SIGNAL TRANSDUCTION MECHANISMS OF HAMP AND PAS DOMAINS IN BACTERIAL CHEMOTAXIS

A Dissertation

Presented to the Faculty of the Graduate School

of Cornell University

In Partial Fulfillment of the Requirements for the Degree of

Doctor of Philosophy

by

Nattakan Sukomon

January 2017

ABSTRACT

Bacteria utilize two-component systems to respond and adapt to changes in their environments. Central to the systems are modular receptors that comprise various functional domains to detect those changes and relay signals to effector domains. HAMP (**H**istidine kinases, **A**denylate cyclases, **M**ethyl accepting proteins and **P**hosphatases) and PAS (**P**er–**A**rnt–**S**im) are two of the most common domains that couple various effectors to regulate a wide range of cellular activities.

HAMP domains are signal relay modules that connects input and output domains. The HAMP domain from the *E. coli* serine receptor Tsr has been extensively studied by using genetic techniques, which leads to a model of HAMP biphasic stability that explains the behaviors of Tsr mutant receptors. However, limited biophysical data on the Tsr HAMP are available due to the instability of the domain. In order to provide stability to the Tsr HAMP, a chimera containing Tsr spliced into the poly-HAMP domains from *Pseudomonas aeruginosa* Aer2 (PaAer2) was created. Within the chimera, the Tsr HAMP maintains its characteristic four-helix coiled-coil structure with the distinctively lowered melting temperature compared to the PaAer2. This chimera was used to study three well-characterized HAMP mutational phenotypes differentiated by flagella-rotation patterns and CheA kinase activities: functional counterclockwise flagella rotation [CCW(A), kinase off], functional clockwise flagella rotation (CW, kinase on), and lesion-induced counterclockwise rotation [CCW(B), kinase off]. The stabilities and structural dynamics of the three phenotypes conform to the biphasic model. The transitions between functional on and off states are mediated by helix rotations and scissor-type movements. In the lesion-induced kinase off, the AS1 helices dissociate from the bundle while the AS2 helices form a two-helix colied coil. Overall, this study provides insights into relationships between HAMP conformational behaviors and their corresponding functional outputs.

PAS domains are sensor motifs that are critical in signal transductions of prokaryotic and eukaryotic sensory proteins including chemoreceptors. *Vibrio cholerae* Aer2 (VcAer2), a PaAer2 homolog, has been shown to mediate responses to oxygen through the heme-binding PAS domains. Substitution of the conserved Trp 276 in the PAS2 domain to Leu abolished the O_2-stabilizing ability, which corroborates its O_2-ligating role. The crystal structure of the VcAer2 W276L is highly similar to the CN-bound PAS domain from PaAer2, suggesting the structure of the W276L mutant might represent the ligand-binding state. VcAer2 can serve as a promising alternative to *E. coli* Aer or PaAer2 for investigating PAS-mediated chemotaxis.

BIOGRAPHICAL SKETCH

Nattakan Sukomon was born and raised in Chiangrai, Thailand. She attended King Mongkut's Institute of Technology Ladkrabang (KMITL), Bangkok, Thailand obtaining a Bachelor of Science and a Master of Science in Biotechnology. During her years at KMITL, she conducted her research on plant metabolites that conferred resistance to low temperature under the direction of Prof. Kanokporn Sompornpailin. After graduation, she started her research career as a research assistant at the National Medical Biotechnology Research Lab, Bangkok, Thailand, where she conducted the research on the trafficking mechanism of a kidney anion exchanger 1 under the supervision of Prof. Pa-thai Yenchitsomanus. In 2009, she joined the Biochemistry, Molecular, and Cell Biology Department of Cornell University to pursue a doctoral degree, and conducted the researched on the "Signal Transduction Mechanisms of HAMP and PAS domains in bacterial chemotaxis" under the supervision of Prof. Brian Crane. Apart from science, she enjoys learning Chinese, business and finance.

Dedicated to my family, mentors and friends

ACKNOWLEDGMENTS

I am ever thankful to my advisor, Prof. Brian Crane, for his invaluable suggestions, guidance, and encouragements. I greatly appreciate my committee members, Prof. Richard A. Cerione and Prof. John D. Helmann, for their guidance and support. I acknowledge the continuous helps and encouragements from the former and current members in the Crane lab, especially Michael Airola, Xiaoxiao Li and Ria Sircar for their mentorships. I am thankful for Cornell University, the Department of Biochemistry, Molecular and Cell Biology, and the Department of Chemistry and Chemical Biology for the opportunities to learn and grow both professionally and personally. I consider myself very lucky to have friends with various backgrounds both at and outside of Cornell. I am very grateful for their continuous support and inspirations. Last bust not least, I am very thankful to my family for their love, encouragement and support.

TABLE OF CONTENTS

LIST OF FIGURES

LIST OF TABLES

CHAPTER 1

Introduction

1.1 Overview of bacterial chemotaxis

Many bacteria monitor and respond to chemical gradients in their environment by means of a chemotactic sensing pathway. Central to chemotaxis are chemoreceptors known as methyl-accepting chemotaxis proteins (MCPs).

Escherichia coli has served as a model organism for bacterial chemotaxis research. In *E. coli*, there are five different chemoreceptors: Tsr (detects serine), Tar (aspartate and maltose), Tap (dipeptides and pyrimidines), Trg (ribose and galactose), and Aer (oxygen through monitoring of internal redox states) [1-6]. Tsr, Tar, Tap and Trg are canonical transmembrane receptors with a periplamic domains that bind directly to small molecule ligands , or indirectly to periplasmic periplasmic substrate-binding proteins (Figure 1-1) [2, 5, 6]. In contrast, Aer does not contain a periplasmic ligand-binding domain. Rather, Aer detects changes in intracellular redox states through a flavin adenine dinucleotide (FAD) that binds to an N-terminal PAS domain (Figure 1-1) [7-12].

Chemoreceptors, also known as methyl-accepting chemotaxis proteins (MCPs) mediate chemotaxis by interacting with the two-component system consisting of the histidine kinase CheA and the response regulator CheY (Figure 1-2) [1-3, 13, 14]. Three MCP homodimers trimerize into a “trimer-of-dimers” to interact with an adaptor protein CheW and CheA to form a ternary signaling complex. MCPs regulate

the autophosphorylation activity of CheA depending on the levels and types of chemoeffectors [4-6].

E. coli cells contain four to six peritrichous flagella that rotate in the counterclockwise (CCW) direction as the default. CCW rotation causes forward swimming (Figure 1-2B) [1, 3, 15]. Repellent binding or attractant dissociation promotes CheA kinase activity, increasing levels of phosphorylated CheY (CheY-P). The interaction of CheY-P and flagella motors induces the rotational switching to clockwise (CW), which destabilizes the flagella bundle, and causes the cell to tumble (Figure 1-2B) [1, 5, 6, 15].

A sensory adaptation system regulates the kinase activity by adjusting detection sensitivity to the pre-stimulus level. In *E. coli*, the adaptation mechanism is accomplished by methylation and demethylation of several conserved Glu residues on the kinase control domain of the cytoplasmic region of the MCP (Figure 1-1). Methylation is catalyzed by the SAM-dependent methylase CheR, and demethylation (as well as deamidation) is catalyzed by CheB (Figure 1-2A) [16-19]. The adaptation system provides a short-term memory for bacterial cells to compare current and previous ligand concentrations, and allow chemoreceptors to operate over a wide range of concentrations [14].

1.1.1 Structures of bacterial chemoreceptors

The canonical MCP is homodimeric with ~500 amino acids per subunit. Each subunit forms an extended, mostly α-helical coiled coil, but has a modular structure

that is organized into three functional elements, including a sensing module, a signal relaying HAMP domain, and a kinase control module (KCM) (Figure 1-1) [1-3].

The sensing module is composed of a periplasmic ligand binding domain connected to a transmembrane region. The crystal structures of Tar periplasmic domain reveal a dimer of symmetric four-helix bundles (α1-α4) that form the ligand-binding site [20-22]. The biochemical and structural studies indicate that, out of the two binding sites, only one is occupied by the aspartate ligand at any one time, which generates negative cooperativity between the two subunits. [23]. The α1 and α4 helices of each subunit span the membrane, providing two transmembrane helices (TM1 and TM2) that, together with the second subunit, form four membrane-spanning helices. The TM2 helices connect to the HAMP domain through a five-residue control cable [3, 24, 25]. The TM2 helices of MCPs contain one or more aromatic residues at their C-termini end near the membrane-cytoplasm interface. These residues form an aromatic belt, which plays a role in transmembrane signaling by constraining the displacement of TM2 [26-30].

The intervening HAMP domain plays a crucial role in mediating signal transmission between the sensing domain and the KCM [31]. Biochemical and structural studies suggest several mechanisms in signal transduction from TM2 to HAMP, including a piston-like downward movement of TM2 relative to TM1, scissor motions, and helix rotation [32-35]. HAMP domains from various microorganisms have a conserved structure of a dimeric protein with each monomer providing two helices (AS1 and AS2) that together form a parallel four-helix coiled-coil [32-34, 36] (see section 1.2).

The cytoplasmic KCM is an antiparallel, four-helix coiled-coil bundle with the adaptation region, the flexible glycine hinge, and the protein-interacting tip that directly binds to CheW and CheA. The protein-interacting region is highly conserved with trimer-formation determinants that are nearly identical across all receptor types in *E. coli*. As a result, the low-abundance receptors (Aer, Tap and Trg) can participate in signaling clusters that are dominated by the high-abundance receptors (Tar and Tsr). MCPs in *E. coli* and *Salmonella typhimurium* contain a pentapeptide motif (NWETF) at the C-termini, which localizes CheR and CheB to the KCM domain. [37-40]. Trg and Tap lack the dipeptide motif, thus requiring Tar and Tsr to recruit CheR and CheB [41].

Newly-synthesized receptor molecules contain two Glu and two Gln residues per subunit (QEQE) at the adaptation region (Figure 1-1) [2, 3]. The receptors with the QEQE state have intermediate CheA activities, and are the target for subsequent CheB-mediated deamidation to the EEEE state, which can subsequently undergo CheR-mediated methylation at each site [42, 43]. Mutational studies have shown that substitution of Glu for Gln at the adaptation sites mimic the effects of the adaptation system. The receptors with the QQQQ state represent the fully methylated or kinase-on output, whereas those with the EEEE state mimic the fully demethylated or kinase-off output [44, 45]. Recently, the fifth methylation site (Glu502) has been identified in Tsr [46]. However, this site may not be critical for chemotaxis as amino acid replacements of this residue do not affect chemotactic responses [46].

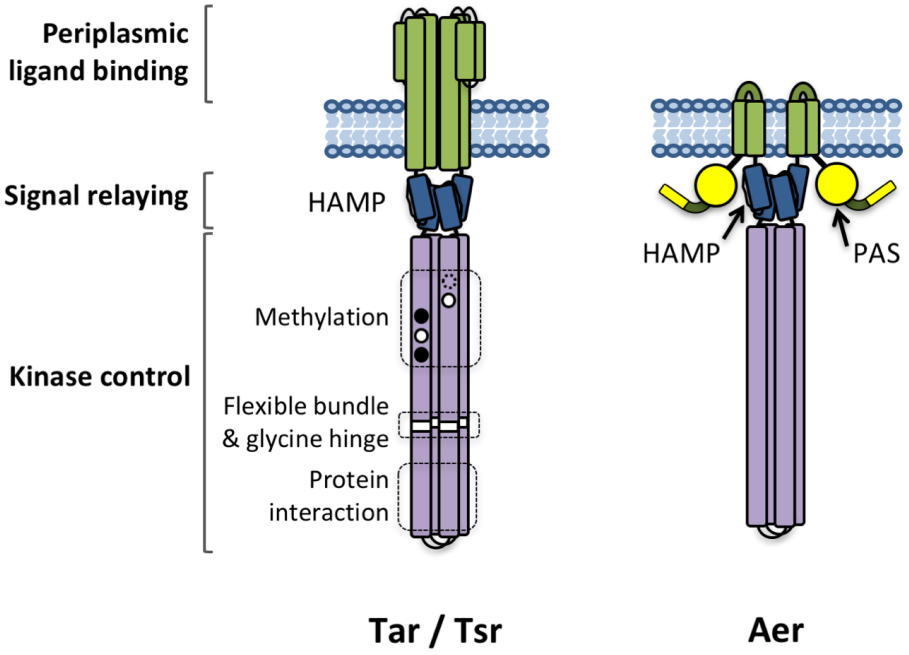

Figure 1-1 Architectures of *E. coli* chemoreceptors. *E. coli* contains four transmembrane MCP, including Tsr, Tar, Tap, and Trg. The *E. coli* MCPs (left) are homodimeric, extended coiled coils with three functional modules: 1) the periplasmic ligand-binding domain, 2) the signal relay or HAMP domain, and 4) the kinase control module. The fifth MCP-related receptor, Aer (right), does not possess the periplasmic ligand-binding site, but senses cellular redox states through the FAD-binding PAS domain. The MCP kinase control module contains four canonical methylation sites per subunit in the adaptation region which are translated as two Glu and two Gln residues (shown as white and black circles, respectively), which represent the targets for CheR or CheB. Tsr possesses the fifth methylation site (Glu502, dashed circle). The fifth site is not critical for function. The Aer kinase control domain does not contain methylation sites, and its adaptation system probably involves interactions with the other receptors.

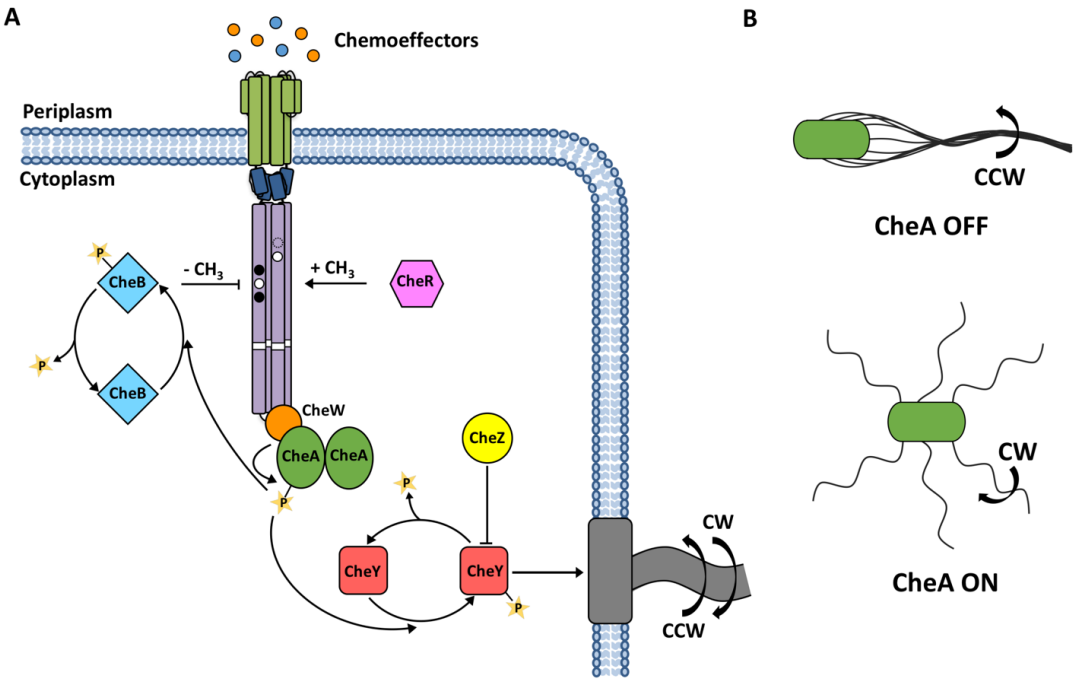

Figure 1-2 Chemotaxis signal transduction in *E. coli*.

(A) Overview of chemotaxis. The MCP periplasmic ligand-binding domain of MCP monitors the level of chemoeffectors. In the presence of repellents or the absence of attractants, the KCM interacts with the histidine kinase CheA and the adaptor protein CheW, which leads to the autophosphorylation of CheA (ON), and subsequently, phosphoryl-group (P) transfer to the response regulator CheY. Phosphorylated CheY interacts with the basal body of flagellar motor, and causes clockwise (CW) rotation. Repellent dissociation or attractant binding deactivates CheA (OFF) and decreases the level of phosphorylated CheY, which switches the rotational bias from CW to counterclockwise (CCW). The effects of chemoeffectors are countered by the sensory adaptation system, which restores the pre-stimulus CheA activity by covalently modifying specific residues in the KCM. The CheR methyltransferase methylates conserved Glu residues (shown in white circles) to shift receptors toward the kinase-

on state. CheB, a methylesterase and deamidase, hydrolyzes methylated glutamates, or deamidates Gln (shown in black circles) to Glu in newly synthesized receptors. CheB is the second response regulator of the system and must be phosphorylated by CheA to be active.

(B) Chemotaxis signaling outputs. The signaling state of chemoreceptors transitions between ON and OFF states. The ON state causes the CW rotational bias and cell tumbling. In contrast, the OFF state switches the rotational bias to CCW and straight swimming.

1.1.2 Signal propagation through MCPs

The signaling properties of MCPs comply with a two-state model, which emphasizes the transition between two dominant signaling outputs: kinase-on (cell tumbling), and kinase-off (straight swimming) [1-3]. This signal mechanism is mediated by allosteric coupling between the cytoplasmic protein-interacting tip and the periplasmic ligand-binding domain, which are located 380 Å away from each other [1].

In the bacterial chemotaxis system, signal transduction is triggered by the binding of chemoeffectors to MCPs. Crystal structures and crosslinking studies of the *E. coli* aspartate chemoreceptor Tar indicate a "piston"-like downward movement of helix 4 in the ligand binding domain, which becomes the second transmembrane helix (TM2), toward the cytoplasm after attractant binding [20, 47]. In addition to chemoreceptors, TM helix-HAMP signal transmission can be found in membrane-associated phototactic transducer HtrII, as well as sensor histidine kinases of various types, such as the osmolarity sensor EnvZ, acidic pH and cationic antimicrobial peptide sensor PhoQ, and nitrate/nitrite sensor NarX [31, 48-50]. The evidence suggests a common theme of HAMP-mediated signal transduction in bacterial transmembrane receptors. Mutational studies of Tar suggest the importance of aromatic residues at the cytoplasmic end of TM2 (Trp209 and Tyr210) localizing to the membrane/cytoplasm interfaces [29]. Furthermore, molecular simulations of Tar indicate a strong correlation between the small, piston-like movement of TM2 (~1.5 Å) and changes in signaling activities [20]. However, other molecular dynamic studies of Tar that is bound to various agonists and antagonists suggest that TM2 displays both

piston-like motion and helix rotation after binding to ligands [51]. The combination of displacement and rotation is also observed in the TM2 of *Natronomonas pharaonis* phototransducer HtrII (NpHtrII) [52-55]. NpHtrII forms a complex with the photoreceptor NpSRII to regulate phototaxis, and is structurally homologous to other transmembrane chemoreceptors with two contiguous HAMP domains [56]. Electron paramagnetic resonance and X-ray structural analysis reveal that NpHtrII responds to NpSRII activation by a clockwise rotation of ~15° of TM2, and a piston displacement of this helix by 0.9 Å toward cytoplasm, which is smaller compared to that observed from chemoreceptors [52].

Several models for HAMP signal propagation have been purposed. The static two-state model originates from the structure of the HAMP domain from the *Archeoglobus fulgidus* hypothetical receptor Af1503 [32]. This model emphasizes two discrete HAMP conformations that mediate the two opposing signaling outputs (the ON and OFF states). The conformational switching is accomplished by gearbox-like rotations of the AS1 and AS2 helices [32, 35, 57]. However, subsequent biochemical and structural studies of HAMP domains from various organisms suggest additional motions for HAMP conformational switching that include translations and scissor-type motions of AS1 and AS2 [34, 48, 58]. Importantly, these motions are not necessarily mutually exclusive [34, 59].

A second dynamic model for HAMP signaling arose from comprehensive functional characterization of the Tsr HAMP domain [60-63]. In contrast to the static model, this model proposed that the ensemble of HAMP conformations with comparable helix-packing stability (and thus dynamic motions) mediate similar

signaling outputs. HAMP conformations with either very stable or very unstable helix packing promote the kinase-off output, and conformations with intermediate stability provoke the kinase-on state (see section 1.2) [60, 61, 63].

Conformational switching of the HAMP domain or the changes in HAMP packing stability modulate the signaling output through the HAMP-KCM interplays [2, 3]. Several studies have shown that the signals from the HAMP domain propagates through the KCM by means of dynamic alterations along the helices. Disulfide crosslinking analyses of engineered Cys residues on the KCM in the kinase-on and OFF states has led to the "yin-yang" hypothesis that explains the signal propagation from the HAMP domain to the protein-interacting region of the KCM [3, 58]. In this model, the HAMP domain transmits the ON and OFF signals directly to the N-termini of the KCM helices through the opposite displacements. In the kinase-on state, the C-termini of the HAMP AS2 adopt an "open" conformation, resulting in the stabilization of the adaptation region, but the disruption of the protein interaction region. The reverse trend is expected for the kinase-off state [58]. In contrast to the yin-yang hypothesis, the recent EPR study using the Tar KCM coupled with PaAer2 HAMP domains have suggested that the protein-interacting region is more rigid in the kinase-on state, but more dynamic in the kinase-off state. Moreover, the HAMP domains in each signaling state cannot be differentiated by simple conformational transitions [64].

Several studies indicate the impact of adaptational modification on the packing stability of the KCM helices. Neutralization of the adaptation Glu residues, either by the methylation activity of CheR or by amino-acid replacement to Gln (QQQQ state), stabilizes the helical packing in the adaptation region, and favors the kinase-on output

[58, 64]. On the other hand, mutagenesis of the methylation sites to EEEE increases charge at the adaptation region [58, 64], and destabilizes the helix packing by causing HAMP-connecting KCM helices (CD1) to detach from the four-helix bundle [64]. As a result, the receptor favors the kinase-off output. Interestingly, EPR studies have shown that the adaptation can switch the signaling conformations of the HAMP domain, suggesting that adaptation impacts the dynamical properties of both the upstream and downstream domains [64]. Moreover, the dynamic state of the KCM helices determine the substrate preferences of the adaptation enzymes. CheR preferentially interacts with KCM helices in the EEEE (ON) state, and shifts the receptor to the OFF state by transferring methyl groups to the glutamyl residues and converting them to glutamyl methyl esters. On the contrary, CheB prefers the more compact KCM helices of the QQQQ (OFF) state, and shifts the receptor to the OFF state by hydrolyzing methylated glutamates [60, 61].

The dynamic properties of the receptor tip are crucial for controlling CheA kinase activities [1-3, 65, 66]. Mutational studies of the highly conserved hairpin residues have revealed that Glu391, which locates at the apex of the hairpin tip in Tsr and Tar, controls the conformational transitions between the ON and OFF states of the receptors. Substitutions of the Glu391 residues with non-polar residues with large side-chain sizes result in fast switching of the flagellar motors, suggesting that Glu391 regulates dynamic motions of the hairpin tip [67]. Moreover, molecular dynamic studies of the Tsr KCM have shown that the conserved Phe396 at the protein-interacting hairpin tip plays a critical role in controlling conformational switching of

the hairpin tip, as well as modulating kinase activities through rotameric switching and alternative stacking arrangements [68].

1.2 Signal transduction mechanism of HAMP domain

HAMP domains are signal transduction modules that couple diverse extracellular input signals into intracellular responses [31]. The first HAMP domain was genetically identified in *E. coli* serine receptor (Tsr) as the region connecting the transmembrane helix TM2 to the kinase control domain [31]. To date, HAMP domains are found in over to 26,000 proteins that are characterized as **h**istidine kinase, **a**denylate cyclases, **m**ethyl-accepting chemotaxis proteins (MCP), and **p**hosphatases in archaea, bacteria, and lower eukaryotes [31, 69-71].

1.2.1 HAMP structure

The sequence analyses classify HAMP into two groups, including canonical and divergent HAMP [71]. The canonical HAMP domains contain the conserved Pro in AS1 and the DExG motif at the N-terminus of AS2 [59, 71]. These two conserved features of the canonical HAMP are essential for signal transmission from the transmembrane helices. The divergent HAMP domains are almost always present as poly HAMP arrays that can extend from 2-31 contiguous domains [71]. HAMP domains in the divergent group lack the conserved Pro and DExG motifs, as such signal transmission may be different [34, 71]. HAMP sequence comparisons show poor pairwise identity. However, the domains are highly conserved at the secondary-structure level [31, 34]. The first high-resolution structure of HAMP domain was

determined from Af1503, a hypothetical receptor from thermophile *Archaeoglobus fulgidus* (Figure 1-3A) [32]. HAMP domain is defined as a small, homodimeric protein with ~ 50 residues in each subunit. The HAMP fold is a homodimeric, parallel four-helix bundle with each monomer supplying two amphipathic α-helices (AS1 and AS2). Each helix comprises of a heptad repeat (a-g) with hydrophobic residues occupying the a and d positions to form a buried hydrophobic core [31, 32, 34]. However, variations in helical packing can be found in HAMP domains. For example, the wild-type Af1503 HAMP domain adopts an unusual x-da helical packing (Figure 1-4A) [32]. AS1 and AS2 are connected by a 14-residue non-helical linker (CTR), which provides two hydrophobic residues (HR1 and HR2) that play a role in HAMP stability [31, 34, 72]. Subsequent cysteine cross-linking analyses in aerotaxis receptor Aer and aspartate receptor Tar from *E. coli* as well as sensor kinase PhoQ from *Salmonella enterica* confirm the conserved four-helix bundle structure of HAMP domains [33, 36, 48, 73].

In addition to the biochemical studies, the crystal structure of three contiguous HAMP domains (HAMP1-2-3) from *Pseudomonas aeruginosa* Aer2 (PaAer2) further corroborates the parallel four-helix bundle as a universal HAMP architecture (Figure 1-3B) [34]. Regardless of the highly conserved fold, the superposition of the PaAer2 HAMP domains, together with the Af1503 HAMP structure, reveals two distinct HAMP conformations [34]. Conformation A, which is held by HAMP1 and HAMP3, resembles Af1503 HAMP with several minor variations from helix tilting and rotation (Figure 1-3B). In this conformation, the AS1 and AS2 helices are in-register with the side chains of hydrophobic residues positioned to the core. However, PaAer2 HAMP1

and HAMP3 do not exclusively utilize the x-da packing mode. Rather, they adopt a variety of packing arrangements, including canonical knobs-into-holes, x-da, and x-x modes [34]. This difference is likely because the Af1503 and PaAer2 HAMP domains belong to distinct groups based on the sequence analysis [34, 71]. On the other hand, HAMP2 adopts the conformation B, which is a unique parallel four-helix bundle with an offset ridges-into-grooves interaction. Compared to HAMP1 and HAMP3, HAMP2 shows drastic differences in helix crossing angles and rotation such that an interaction approximating a two-helix coiled coil is formed by the AS2 helices (Figure 1-3B) [34]. The two distinct HAMP conformations observed in PaAer2 may represent different HAMP signaling states.

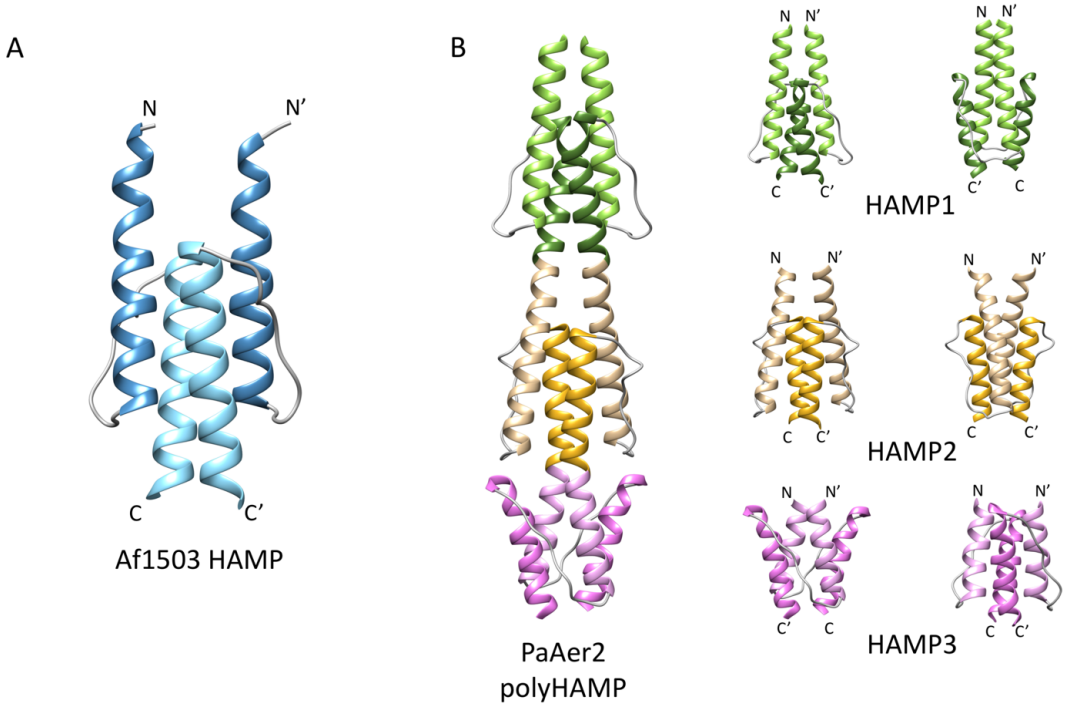

Figure 1-3 High-resolution structures of HAMP domains.

(A) The NMR structure of the Af1503 HAMP domain from *A. fulgidus* (PDB: 2L7H). The HAMP domain represents a homodimeric, four-helix coiled coil fold with an unusual x-da helical packing arrangement.

(B) The crystal structure of the PaAer2 poly-HAMP domains (PDB: 3LNR) from *P. aeruginosa*. The PaAer2 HAMP structures confirm the universal four-helix coiled coil fold. However, the poly-HAMP domains adopt two distinct conformations. The HAMP1 and HAMP 3 domains represent conformation A, which resembles that of Af1503 HAMP, but do not exclusively utilize the x-da packing mode. Ra The HAMP2 domain represents conformation B, which is distinct from conformation A in helix crossing angles, rotations, and translation.

1.2.2 HAMP signal transduction mechanism

Signal transduction within signaling proteins occurs via sequential conformational changes through linked modules. In chemoreceptors, ligand-induced movements of TM2 mediate the structural changes of the HAMP domain, which is subsequently transmitted to the downstream kinase control module [20, 47].

The AS1 helices of Tsr and Tar HAMP domains are connected to TM2 through a five-residue control cable segment [24, 25, 31]. Mutational analyses of the control cable from Tsr have led to the helix-clutch model, which emphasizes the role of the control cable helicity on the downstream HAMP structures and signaling outputs. However, only Ile214 is critical to signal transmission to the HAMP domain [25, 74]. It has been proposed that the control cable creates a mismatch between the registers of TM2 and the HAMP AS1 helices. The inward piston-like movements of TM2 disengage the "structural clutch" of the aromatic residues at the cytoplasmic end of TM2. This disengagement creates a break in helicity that reduces the register mismatch of TM2 and AS1, thus affecting the HAMP conformations [24].

Several models have been proposed for conformational signal propagation through HAMP domains. To date, there are two distinct models, including a static, two-state model and a dynamic bundle model [31, 75].

The static, two-state model emphasizes the two distinct conformations of HAMP domains that mediate opposite CheA activities, and thus signaling outputs [75]. A well-known example is the gearbox model, which originated from the structure of Af1503 HAMP [32, 35, 57, 76]. The wild type Af1503 HAMP adopts an unusual x-da packing arrangement of the helical heptad repeat (Figure 1-4A) [32]. Subsequent

biophysical studies of the key residue A291, which residues in the hydrophobic core, have shown that substitutions of A291 with residues of larger side chains switch the core packing arrangement from the x-da mode to the canonical knobs-into-holes mode by a concerted 26° axial rotation of all helices (Figure 1-4A and 1-4B) [57, 76]. Furthermore, the types of packing arrangements, and thus HAMP conformations, correlate with adenylyl cyclase activity in biochemical experiments using a chimeric system composing of the ligand-binding domain and transmembrane region of Tsr, Af1503 HAMP, and cyclase domain of Rv3645 [57].

Cysteine-crosslinking experiments of Tar further support the two-state model. Rather than helix rotation, however, conformation signals generated by attractant-induced piston movements of TM2 induce a scissors-type displacement of HAMP, thus causing a structural rearrangement that is transmitted to the C-termini of the AS-2 helices [58]. This displacement couples with helices of the kinase control domain at the N-termini, and strains its four-helix bundle packing to favor the CheA OFF state [33].

The crystal structure of the poly HAMP domains from PaAer2 indicates two distinct HAMP conformations distinguished by four- (conformation A, represented by HAMP1) or two- (conformation B, represented by HAMP2) helix coiled-coil structures at the C-termini [34]. The *in vivo* chemotaxis experiments using the Tar-PaAer2 HAMP system have shown that HAMP1 and HAMP2 mediate opposite signaling outputs as expected from the two-state model [77]. The HAMP1 conformation activates CheA and generates CW flagella rotation. On the contrary, the conformation of HAMP2 inhibits CheA, and induces CCW flagella rotation. The

transition between the two conformations can be achieved by the combination of several mechanisms, including helix translation, tilting and rotation [59]. Furthermore, substitution of Ile88 to Gly converts both conformation and signaling output of HAMP2 to those of HAMP1. Ile88 is an HR2 residue in the CTR of HAMP2. The side chain of Ile88 inserts into the HAMP2 bundle, and plays a role in stabilizing the hydrophobic core. Thus, the conformational and output switching behaviors of I88G mutant validate the conformation-dependent signaling mechanism of HAMP domains [59]. However, it should be noted that the ON state of HAMP1 appears to be much more conformationally dynamic than the OFF state of HAMP2, and this difference is in keeping with the dynamic bundle model discussed below [77].

Structural and biochemical studies of HAMP domains from other classes of bacterial receptors also indicate the two-state model as the signaling mechanism. Studies of the first HAMP domain of NpHtrII indicate a signal-induced helix rotation similar to that observed in the Af1503 HAMP. Moreover, signal propagation is also associated with the inverse helical displacements in that the AS1 and AS2 helices shift in the opposite directions [54, 55]. In addition, cysteine cross-linking analysis and molecular modeling also confirm the two-state signaling mechanism of the PhoQ HAMP domain [48, 50]. However, the conformational switching is mediated by helix rotation along with the opposite tilting of the AS1 and AS2 helices [75].

Overall, evidence for a two-state model of signaling is supported by studies of HAMP domains from various receptor types. However, HAMP signal transduction mechanisms may not necessarily involve similar conformational transitions.

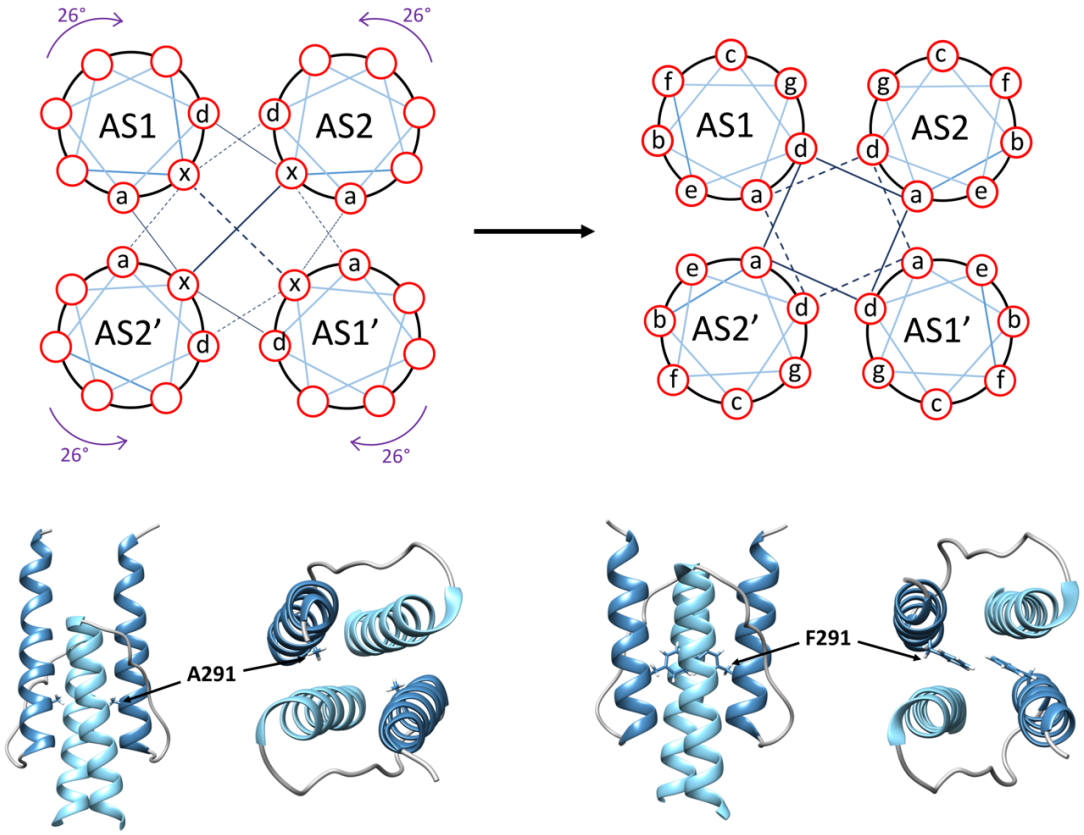

Figure 1-4 The gearbox model for HAMP signal transduction

(A) Schematic representation of the gearbox model. The helical wheel diagrams show two possible HAMP packing modes: complementary x-da (left) and knobs-into-holes (right). HAMP domains with the x-da packing mode interconvert to the canonical knob-into-holes packing mode by a concerted 26° axial rotation of all four helices (depicted as arrows). The complementary x-da packing forms the hydrophobic core by utilizing three positions, including one in x-geometry and two in da-geometry. In contrast, the knobs-into-holes packing uses two core residues, which reside in a and d positions, to form the hydrophobic core. The dark blue lines in solid and dashed represent two successive layers.

(B) The WT Af1503 (left) (PDB: 2L7H) assumes the complementary x-da packing mode, which is stabilized by the core residue A291. Mutations of A291 to Phe (A291F, PDB: 2L7I) (right), or amino acids with larger side chain allow the HAMP domain to convert to the canonical knobs-into-holes packing mode by axial helix rotation. The AS1 and AS2 helices are shown in dark blue and light blue, respectively. The connectors are shown in grey.

Extensive mutational analyses of the Tsr HAMP domain provide insight into the HAMP signal transduction mechanism that leads to the dynamic bundle model [60-63]. This model emphasizes the relationship between HAMP bundle stability (or dynamics) and signaling outputs represented by kinase activities or flagella rotation. Rather than discrete conformational states, HAMP signaling states correspond to ensembles of structures with similar stabilities (Figure 1-5A). HAMP bundles of both dynamic extremes, highly stable and highly unstable, mediate kinase-off or CCW flagella rotation behavior. HAMP bundles with intermediate stabilities cause the kinase-on (CW) output [31, 59-61, 63].

The stable state [CCW(A)] is the functional off phenotype. The residues whose mutations cause CCW(A) phenotype specifically locate at the membrane-proximal end of the Tsr HAMP, such as Pro221 and Asp248 (Figure 1-5B). The substitutions of these residues, mostly to hydrophobic amino acids, are likely to increase helix-packing interactions, and thus mimic the effect of attractants [61, 63].

On the other hand, the very unstable state [CCW(B)] is caused by lesions that destabilize the HAMP bundle, and is found to associate with the core residues, such as Met222, Ile229, and Leu252 (Figure 1-5B). Therefore, substitutions with polar and charged amino acid residues or Pro residues destabilize the HAMP bundle, and impair the ability for ternary-complex assembly of the receptor [61, 63].

The kinase-on (CW) output is exclusively found in mutations of the residues that locate in the membrane-distal part of the HAMP domain, such as Ala233 and Met259 (Figure 1-5B). The hydrophobic replacements of this residue most likely distort the stability of the C-terminal half of the HAMP domain. The wild-type Tsr

HAMP has stability within this range and generates the CW-biased phenotype by default (with ~75% CW) in absence of the adaptation system [61, 63].

In addition, HAMP signaling states are not only determined by the stability of the helical bundle, but are also modulated by conformational rearrangements of the control cable, as well as by changes in the kinase control domain [24, 25, 64].

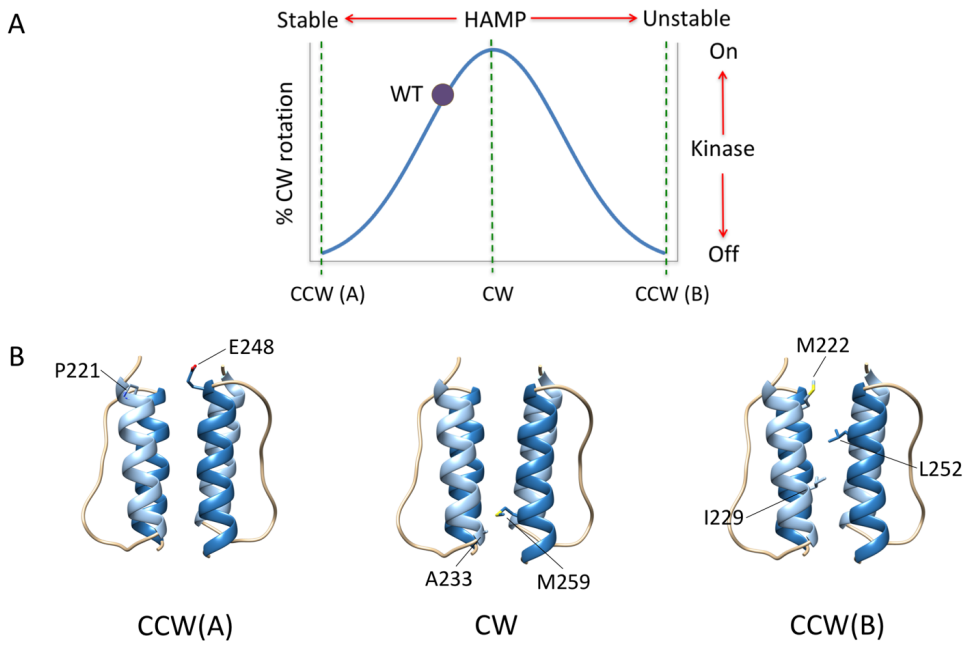

Figure 1-5 The dynamic bundle model for the HAMP signaling mechanism

(A) The dynamic bundle model emphasizes the relationships between the stabilities of the HAMP bundle and the signaling outputs. The HAMP bundle with stability at either two extremes causes CCW output. CCW(A) is most likely functional off state that mimics the effect of attractants. On the other hand, the CCW(B) state is caused by lesions that destabilize the HAMP bundle and distort the domain outside of the physiological range. The HAMP bundle with intermediate stability mediates CW output. The wild-type (WT) Tsr HAMP has stability in this range, generating approximately 75% CW output in the absence of the adaptation system.

(B) Examples of residues whose substitutions generate the CCW(A), CW, and CCW(B) signaling outputs. The atomic coordinate for the homology model of Tsr HAMP was generates by threading the Tsr HAMP sequence onto the Af1503 A291F HAMP (PDB: 2L7I) using SWISS-MODEL.

1.3 Signal transduction mechanism of PAS domain

Per-ARNT-Sim (PAS) motifs were originally identified by sequence homology of *Drosophil*a **per**iod, vertebrate **a**ryl hydrocarbon **r**eceptor **n**uclear **t**ransport (ARNT), and *Drosophila* **si**ngle-**m**inded [78-80]. Found in all kingdoms of life, PAS domains serve as sensor and protein interaction modules [81, 82]. To date, PAS domains have been found in over 29,000 proteins that play a role in the signal transduction of diverse processes, such as chemical sensing, nitrogen fixation, phototropism, and circadian behavior [81-84].

In general, PAS-containing proteins are modular. PAS domains act as sensors that detect various chemical and physical stimuli, and regulate the activity of effector domains [81, 82]. The analysis of Pfam-annotated PAS-containing proteins indicates that histidine kinases are the most prominent effector domains that are found in conjunction with PAS domains [81]. Other effector domains include phosphodiesterases, methyl-accepting chemotaxis protein (MCP), serine/threonine kinases and transcription factors [82].

1.3.1 PAS structure and oligomerization

PAS domains share relatively low sequence homology with the average pairwise sequence identity of 20% or lower, which leads to complication in sequence-based identification of PAS domains [85, 86]. In 1995, the crystal structure of *Halorhodospira halophile* photoactive yellow protein (PYP) was determined, which provided the first view of three-dimensional structures of PAS domains (Figure 1-6) [87].

Regardless of low sequence identity, PAS domains adopt a conserved, single globular fold of approximately 100 residues [88]. A canonical PAS domain comprises a core with five antiparallel β strands (designated Aβ, Bβ, Gβ, Hβ, and Iβ) in the topological order of 2-1-5-4-3. The PAS core is flanked by several α helices, namely Cα, Dα, Eα, and Fα (Figure 1-6 and 1-7) [81, 82, 84]. Structural superposition of 47 PAS domains indicates that the PAS core is the most conserved region with the root-mean-square deviation of any two PAS β backbones of 1.9 ± 0.6 Å. On the contrary, the flanking helices vary in both length and structure [82].

Various PAS domains contain α-helical extensions at their N-termini, which are referred to as N-terminal caps (N-caps) (Figure 1-6). Even though N-caps are the least conserved segments of PAS domains, they play a role in protein stabilization [84]. The N-cap truncation of *E. coli* aerotaxis receptor (EcAer) leads to a lower cellular level of the receptor, confirming the role of PAS domains in structure stabilization [89]. Several studies have also suggested the role of N-caps in PAS functions. Structural comparisons between the ligand-free and CN^--bound PAS domains from PaAer2 receptor reveal that the N-cap undergoes repositioning as the receptor senses signals [77, 90]. The N-cap deletion of the PAS-A domain from aryl hydrocarbon receptor (AHR) dramatically lower the transcriptional activity of this variant compared to the wild type [91]. In addition, the mutational studies of human Kv11.1a potassium channel have revealed the critical role of the N-cap in channel trafficking and stability [92, 93].

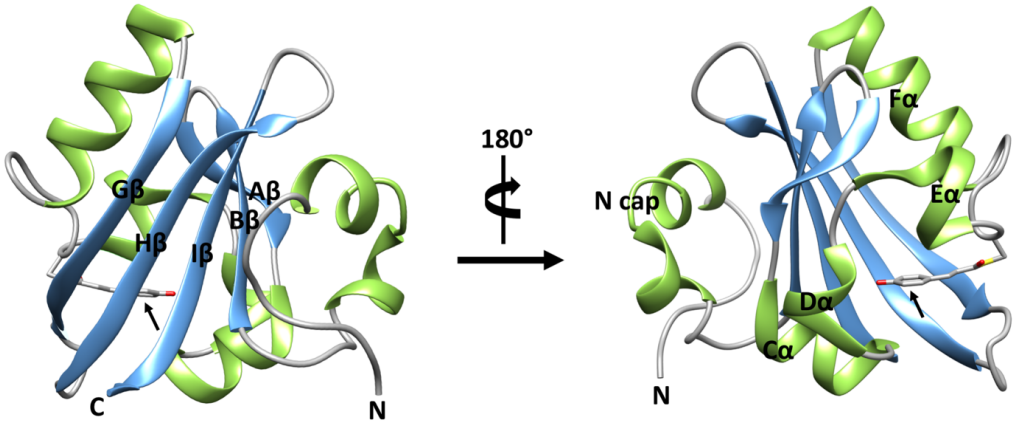

Figure 1-6 Three-dimensional structure of *Halorhodospira halophile* photoactive yellow protein (PYP) (PDB: 2PHY). PYP represents the conserved PAS fold, which is composed of a 5-stranded β scaffold and flanking α helices. The secondary structure elements are as denoted with β strands in blue, α helices in green, and connectors in grey. The 4-hydroxycinnamyl chromophore is covalently linked to Cys69 in the connector between Eα and Fα by a thioester bond, and is marked by an arrow.

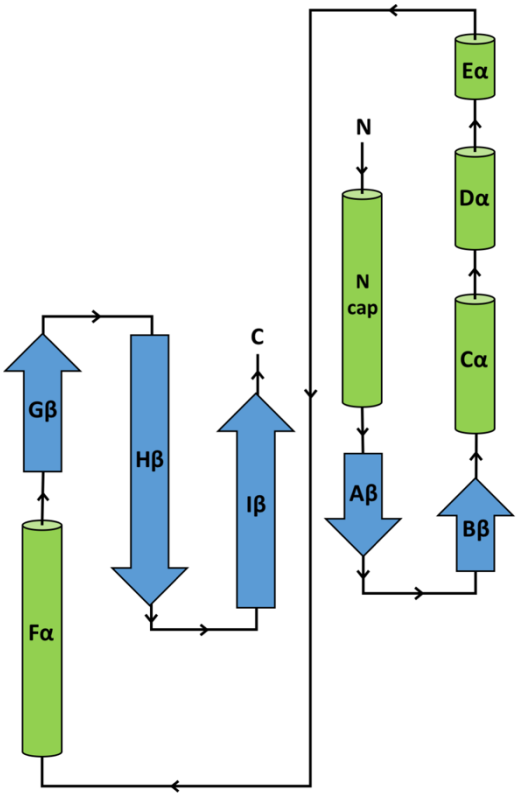

Figure 1-7 Topology diagram of canonical PAS domains. The PAS core is composed of five antiparallel β-strands in the order of B-A-I-H-G. Several α helices, including Cα, Dα, Eα and Fα, flank the β scaffold. Several PAS domains contain N-terminal α helices (N cap), which are important for PAS signal transduction. (Adapted from [82])

Several studies have shown that PAS domains mediate protein-protein interactions by promoting oligomerization [78, 82, 84]. In many cases PAS oligomerization is necessary for function. PAS monomer interfaces are plastic [82]. As a result, PAS domains can display a variety of oligomerization patterns, which can be parallel dimers, antiparallel dimers, or intermediate orientations [82, 94]. PAS domains from several prokaryotic proteins, such as PaAer2 [77, 90], NpSTHK [95], EcDOS [96, 97], AvNifL [98], KpCitA [99] and RmFixL [100], adopt a parallel homodimeric arrangement with their N-termini and/or β cores in close proximity (Figure 1-8A). Antiparallel homodimerization can be found in some PAS domains, such as *Chlamydomonas reinhardtii* Phot-LOV1 [101], *Arabidopsis thaliana* LOV1 [102], and PAS-B domain from human HIF2α/Arnt [103, 104] (Figure 1-8B). On the other hand, PAS domains from some proteins, such as BjFixL [105] and BsKinA [106], form dimers with several different quaternary structures under the same crystallization conditions. However, it should be noted that crystal structures of PAS domains are often obtained outside of the context of the respective full-length protein; and thus, the association state found in the crystal may be misleading.

In addition to mediating homo-oligomerization, PAS domains often associate with effector domains [82]. For example, a dioxin receptor contains a bHLH domain in addition to a PAS domain (ARNT) [107]. The isolated bHLH domain forms homodimeric complexes. However, the presence of the ARNT domain induces heterodimeric formation that is sufficient for DNA binding *in vitro* and *in vivo* [103, 108-110].

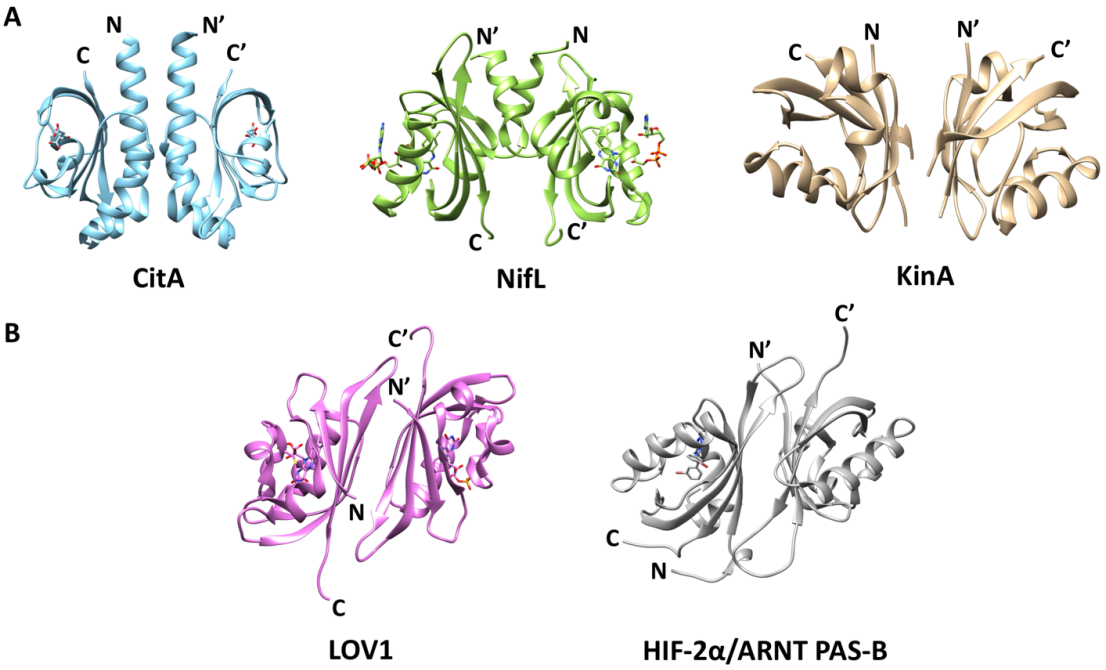

Figure 1-8 PAS homodimeric properties.

(A) PAS domains that form parallel homodimers can adopt several dimerization modes, including α helix to α helix represented by *Klebsiella pneumoniae* CitA (PDB: 2J80), α helix to β sheet represented by Azotobacter vinelandii NifL (PDB: 2GJ3), and β sheet to β sheet represented by *Bacillus subtilis* KinA (PDB: 2VLG). CitA and NifL contain cofactors, namely citrate and FAD, and are included in the ribbon diagrams. (B) Antiparallel homodimeric organization of the PAS domains. LOV1 domain from *Arabidopsis thaliana* phototropin 2 (PDB: 2Z6D) and PAS-B domain from human HIF-2α/ARNT (PDB: 4XT2) adopt the β sheet/β sheet dimerization mode to form antiparallel homodimers. The FAD cofactor of LOV1 and the antagonist for HIF-2α/ARNT are shown in the structure.

1.3.2 PAS signaling mechanism

Cofactor binding and signal detection

Various PAS domains bind to cofactors covalently or non-covalently [81, 82]. The structural comparisons of PAS domains that bind to different cofactors, including flavin nucleotide, 4-hydroxycinnamic acid, heme, and carbon metabolites, indicate a conserved cofactor binding-cleft at the inner surface of the β scaffold and the Eα and Fα helices [81]. In some PAS sensors, such as the citrate-sensor histidine kinase CitA from *Klebsiella pneumoniae*, cofactors constitute signals. In this case, the binding initiates signal transduction cascades [99]. However, in general, PAS cofactors play a role in signal detection. Therefore, cofactor ligations require precise coordination with the PAS β cores [81].

Certain PAS domains sense diatomic ligands through heme cofactors. *Alphaproteobacteria* FixL and *E. coli* DosP contain a *b*-type heme molecule that is covalently ligated via a conserved His residue [105, 111, 112]. Similar His-mediated heme ligation is observed in the PaAer2 PAS domain, which binds to a *b*-type heme molecule [77, 90]. However, GSU0935 and GSU0582, the methyl-accepting chemotaxis proteins from *Geobactor sulfurreducens*, bind to heme *c* via a conserved bi-cysteine ligation site, which is located outside of the PAS cores [113, 114].

The light, oxygen, or voltage (LOV) family is a subset of the PAS superfamily that functions as blue-light photoreceptors [115-118]. The crystal structure of the plant phototropin phy3 LOV2 from *Adiantum capillus-veneris* reveals a binding pocket in the β core that promotes noncovalent binding with flavin mononucleotide (FMN) [119]. Even though first identified as phototropins in higher plants, LOV domains are

also present in fungi and bacteria [115, 120, 121]. In addition to LOV domains, there are other PAS domains that contain flavin cofactors, such as EcAer and *Azotobacter vinelandii* NifL [7, 122]. EcAer and NifL contain flavin adenine nucleotide (FAD), and function as cellular redox sensors by monitoring oxygen levels. The sequence and structural analyses reveal that EcAer and NifL bind to FAD via conserved polar interactions with Asp and Lys/Arg residues and aromatic stacking interaction with Trp in the flavin-binding pockets [10, 122, 123].

Common themes in PAS signaling mechanism

The similarities in PAS ternary structures suggest the common theme in their signal transduction mechanisms. In fact, some PAS domains are interchangeable, as demonstrated by the recombinant receptor containing the LOV domain from *Bacillus subtilis* YtvA connected to the histidine kinase domain from *Bradyrhizobium japonicum* FixL. The resultant chimeric protein maintains the histidine kinase activity of FixL, and responds to blue light instead of oxygen [124].

High-resolution structural information of several PAS domains in the absence and presence of signals indicate small signal-induced conformational changes that are mostly concentrated in the cofactor binding sites of the β scaffold. Time-resolved crystallography of PYP from nano- to milliseconds demonstrates that the PYP-β core rearrangement following photon absorption and isomerization of 4-hydroxycinnamic acid chromophore. This conformational change propagates to the N-terminal cap, which locates opposite to the chromophore [125].

Similar to PYP, heme-binding PAS domains demonstrate ligand-induced conformational changes, which ultimately propagate to effector domains [77, 90, 96, 105, 126, 127]. The crystal structures of the PaAer2 PAS domain reveal the β-core rearrangement as Iβ Trp283 rotates and Hβ Leu 264 contracts following the binding of diatomic ligands to the heme. These changes lead to the displacement of the C-terminal DxT motif, which connects to the HAMP domain [77]. In EcDOS and FixL, bound O_2 is stabilized by Arg in the heme-binding pockets. O_2 binding leads to the rearrangement of the side chain of the Arg residue, as well as the Fα-Gβ loop [96, 105, 127].

Flavin-containing PAS domains employ common signal-induced structural changes through internal hydrogen-bond rearrangement in response to light or cellular redox states. The LOV2 domain of *Adiantum* phytochrome3 binds to the FMN cofactor by the hydrogen bond between the side chain of the Eβ Gln1029 and the N5 atom of FMN. Upon adduct formation in response to light, this hydrogen bond interaction is reoriented by the rotation of Gln1029 [119]. Similar signaling mechanisms have been observed in the redox sensor NifL from *Azotobacter vinelandii*, which contains an FAD-binding PAS domain [122, 128]. Prolonged illumination of AvNifL leads to changes in the position of the Glu70 side chain, which resides in the FAD cavity. The Glu70 side chain forms hydrogen bonds with the protonated N5 atom of FAD as well as the Ser39 side chain in the core β-sheet, thus initiating a signal that propagates to the β-sheet interface between the PAS monomers [122].

Signal propagation to effector domains

PAS domains are often linked to effector domains in larger proteins. Therefore, signals generated at PAS domains must be transduced to effector domains. In EcDOS, the signal propagation is expected to occur through the association/dissociation of the PAS and the effector domain [97]. The redox sensor EcDOS comprises of a tandem repeat of a heme-binding PAS-A and a heme-free PAS-B domain, and a C-terminal phosphodiesterase domain (PDE) that regulates cellular cAMP levels [96, 97, 129]. In the inactive state, the Fe(III) heme-bound PAS-A directly interacts with the PDE and inhibits catalysis. Structural changes of the PAS domain in response to O_2 binding (as mentioned above) lead to the dissociation of the Fe(II) PAS-A from the PDE domain, resulting in an active enzyme [97].

In chemotaxis systems mediated by Aer and Aer2, the signals initiated from the PAS domain are transmitted to the kinase control domain through the signal-transducer HAMP domain(s) [11, 130]. There are two proposed mechanisms for how the signals are propagated from PAS to HAMP domains: the direct-interaction and the in-line model [77, 131, 132]. Biochemical and mutational studies have shown that EcAer adopts the direct-interaction mechanism, where its FAD-binding PAS domain directly associate with the HAMP domain [11, 131, 132]. In the condition where the environmental O_2 concentration is insufficient to maintain the proper electron transfer rate in the electron transport system, the FAD cofactor of the EcAer PAS domain is reduced to the anionic semiquinone state [8], leading to the reorganization of the hydrogen-bond network and conformational changes of the PAS β-scaffold at the PAS-HAMP interface [131, 132]. These changes destabilize the PAS-HAMP

interaction and allow the HAMP domain to assume a more dynamic state. In contrast, the PAS FAD becomes oxidized in an aerobic condition, which results in a strengthened PAS-HAMP interaction and a more static HAMP domain [131, 132]. Unlike EcAer, PaAer2 utilizes the in-line mechanism. The diatomic ligand-induced structural changes of the β-scaffold leads to the reorientation of the C-terminal helix of the PaAer2 PAS, which connects and propagates the signal to the following HAMP domains [77].

As effector domains are highly diverse regardless of PAS structural uniformity, how signals initiated by structural changes to PAS domains are propagated to effector domains remains an active research topic. High-resolution structures of PAS-containing proteins in the absence and presence of signals will be valuable in elucidating PAS-signaling mechanisms.

REFERENCES

[1] Wadhams GH, Armitage JP. Making sense of it all: bacterial chemotaxis. Nat Rev Mol Cell Biol. 2004;5:1024-37.

[2] Bi S, Lai L. Bacterial chemoreceptors and chemoeffectors. Cell Mol Life Sci. 2015;72:691-708.

[3] Parkinson JS, Hazelbauer GL, Falke JJ. Signaling and sensory adaptation in Escherichia coli chemoreceptors: 2015 update. Trends in Microbiology. 2015;23:257-66.

[4] Studdert CA, Parkinson JS. Crosslinking snapshots of bacterial chemoreceptor squads. Proceedings Of The National Academy Of Sciences Of The United States Of America. 2004;101:2117-22.

[5] Hazelbauer GL, Falke JJ, Parkinson JS. Bacterial chemoreceptors: high-performance signaling in networked arrays. Trends In Biochemical Sciences. 2008;33:9-19.

[6] Hazelbauer GL, Lai WC. Bacterial chemoreceptors: providing enhanced features to two-component signaling. Current Opinion in Microbiology. 2010;13:124-32.

[7] Taylor BL, Zhulin IB, Johnson MS. Aerotaxis and other energy-sensing behavior in bacteria. Annual Review Of Microbiology. 1999;53:103-28.

[8] Repik A, Rebbapragada A, Johnson MS, Haznedar JO, Zhulin IB, Taylor BL. PAS domain residues involved in signal transduction by the Aer redox sensor of Escherichia coli. Molecular Microbiology. 2000;36:806-16.

[9] Ma QH, Roy F, Herrmann S, Taylor BL, Johnson MS. The Aer protein of Escherichia coli forms a homodimer independent of the signaling domain and flavin adenine dinucleotide binding. Journal Of Bacteriology. 2004;186:7456-9.

[10] Herrmann S, Ma QH, Johnson MS, Repik AV, Taylor BL. PAS domain of the Aer redox sensor requires C-terminal residues for native-fold formation and flavin adenine dinucleotide binding. Journal Of Bacteriology. 2004;186:6782-91.

[11] Taylor BL. Aer on the inside looking out: paradigm for a PAS-HAMP role in sensing oxygen, redox and energy. Molecular Microbiology. 2007;65:1415-24.

[12] Bibikov SI, Biran, R., Rudd, K.E., and Parkinson, J.S. A signal tranducer for aerotaxis in Escherichia coli. J Bacteriol. 1997;179:4075-9.

[13] Porter SL, Wadhams GH, Armitage JP. Signal processing in complex chemotaxis pathways. Nature Reviews Microbiology. 2011;9:153-65.

[14] Sourjik V, Wingreen NS. Responding to chemical gradients: bacterial chemotaxis. Current Opinion in Cell Biology. 2012;24:262-8.

[15] Berg HC, Tedesco PM. Transient response to chemotactic stimuli in Escherichia coli. Proc Natl Acad Sci U S A. 1975;72:3235-9.

[16] Springer MS, Goy MF, Adler J. Protein methylation in behavioural control mechanisms and in signal transduction. Nature. 1979;280:279-84.

[17] Stock JB, Koshland DE, Jr. A protein methylesterase involved in bacterial sensing. Proc Natl Acad Sci U S A. 1978;75:3659-63.

[18] Kehry MR, Dahlquist FW. Adaptation in bacterial chemotaxis: CheB-dependent modification permits additional methylations of sensory transducer proteins. Cell. 1982;29:761-72.

[19] Kehry MR, Doak TG, Dahlquist FW. Sensory adaptation in bacterial chemotaxis: regulation of demethylation. J Bacteriol. 1985;163:983-90.

[20] Milburn MV, Prive GG, Milligan DL, Scott WG, Yeh J, Jancarik J, et al. Three-dimensional structures of the ligand-binding domain of the bacterial aspartate receptor with and without a ligand. Science. 1991;254:1342-7.

[21] Yeh JI, Biemann HP, Prive GG, Pandit J, Koshland DE, Kim SH. High-resolution structures of the ligand binding domain of the wild-type bacterial aspartate receptor. Journal Of Molecular Biology. 1996;262:186-201.

[22] Chi YI, Yokota H, Kim SH. Apo structure of the ligand-binding domain of aspartate receptor from Escherichia coli and its comparison with ligand-bound or pseudoligand-bound structures. Febs Letters. 1997;414:327-32.

[23] Mise T. Structural Analysis of the Ligand-Binding Domain of the Aspartate Receptor Tar from Escherichia coli. Biochemistry. 2016;55:3708-13.

[24] Ames P, Hunter S, Parkinson JS. Evidence for a Helix-Clutch Mechanism of Transmembrane Signaling in a Bacterial Chemoreceptor. J Mol Biol. 2016.

[25] Kitanovic S, Ames P, Parkinson JS. Mutational Analysis of the Control Cable That Mediates Transmembrane Signaling in the Escherichia coli Serine Chemoreceptor. Journal of Bacteriology. 2011;193:5062-72.

[26] Miller ASaF, J.J. Side chains at the membrane-water interface modulate the signaling state of a transmembrane receptor. Biochemistry. 2004;43:1763-70.

[27] Draheim RR, Bormans AF, Lai RZ, Manson MD. Tryptophan residues flanking the second transmembrane helix (TM2) set the signaling state of the Tar chemoreceptor. Biochemistry. 2005;44:1268-77.

[28] Draheim RR, Bormans AF, Lai RZ, Manson MD. Tuning a bacterial chemoreceptor with protein-membrane interactions. Biochemistry. 2006;45:14655-64.

[29] Adase CA, Draheim RR, Manson MD. The Residue Composition of the Aromatic Anchor of the Second Transmembrane Helix Determines the Signaling Properties of the Aspartate/Maltose Chemoreceptor Tar of Escherichia coli. Biochemistry. 2012;51:1925-32.

[30] Adase CA, Draheim RR, Rueda G, Desai R, Manson MD. Residues at the Cytoplasmic End of Transmembrane Helix 2 Determine the Signal Output of the Tar(Ec) Chemoreceptor. Biochemistry. 2013;52:2729-38.

[31] Parkinson JS. Signaling Mechanisms of HAMP Domains in Chemoreceptors and Sensor Kinases. In: Gottesman S, Harwood CS, editors. Annual Review of Microbiology, Vol 64, 20102010. p. 101-22.

[32] Hulko M, Berndt F, Gruber M, Linder JU, Truffault V, Schultz A, et al. The HAMP domain structure implies helix rotation in transmembrane signaling. Cell. 2006;126:929-40.

[33] Swain KE, Falke JJ. Structure of the conserved HAMP domain in an intact, membrane-bound chemoreceptor: A disulfide mapping study. Biochemistry. 2007;46:13684-95.

[34] Airola MA, Watts KJ, Crane BR. Structure of concatenated HAMP domains provides a mechanism for signal transduction. Structure. 2010;18:436-48.

[35] Ferris HU, Zeth K, Hulko M, Dunin-Horkawicz S, Lupas AN. Axial helix rotation as a mechanism for signal regulation inferred from the crystallographic analysis of the E. coli serine chemoreceptor. J Struct Biol. 2014;186:349-56.

[36] Watts KJ, Johnson MS, Taylor BL. Different Conformations of the Kinase-On and Kinase-Off Signaling States in the Aer HAMP Domain. Journal of Bacteriology. 2011;193:4095-103.

[37] Wu J, Li J, Li G, Long DG, Weis RM. The receptor binding site for the methyltransferase of bacterial chemotaxis is distinct from the sites of methylation. Biochemistry. 1996;35:4984-93.

[38] Barnakov AN, Barnakova LA, Hazelbauer GL. Location of the receptor-interaction site on CheB, the methylesterase response regulator of bacterial chemotaxis. J Biol Chem. 2001;276:32984-9.

[39] Djordjevic S, Stock AM. Chemotaxis receptor recognition by protein methyltransferase CheR. Nat Struct Biol. 1998;5:446-50.

[40] Shiomi D, Zhulin IB, Homma M, Kawagishi I. Dual recognition of the bacterial chemoreceptor by chemotaxis-specific domains of the CheR methyltransferase. J Biol Chem. 2002;277:42325-33.

[41] Barnakov AN, Barnakova LA, Hazelbauer GL. Comparison in vitro of a high- and a low-abundance chemoreceptor of Escherichia coli: similar kinase activation but different methyl-accepting activities. J Bacteriol. 1998;180:6713-8.

[42] Kehry MR, Bond MW, Hunkapiller MW, Dahlquist FW. Enzymatic deamidation of methyl-accepting chemotaxis proteins in Escherichia coli catalyzed by the cheB gene product. Proc Natl Acad Sci U S A. 1983;80:3599-603.

[43] Sourjik V, Berg HC. Receptor sensitivity in bacterial chemotaxis. Proc Natl Acad Sci U S A. 2002;99:123-7.

[44] Dunten P, Koshland DE. TUNING THE RESPONSIVENESS OF A SENSORY RECEPTOR VIA COVALENT MODIFICATION. Journal of Biological Chemistry. 1991;266:1491-6.

[45] Bornhorst JA, Falke JJ. Evidence that both ligand binding and covalent adaptation drive a two-state equilibrium in the aspartate receptor signaling complex. Journal Of General Physiology. 2001;118:693-710.

[46] Han XS, Parkinson JS. An Unorthodox Sensory Adaptation Site in the Escherichia coli Serine Chemoreceptor. Journal of Bacteriology. 2014;196:641-9.

[47] Chervitz SA, Falke JJ. Molecular mechanism of transmembrane signaling by the aspartate receptor: a model. Proc Natl Acad Sci U S A. 1996;93:2545-50.

[48] Matamouros S, Hager KR, Miller SI. HAMP Domain Rotation and Tilting Movements Associated with Signal Transduction in the PhoQ Sensor Kinase. MBio. 2015;6:e00616-15.

[49] Dutta R, Qin L, Inouye M. Histidine kinases: diversity of domain organization. Mol Microbiol. 1999;34:633-40.

[50] Molnar KS, Bonomi M, Pellarin R, Clinthorne GD, Gonzalez G, Goldberg SD, et al. Cys-scanning disulfide crosslinking and bayesian modeling probe the transmembrane signaling mechanism of the histidine kinase, PhoQ. Structure. 2014;22:1239-51.

[51] Yu D, Ma X, Tu Y, Lai L. Both piston-like and rotational motions are present in bacterial chemoreceptor signaling. Sci Rep. 2015;5:8640.

[52] Moukhametzianov R, Klare JP, Efremov R, Baeken C, Goppner A, Labahn J, et al. Development of the signal in sensory rhodopsin and its transfer to the cognate transducer. Nature. 2006;440:115-9.

[53] Wegener AA, Klare JP, Engelhard M, Steinhoff HJ. Structural insights into the early steps of receptor-transducer signal transfer in archaeal phototaxis. EMBO J. 2001;20:5312-9.

[54] Inoue K, Sasaki J, Spudich JL, Terazima M. Signal transmission through the HtrII transducer alters the interaction of two alpha-helices in the HAMP domain. J Mol Biol. 2008;376:963-70.

[55] Wang J, Sasaki J, Tsai AL, Spudich JL. HAMP domain signal relay mechanism in a sensory rhodopsin-transducer complex. J Biol Chem. 2012;287:21316-25.

[56] Gordeliy VI, Labahn J, Moukhametzianov R, Efremov R, Granzin J, Schlesinger R, et al. Molecular basis of transmembrane signalling by sensory rhodopsin II-transducer complex. Nature. 2002;419:484-7.

[57] Ferris HU, Dunin-Horkawicz S, Mondejar LG, Hulko M, Hantke K, Martin J, et al. The Mechanisms of HAMP-Mediated Signaling in Transmembrane Receptors. Structure. 2011;19:378-85.

[58] Swain KE, Gonzalez MA, Falke JJ. Engineered Socket Study of Signaling through a Four-Helix Bundle: Evidence for a Yin-Yang Mechanism in the Kinase Control Module of the Aspartate Receptor. Biochemistry. 2009;48:9266-77.

[59] Airola MV, Sukomon N, Samanta D, Borbat PP, Freed JH, Watts KJ, et al. HAMP domain conformers that propagate opposite signals in bacterial chemoreceptors. PLoS Biol. 2013;11:e1001479.

[60] Ames P, Zhou Q, Parkinson JS. HAMP domain structural determinants for signalling and sensory adaptation in Tsr, the Escherichia coli serine chemoreceptor. Molecular Microbiology. 2014;91:875-86.

[61] Zhou Q, Ames P, Parkinson JS. Biphasic control logic of HAMP domain signalling in the Escherichia coli serine chemoreceptor. Molecular Microbiology. 2011;80:596-611.

[62] Lai R-Z, Parkinson JS. Functional Suppression of HAMP Domain Signaling Defects in the E. coli Serine Chemoreceptor. Journal of Molecular Biology. 2014;426:3642-55.

[63] Zhou Q, Ames P, Parkinson JS. Mutational analyses of HAMP helices suggest a dynamic bundle model of input-output signalling in chemoreceptors. Molecular Microbiology. 2009;73:801-14.

[64] Samanta D, Borbat PP, Dzikovski B, Freed JH, Crane BR. Bacterial chemoreceptor dynamics correlate with activity state and are coupled over long distances. Proceedings of the National Academy of Sciences of the United States of America. 2015;112:2455-60.

[65] Piasta KN, Ulliman CJ, Slivka PF, Crane BR, Falke JJ. Defining a Key Receptor-CheA Kinase Contact and Elucidating Its Function in the Membrane-Bound Bacterial Chemosensory Array: A Disulfide Mapping and TAM-IDS Study. Biochemistry. 2013;52:3866-80.

[66] Pedetta A, Parkinson JS, Studdert CA. Signalling-dependent interactions between the kinase-coupling protein CheW and chemoreceptors in living cells. Molecular Microbiology. 2014;93:1144-55.

[67] Mowery P, Ostler JB, Parkinson JS. Different Signaling Roles of Two Conserved Residues in the Cytoplasmic Hairpin Tip of Tsr, the Escherichia coli Serine Chemoreceptor. Journal of Bacteriology. 2008;190:8065-74.

[68] Ortega DR, Yang C, Ames P, Baudry J, Parkinson JS, Zhulin IB. A phenylalanine rotameric switch for signal-state control in bacterial chemoreceptors. Nature Communications. 2013;4.

[69] Letunic I, Doerks T, Bork P. SMART 7: recent updates to the protein domain annotation resource. Nucleic Acids Res. 2012;40:D302-5.

[70] Aravind L, Galperin MY, Koonin EV. The catalytic domain of the P-type ATPase has the haloacid dehalogenase fold. Trends Biochem Sci. 1998;23:127-9.

[71] Dunin-Horkawicz S, Lupas AN. Comprehensive Analysis of HAMP Domains: Implications for Transmembrane Signal Transduction. Journal of Molecular Biology. 2010;397:1156-74.

[72] Ames P, Zhou Q, Parkinson JS. Mutational analysis of the connector segment in the HAMP domain of Tsr, the Escherichia coli serine chemoreceptor. Journal Of Bacteriology. 2008;190:6676-85.

[73] Watts KJ, Johnson MS, Taylor BL. Structure-function relationships in the HAMP and proximal signaling domains of the aerotaxis receptor Aer. J Bacteriol. 2008;190:2118-27.

[74] Kitanovic S, Ames P, Parkinson JS. A Trigger Residue for Transmembrane Signaling in the Escherichia coli Serine Chemoreceptor. Journal of Bacteriology. 2015;197:2568-79.

[75] Bhate MP, Molnar KS, Goulian M, DeGrado WF. Signal transduction in histidine kinases: insights from new structures. Structure. 2015;23:981-94.

[76] Ferris HU, Dunin-Horkawicz S, Hornig N, Hulko M, Martin J, Schultz JE, et al. Mechanism of Regulation of Receptor Histidine Kinases. Structure. 2012;20:56-66.

[77] Airola MV, Huh D, Sukomon N, Widom J, Sircar R, Borbat PP, et al. Architecture of the Soluble Receptor Aer2 Indicates an In-Line Mechanism for PAS and HAMP Domain Signaling. Journal of Molecular Biology. 2013;425:886-901.

[78] Huang ZJ, Edery I, Rosbash M. PAS is a dimerization domain common to Drosophila period and several transcription factors. Nature. 1993;364:259-62.

[79] Nambu JR, Lewis JO, Wharton KA, Jr., Crews ST. The Drosophila single-minded gene encodes a helix-loop-helix protein that acts as a master regulator of CNS midline development. Cell. 1991;67:1157-67.

[80] Hoffman EC, Reyes H, Chu FF, Sander F, Conley LH, Brooks BA, et al. Cloning of a factor required for activity of the Ah (dioxin) receptor. Science. 1991;252:954-8.

[81] Henry JT, Crosson S. Ligand-binding PAS domains in a genomic, cellular, and structural context. Annu Rev Microbiol. 2011;65:261-86.

[82] Moglich A, Ayers RA, Moffat K. Structure and signaling mechanism of Per-ARNT-Sim domains. Structure. 2009;17:1282-94.

[83] Schultz J, Milpetz F, Bork P, Ponting CP. SMART, a simple modular architecture research tool: identification of signaling domains. Proc Natl Acad Sci U S A. 1998;95:5857-64.

[84] Taylor BL, Zhulin IB. PAS domains: internal sensors of oxygen, redox potential, and light. Microbiol Mol Biol Rev. 1999;63:479-506.

[85] Finn RD, Mistry J, Tate J, Coggill P, Heger A, Pollington JE, et al. The Pfam protein families database. Nucleic Acids Res. 2010;38:D211-22.

[86] Finn RD, Mistry J, Schuster-Bockler B, Griffiths-Jones S, Hollich V, Lassmann T, et al. Pfam: clans, web tools and services. Nucleic Acids Res. 2006;34:D247-51.

[87] Borgstahl GE, Williams DR, Getzoff ED. 1.4 A structure of photoactive yellow protein, a cytosolic photoreceptor: unusual fold, active site, and chromophore. Biochemistry. 1995;34:6278-87.

[88] Hefti MH, Francoijs KJ, de Vries SC, Dixon R, Vervoort J. The PAS fold. A redefinition of the PAS domain based upon structural prediction. Eur J Biochem. 2004;271:1198-208.

[89] Watts KJ, Sommer K, Fry SL, Johnson MS, Taylor BL. Function of the N-terminal cap of the PAS domain in signaling by the aerotaxis receptor Aer. Journal Of Bacteriology. 2006;188:2154-62.

[90] Sawai H, Sugimoto H, Shiro Y, Ishikawa H., Y. M, S. A. Structural basis for oxygen sensing and signal transduction of the heme-based sensor protein Aer1 from Psuedomonas aeruginosa. Chem Commun. 2012;48:6523-65.

[91] Hao N, Whitelaw ML, Shearwin KE, Dodd IB, Chapman-Smith A. Identification of residues in the N-terminal PAS domains important for dimerization of Arnt and AhR. Nucleic Acids Res. 2011;39:3695-709.

[92] Ke Y, Hunter MJ, Ng CA, Perry MD, Vandenberg JI. Role of the cytoplasmic N-terminal Cap and Per-Arnt-Sim (PAS) domain in trafficking and stabilization of Kv11.1 channels. J Biol Chem. 2014;289:13782-91.

[93] Ke Y, Ng CA, Hunter MJ, Mann SA, Heide J, Hill AP, et al. Trafficking defects in PAS domain mutant Kv11.1 channels: roles of reduced domain stability and altered domain-domain interactions. Biochem J. 2013;454:69-77.

[94] Ayers RA, Moffat K. Changes in quaternary structure in the signaling mechanisms of PAS domains. Biochemistry. 2008;47:12078-86.

[95] Ma XL, Sayed N, Baskaran P, Beuve A, van den Akker F. PAS-mediated dimerization of soluble guanylyl cyclase revealed by signal transduction histidine kinase domain crystal structure. Journal of Biological Chemistry. 2008;283:1167-78.

[96] Kurokawa H, Lee DS, Watanabe M, Sagami I, Mikami B, Raman CS, et al. A redox-controlled molecular switch revealed by the crystal structure of a bacterial heme PAS sensor. J Biol Chem. 2004;279:20186-93.

[97] Sasakura Y, Yoshimura-Suzuki T, Kurokawa H, Shimizu T. Structure-function relationships of EcDOS, a heme-regulated phosphodiesterase from Escherichia coli. Acc Chem Res. 2006;39:37-43.

[98] Key J, Hefti M, Purcell EB, Moffat K. Structure of the redox sensor domain of Azotobacter vinelandii NifL at atomic resolution: signaling, dimerization, and mechanism. Biochemistry. 2007;46:3614-23.

[99] Sevvana M, Vijayan V, Zweckstetter M, Reinelt S, Madden DR, Herbst-Irmer R, et al. A ligand-induced switch in the periplasmic domain of sensor histidine kinase CitA. J Mol Biol. 2008;377:512-23.

[100] Miyatake H, Mukai M, Park SY, Adachi S, Tamura K, Nakamura H, et al. Sensory mechanism of oxygen sensor FixL from Rhizobium meliloti: crystallographic, mutagenesis and resonance Raman spectroscopic studies. J Mol Biol. 2000;301:415-31.

[101] Fedorov R, Schlichting I, Hartmann E, Domratcheva T, Fuhrmann M, Hegemann P. Crystal structures and molecular mechanism of a light-induced signaling

switch: The Phot-LOV1 domain from Chlamydomonas reinhardtii. Biophys J. 2003;84:2474-82.

[102] Nakasako M, Zikihara K, Matsuoka D, Katsura H, Tokutomi S. Structural basis of the LOV1 dimerization of Arabidopsis phototropins 1 and 2. J Mol Biol. 2008;381:718-33.

[103] Erbel PJA, Card PB, Karakuzu O, Bruick RK, Gardner KH. Structural basis for PAS domain heterodimerization in the basic helix-loop-helix-PAS transcription factor hypoxia-inducible factor. Proceedings of the National Academy of Sciences of the United States of America. 2003;100:15504-9.

[104] Card PB, Erbel PJA, Gardner KH. Structural basis of ARNT PAS-B dimerization: Use of a common beta-sheet interface for hetero- and homodimerization. Journal of Molecular Biology. 2005;353:664-77.

[105] Hao B, Isaza C, Arndt J, Soltis M, Chan MK. Structure-based mechanism of O2 sensing and ligand discrimination by the FixL heme domain of Bradyrhizobium japonicum. Biochemistry. 2002;41:12952-8.

[106] Lee J, Tomchick DR, Brautigam CA, Machius M, Kort R, Hellingwerf KJ, et al. Changes at the KinA PAS-A dimerization interface influence histidine kinase function. Biochemistry. 2008;47:4051-64.

[107] Pongratz I, Antonsson C, Whitelaw ML, Poellinger L. Role of the PAS domain in regulation of dimerization and DNA binding specificity of the dioxin receptor. Mol Cell Biol. 1998;18:4079-88.

[108] Wu D, Potluri N, Kim Y, Rastinejad F. Structure and dimerization properties of the aryl hydrocarbon receptor PAS-A domain. Mol Cell Biol. 2013;33:4346-56.

[109] Zelzer E, Wappner P, Shilo BZ. The PAS domain confers target gene specificity of Drosophila bHLH/PAS proteins. Genes Dev. 1997;11:2079-89.

[110] Kewley RJ, Whitelaw ML, Chapman-Smith A. The mammalian basic helix-loop-helix/PAS family of transcriptional regulators. Int J Biochem Cell Biol. 2004;36:189-204.

[111] Rey FE, Harwood CS. FixK, a global regulator of microaerobic growth, controls photosynthesis in Rhodopseudomonas palustris. Mol Microbiol. 2010;75:1007-20.

[112] Delgado-Nixon VM, Gonzalez G, Gilles-Gonzalez MA. Dos, a heme-binding PAS protein from Escherichia coli, is a direct oxygen sensor. Biochemistry. 2000;39:2685-91.

[113] Londer YY, Dementieva IS, D'Ausilio CA, Pokkuluri PR, Schiffer M. Characterization of a c-type heme-containing PAS sensor domain from Geobacter

sulfurreducens representing a novel family of periplasmic sensors in Geobacteraceae and other bacteria. FEMS Microbiol Lett. 2006;258:173-81.

[114] Pokkuluri PR, Pessanha M, Londer YY, Wood SJ, Duke NE, Wilton R, et al. Structures and solution properties of two novel periplasmic sensor domains with c-type heme from chemotaxis proteins of Geobacter sulfurreducens: implications for signal transduction. J Mol Biol. 2008;377:1498-517.

[115] Krauss U, Minh BQ, Losi A, Gartner W, Eggert T, von Haeseler A, et al. Distribution and phylogeny of light-oxygen-voltage-blue-light-signaling proteins in the three kingdoms of life. J Bacteriol. 2009;191:7234-42.

[116] Briggs WR, Christie JM, Salomon M. Phototropins: A new family of flavin-binding blue light receptors in plants. Antioxidants & Redox Signaling. 2001;3:775-88.

[117] Christie JM, Reymond P, Powell GK, Bernasconi P, Raibekas AA, Liscum E, et al. Arabidopsis NPH1: a flavoprotein with the properties of a photoreceptor for phototropism. Science. 1998;282:1698-701.

[118] Crosson S, Rajagopal S, Moffat K. The LOV domain family: Photoresponsive signaling modules coupled to diverse output domains. Biochemistry. 2003;42:2-10.

[119] Crosson S, Moffat K. Photoexcited structure of a plant photoreceptor domain reveals a light-driven molecular switch. Plant Cell. 2002;14:1067-75.

[120] Glantz ST, Carpenter EJ, Melkonian M, Gardner KH, Boyden ES, Wong GK, et al. Functional and topological diversity of LOV domain photoreceptors. Proc Natl Acad Sci U S A. 2016;113:E1442-51.

[121] Herrou J, Crosson S. Function, structure and mechanism of bacterial photosensory LOV proteins. Nat Rev Microbiol. 2011;9:713-23.

[122] Key J, Hefti M, Purcell EB, Moffat K. Structure of the redox sensor domain of Azotobacter vinelandii NifL at atomic resolution: Signaling, dimerization, and mechanism. Biochemistry. 2007;46:3614-23.

[123] Bibikov SI, Barnes LA, Gitin Y, Parkinson JS. Domain organization and flavin adenine dinucleotide-binding determinants in the aerotaxis signal transducer Aer of Escherichia coli. Proc Natl Acad Sci U S A. 2000;97:5830-5.

[124] Moglich A, Ayers RA, Moffat K. Design and signaling mechanism of light-regulated histidine kinases. J Mol Biol. 2009;385:1433-44.

[125] Tenboer J, Basu S, Zatsepin N, Pande K, Milathianaki D, Frank M, et al. Time-resolved serial crystallography captures high-resolution intermediates of photoactive yellow protein. Science. 2014;346:1242-6.

[126] Key J, Moffat K. Crystal structures of deoxy and CO-bound bjFixLH reveal details of ligand recognition and signaling. Biochemistry. 2005;44:4627-35.

[127] Park H, Suquet C, Satterlee JD, Kang C. Insights into signal transduction involving PAS domain oxygen-sensing heme proteins from the X-ray crystal structure of Escherichia coli Dos heme domain (Ec DosH). Biochemistry. 2004;43:2738-46.

[128] Woodley P, Drummond M. Redundancy of the conserved His residue in Azotobacter vinelandii NifL, a histidine autokinase homologue which regulates transcription of nitrogen fixation genes. Mol Microbiol. 1994;13:619-26.

[129] Yoshimura-Suzuki T, Sagami I, Yokota N, Kurokawa H, Shimizu T. DOS(Ec), a heme-regulated phosphodiesterase, plays an important role in the regulation of the cyclic AMP level in Escherichia coli. J Bacteriol. 2005;187:6678-82.

[130] Watts KJ, Taylor BL, Johnson MS. PAS/poly-HAMP signalling in Aer-2, a soluble haem-based sensor. Molecular Microbiology. 2011;79:686-99.

[131] Garcia D, Watts KJ, Johnson MS, Taylor BL. Delineating PAS-HAMP interaction surfaces and signalling-associated changes in the aerotaxis receptor Aer. Mol Microbiol. 2016;100:156-72.

[132] Campbell AJ, Watts KJ, Johnson MS, Taylor BL. Gain-of-function mutations cluster in distinct regions associated with the signalling pathway in the PAS domain of the aerotaxis receptor, Aer. Molecular Microbiology. 2010;77:575-86.

CHAPTER 2

Stability and conformation of the HAMP domain from the chemoreceptor Tsr within a poly-HAMP chimera

2.1 Abstract

HAMP domains are dimeric, all-parallel 4-helix bundles that transduce conformational signals in bacterial receptors. Extensive genetic studies of the *E. coli* serine receptor (Tsr) have provided an opportunity to understand HAMP conformational behavior in terms of functional output. To stabilize the Tsr HAMP for biophysical investigations, the domain was spliced into a poly-HAMP unit from the *P. aeruginosa* Aer2 receptor. Within the chimera, the Tsr HAMP maintains its α-helical, 4-helix coiled-coil structure but undergoes a thermal melting transition at a temperature much lower than that of the Aer2 HAMP domains. Pulse-dipolar ESR spectroscopy (PDS) and site-specific spin labeling reveal that the N-terminal AS1 helices of the Tsr HAMP are conformationally variable and spread out toward their C-termini, whereas the C-terminal AS2 helices are more stable and relatively straight. PDS was also used to study three well-characterized HAMP mutational phenotypes: those that cause flagellar rotation that is counterclockwise (CCW(A)) and kinase-off; CCW(B) and also kinase-off, and, clockwise (CW) and kinase-on. The behaviors of the three HAMP variants support the biphasic model of dynamic bundle stability. Functional kinase-on (CW) and kinase-off (CCW(A) states are also distinguished by concerted changes in the positions of spin-label sites at the base of the bundle.

Opposite changes in the subunit separation distances of neighboring residues at the C termini of the AS1 and AS2 helices are consistent with either a scissors motion of the helices or a "gearbox" rotational model of HAMP activation. In the drastic kinase-off lesion of CCW(B) the AS1 helices unfold and the AS2 helices form a tight 2-helix coiled-coil. The substitution of a critical residue in the Tsr N-terminal linker or "control cable" reduces conformational heterogeneity at the N-terminus of AS1 but does not affect structure at the C-terminus of AS2. Overall, the data suggest that transitions from on to off states involve decreased dynamics of the Tsr HAMP coupled with helix rotations and movements toward a more 2-helix packing mode.

2.2 Introduction

Bacteria employ transmembrane receptors to sense and respond to their changing environment [1-3]. Essential components of these receptors are so called "HAMP" domains (for Histidine Kinase, Adenylate Cyclase and Methyl-accepting Chemotaxis Proteins (MCP) and some Phophatases) [4-7]. Found in over 26,000 receptors [8], they often lie proximal to the cytoplasmic leaflet of the membrane and act to couple extracellular signals to intracellular responses [9].

The HAMP domain as a small, homodimeric protein with ~50 residues in each subunit [9, 10]. HAMP structures are parallel four-helix bundles with each subunit supplying two α helices (AS1 and AS2) that each contain typical heptad sequence repeats reflecting internal hydrophobic packing and the helix periodicity (residue positions, a-g, where a, d, and to a lesser extent e, and g are held by hydrophobic residues) [10, 11]. A non-helical linker (CTR) connects the AS1 and AS2 helices and

contains two conserved hydrophobic residues (HR1 and HR2) that are important for stability and function [9, 12, 13]. Subsequent biochemical and structural studies of HAMP domains in both MCPs and histidine kinases show high conservation of these general properties [14-16]. However, among the known structures, HAMP domains display a range of conformations that differ in terms of helix rotation, translation, and crossing angles [10, 12, 17-21].

HAMP domains have been extensively studied in the context of MCPs, which regulate chemotaxis in eubacteria and archaea [2, 22]. MCPs are modular receptors comprising a ligand-sensing domain, a transmembrane domain, HAMP domain(s), and a kinase control module (KCM) [23, 24]. In general, the periplasmic ligand-binding domain monitors chemoeffector levels, and the KCM interacts with the histidine kinase CheA and the adaptor protein CheW CheA transfers phosphoryl groups from ATP to the response regulator CheY depending on the ligand occupancy of the receptor. Phosphorylated CheY (CheY-P) interacts directly with the flagellar motor to change the rotational bias from counterclockwise (CCW) to clockwise (CW) [23-25]. In *E coli*, CheA is activated when attractants dissociate or repellants bind (kinase-on). These effects cause higher levels of CheY-P, clockwise (CW) rotation and cell tumbling. Attractant binding, or repellant dissociation deactivates CheA (kinase-off) and lowers the level of CheY-P, which causes counterclockwise (CCW) rotation and straight swimming [23-25]. In MCPs, the effects of ligand binding are countered by covalent modification through the activities of the CheR methyl transferase and CheB methyl-esterase, which together provide a feedback system that adapts receptor output to current conditions. CheR methylates conserved Glu residues to shift the receptors

toward kinase-on states. Methylation can be generally mimicked by Glu to Gln substitutions [24, 26, 27]. Functional studies of *E. coli* serine receptor (Tsr) have shown that the HAMP domain is critical for switching CheA activity states upon receptor stimulation [9, 24, 27-29].

Several models have been purposed to elucidate how conformational signals propagate through HAMP domains. These models range from those that emphasize more static two-state behavior to those that emphasize the dynamics (stabilities) of on- and off- conformations [9, 21]. The two-state models focus on discrete kinase-on and kinase-off states, which invoke the opposite physiological outputs. A well-known example is the gearbox model, which arose from the discovery of an unusual x-da hydrophobic packing arrangement of the Af1503 helical heptad repeat positions (a-g) and the subsequent study of a key residue A291 in AS1 of Af1503 [10, 17, 30, 31]. Increase in the volume of this core residue promotes HAMP packing to switch from the complementary x-da packing mode to the more conventional, knobs-into-hole (a-d) arrangement [17]. The packing change is proposed to induce a gearbox-type counter rotation of the AS1 and AS2 helices [10, 17, 30, 31]. Another proposal for a two-state conformational switching involves scissor-type motions of the AS1 and AS2 helices that explain changes in cross-linking of cysteines engineered into the *E. coli* aspartate receptor Tar [18]. Notably, rotational and scissor motions of helices are not necessarily mutually exclusive.

The functional characterization of Tsr HAMP has led to the biphasic dynamic bundle model of HAMP stability that well explains the behavior of a large number of Tsr mutant receptors [27-29, 32]. This model proposes that HAMP domains operate in

regimes of conformational dynamics. The signaling outputs correspond to the ensembles of HAMP structures with similar stabilities rather than discrete conformations. HAMP domains at both dynamic extremes (highly unstable and highly stable) promote the kinase-off state. Of these, the more stable state [CCW(A)] is most likely the functional off configuration, as the highly unstable form [CCW(B)] results from lesions that distort the domain outside of its physiological range. HAMP bundles with stabilities intermediate to these two extremes cause the kinase-on (CW) output. Over the physiological regime then, the kinase-on states have HAMP domains that are more dynamic than those of the kinase-off states [27, 28, 32, 33].

Structural and biochemical studies of the concatenated HAMP domains from *P. aeruginosa* Aer2 support an intermediate view [12, 33]. The Aer2 poly-HAMP structure contains three N-terminal HAMP domains, of which two (HAMP1 and HAMP3) have similar conformations, whereas a second (HAMP2), is quite different [12]. The HAMP1/3 and HAMP2 structures were distinguished by complex differences in helical register, rotation, and tilting, which include a rotation at the end of AS2 [12, 33]. In vitro and in vivo experiments showed that when the HAMP1 and HAMP2 conformers are fused to the Tar KCMs, they elicit opposite effects on kinase activities and cell swimming responses [34]. The two conformers and their functional consequences are convertible by mutation of conserved hydrophobic residue HR2, which plays an important role in stabilizing the HAMP2 conformer. Nonetheless, pulse-ESR experiments of spin-labeled proteins also indicate that the HAMP1 and HAMP2 conformers have very different dynamic properties, with the HAMP1 kinase-

on form much more dynamic than the HAMP2 kinase-off form, as predicted by the dynamic bundle model [12, 33].

HAMP domains from other classes of bacterial transmembrane receptors, including sensor histidine kinases and sensory rhodopsin transducers also suggest a range of activation mechanisms [9, 16, 35]. For example, cysteine cross-linking analyses on variants of PhoQ, a sensor histidine kinase in *Salmonella enterica*, indicate a change from a-d to x-da helix packing in the HAMP domain along with a tilt of the AS1 helices [16, 36]. Helix tilt angles do vary among known HAMP structures with tilts of AS1 compensated by opposite tilts of AS2 [21]. In contrast, studies of the sensory rhodopsin transducer HtrII indicate that signal propagation is associated with helix displacements along the long axis (piston motions) and again there are compensating shifts between AS1 and AS2 [37, 38]. Computational studies of isolated HAMP domains emphasize such piston motions over rotations, but the simulated HAMP domains are not coupled to input and output modules that may otherwise dampen such motions [39, 40]. In line with the dynamic bundle model, several other studies have also suggested changes in HAMP dynamics, compactness, and folding upon activation, but the signs of the changes do not always correlate among different systems [9, 37, 41, 42]. While signal transduction by different HAMP domains need not involve the same conformational transitions, the conservation of residues involved in interactions among AS1, and AS2, at the dimer interface and involving the connector, hint at some commonality of mechanism.

Despite the rich genetic and functional data available for the Tsr HAMP, there is limited structural and biophysical data on this system due to the instability of the

isolated domain, and the difficulty in producing the functional intact membrane protein for biophysical studies. The effects of the residue substitutions on domain stability have mainly been inferred from the likely consequences of similar substitutions on known HAMP structures [13, 28, 29]. In order to provide access to structural and biophysical studies of Tsr HAMP, we created a chimeric protein containing Tsr HAMP spliced into the poly-HAMP domains from *P. aeruginosa* Aer2. This work reports its initial characterization. Furthermore, we demonstrate that residue substitutions in the Tsr HAMP domain indeed alter its stability as suggested by the bistability model. However, changes in stability are also accompanied by conformational changes consistent with helical rotations. Additionally, we show that the substitution of a critical residue in the so-called Tsr "control cable" that joins HAMP to the transmembrane helices produces complex effects, but in this system does not appear to alter structure near the C-terminal output of AS2. Although we investigate the Tsr HAMP outside of its normal environment, our findings do demonstrate how single residue substitutions can affect HAMP structure, dynamics and stability and thus provide a general rationale for the types of changes expected by HAMP mutational alternations. Moreover, the properties of the variants correlate reasonably well with prevailing models.

2.3 Materials and methods

Cloning and Mutation

The coding region for the Tsr HAMP domain (residues 212 – 264) was PCR-amplified from *E. coli* genomic DNA. The coding region for the Aer2 poly-HAMP

(residues 1-172) was previously cloned in pET28a [12]. The chimeric Tsr-Aer2H1-3 was cloned into pET28a by the following steps. First, the Tsr HAMP coding region was fused upstream of the Aer2 linker-Aer2H2-3 coding region (residues 57-172) using PCR overlap extension. Then, the Aer2H1-Aer2 linker coding region (residues 1-62) was introduced upstream of the former construct by also using overlap extension, resulting in a chimeric Tsr-Aer2H1-3 construct that contains the Tsr HAMP domain (residue 216-264) embedded between Aer2H1 and Aer2H2-3 with the Aer2 H1-H2 linker sequence repeated at both ends of the Tsr HAMP. During this step, the primers for overlap extension were designed to generate two sets of substitutions. In the first, silent mutations were introduced at the E61 and L62 positions in the first Aer2H1-2 linker to create more unique restriction sites. In the second, the Aer2 residue 1-4 (Met Gly Leu Phe), which is located before the N-terminus of the Aer2 H1, was modified to His Met Ala Ser to aid expression and stability. Point mutations of the recombinant HAMP domains were introduced by using either the QuikChange PCR protocol (Agilent Technologies) or overlap extension methodology [43].

Expression and Purification of Proteins

All of the proteins were expressed in *E. coli* BL21(DE3) under 0.4 mM isopropyl β-D-1-thiogalactopyranoside (IPTG) induction at 4°C for 16 hours. The proteins were purified by Ni-NTA affinity chromatography under the manufacturers protocols. After overnight digestion with thrombin (0.7 μg/ml), the tag-free proteins were subjected to a Superdex 75 26-60 size exclusion column and eluted in 10 mM Tris (pH 8.0), 150 mM NaCl, and 10% (vol/vol) glycerol.

Circular Dichroism Spectroscopy

Circular dichroism experiments on the recombinant HAMP domains were carried out with a AVIV Biomedical (model 202-01) spectropolarimeter. The proteins were prepared at a concentration of 10 μM (250 mg/ml) in 10 mM sodium phosphate buffer (pH 7.5), 150 mM NaCl, and 10% (vol/vol) glycerol. The α-helical property of the proteins was confirmed using wavelength scan experiments at 4°C. For the temperature scan experiments, the protein samples were heated at the rate of 1°C per minute, and allowed to reach equilibrium for 1 minute. The degree ellipticity was then measured as an average over 1 minute.

Site-directed Spin Labeling

Cysteine was substituted for selected residues in the recombinant HAMP domain with QuikChange mutagenesis or overlap extension. Cysteine-substituted molecules were over expressed with an N-terminal His-6 tag. Then, the His-tagged proteins were purified using a Ni-NTA affinity column. The purified proteins were reacted with cysteine-specific nitroxide S-(1-oxyl-2,2,5,5-tetramethyl-2,5-dihydro-1H-pyrrol-3-yl)methyl methanesulfonothioate spin label (MTSL) (Toronto Research Chemicals Inc.) on column for 4 hours at room temperature, and subsequently at 4°C for 8 hours. The proteins were eluted with 20 mM Tris (pH 8.0), 250 mM imidazole (pH 8.0), 500 mM NaCl, and 10% (vol/vol) glycerol. The samples were subjected to size-exclusion chromatography (Superdex 75 26-60) for further purification and removal of unreacted MTSL.

PDS Measurements

The spin-labeled samples (100 μM) were prepared in 10 mM Tris (pH 8.0), 150 mM NaCl, and 35% (vol/vol) glycerol. The distance distributions between the two spins were detected with double electron-electron resonance (DEER) on a home-built 2D Fourier-transform-ESR instrument [44-46]. The dipolar evolution was measured at 17.35 GHz with four-pulse double-electron electron resonance with a 16-ns π-pump pulse centered on the nitroxide spectrum in a 16/32/32-ns pulse sequence. The PDS signals were analyzed after correcting the baseline of the time domain data with a log-linear polynomial function. Subsequently, the DEER signals were converted to distance distributions with Tikhonov regularization, and further refined by maximum entropy refinement [44, 47, 48].

2.4 Results

Expression of a Tsr HAMP within the Aer2 poly-HAMP

The Tsr HAMP domain was expressed with the *P. aeruginosa* Aer2 poly-HAMP 1-2-3 domains in the context of a chimeric protein (Aer2H1-3; Figure 2-1). Fusion points were chosen by aligning the respective HAMP sequences. The Tsr sequence A216-M264 was inserted at residue 62 of Aer2, after a helical linker following Aer2 HAMP1. This linker (residues 57-62 of Aer2) was then repeated at the C-terminus of Tsr to provide some spacing and flexibility for the connection to the HAMP2 domain of Aer2 (Figure 2-1). The circular dichroism (CD) spectrum of the chimeric poly-HAMP protein (Tsr-Aer2H1-3) showed typical α-helical structure, with roughly 3/4 the helical signal of the parent Aer2H1-3 (Figure 2-2A). Aer2H1-3

thermally unfolded with a single transition of Tm = 53 °C ([33] and Figure 2-2B). In contrast, Tsr-Aer2H1-3 unfolds in two stages with a lower transition temperature of 26°C in addition to a higher temperature of 57°C. The lower temperature transition accounts for roughly 1/4 of the helical content loss (Figure 2-2B) and we assign it to the Tsr HAMP domain, which, as expected, would be very unstable if expressed separately. Fusion into Aer2H1-3 appears to protect the domain from aggregation and allows it to assume helical structure at low temperature. We note that the melting curves of the HAMP chimeras and their variants (discussed below) are at best only partially reversible. This behavior may relate to the dissociation of subunits that accompanies unfolding. Thus, although thermodynamic quantities cannot be derived from the melting curves, the curves can report on the relative helical stabilities of different variants. Comparative measurements were taken with the same concentrations of proteins to limit subunit dissociation effects on the Tm values. Fortunately, as shown below, substantial changes in the melting curve behavior of the HAMP variants support general inferences about the consequences of the amino-acid replacements.

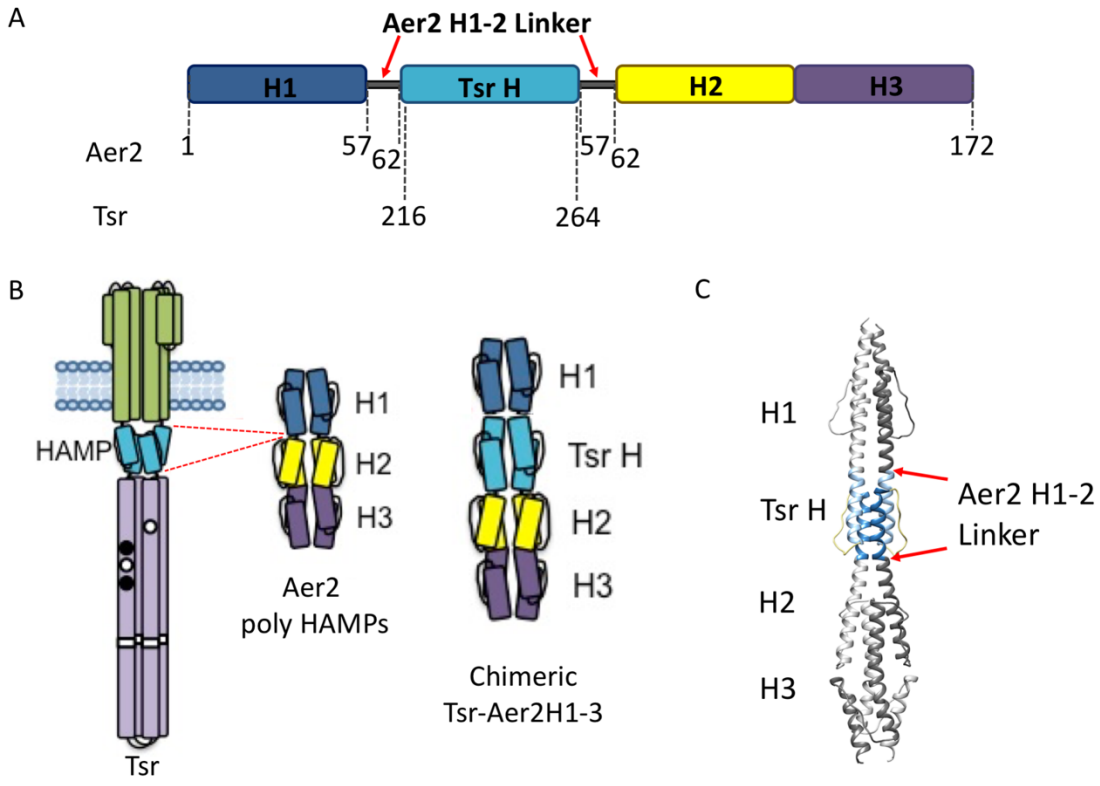

Figure 2-1 Schematic representations of the recombinant Tsr-Aer2 HAMP domains. (A) Domain organization of the chimeric Tsr-Aer2H1-3 protein that is composed of the Tsr HAMP (Tsr H) and the PaAer2 poly-HAMP domains (H1, H2 and H3). The HAMP domains are represented as cylinders, and the PaAer2 linker is shown as grey lines. The actual residue numbers for each domain are as depicted: Aer2H1: 8-56, Aer2H2-H3: 62-172, Aer2H1-2 linker: 57-62, Tsr HAMP: 216-264.

(B) Schematic diagram of the domain architecture the recombinant Tsr-Aer2 HAMP domains. The Tsr HAMP domain is fused between the PaAer2H1-2 domains with the Aer2H1-2 linkers at both ends. The α helices are depicted as cylinders, which represent the dimeric parallel coiled coil structure of HAMP domains. The linkers Aer2 H1-2 linkers are represented as lines.

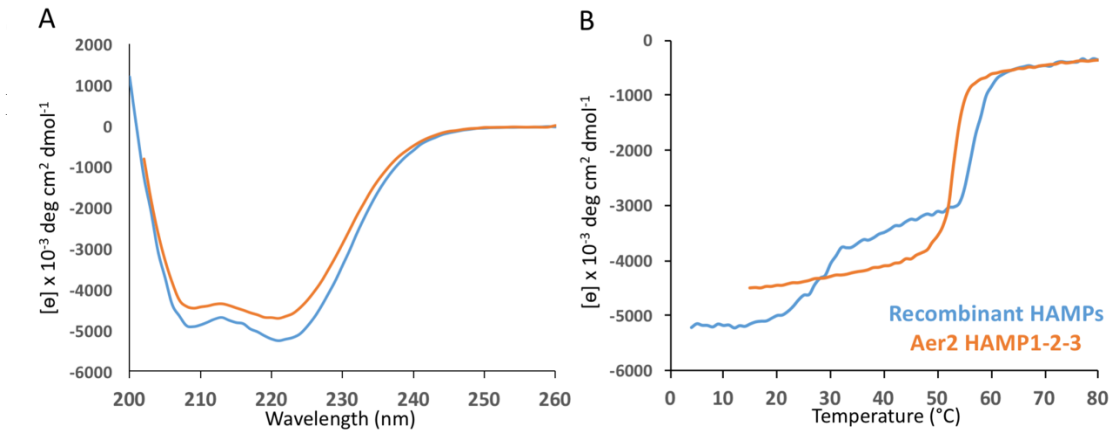

Figure 2-2 Helical content and thermostability of the chimeric Tsr-Aer2H1-3 protein compared to that of Aer2H1-3.

(A) The CD wavelength scans show the overall α-helical structure of Tsr-Aer2H1-3 and Aer2H1-3 alone.

(B) The CD melting curves show the two-step unfolding character of the chimeric protein. An additional transition in the chimera at 26°C is not present in the Aer2H-13 domain, which has a melting temperature of 53°C.

Site-specific spin labeling and pulse-dipolar ESR spectroscopy (PDS) were used to verify the dimeric coiled-coil structure of the Tsr domain within the context of Tsr-Aer2H1-3. Nine engineered cysteine residues were introduced along the AS1 and AS2 helices of the Tsr HAMP domain and subsequently labeled with the nitroxide spin-probe MTSL. Owing to HAMP dimerization, one spin-probe site will produce a dipolar interaction with its symmetric position on the adjacent subunit. The chosen residues were mainly located at the exposed b, c and f positions of the helical heptad repeats (Figure 2-3). The distance distributions between spin pairs generated by the HAMP dimers were measured by double electron-electron resonance (DEER) [44, 49, 50].

DEER modulation depths were monitored to evaluate oligomeric states and aggregration properties of the engineered HAMP domains. The modulation depth of the time-domain DEER spectrum (Δ) is defined as $\Delta(p) = \frac{DEER(t=0)-DEER(t=\infty)}{DEER(t=0)}$, where p is the fraction of spins flipped by the pump π-pulse [51-54]. Δ depends on the number of interacting spins, N, as $\Delta(p,N) = 1-(1-p)^{N-1}$ [51-53, 55]. For a dimer, $\Delta(p,2) = p$ and for an oligomer, $\Delta > p$. Under our experimental conditions (16 ns π-pulse pumped at the center of the nitroxide spectrum) Δ is ~0.35 for a dimer, and ~0.73 for a tetramer with all spins interacting. Most of the samples examined in this study have Δ in the range of 0.35, with some values slightly larger, perhaps owing to modest oligomerization (Figures 2-4 and 2-5). Exceptions are the WT protein spin-labeled at the 220 and 230 positions (Figures 2-6 and 2-7). For 220, the protein eluted on SEC with a bimodal peak (Figure 2-6). Protein from the larger, fast eluting

fractions gave Δ ~ 0.6, whereas the lighter slow-eluting fractions gave values consistent with a dimer Δ ~ 0.4 (Figure 2-6). Diluting samples from the larger fraction also lowered the modulation depth, as would be expected on dissociation of weakly associating tetramer. The resulting distance distributions [P(r)] reflect the oligomerization in the larger species, and thus, only the [P(r)] from the dimeric fraction was used in further analysis. In the case of position 230, the SEC profile was more uniform, but the modulation depth remained high (~0.7) for all fractions across the elution peak, expect for the remote shoulder, where it began to diminish only slightly (Figure 2-7). Thus, WT Tsr-Aer2H1-3 labeled at the 230 site forms a tight, likely tetrameric state, whose overall structure is uncertain, but may contain the typical HAMP dimer (see below).

The derived distance distributions from all spin-labeled residues showed similar separations of approximately 21-26Å (Figure 2-3A,B and 2-4 and Table 2-1), which are generally expected based on structurally characterized HAMP domains (Figure 2-3B). In general the (f) positions give the longest distances followed by the (b) and (c) positions and then the (e) and (d) positions, as would be expected from their placement in the 4-helix bundle (Fig 2-3C,D). For example, the 232 (d) position, which is predicted to orient toward the interior of the helix bundle produces the shortest distance of the AS1 sites. As mentioned above, labeling at the 230 site favors formation of a higher-order oligomer probably a tetramer. Nevertheless, the resulting 230 P(r) is indicative of (b) position and is very similar to the 250 (b) site (Fig. 2-3A). Thus, the average spin-separation within the 230 tetramer may be close to the intersubunit spacing in the dimer. Three neighboring sites at the C-terminus of AS2

agree well with predictions of canonical coiled-coil structure: the 260 (e) position gives the shortest distance, followed by the 258 (c) position and then the 261 (f) position. Broader spatial P(r) distributions correlate with larger spin-label amplitude motions [34], and the overall pattern of P(r) breadth indicate that AS1 of the Tsr HAMP may be more dynamic than AS2 (Table 2-1). In summary, the Tsr HAMP structure in the context of Tsr-Aer2H1-3 meets the expectations of a parallel four-helix bundle, with the AS-1 helices slightly more destabilized compared to the AS-2 helices.

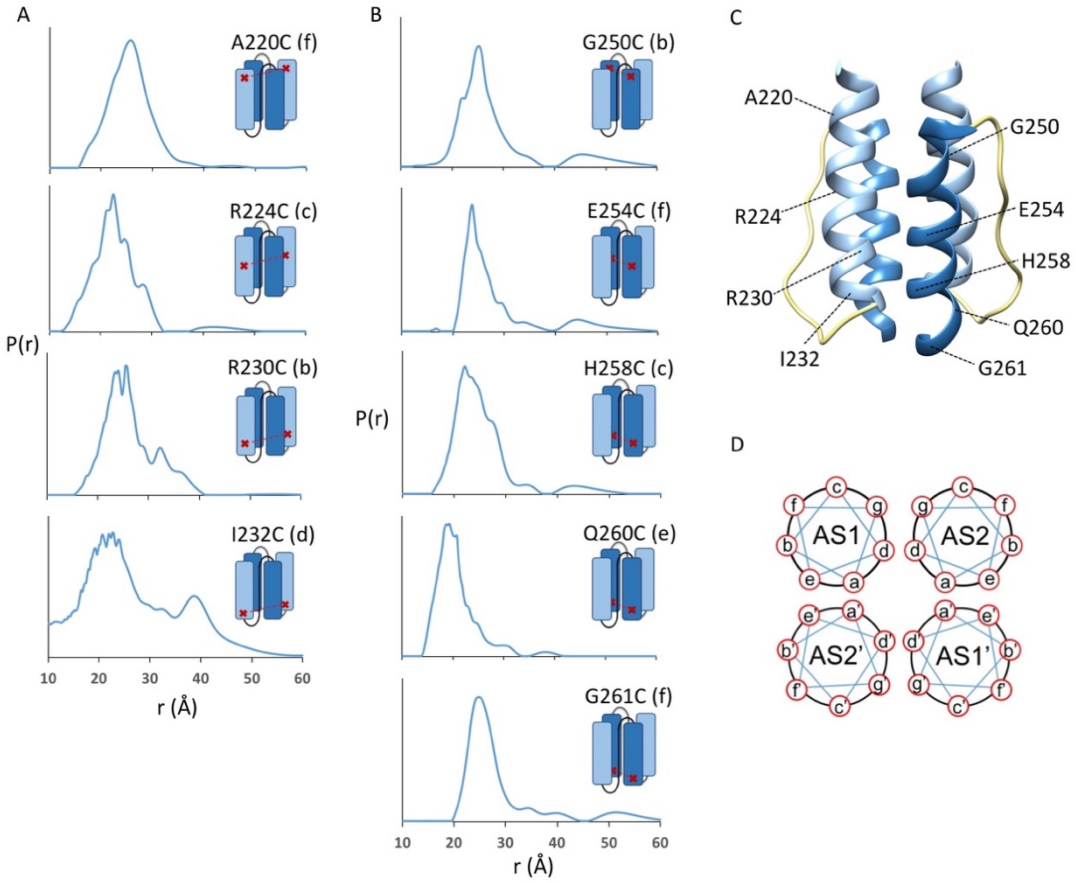

Figure 2-3 Structural properties of the Tsr HAMP domain as revealed by PDS.

(A) Inter-subunit spin probe distances of nitroxide-labeled proteins measured by PDS. The chosen sites are marked on the AS1 and AS2 of one subunit in the schematic diagrams of the Tsr HAMP domain. Pair-wise distance distributions [P(r)] were generated each pair of spins on adjacent subunits. Based on sequence alignments [12, 28], the heptad positions of the spin label sites are defined as follows: AS-1: 220 – f; 224 –c; 230 – b; 232 - d; AS-2: 250 - b; 254 - f; 258 - c; 260 - e, 261 - f;

(B) Homology model of the Tsr HAMP domain. The atomic coordinates for the model wereobtained by threading the Tsr HAMP sequence onto the Af1503 A291F HAMP using SWISS-MODEL. The Tsr HAMP domain is depicted as a dimeric 4-helix

bundle with the AS1 helices in light blue, the AS2 helices in dark blue, and the CTR in gold. The spin-label positions are shown on only one subunit; AS1 on the left and AS2 on the right.

(C) Helical wheel representation of the heptad repeat positions of a parallel 4-helix bundle with a-d, knobs-into-holes, packing.

Table 2-1 Mean distances and width at half height of PDS distance distributions (P(r)) of the chimeric Tsr-Aer2H1-3 with the WT Tsr HAMP.

MTSL Spin Label Position	Mean Distances (Å)	Width at Half Height of P(r) (Å)
A220	26	9
R224	23	8
R230	24, 26	4, 3
I232	22, 39	11, 7
G250	25	7
E254	24	5
H258	22	9
Q260	19	6
G261	25	6

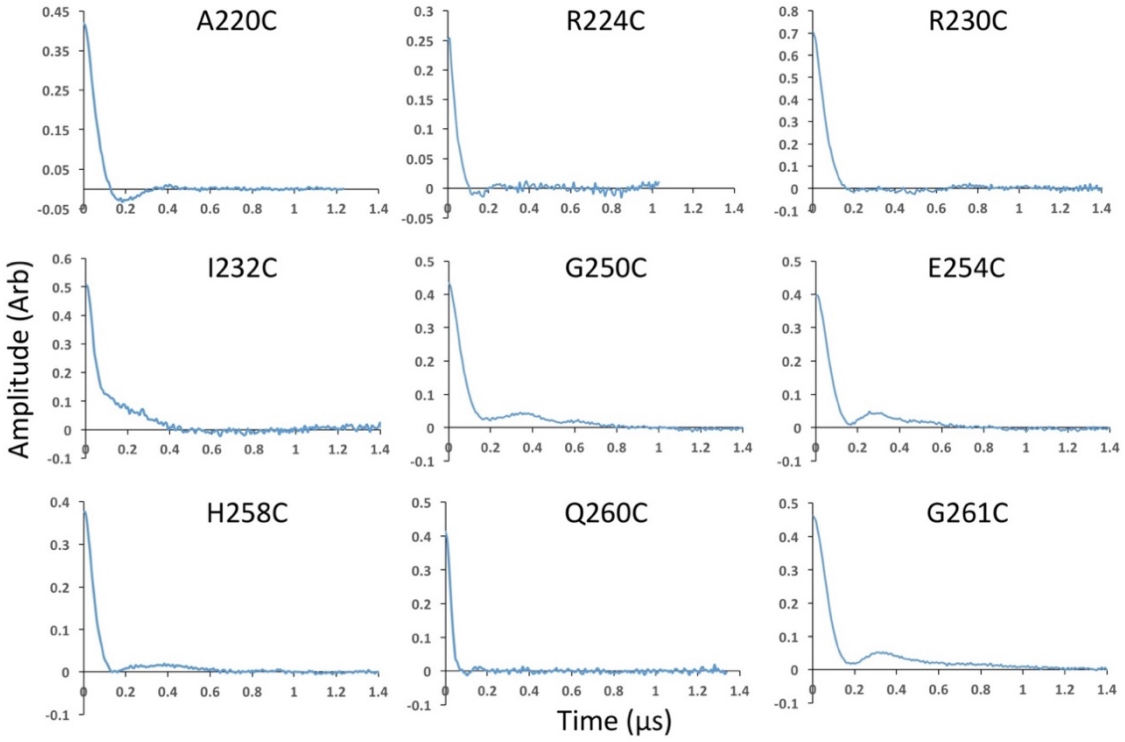

Figure 2-4 Time domain signals measured by PDS for the chimeric Tsr-Aer2H1-3 with the WT Tsr HAMP. The chosen spin-labeled sites are as indicated.

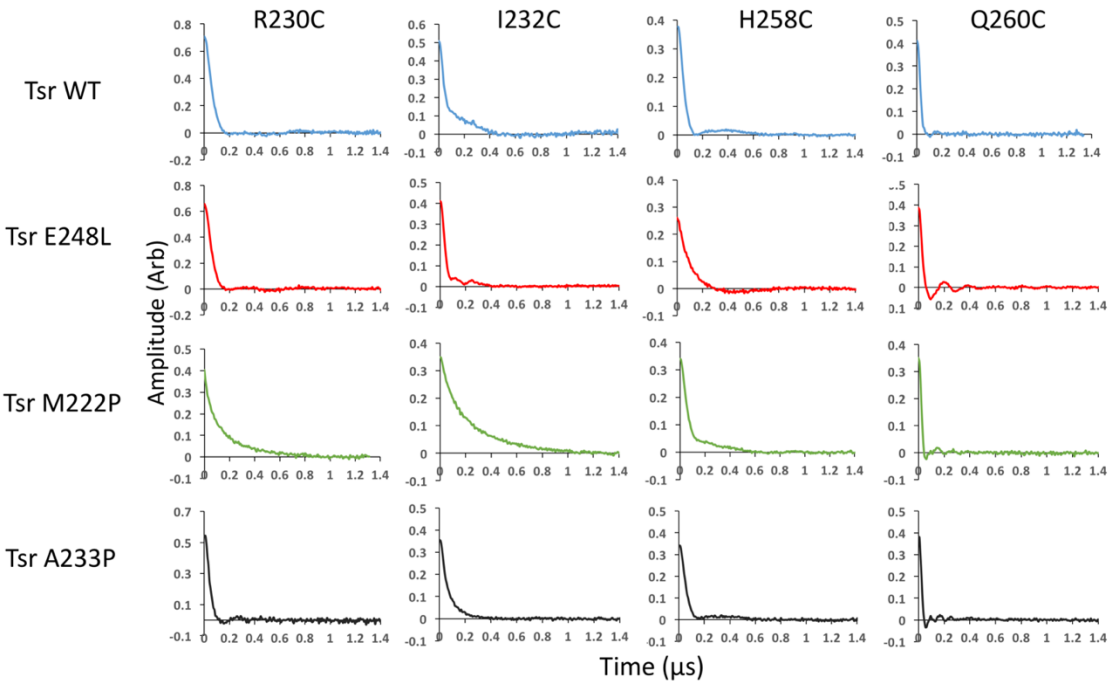

Figure 2-5 Time domain signals measured by PDS for the chimeric Tsr-Aer2H1-3 with the WT Tsr HAMP and variants. The chosen spin-labeled sites are as indicated.

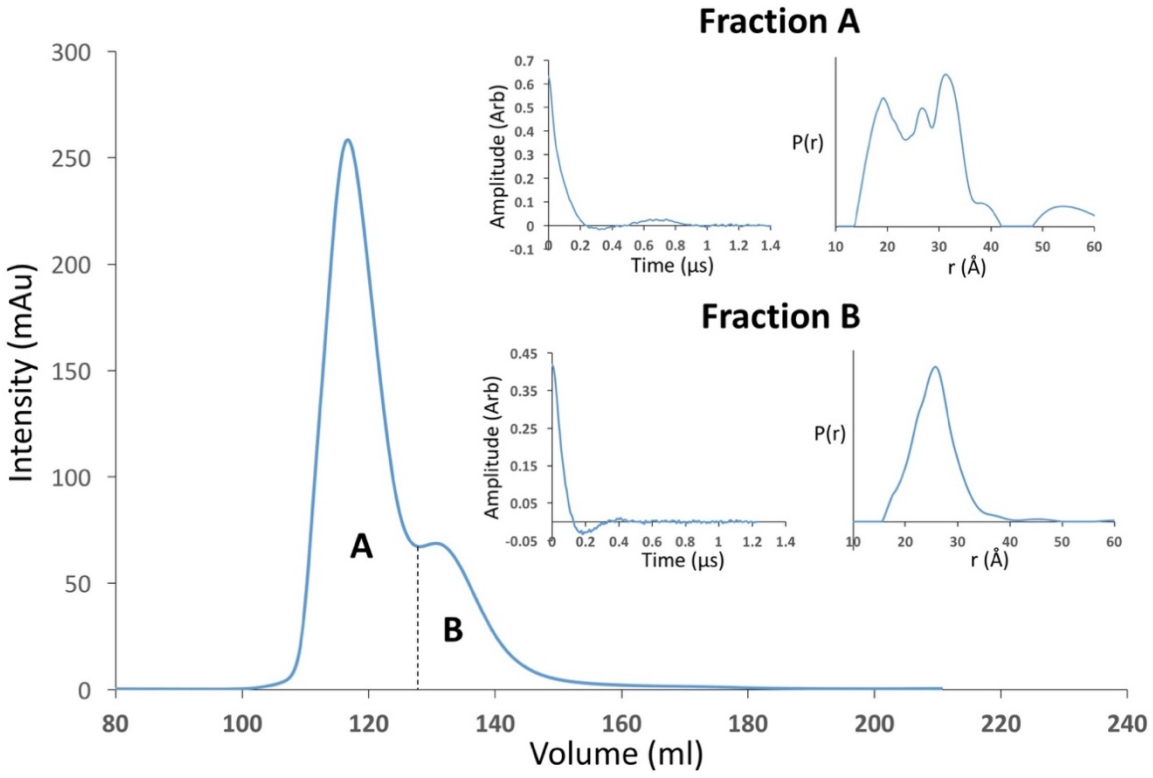

Figure 2-6 SEC profile and effects of oligomerization on PDS results for the Tsr-Aer2H1-3 spin-labelled at the A220 position (A220C). The SEC profile for A220C displayed a bimodal peak with the larger (fraction A), and the smaller (fraction B) species. The time domain signals and distance distributions [P(r)] for each fraction are shown as insets. The time-domain DEER spectrum of fraction A suggests the formation of oligomers, which is consistent with its P(r) data. The oligomers dissociate in fraction B, whose time domain signals and P(r) indicate proper dimerization of the protein.

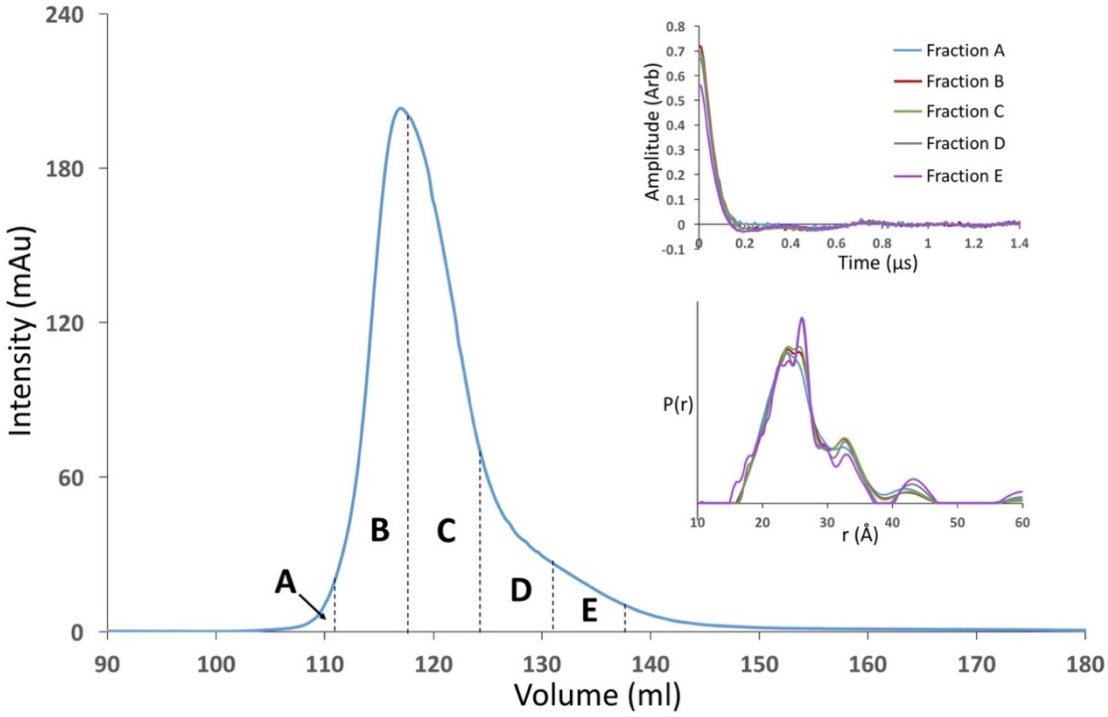

Figure 2-7 SEC profile and effects of oligomerization on PDS results for the Tsr-Aer2H1-3 spin-labelled at the R230 position (R230C). The SEC profile of R230C was uniform. PDS was performed on each SEC fraction denoted as A-E. The time domain signals and P(r) for each fraction are shown as insets. The PDS profiles of all SEC fractions are consistent except small changes of fractions with small species.

Effects of amino-acid replacements on the stability of Tsr HAMP domain

Single amino-acid replacements in the Tsr HAMP domain dramatically alter signaling responses of chemoreceptors [28, 32, 56]. We employed the recombinant Tsr-Aer2H1-3 to investigate the types of physical changes in Tsr HAMP that such residue substitutions may generate. In this initial study we focused on replacements that give three types of phenotypes: CCW(A), caused by Tsr E248L; CCW(B), caused by Tsr M222P, and CW, caused by Tsr A233P [28].

The Tsr E248L substitution was chosen from the group of replacement mutants that give an attractant-mimic [kinase-off; CCW(A)] phenotype. E248 is a conserved residue at the very N-terminus of the AS2 helix in a predicted f position. E248L increased helical content of Tsr-Aer2H1-3 and also substantially raised the Tm of the lower transition to 31°C (Figure 2-8B). Thus, E248L stabilizes the Tsr HAMP bundle. The higher melting transition showed a slightly decreased Tm, reflecting a small compensating destabilization of the Aer2 HAMP domains. The primary effect of this substitution on the lower transition temperature supports the assignment of this transition to the Tsr HAMP.

Tsr M222P was chosen to represent those mutations that cause a kinase-off; CCW(B) phenotype [28]; i.e. a HAMP off state that results from major destabilization of the helix bundle. M222 resides in AS1 at an (a) position within the hydrophobic core of the four-helix coiled coil. Replacements of this residue to proline [28] or polar amino acids generally give non-functional receptors; i.e. CheA is not active and there is no cell tumbling [CCW(B)]. Not surprisingly, this variant partially lost α-helical content (Figure 2-8A) and showed helical melting in a single step with a low Tm of

37 °C (Figure 2-8B). Thus, M222P appears to destabilize Tsr-Aer2H1-3 in entirety and causes the protein to unfold as a single unit.

Tsr A233P was studied as a mutation that produces high CheA activity [kinase on; CW] when receptors are in their default QEQEE modification state ($CheRB^{-}$). The A233P substitution resides on AS1 in an (e) position and slightly increases the CW bias of Tsr receptors from 75% to 81% in *E. coli* cells that lack the adaptation system [28]. The A233P variant also responds to the adaptation system, producing 15% CW rotation in $CheRB^{+}$ cells, which is a lower level than that of WT Tsr (25 ± 4%) [9, 28]. Based on the bistability model [9], residue replacements that yield CW phenotypes are expected to be less destabilizing to the HAMP bundle compared to those that generate CCW(B) phenotypes, but more destabilizing compared to those that generate CCW(A) phenotypes. In the context of Tsr-Aer2H1-3, A233P had reduced α-helical content and a less well-defined lower transition temperature compared to WT (Figure 2-8A, B) Furthermore, the upper transition associated with Aer2H1-3 also had a lowered melting temperature compared to WT (Figure 2-8B). Although the stability effects of Aer2H1-3 cannot be easily separated into Tsr and Aer2 effects, the net result of the substitution is destabilization of the protein. In summary, the stability behavior of these three Tsr mutations largely follows the expectations of the bistability model.

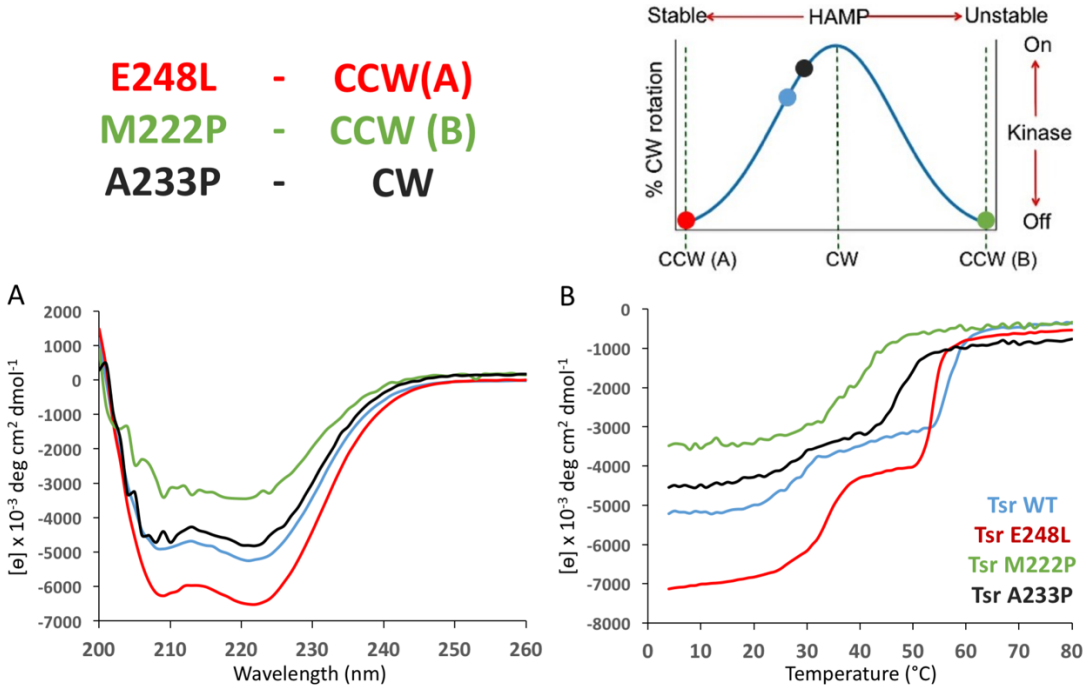

Figure 2-8 Effects of single residue substitutions on the secondary structure and thermal stability of the Tsr HAMP domain.

(A) The CD spectra of the recombinant HAMP domains containing the WT Tsr HAMP (blue) compared to the E248L (red), M222P (green), and A233P (black) variants. The recombinant proteins with the WT Tsr, E248L, and A233P variants maintain their overall α-helical structure. The M222P variant shows the most reduced helical content.

(B) CD thermal melts of the variant Tsr-Aer2H1-3 proteins. The E248L, and A233P mutations do not affect the two-step unfolding of the recombinant protein, but have altered transition temperatures. The E248L variant has melting transitions at 33 and 54°C, and the A233P variant has transitions at 27 and 48°C. In contrast, the M222P variant unfolds in a single step at 39°C.

Effects of mutations on the structure and dynamics of the Tsr HAMP domain

The structural variation of HAMP domains from different proteins suggest that the HAMP fold can assume different conformational states that could relate to their signal transduction mechanism. We applied PDS and site-specific spin labeling to characterize changes in structure and dynamics associated with the CCW(A), CCW(B) and CW phenotype-causing mutants studied above. Additional cysteine residues were introduced into the Tsr unit of Tsr-Aer2H1-3 for nitroxide labeling. Residues R230 & I232 at the C-terminal end of AS1, and H258 & Q260 at the C-terminal end of AS-2 were chosen as the spin-label positions. To simplify subsequent discussion, the proteins with reporter sites will still be referred to as WT. The conformation of the AS2 C-terminus was of interest because it normally couples to the KCM of the receptor. The two residues on each helix reside at different heptad positions but are close in sequence and should report on rotational as well as translational motions.

The changes in spin-label distance distributions for the four probe sites are not dramatic but show some clear trends (Figure 2-5 and 2-9; Table 2-2). Foremost, the AS1 sites give quite different P(r) widths, indicative of changes in conformational heterogeneity. The CCW(B) M222P variant is the most unstable, showing a very broad AS1 signal for both the 230 (b) and the 232 (d) sites. Furthermore, the 230 site now gives a modulation depth below 0.4 (Figure 2-5). These signals suggest that AS1 is essentially unfolded in and that higher order oligomerization has diminished. The next most dynamic AS1 is found in the CW state, followed by WT and then by E248L CCW(A); very much in keeping with predictions of the bistability model [28]. However, the same trend is not observed for AS2, where the two probe positions show

similar P(r) widths for the four variants. That said, E248L tends to give the sharpest distributions. Changes in the mean positions of the distributions are also evident among the variants. Comparisons are perhaps most instructive between the sites that give opposing functional phenotypes: CCW(A) E248L and CW A233P. Of the two AS1 reporter sites, the 232 (d) separation increases from CCW(A) to CW, whereas. 230 (b) decreases. For the 230 site, oligomerization may again complicate this interpretation, but, assuming the dimeric bundle structures are largely the same for 230 and 232 opposite changes in distance are consistent with a counterclockwise rotation at the C-terminal end of the AS1 helices. A gearbox-type rotation of the bundle would necessitate a compensating clockwise rotation of the AS2 helices. Consistent with an AS2 clockwise rotation, 260 (e) transition to a shorter separation on transition from CCW(A) to CW and the 258 position undergoes a slight shift in the distribution mean to longer distances. The broad distribution of the 258 position (which could be due to spin label conformational heterogeneity) may mask a more definitive shift in separation distance. The WT distribution lies in between the two extremes of CW and CCW(A) for position 232, resembles CCW(A) for position 230, and resembles CW for 260, which in sum are consistent with an intermediate phenotype. These patterns thus suggest that the CCW(A) and CW mutations are distinguished by conformational changes in both the AS1 and AS2 helices, that can be interpreted as rotations. Nonetheless, other motions, such as helix translation and tilting, could also contribute to the altered PDS distance distributions. Notably, both the AS1 and AS2 helices are more dynamic in the CW state. For CCW(B) the AS1 helix is essentially unfolded but the AS2 helices maintain close interactions characteristic of a two-helix coiled-coil.

Interestingly, for CCW(B) the most C-terminal 260 site shows a sharp, short, bimodal distribution very similar to that of the Aer2 HAMP2 domain fused to the KCM of the Tar receptor [34]. Like the HAMP2-Tar chimera [33], the CCW(B) variant in Tsr also gives an exclusively CCW phenotype and a kinase-off state.

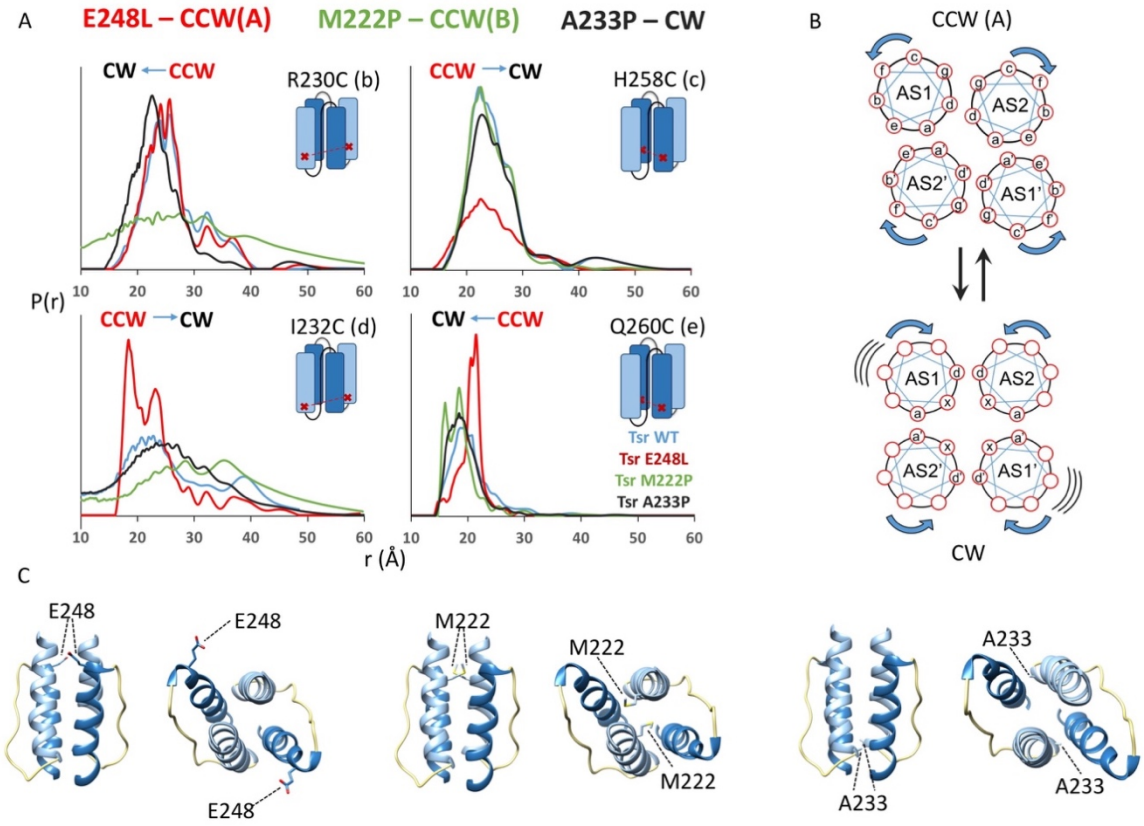

Figure 2-9 Effects of single residue substitutions on the structural properties of the Tsr-Aer2H1-3 chimeric protein.

(A) PDS distance distributions. Schematic diagrams for the Tsr HAMP are marked with the spin-label sites. Distance distributions [P(r)] measured by PDS are shown for the Tsr WT (blue) and variants E248L – CCW(A) (red), M222P – CCW(B) (green), and A233P – CW (black).

(B) Schematic diagram summarizing the possible conformational changes relating CCW(A) and CW as inferred by the four spin-label positions at the base of AS1 and AS2. For AS1, increase in the d-d separation and decrease in the b-b separation suggest a counterclockwise rotation in switching from the CCW(A)-kinase off state to

the CW kinase-on state. For AS2, decrease in the e-e separation indicates a corresponding clockwise rotation. The c-c position of AS2 shows little change, probably due to breadth of the distribution.

(C) Schematic diagrams showing the positions of the residues chosen for substitutions on the Tsr HAMP domain. E248 resides at the very N-terminus of AS2 and assumes a predicted f position. M222 locates at a position of AS1 in the hydrophobic core of the Tsr HAMP. A233 resides at e position at N-terminus of AS1.

Table 2-2 Mean distances and width at half height of PDS distance distributions (P(r)) of the chimeric Tsr-Aer2H1-3 with WT Tsr HAMP and variants

Genotype	MTSL Spin Label Position	Mean Distances (Å)	Width at Half Height of P(r) (Å)
WT	R230	24, 26	4, 3
	I232	22, 39	11, 7
	H258	22	9
	Q260	19	6
E248L	R230	24, 26	7
	I232	18, 23	4, 2
	H258	23	11
	Q260	21	3
M222P	R230	26*	28
	I232	28, 36*	11, 11
	H258	23	9
	Q260	16, 18	2, 3
A233P	R230	23	8
	I232	24	16
	H258	23	9
	Q260	18	6

* Indicates broad distribution

Effects of the N-terminal linker sequence on Tsr structure and dynamics

The five-residue control cable of Tsr links transmembrane TM2 to the HAMP domain and transmits the piston displacement of TM2 that down-regulates kinase activity [1, 56-58]. The linker sequence is similar to that of Aer2 used in the chimera, but differs in one important way. Functional studies of Tsr have shown that I214 on the control cable is critical for triggering responses, possibly through the interaction of its side chain with the aromatic residues at TM2 C-terminus [56, 59-62]. Glu substitution at this position (61), as found in Aer2, has impaired function [56]. Thus, we altered Glu61 to Ile to better reflect the control cable sequence, and investigated the impact on stability and conformation.

E61I Tsr-Aer2H1-3 showed substantially higher thermal stability of both Tsr HAMP (36°C) and Aer2 HAMP1-2-3 domains (67°C) than the WT counterparts (26 and 57°C, respectively) (Figure 2-10C). In PDS studies (Figure 2-10D and 2-11; Table 2-3), the substitution substantially ordered a probe site at the N-terminus of AS1, showing that increased hydrophobicity in this position of the control cable stabilizes the otherwise variable AS1. However, little change of the substitution is observed at the 258 position at the C-terminus of AS2. Thus, in the context of the chimera, the control cable conformation does not greatly impact AS2 (Figure 2-10D). This result further confirms the stable nature of Tsr AS2.

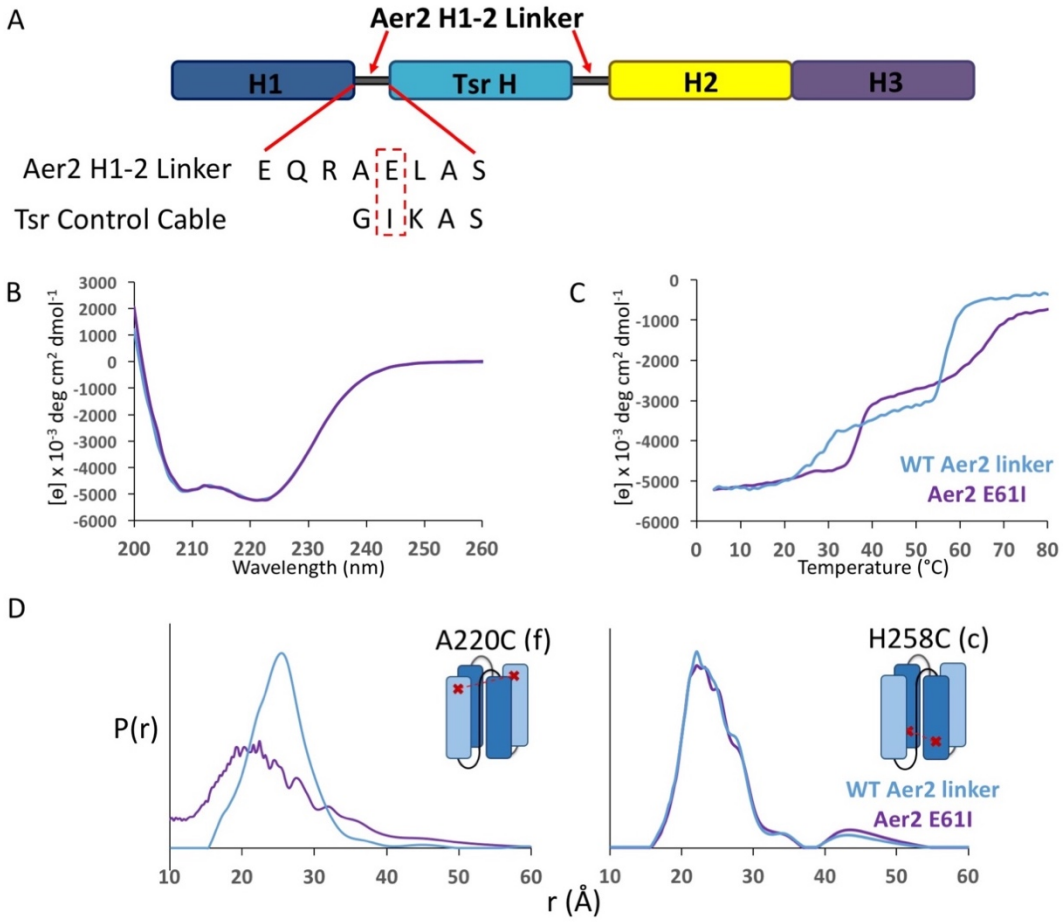

Figure 2-10 Effects of the linker sequence on the Tsr HAMP domain structure and stability.

(A) Schematic of the chimeric Tsr-Aer2H1-3 domain structure and linker sequence. Sequence for the PaAer2 linker and Tsr control cable are similar but differ in the critical residue Tsr I214 which in PaAer2 is E61 (red box.)

(B) CD spectra showing the secondary structure properties of the chimeric proteins containing either the WT Aer2 linker (blue) or the Aer2 E61I substitution (purple). The two proteins have nearly identical α-helical content.

(C) Thermal stabilities of the chimeric Tsr-Aer2H1-3 proteins with either the WT Aer2 linker or the Aer2 E61I substitution as measured by CD spectroscopy. The E61I substitution increased the melting temperatures for both the Tsr HAMP and the Aer2 poly HAMP domains to 37 and 65°C, respectively.

(D) PDS distance distributions of the Tsr HAMP domain in the recombinant protein with and without the Aer2 E61I substitution. The spin-label sites A220 and H258 are depicted as red stars.

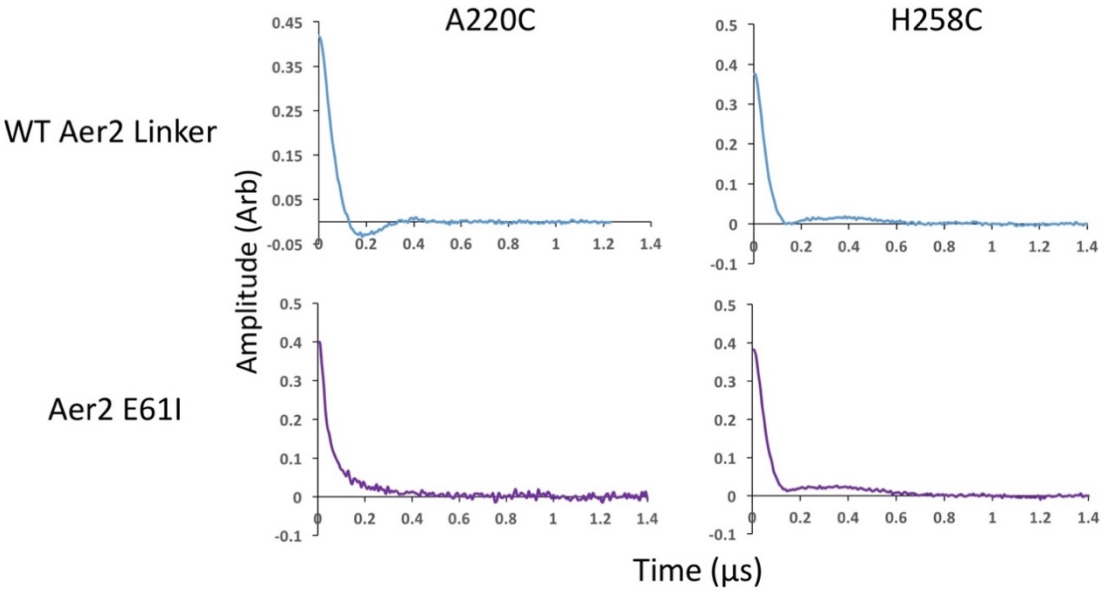

Figure 2-11 Time domain signals measured by PDS for the chimeric Tsr-Aer2H1-3 with the WT Aer2 linker and the Aer2 E61I mutant. The chosen spin-labeled sites are as indicated.

Table 2-3 Mean distances and width at half height of PDS distance distributions (P(r)) of the chimeric Tsr-Aer2H1-3 with WT Aer2 linker and Aer2 E61I

Variant	MTSL Spin Label Position	Mean Distances (Å)	Width at Half Height of P(r) (Å)
WT Aer2 Linker	A220	26	9
	H258	22	9
Aer2 E61I	A220	21	9
	H258	23	14

2.5 Discussion

To permit expression of the otherwise unstable Tsr HAMP, we generated a chimeric protein containing the Tsr HAMP domain spliced into the Aer2 poly HAMP. Under these circumstances, the Tsr HAMP maintained its α-helical, four-helix coiled-coil structure although the AS1 helix appeared more conformationally variable toward its N-terminus than the AS2 helix. Compared to Aer2 poly HAMP alone, the thermal denaturation profile of the chimeric protein revealed an additional lower temperature transition, that we attribute to Tsr HAMP. The chimeric protein thus provided an opportunity to evaluate the effects of residue substitutions of known functional consequence on the stability and conformational properties of the Tsr HAMP.

A common signaling mechanism of HAMP domains is supported by the ability to swap HAMP domains among various proteins while maintaining function [63, 64]. The structural studies of several HAMP domains have led to a two-state model for HAMP signaling mechanism. The gearbox model proposes conversion between a-d and x-da packing arrangements of HAMP bundles [10, 15, 17, 31]. Chemoreceptors in off states are associated with the a-d packing mode and on-states with the x-da mode [17, 29, 65]. In contrast, the extensive genetic studies of Tsr HAMP mutations have led to the dynamic bundle model, which accounts for the observations that multiple amino acid substitutions of similar character invoke the same signaling outputs. This model purposes that, for each signaling state, HAMP domains operate in a range of related conformations with different helix-packing stabilities [28, 29, 32]. In the context of the Tsr receptor, the packing stabilities of HAMP helical bundles are expected to oppose those of the KCM helical bundles owing to a mismatched phase of

hydrophobic packing between AS2 and the methylation helices of the kinase control module; i.e. one of the two bundles can pack in stable fashion, but not both simultaneously [19, 29, 34].

This initial evaluation of three residue substitutions representative of the CCW(A), CCW(B) and CW states defined in the dynamic bundle model provides some insight into how such changes alter Tsr HAMP stability and structure. The CCW(B) mutation, M222P, which replaces an internal hydrophobic residue with a helix-breaking proline, greatly destabilizes the AS1 helix and produces an extremely broad PDS distribution. However, the AS2 helices remains folded and associated; thus, the domain has effectively become a two-helix coiled-coil and hydrophobic packing of AS2 can occur independently from that of AS1. Indeed, deletion of the Tsr AS1 helices causes CCW locked behavior [27] (which depends on the C-terminal packing residues of AS2). The two substitutions that produce CCW(A) and CW phenotypes represent differences in functional states. The CCW(A) substitution, E248L, resides in the DExG motif (NEMG in the Tsr HAMP) at the connector to AS2. The DExG motif is highly conserved in canonical HAMP domains, and is critical for coupling transmembrane signals [5, 33]. The CW phenotype of A223P in QEQEE cells, which increases only slightly over WT, tolerates the substitution of a larger residue in the (e) position near the end of AS1 [28]. As evaluated by thermal melts, the CCW(A) mutation produces a domain more stable than the WT, whereas the CW mutation produces a domain less stable than the WT. The breadth of the PDS distributions reflects these trends, with increased conformational heterogeneity most evident in AS1.

When comparing E248L (CCW(A) and A233P (CW), the centers of the PDS distributions at the C-terminal ends of AS1 and AS2 also indicate a conformational change consistent with concerted helical rotation. Under this premise, the internal hydrophobic packing converts between the x-da arrangement to a more canonical a-d (knobs-into-holes) packing (Fig. 3). In transition from a-d to x-da packing, the AS1 helices rotate counterclockwise and the AS2 helices rotate clockwise. Opposite shifts in separation of neighboring residues can be explained by such motions but are not consistent with an exclusive helical tilt away from the dimer axis or a piston motion, wherein the spacing of two closely spaced positions on the same helix would rather both change in the same direction or stay the same. However, translations in a plane perpendicular to the dimer axis or a scissors motion of symmetric helical pairs could also generate the observed distance changes. These types of distortion would produce a more rhombic structure in one of the states (Figure 2-9). Ambiguities arising from flexibility in the spin-label prevent a further discrimination of these models, and thus we presume that the actual transition contains elements of both. Interestingly, the residue substitutions that cause CCW(A) and CCW(B) states have very different adaptational modification properties, which predicted that their AS2 structures should be different [28]. Indeed, the CCW(A) and CCW(B) representative variants do not produce the same conformations at the C-terminus of AS2, as reported by the spin-probe at position 260. It is possible that the rotational "phase" of the AS2 helix rotation must be within a specific range for the downstream helices of the KCM to be stable, as has been seen in other helical signaling systems [66, 67]. The distance distributions for both the WT and CW states lie between those of CCW(A) and

CCW(B). CCW output may result if HAMP AS2 enforces the downstream helices to be either over or underwound. Fusion of the Aer2 HAMP1 or HAMP2 to the Tar KCM causes opposite effects on KCM dynamics, kinase activity and cell swimming behavior [33, 68] At their C-termini the Aer2 HAMP1 and more rhombic HAMP2 domains also differ by AS2 rotation and positioning, with the off-state involving closer 2-helix knobs-into-holes (a-d) packing of HAMP2 [33, 34].

In the context of transmembrane chemoreceptors, the five-residue control cable connects and transmits piston displacements of the ligand-bound TM2 to the AS1 helix of the HAMP domain [9, 56, 59]. The genetic studies in the Tsr receptor have shown that the control cable helicity enables Tsr to adopt proper signaling states by modulating the structural mismatches between the TM2 and the AS1 helix. However, only isoleucine 214 on the control cable is critical for this transmission mechanism [56, 58, 59, 62]. *E. coli* cells expressing the Tsr receptor with the I214E substitution showed higher CW flagella rotation (88%) compared to cells expressing the WT receptor (75%) [56]. Changing Aer2 Glu61 to Ile increased stability of the Tsr HAMP as judged by thermal melts and reduced conformational heterogeneity in AS1. However, there appeared to be little change at the AS2 C-terminus. Hence, the Tsr I214 control cable residue may have less impact on the AS2 conformation in this chimeric system than in the native receptors where I214 resides close to the membrane.

In summary, the Tsr-Aer2H1-3 chimera has allowed us to study the effects of mutations of known functional consequences on Tsr HAMP conformation and stability. Although the Tsr HAMP is not in its native context, it is coupled to other dimeric helical bundles, as it is in the chemoreceptor. The results of the residue

substitutions on biophysical properties of Tsr HAMP match expectations of prevailing models for HAMP activation. CW and CCW causing mutations differ by changes that can be interpreted in terms of helix rotation, juxtaposition and altered stability. The activating states of HAMP appear to be associated with more conformational variability, less stability versus an unfolded state and movement of the AS2 helices at their C-termini that bring symmetric (e) sites closer together and symmetric (c) sites further apart. A clockwise rotation toward x-da packing is consistent with such a change. Inactivating states are associated with a stable association of the AS2 helices that favors a more a-d arrangement. Importantly, multiple conformational states are likely capable of inducing either on or off behavior. For activating states, an ensemble of dynamic HAMP conformations may allow the KCM to assume its favored conformation. In contrast, for deactivating states, a stable 2-helix coil in HAMP may over or underwind the KCM to push its conformation outside of the range that allows kinase activation.

REFERENCES

[1] Falke JJ, Hazelbauer GL. Transmembrane signaling in bacterial chemoreceptors. Trends Biochem Sci. 2001;26:257-65.

[2] Falke JJ, Piasta KN. Architecture and signal transduction mechanism of the bacterial chemosensory array: Progress, controversies, and challenges. Curr Opin Struct Biol. 2014;29:85-94.

[3] Blair DF. How bacteria sense and swim. Annu Rev Microbiol. 1995;49:489-522.

[4] Aravind L, Galperin MY, Koonin EV. The catalytic domain of the P-type ATPase has the haloacid dehalogenase fold. Trends Biochem Sci. 1998;23:127-9.

[5] Dunin-Horkawicz S, Lupas AN. Comprehensive Analysis of HAMP Domains: Implications for Transmembrane Signal Transduction. J Mol Biol. 2010;397:1156-74.

[6] Schirmer T. C-di-GMP synthesis: Structural aspects of evolution, catalysis and regulation. J Mol Biol. 2016.

[7] Butler SL, Falke JJ. Cysteine and disulfide scanning reveals two amphiphilic helices in the linker region of the aspartate chemoreceptor. Biochemistry. 1998;37:10746-56.

[8] Letunic I, Doerks T, Bork P. SMART 7: recent updates to the protein domain annotation resource. Nucleic Acids Res. 2012;40:D302-5.

[9] Parkinson JS. Signaling Mechanisms of HAMP Domains in Chemoreceptors and Sensor Kinases. In: Gottesman S, Harwood CS, editors. Annual Review of Microbiology, Vol 64, 20102010. p. 101-22.

[10] Hulko M, Berndt F, Gruber M, Linder JU, Truffault V, Schultz A, et al. The HAMP domain structure implies helix rotation in transmembrane signaling. Cell. 2006;126:929-40.

[11] Williams SB, Stewart V. Functional similarities among two-component sensors and methyl-accepting chemotaxis proteins suggest a role for linker region amphipathic helices in transmembrane signal transduction. Mol Microbiol. 1999;33:1093-102.

[12] Airola MA, Watts KJ, Crane BR. Structure of concatenated HAMP domains provides a mechanism for signal transduction. Structure. 2010;18:436-48.

[13] Ames P, Zhou Q, Parkinson JS. Mutational analysis of the connector segment in the HAMP domain of Tsr, the Escherichia coli serine chemoreceptor. J Bacteriol. 2008;190:6676-85.

[14] Kishii R, Falzon L, Yoshida T, Kobayashi H, Inouye M. Structural and functional studies of the HAMP domain of EnvZ, an osmosensing transmembrane histidine kinase in Escherichia coli. J Biol Chem. 2007;282:26401-8.

[15] Wang C, Sang J, Wang J, Su M, Downey JS, Wu Q, et al. Mechanistic insights revealed by the crystal structure of a histidine kinase with signal transducer and sensor domains. PLoS Biol. 2013;11:e1001493.

[16] Matamouros S, Hager KR, Miller SI. HAMP Domain Rotation and Tilting Movements Associated with Signal Transduction in the PhoQ Sensor Kinase. MBio. 2015;6:e00616-15.

[17] Ferris HU, Dunin-Horkawicz S, Mondejar LG, Hulko M, Hantke K, Martin J, et al. The Mechanisms of HAMP-Mediated Signaling in Transmembrane Receptors. Structure. 2011;19:378-85.

[18] Swain KE, Falke JJ. Structure of the conserved HAMP domain in an intact, membrane-bound chemoreceptor: A disulfide mapping study. Biochemistry. 2007;46:13684-95.

[19] Swain KE, Gonzalez MA, Falke JJ. Engineered Socket Study of Signaling through a Four-Helix Bundle: Evidence for a Yin-Yang Mechanism in the Kinase Control Module of the Aspartate Receptor. Biochemistry. 2009;48:9266-77.

[20] Watts KJ, Johnson MS, Taylor BL. Structure-function relationships in the HAMP and proximal signaling domains of the aerotaxis receptor Aer. J Bacteriol. 2008;190:2118-27.

[21] Bhate MP, Molnar KS, Goulian M, DeGrado WF. Signal transduction in histidine kinases: insights from new structures. Structure. 2015;23:981-94.

[22] Sourjik V, Wingreen NS. Responding to chemical gradients: bacterial chemotaxis. Curr Opin Cell Biol. 2012;24:262-8.

[23] Hazelbauer GL, Falke JJ, Parkinson JS. Bacterial chemoreceptors: high-performance signaling in networked arrays. Trends BiochemSci. 2008;33:9-19.

[24] Parkinson JS, Hazelbauer GL, Falke JJ. Signaling and sensory adaptation in Escherichia coli chemoreceptors: 2015 update. Trends Microbiol. 2015;23:257-66.

[25] Pedetta A, Parkinson JS, Studdert CA. Signalling-dependent interactions between the kinase-coupling protein CheW and chemoreceptors in living cells. Mol Microbiol. 2014;93:1144-55.

[26] Wadhams GH, Armitage JP. Making sense of it all: bacterial chemotaxis. Nat Rev Mol Cell Biol. 2004;5:1024-37.

[27] Ames P, Zhou Q, Parkinson JS. HAMP domain structural determinants for signalling and sensory adaptation in Tsr, the Escherichia coli serine chemoreceptor. Mol Microbiol. 2014;91:875-86.

[28] Zhou Q, Ames P, Parkinson JS. Biphasic control logic of HAMP domain signalling in the Escherichia coli serine chemoreceptor. Mol Microbiol. 2011;80:596-611.

[29] Lai R-Z, Parkinson JS. Functional Suppression of HAMP Domain Signaling Defects in the E. coli Serine Chemoreceptor. J Mol Biol. 2014;426:3642-55.

[30] Ferris HU, Dunin-Horkawicz S, Hornig N, Hulko M, Martin J, Schultz JE, et al. Mechanism of Regulation of Receptor Histidine Kinases. Structure. 2012;20:56-66.

[31] Ferris HU, Zeth K, Hulko M, Dunin-Horkawicz S, Lupas AN. Axial helix rotation as a mechanism for signal regulation inferred from the crystallographic analysis of the E. coli serine chemoreceptor. J Struct Biol. 2014;186:349-56.

[32] Zhou Q, Ames P, Parkinson JS. Mutational analyses of HAMP helices suggest a dynamic bundle model of input-output signalling in chemoreceptors. Mol Microbiol. 2009;73:801-14.

[33] Airola MV, Sukomon N, Samanta D, Borbat PP, Freed JH, Watts KJ, et al. HAMP domain conformers that propagate opposite signals in bacterial chemoreceptors. PLoS Biol. 2013;11:e1001479.

[34] Samanta D, Borbat PP, Dzikovski B, Freed JH, Crane BR. Bacterial chemoreceptor dynamics correlate with activity state and are coupled over long distances. Proc Natl Acad Sci U S A. 2015;112:2455-60.

[35] Dutta R, Qin L, Inouye M. Histidine kinases: diversity of domain organization. Mol Microbiol. 1999;34:633-40.

[36] Molnar KS, Bonomi M, Pellarin R, Clinthorne GD, Gonzalez G, Goldberg SD, et al. Cys-scanning disulfide crosslinking and bayesian modeling probe the transmembrane signaling mechanism of the histidine kinase, PhoQ. Structure. 2014;22:1239-51.

[37] Inoue K, Sasaki J, Spudich JL, Terazima M. Signal transmission through the HtrII transducer alters the interaction of two alpha-helices in the HAMP domain. J Mol Biol. 2008;376:963-70.

[38] Wang J, Sasaki J, Tsai AL, Spudich JL. HAMP domain signal relay mechanism in a sensory rhodopsin-transducer complex. J Biol Chem. 2012;287:21316-25.

[39] Gushchin I, Gordeliy V, Grudinin S. Two Distinct States of the HAMP Domain from Sensory Rhodopsin Transducer Observed in Unbiased Molecular Dynamics Simulations. Plos One. 2013;8.

[40] Zhu L, Bolhuis PG, Vreede J. The HAMP signal relay domain adopts multiple conformational states through collective piston and tilt motions. PLoS Comput Biol. 2013;9:e1002913.

[41] Schultz JE, Natarajan J. Regulated unfolding: a basic principle of intraprotein signaling in modular proteins. Trends Biochem Sci. 2013;38:538-45.

[42] Klose D, Voskoboynikova N, Orban-Glass I, Rickert C, Engelhard M, Klare JP, et al. Light-induced switching of HAMP domain conformation and dynamics revealed by time-resolved EPR spectroscopy. FEBS letters. 2014;588:3970-6.

[43] Bryksin AV, Matsumura I. Overlap extension PCR cloning: a simple and reliable way to create recombinant plasmids. BioTechniques. 2010;48:463-5.

[44] Borbat PP, Freed JH. Pulse Dipolar Electron Spin Resonance: Distance Measurements. In: Timmel CR, Harmer JR, editors. Structural Information from Spin-Labels and Intrinsic Paramagnetic Centres in the Biosciences2014. p. 1-82.

[45] Borbat PP, Crepeau RH, Freed JH. Multifrequency two-dimensional Fourier transform ESR: an X/Ku-band spectrometer. J Magn Reson. 1997;127:155-67.

[46] Georgieva ER, Borbat PP, Ginter C, Freed JH, Boudker O. Conformational ensemble of the sodium-coupled aspartate transporter. Nat Struct Mol Biol. 2013;20:215-21.

[47] Chiang YW, Borbat PP, Freed JH. The determination of pair distance distributions by pulsed ESR using Tikhonov regularization. J Magn Reson. 2005;172:279-95.

[48] Chiang YW, Borbat PP, Freed JH. Maximum entropy: A complement to Tikhonov regularization for determination of pair distance distributions by pulsed ESR. Journal Of Magnetic Resonance. 2005;177:184-96.

[49] Borbat PP, Freed JH. Double-Quantum ESR and Distance Measurements. In: Berliner LJ, Eaton GR, Eaton SS, editors. Distance Measurements in Biological Systems by EPR. New York: Kluwer Academic/Plenum Publishers; 2000. p. 383-459.

[50] Jeschke G, Polyhach Y. Distance measurements on spin-labelled biomacromolecules by pulsed electron paramagnetic resonance. Physical Chemistry Chemical Physics. 2007;9:1895-910.

[51] Milov ADaP, A.B. and Tsvetkov, Y.D. Electron-electron double resonance in electron spin echo: model biradical systems and the sensitized photolysis of decalin. Chem, POhys Lett. 1984;110:67-72.

[52] Bode AEaM, D. and Plackmeyer, J. and Dumer, G. and Prisner, T.F. and Schiemann. Counting the monomers in nanometer sized oligomers by pulsed electron-electron double resonance. J Am Chem Soc. 2007;129:6736-45.

[53] Bhatnagar J, Sircar R, Borbat P, Freed JR, Crane BR. Self Association of the Histidine Kinase CheA as Studied by
Pulsed Dipolar ESR Spectroscopy
. Biophysical J. 2012;102:2192-201.

[54] Georgieva ER, Borbat PP, Norman HD, Freed JH. Mechanism of influenza A M2 transmembrane domain assembly in lipid membranes. Scientific reports. 2015;5:11757.

[55] Georgieva ER, Ramlall TF, Borbat PP, Freed JH, Eliezer D. Membrane-bound alpha-synuclein forms an extended helix: Long-distance pulsed ESR measurements using vesicles, bicelles, and rodlike micelles. J Am Chem Soc. 2008;130:12856-+.

[56] Kitanovic S, Ames P, Parkinson JS. Mutational Analysis of the Control Cable That Mediates Transmembrane Signaling in the Escherichia coli Serine Chemoreceptor. J Bacteriol. 2011;193:5062-72.

[57] Park H, Im W, Seok C. Transmembrane Signaling of Chemotaxis Receptor Tar: Insights from Molecular Dynamics Simulation Studies. Biophys J. 2011;100:2955-63.

[58] Wright GA, Crowder RL, Draheim RR, Manson MD. Mutational analysis of the transmembrane helix 2-HAMP domain connection in the Escherichia coli aspartate chemoreceptor tar. J Bacteriol. 2011;193:82-90.

[59] Kitanovic S, Ames P, Parkinson JS. A Trigger Residue for Transmembrane Signaling in the Escherichia coli Serine Chemoreceptor. J Bacteriol. 2015;197:2568-79.

[60] Draheim RR, Bormans AF, Lai RZ, Manson MD. Tryptophan residues flanking the second transmembrane helix (TM2) set the signaling state of the Tar chemoreceptor. Biochemistry. 2005;44:1268-77.

[61] Adase CA, Draheim RR, Manson MD. The Residue Composition of the Aromatic Anchor of the Second Transmembrane Helix Determines the Signaling Properties of the Aspartate/Maltose Chemoreceptor Tar of Escherichia coli. Biochemistry. 2012;51:1925-32.

[62] Ames P, Hunter S, Parkinson JS. Evidence for a Helix-Clutch Mechanism of Transmembrane Signaling in a Bacterial Chemoreceptor. J Mol Biol. 2016.

[63] Appleman JA, Chen LL, Stewart V. Probing conservation of HAMP linker structure and signal transduction mechanism through analysis of hybrid sensor kinases. J Bacteriol. 2003;185:4872-82.

[64] Zhu Y, Inouye M. Analysis of the role of the EnvZ linker region in signal transduction using a chimeric Tar/EnvZ receptor protein, Tez1. J Biol Chem. 2003;278:22812-9.

[65] Mondejar LG, Lupas A, Schultz A, Schultz JE. HAMP domain-mediated signal transduction probed with a mycobacterial adenylyl cyclase as a reporter. J Biol Chem. 2012;287:1022-31.

[66] Moglich A, Ayers RA, Moffat K. Design and signaling mechanism of light-regulated histidine kinases. J Mol Biol. 2009;385:1433-44.

[67] Wang B, Zhao A, Novick RP, Muir TW. Activation and inhibition of the receptor histidine kinase AgrC occurs through opposite helical transduction motions. Mol Cell. 2014;53:929-40.

[68] Samanta D, Borbat PP, Dzikovski B, Freed JH, Crane BR. Bacterial chemoreceptor dynamics correlate with activity state and are coupled over long distances. Proc Natl Acad Sci U S A. 2015;112:2455-60.

CHAPTER 3

Structural and functional analyses of PAS domains from the *Vibrio cholerae* Aer2 receptor

3.1 Abstract

Vibrio cholerae Aer2 (VcAer2) is a soluble receptor that is homologous to *Pseudomonas aeruginosa* Aer2 (PaAer2). VcAer2 contains two tandem heme-binding PAS domains, namely VcPAS1 and VcPAS2, following by two continuous HAMP domains and a kinase control domain. The sequence alignment and biophysical studies indicate the high similarities in both sequence and O_2-binding affinity of VcPAS2 to PaAer2 PAS (PaPAS). In addition, the 1.65 Å-resolution crystal structure of the ligand-free VcPAS2 W276L represents the conserved PAS fold that is highly similar to that of PaPAS. The Trp276 locates in the Iβ strand at the C-terminal region of the PAS domain, and is a conserved residue that is crucial for O_2-binding stability in VcPAS2 and PaPAS. Surprisingly, the ligand-free VcPAS2 W276L shows the higher similarity in the structural arrangement with the CN^--bound PaPAS, especially at the Iβ strand, which propagates signals to the downstream HAMP domains. Unlike VcPAS2 and PaPAS, the Iβ Trp is not required for stabilizing O_2-binding in VcPAS1. The VcPAS1 homology model suggests that it may adopt a different O_2-ligation mechanism, which contributes to higher O_2-binding stability compared to VcPAS2 and PaPAS. As a PaAer2 homolog, VcAer2 can serve as a promising system to investigate the signal transduction mechanism of multi-domain receptors.

3.2 Introduction

Microorganisms utilize modular proteins in signal transduction. Multi-component proteins often initiate signaling cascades and transduce information within the cell to properly respond to environmental changes. Found in over 99,000 proteins [1], Per-ARNT-Sim (PAS) domains are widespread components of modular signaling proteins [2-4]. They were originally identified as homologous regions of *Drosophila* period (Per) and single-minded (Sim), and the vertebrate aryl hydrocarbon receptor nuclear transporter (ARNT) [5-7]. PAS domains serve as universal signal sensors and they regulate diverse processes [2, 4]. Although sharing relatively low sequence identity overall [8, 9], PAS domains are highly conserved at the structural level. The canonical PAS domain comprises of a central five-stranded antiparallel β-sheet and several flanking α-helices [2, 4]. In bacteria, PAS domains are often found in conjunction with other signaling domains, including: sensory input (GAF), signal relay (HAMP), and output (histidine kinase, GGDEF, and kinase control module (KCM) of methyl-accepting chemotaxis proteins) [2, 4, 10-12].

Heme proteins are one of the most studied metalloenzymes. They regulate a variety of functions ranging from catalysis, electron transfer, O_2 transport and storage to signaling [13, 14]. Recently, heme-based sensors have emerged as a new protein family that functions to detect diatomic gases (O_2, CO and NO) [15-20]. Heme proteins adopt various folds, such as globin, GAF, H-NOX and PAS, to accommodate the heme cofactor [21-23]. In all cases the binding of diatomic gases to the heme iron triggers conformational changes around the porphyrin molecule [16, 21-27].

Importantly, PAS domains will also bind the heme cofactor, which serves to initiate signaling events in response to diatomic gases.

In bacteria and archaea, heme-containing PAS domains often mediate O_2 sensing. In the well-studied example of *Rhizobium*, FixL, an O_2-sensing protein kinase, a heme-containing PAS domain acts as a sensor domain [3, 13, 17, 28, 29]. Under low O_2 condition, FixL phosphorylates its response regulator FixJ, which in turn activates the expression of genes such as NifA and FixK, which are involved in nitrogen fixation and respiration [30-33]. In another example, EcDOS is a heme-containing PAS protein in *E. coli* that acts as a direct O_2 sensor [18, 19, 29, 34, 35]. EcDOS contains two N-terminal PAS domains, a FixL-like heme-containing PAS-A and a heme-free PAS-B, followed by a C-terminal phosphodiesterase domain [19, 35]. Several studies have shown that EcDOS senses environmental O_2 concentrations and responds by modulating the cellular cAMP levels, which in turn regulates transcription of related genes [19, 36].

How PAS domains communicate with other modules to mediate signal transduction remains an active area of research. Several PAS-containing sensor proteins couple with HAMP and KCM domains to mediate aerotaxis, a term describing the movement of cells toward preferred O_2 concentrations or redox condition [26, 27, 37-41]. *E. coli* Aer (EcAer) is an integral membrane protein with an FAD-binding PAS domain coupled with HAMP and KCM domains (Figure 3-1) [40, 42, 43]. Rather than directly sensing O_2 levels, EcAer responds to changes in the electron transport chain (ETC) via its effect on the redox state of its FAD cofactor. ETC activity then serves as a proxy for O_2 availability and allows EcAer to monitor

the internal energy levels of cells [37, 40, 44, 45]. There are substantial details regarding the mechanism of EcAer signaling. The EcAer PAS domain directly interacts with the HAMP domain [26, 43]. Cysteine crosslinking experiments have shown that the PAS-HAMP interaction is loosened when the ambient O_2 concentration is below the requirement for maintaining the electron transport system [41]. Under this condition, the FAD Aer PAS domain is reduced, causing the reorientation of the N-cap and the conformational change of the β-scaffold of the PAS domain that is in contact with the AS2 helix of the HAMP domain [26, 38]. These conformational changes destabilize the PAS-HAMP interaction, which allow the HAMP domain to be more dynamic, and subsequently lead to a kinase-on output. In an aerobic environment, the FAD is oxidized, and the PAS domain undergoes structural reorientations that strengthen the PAS-HAMP interaction [26, 41], causing the HAMP domain to be more static and produce a kinase-off output [41]. Unfortunately, high-resolution structural information on these conformational changes is still unavailable due to the transmembrane nature of EcAer.

Pseudomonas aeruginosa Aer2 (PaAer2) is a soluble receptor that is comprised of poly-HAMP, heme-binding PAS, tandem HAMP and KCM domains (Figure 3-1 and 3-2) [25, 46]. The biological function of PaAer2 is still unclear. When expressed in *E. coli*, however, PaAer2 is able to interact with the chemotaxis system in the host cells to mediate the response to diatomic gases [46]. Recently, PaAer2 has emerged as a promising system to probe PAS-HAMP interaction due to the availability of the crystal structures of the PaPAS with unligated ferric and cyanide (CN^-)-bound heme [16, 25]. The structural comparison reveals ligand-induced

rearrangements of the core β-sheet and the Aα helix, and identifies Trp283 in the Iβ strand as the CN^--ligating residue [16, 25]. Unlike EcAer, PaPAS and poly-HAMP do not directly interact [25]. PaAer2 is most likely to utilize an in-line signaling mechanism, wherein structural changes in PaPAS are relayed through the PAS-HAMP junction to the KCM domain [25].

Vibrio cholerae Aer2 (VcAer2) is a homolog of PaAer2. VcAer2 is a soluble receptor composed of two tandem N-terminal PAS domains (VcPAS1 and VcPAS2), following by two continuous HAMP domains and a KCM domain (Figure 3-1 and 3-2) [47]. Biochemical studies have shown that the PaPAS and VcPAS2 domains possess comparable affinities to O_2. O_2 ligation in VcPAS2 is facilitated by hydrogen bonding with the conserved Trp276 in the Iβ strand, as observed in PaAer2. Amino-acid substitution at the conserved Trp residue (W276L) reduced O_2-binding stability of the VcPAS2 domain. In contrast, VcPAS1 has higher affinity to O_2 compared to VcPAS2 and PaPAS, and surprisingly, the Iβ Trp residue (Trp151) is not required for VcPAS1 to stabilize O_2 binding. In this study, the crystal structure of the ferric-form of VcPAS2 W276L was determined at 1.65 Å resolution. VcPAS2 maintains the conserved PAS fold. However, the otherwise conserved Aα helix is absent from the structure. VcPAS2 W276L has an overall arrangement of secondary-structure elements similar to PaPAS, but a detailed structure that is more similar to the CN^--bound PaPAS than the analogous ferric form. As a PaAer2 homolog, VcAer2 may serve as a useful, alternative system for investigating PAS-HAMP mediated signal transduction.

3.3 Materials and methods

Cloning and mutation

The DNA encoding full-length VcAer2 was received from Kylie Watts (Loma Linda University). VcAer2 was initially cloned into pProEx. Various fragments of the gene encoding the PAS domains, including VcPAS1-2 (1-282 and 38-282), VcPAS1 (1-157 and 38-157) and VcPAS2 (165-282), were individually amplified using PCR, and subcloned into pET28a vector between NdeI and XhoI restriction sites. Two tryptophan substitutions were introduced to the VcAer2 PAS domains by using the overlap extension methodology [48]: W151L in VcPAS1 (38-157) and W276L in VcPAS2,.

Protein expression and purification

All of the proteins were expressed in *E. coli* BL21(DE3). cells *E. coli* ferrochelatase was co-expressed to promote full heme incorporation in the PAS domain [49]. Protein expression was induced under 0.4 mM isopropyl β-D-1-thiogalactopyranoside (IPTG) at 37°C for 16 hours. Protein purification was carried out using Ni-NTA affinity chromatography under the manufacturer's protocols (QIAGEN).

WT VcPAS1 (38-157), VcPAS1 W151L (38-157), WT VcPAS2, and VcPAS2 W276L were extracted from *E. coli* cells by means of sonication, and were eluted from the Ni-NTA in an elution buffer (10 mM Tris pH 8.0, 500 mM NaCl, 10% glycerol and 250 mM Imidazole pH 8.0). The eluted proteins were subjected to buffer exchange into 20 mM imidazole pH 8.0 and 100 mM NaCl before overnight digestion

with thrombin (0.7 μg/ml). The tag-free proteins were further purified using a Superdex 75 26-60 size exclusion column, and eluted in 20 mM imidazole pH 8.0 and 100 mM NaCl.

Crystallization and data collection

Crystals of VcPAS2 W276L protein (12 mg/ml) were grown using the vapor diffusion method by mixing 1 μl of protein with 1 μl of well solution against a reservoir containing 2.6 M $(NH_4)_2SO_4$, 0.1 M citric acid pH 5.5. The solution of $NiCl_2$ added directly to the protein-well solution mixture (final concentration 10 mM) to influence crystallization and promote better diffraction.

The crystals were tested for diffraction at the Cornell High Energy Synchroton Source (CHESS) at the A1 beamline. Only crystals of VcPAS2 W276L diffracted, and the diffraction data were collected at the same beamline on an ADSC Quantum 210 CCD detector. Data was processed using HKL2000 [50].

Structural determination

The structure of VcPAS2 W276L in the ligand-free form was determined by molecular replacement on PHENIX AutoMR using the CN^--bound PaPAS structure (PDB code: 3VOL) as a model. The structure was built using Coot [51], and refined in PHENIX [52] amid manual model building, minimization, *B*-factor refinement, and non-crystallographic symmetry to generate the final model.

Structural analysis and homology modeling

Homology models were generated for the wild type VcPAS1 (residue 38-157) and wild type VcPAS2 based on the VcPAS2 W276L structure using SWISS-MODEL [53]. A *b* heme molecule was included into the VcPAS1 homology model by manually superimposing heme-containing VcPAS2 onto the VcPAS1 homology model and incorporating the positioned heme group into the VcPAS1 model. A similar heme-ligation pattern was maintained to that observed in the VcPAS2 W276L structure.

3.4 Results

Characterization of VcPAS domains

The *V. cholerae* genome sequence reveals three putative *aer* gene homologs, designated *aer1*, *aer2*, and *aer3* [47]. VcAer2 (VCA1092) is a homolog of PaAer2, a putative diatomic-gas sensor in *Pseudomonas aeruginosa* [46]. The physiological functions of VcAer2 has not been characterized. However, VcAer2 is a heme-containing soluble protein (Figure 3-1) that mediates responses to O_2 (Table 3-1).

VcAer2 contains two tandem N-terminal PAS domains (VcPAS1 and VcPAS2) followed by two continuous HAMP domains (HAMP1 and HAMP2), and then a kinase control domain that also contains an adaptation region (Figure 3-1 and 3-2). Adaptation regions in chemoreceptors undergo reversible methylation reactions on conserved Glu residues in a feedback response mechanism. Based on the sequence alignment, VcPAS1 and VcPAS2 are predicted to maintain the universal PAS fold with the core domain composed of the five-stranded antiparallel β sheet, surrounded by loops and α-helices (Aα, extended Cα/Dα, Eη, and Fα). The two VcPAS domains

share 37.8% sequence similarity to each other, and VcPAS2 has higher sequence similarity with PaPAS (35.3%) compared to VcPAS1 (33.6%) (Figure 3-3).

VcPAS domains have different affinities for *in vitro* O_2 binding. The isolated VcPAS2 and PaPAS domains showed comparable O_2 affinities with the dissociation constants (K_d) of 17 μM and 16 μM, respectively. VcPAS1, however, has approximately higher affinity for O_2 (K_d 12 μM) (Table 3-1) (Kylie Watts, unpublished data). In the context of the receptor, VcAer2 without the VcPAS1 domain (VcAer2 ΔPAS1) had lower O_2 affinity (K_d 20 μM) than the isolated VcPAS1 or VcPAS2. The affinities for O_2 confirm the higher similarities between PaPAS and VcPAS2. Interestingly, VcAer2 could mediate responses to O_2 even when VcPAS1 lacked a heme molecule (Kylie Watts, unpublished data), suggesting that VcPAS2 may serve as an O_2 while VcPAS1 may play a role as a VcPAS2 regulator.

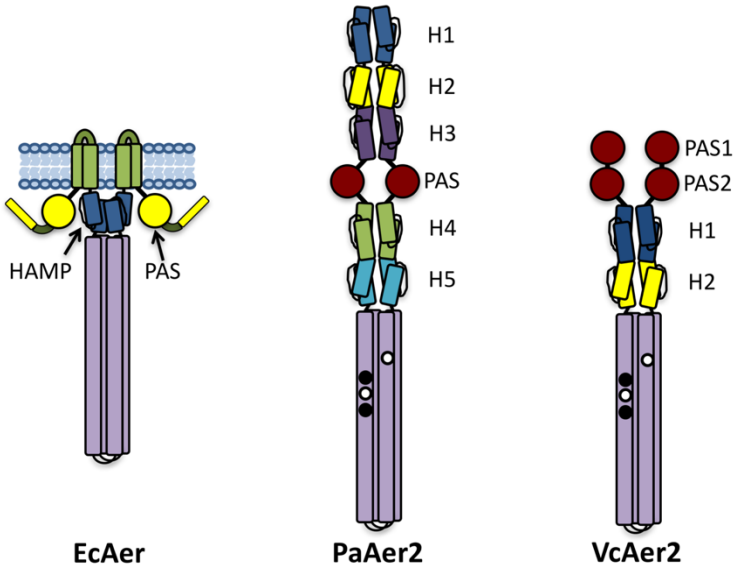

Figure 3-1 Schematic representations of the aerotaxis receptors (EcAer and VcAer2), and a canonical diatomic-gas receptor (PaAer2). The α helices are depicted as cylinders. PAS domains are represented as circles. The linkers are shown as lines. EcAer2 is a transmembrane receptor, whereas PaAer2 and VcAer2 are cytoplasmic receptors. Abbreviations used: EcAer: *E. coli* Aer; PaAer2: *P. aeruginosa* Aer2; VcAer2: *V. cholera* Aer2

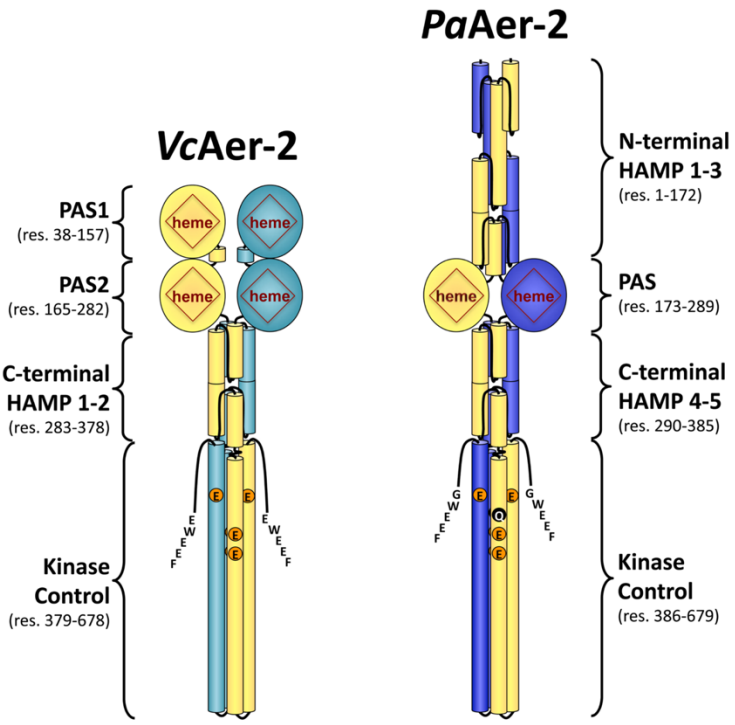

Figure 3-2 Schematic diagrams of the domain architectures of VcAer2 compared to PaAer2. VcAer2 is homologous to PaAer2. Each receptor is composed of three main domains, including heme-binding PAS, HAMP and kinase control domains. VcAer2 contains two continuous PAS domains (PAS1 and PAS2), two HAMP domains (HAMP1 and HAMP2), following by a kinase control domain containing substrate Glu residues for the adaptation system similar to those found in methyl-accepting chemotaxis receptors. The domain architecture of PaAer2 is highly similar to VcAer2 except for the extra three HAMP domains (HAMP1-3) at its N-terminus and only one PAS domain instead of two. The α helices, PAS domains, and linkers are represented as cylinders, circles, and lines, respectively. The residue numbers for each domain are as depicted.

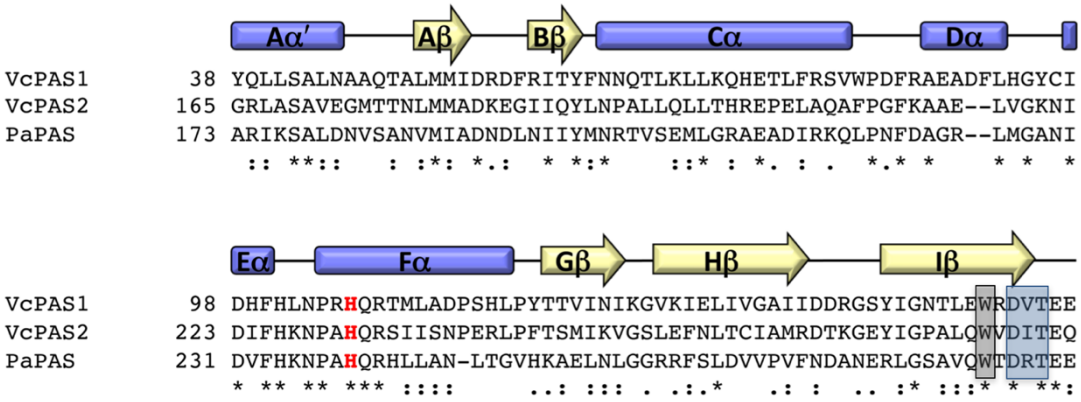

Figure 3-3 Sequence alignment of VcPAS1, VcPAS2 and PaPAS with secondary-structure elements above. The three PAS domains share the identical secondary structure as well as key residues for heme and ligand binding. The proximal heme-coordinating His residues are shown in red. The distal ligand-stabilizing Trp residues are highlighted in the grey box, and the C-terminal DxT motifs are highlighted in the blue box.

Table 3-1 PAS-heme O_2 affinities (Kylie Watts, unpublished data)

PAS domains	O_2-dissociation constant (K_d, μM)
PaPAS	16
VcPAS1	12
VcPAS2	17
VcAer2 ΔPAS1	20
VcPAS1 W151L	17

Crystal structure of VcPAS2 W276L

The structure of VcPAS2 W276L with a ferric (Fe(III)) heme was determined to 1.65 Å resolution (Table 3-2). VcPAS2 W276L maintains the highly conserved PAS fold with several features similar to that of PaPAS (Figure 3-4A and 3-5). First, the core of the PAS domain consists of Aβ, Bβ, Hβ and Iβ. Second, VcPAS2 W276L also contains the extended helix of Cα/Dα with a kink at Arg201 (Ala209 in PaAer2). Third, the Eα helix distorts into Eη, which is actually a 3_{10} helix. Forth, the highly conserved His residue in the Fα helix (His231 in VcPAS2 and His239 in PaPAS) does not serve as a heme-ligating residue as in FixL and EcDOS [17-19, 29, 54, 55]. Rather, the His226 on the Eη helix of VcPAS2 (His234 in PaPAS [16, 25]) is the proximal heme ligand (Figure 3-6). Indeed, the role of H226 in coordinating the heme cofactor was confirmed by the H226A substitution, which substantially lowered the heme-binding capability of VcPAS2 (Kylie Watts, unpublished data).

Despite the overall relatedness of VcPAS2 W276L to PaPAS, there are also some significant structural differences. VcPAS2 W276L contains an additional 3_{10} helix between the Fα helix and the Gβ strand. While the N-terminus of PaPAS forms a helix (Aα) [16, 25], that of VcPAS2 W276L is unstructured. In fact, the electron density of the first five residues of VcPAS2 W276L is not apparent in the crystal structure, which may relate to the absence of α-helical structure at the N-terminus. In addition, VcPAS2 W276L forms an antiparallel dimer in the crystallographic asymmetric unit with extensive β-β contacts (Figure 3-4B). On the contrary, PaPAS forms a parallel dimer mediated by the Aα helices and the β-sheets [25]. Therefore,

the unstructured nature at the N-terminus of VcPAS2 W276L may contribute to its antiparallel dimerization (Figure 3-4B).

Both VcPAS2 and PaPAS contain *b*-type hemes that bind into a hydrophobic pocket of non-polar side chains. For PaPAS, His251 in the Gβ strand forms a hydrogen bond with the 7-propionate of the heme [16, 25]. However, VcPAS2 contains Phe (Phe244) instead of His at this position. However, VcPAS2 His231 may compensate for the loss of His at position 244, as His231 shifts in closer to the heme propionate than its counterpart, His239, in PaPAS (Figure 3-6).

Table 3-2 Data collection and refinement statistics

Wavelength (Å)	0.97720
Resolution range	50 - 1.65 (1.709 - 1.65)
Space group	P 3_2 2 1
Unit cell dimensions	
a, b, c (Å)	62.51, 62.5, 157.024
α, β, γ (°)	90, 90, 120
Total reflections	43,583
Unique reflections	4,170
Completeness (%)	99.18
Wilson B-factor	24.3
R-work	0.2008 (0.3377)
R-free	0.2209 (0.3681)
Number of non-hydrogen atoms	3018
Macromolecules	2589
Ligands	129
Protein residues	339
RMS(bonds)	0.01
RMS(angles)	1.4
Ramachandran favored (%)	97
Ramachandran allowed (%)	2.4
Ramachandran outliers (%)	0.3
Rotamer outliers (%)	1.4
Clashscore	3.48
Average B-factor	31.0
Macromolecules	30.5
Ligands	25.1
Solvent	38.2

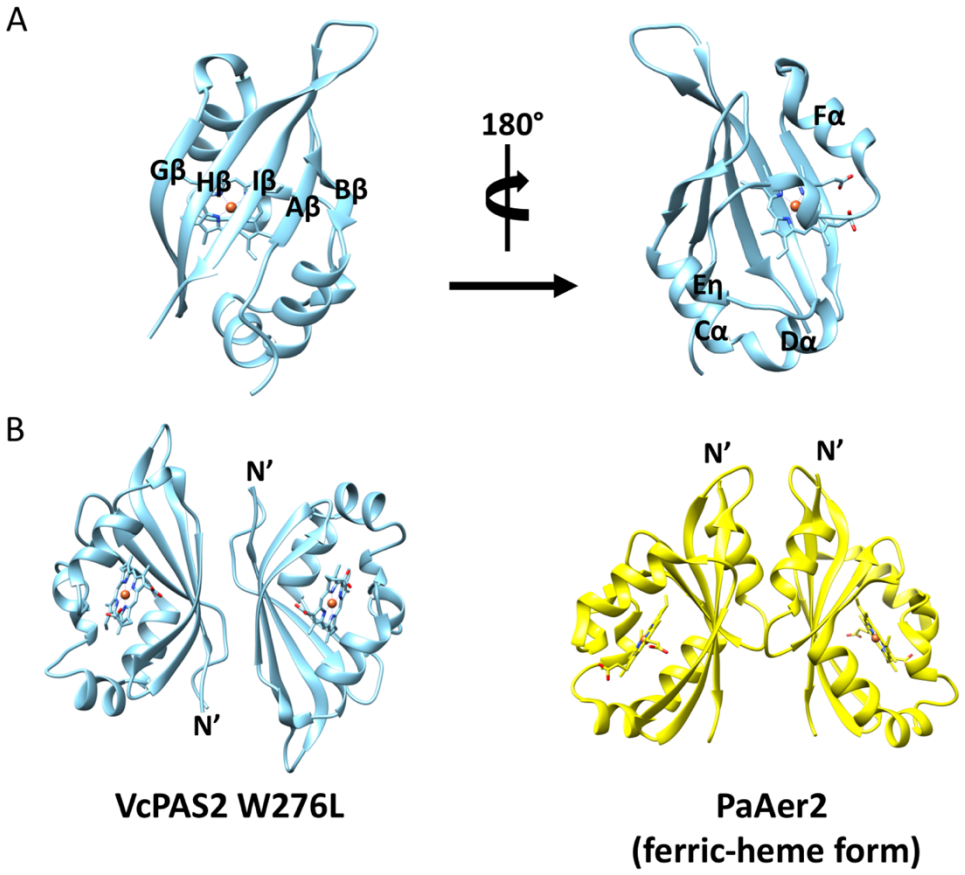

Figure 3-4 Crystal structure VcPAS2 W276L.

(A) The structure of VcPAS2 W276L with ferric heme bound. The protein maintains the canonical PAS fold with the five-stranded antiparallel β sheet composed of Aβ, Bβ, Gβ, Hβ, and Iβ strands. The PAS core is flanked by several α helices, denoted Cα, Dα, Eη and Fα. The conserved N-terminal Aα (also known as N-terminal cap) is disordered in the structure.

(B) The ferric VcPAS2 W276L forms an antiparallel dimer in the crystallographic asymmetric unit with the β sheets at the interface. In contrast, the ferric-heme containing PaPAS2 forms a parallel dimer in the crystal lattice with extensive contacts between the Aα helices and β sheets.

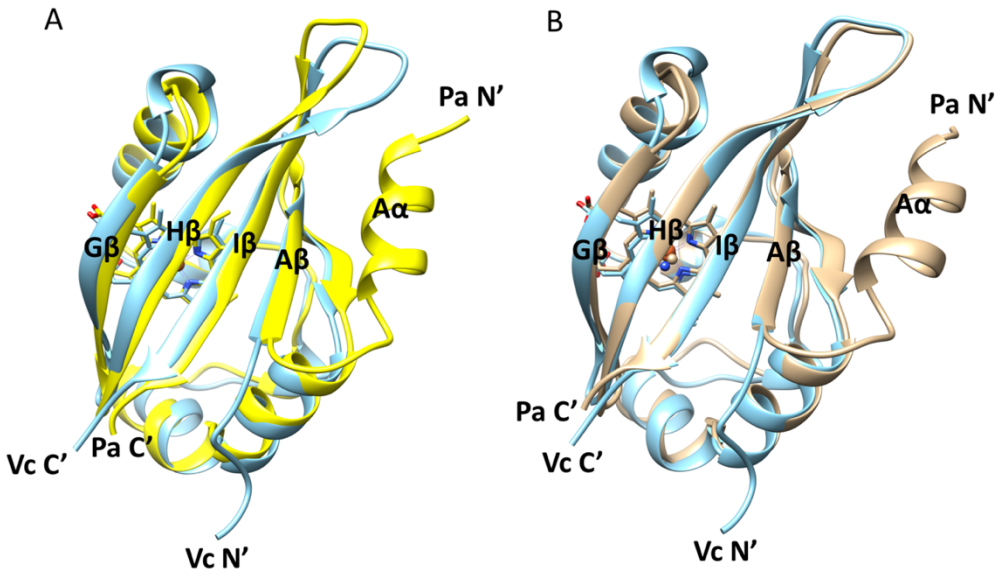

Figure 3-5 Structural comparisons of the VcPAS2 W276L and PaPAS domains

(A) Superposition of VcPAS2 W276L (blue) and PaPAS in the ferric-heme form (PDB code 4HIH, yellow)

(B) Superposition of VcPAS2 W276L (blue) and PaPAS in the CN^-bound form (PDB code 3VOL, khaki)

The structures of the VcPAS2 W276L and both PaPAS domains share high similarity within the PAS β- sheet core and flanking helices. VcPAS2 W276L lacks the N-terminal Aα helix, which is replaced by an unstructured linker. The secondary elements are as indicated. The N- and C- termini of the PaPAS domain are labelled as Pa N'and Pa C', respectively. Those of VcPAS2 W276L are labelled as Vc N'and Vc C'.

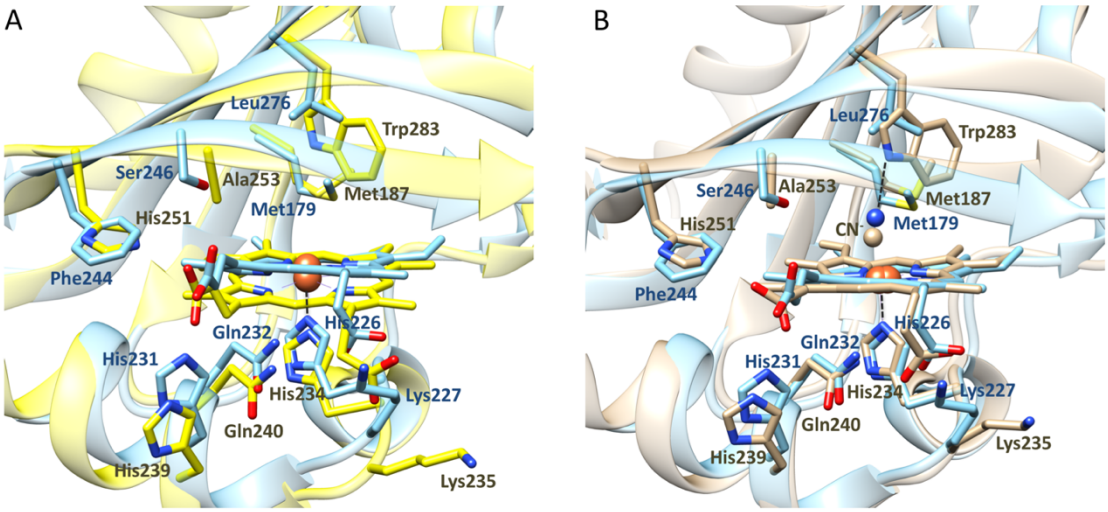

Figure 3-6 Residue alignment in the heme-binding pockets of VcPAS2 and PaPAS.

(A) Superposition of the heme-binding pockets of VcPAS2 W276L (blue) and PaPAS in the ferric-heme form (PDB code 4HIH, yellow).

(B) Superposition of the heme-binding pockets of VcPAS2 W276L (blue) and PaPAS in the CN-bound form (PDB code 3VOL, brown)

The conserved His residues on the Eη helix, namely VcPAS2 His226 and PaPAS His234, act as the proximal heme ligands. Key residues from VcPAS2 W276L are listed in blue, and those from PaPAS are listed in brown.

Consequences of Trp substitution in the distal ligand binding pocket.

The C-terminal Trp residue resides in the distal-heme pocket generated by the Iβ strand, and is conserved between PaPAS (Trp283) and the two VcPAS domains (Trp151 in VcPAS1 and Trp276 in VcPAS2) (Figure 3-3). The resonance Raman and mutagenesis studies indicate that PaPAS utilizes Trp283 to interact with heme-bound O_2 [16]. Mutational studies in VcPAS2 also indicated that the Trp residue was necessary for stabilizing O_2 binding as the VcPAS2 W276L mutant failed to form a stable complex with O_2. However, the Trp substitutions did not affect CO binding in both PaPAS and VcPAS2 (Kylie Watts, unpublished data), which suggests that a distal hydrogen bond to CO is not important for stable CO ligation.

VcPAS2 W276L was crystalized in the ferric form. However, the overall structural arrangement of the ligand-free VcPAS2 W276L is more similar to the CN^--bound PaPAS, especially at the C-terminus, which aligns almost perfectly with that of the cyanide-bound PaPAS (Figure 3-5). The displacement of the Iβ strand at the C-termini of PaPAS is observed when the domain binds to CN^-, which is caused by the rotation of Trp283 [25]. This spatial arrangement of the Iβ strand is crucial for PaAer2 signal transduction because this element connects directly to the downstream HAMP domain [16, 25]. Therefore, the W276L mutation might mimic the ligand-bound state of the VcPAS2 domain.

Structure and function of VcPAS1

The homology model for the wild type VcPAS1 was created by threading the VcPAS1 sequence (residue 38-157) onto the VcPAS2 W276L using SWISS-MODEL. As expected, the VcPAS1 domain shows the conserved PAS fold as observed in VcPAS2, which reflects their high sequence identity (Figure 3-3). VcPAS1 is composed of the antiparallel five-stranded β-sheet and the flanking α-helices. Similar to VcPAS2, the VcPAS1 N-terminus, which is expected to form an α-helix based on the sequence alignment (Figure 3-3), appears unstructured (Figure 3-7A).

In addition to the secondary-structure organization, the heme-binding pockets of VcPAS1 and VcPAS2 also show high similarity for the proximal heme-ligating residue (His101 in VcPAS1 and His226 in VcPAS2) and distal ligand-coordinating residue (Trp151 in VcPAS1 and Trp 276 in VcPAS2) (Figure 3-7). In VcPAS2, His231 in the Fα helix forms a hydrogen bond with the 7-propionate of the heme (Figure 3.6B). Likewise, VcPAS1 His106 in the Fα-helix acts as a hydrogen donor to the 7-propionate of the heme (Figure 3-7).

In VcPAS2, Gln232 in the Fα helix and Lys227 in the upstream linker are most likely key residues for coordinating the 6-propionate of the heme. The Fα-helix Gln residue is conserved between VcPAS and PaPAS domains, suggesting its role in coordinating the heme cofactor is similar (Figure 3-3). However, VcPAS1 lacks a hydrophilic residue analogous to Lys227 in the upstream linker and instead has Leu102 at this position (Figure 3-7). Therefore, the heme coordination at the 6-propionate in VcPAS1 is most likely mediated by the Gln107 or Tyr119.

The Iβ Trp residues are conserved in VcPAS1 and VcPAS2 (Figure 3-3), and reside at analogous sites in the distal ligand-coordinating pocket (Figure 3-6B and 3-7B). In contrast to VcPAS2 and PaPAS, the Iβ Trp (Trp151) is not essential for O_2-binding stability. Substitutions of this Trp do not affect O_2 binding as most of Trp151 mutants have comparable affinities to O_2 with the wild type (Table 3-3) (Kylie Watts, unpublished data). It is possible that other residues contribute to O_2-binding stability in VcPAS1.

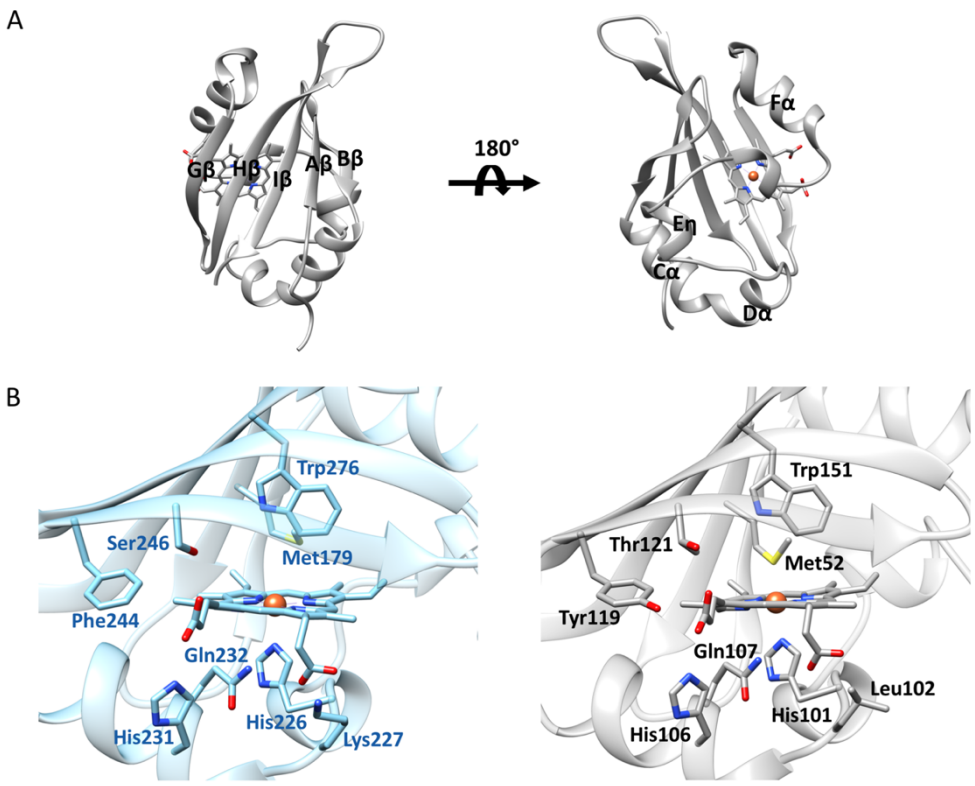

Figure 3-7 Homology model of VcPAS1

(A) VcPAS1 homology model. The model was generated by SWISS-MODEL using the VcPAS2 W276L as a template and the wild type sequence of VcPAS1. The secondary elements are as indicated. VcPAS1 shows the conserved PAS fold with the five-stranded antiparallel β-sheet and the flanking helices as observed in the VcPAS2 W276L structure.

(B) The heme-binding pockets of VcPAS2 (blue) and VcPAS1 (grey). The hypothetical position of the Trp276 residue in VcPAS2 was obtained by threading the wild type sequence of VcPAS2 onto the VcPAS2 W276L structure using SWISS-MODEL.

Table 3-3 O_2-binding affinities of VcPAS1 Trp151 variants (Kylie Watts, unpublished data)

PAS domains	O_2-dissociation constant (K_d, μM)
VcPAS1 WT	12
W151C	15
W151F	14
W151G	11
W151L	17
W151S	10
W151T	10
W151V	13

3.5 Discussion

The VcPAS W276L structure maintains the conserved PAS fold with high similarity in the arrangement of secondary-structure elements with the PAS domain from PaAer2. VcPAS2 W276L contains the *b*-type heme in the ferric form with the heme-ligating residues similar to, although not identical, to those of the PaPAS.

The role of PAS domains in aerotaxis and the PAS-HAMP interaction have been studied extensively in Aer, an integral membrane protein from *E. coli* [26, 27, 37, 38, 40, 41, 44, 45, 56-58]. Recently, PaAer2 has emerged as a promising system for PAS-HAMP signal transduction due to its solubility and availability of high-resolution structures [16, 25, 46]. PaAer2 mediates repellent responses to O_2, NO, and CO when expressed in *E. coli* [46]. As VcAer2 is a PaAer2 homolog, it can potentially serve as an alternative to investigate PAS-HAMP mediated signal transduction.

Crystallographic oligomeric state of VcPAS2 W276L

PAS domains are known to form dimers and higher-order oligomers through hydrophobic patches on the outer surfaces of their β-sheet scaffolds and/or α-helices [4]. The oligomerization modes of PAS domains can vary [4, 59]. Several PAS domains are present as parallel dimers with N-termini from each monomer forming close contacts [18, 60-62]. On the other hand, various PAS domains are found to form antiparallel dimers [63-65] or adopt intermediate orientations [59, 66], which suggests that PAS-subunit interfaces can readily evolve into different configurations [4]. Even though the majority of PAS domains form homo-oligomers, several PAS domains from eukaryotes, such as *Neurospora crassa* white-collar proteins, can form hetero-oligomers [4, 67].

VcPAS2 W276L produces an antiparallel dimer in the crystallographic asymmetric unit with the β-sheets forming the contact interface. This dimerization pattern is different from the other heme-containing PAS domains, such as those from *P. aeruginosa* Aer2 [25], *Rhizobium meliloti* FixL [68], and *E. coli* DOS [18, 69], which have been crystallized as parallel dimers. The antiparallel dimerization of the VcPAS2 W276L domain suggests that this assembly mode is the most stable for the isolated domain. However, this state may not reflect the physiological oligomeric state of the VcAer2 because the other domains may well influence the overall oligomeric state of the protein. In addition, the absence of the Aα helix at the N-terminus may contribute to the antiparallel dimerization of VcPAS2 W276L (Figure 3-4). Nevertheless, the crystal structure confirms the variable nature of PAS domain interfaces [4].

Conformational changes associated with the substitution of the Iβ Tryptophan

Structural studies of various PAS-containing signaling proteins have revealed rearrangements of PAS subunits in response to conformational propagation from the cofactor binding pocket as the mechanism of signal transductions [4]. The crystal structures of the PAS domain from PaAer2 emphasizes the common themes for ligand-induced conformational changes [16, 25]. The structural comparison between the ligand-free and CN^--bound PaPAS signifies a crucial role of Trp283 in sensing and coordinating diatomic gases. Trp283 resides in the C-terminal region of the Iβ strand in the distal heme-binding pocket, and forms a hydrogen bond with a coordinated diatomic ligand [16, 25]. The hydrogen bond between the indole group of Trp283 and the bound CN^- cause the rotation of Trp283 by approximately 90°, which subsequently displaces the DxT motif at the very C-terminus of the PaPAS domain and leads to substantial changes at the junction between the PAS domain and downstream HAMP domain [25].

The Iβ Trp is conserved among PaPAS, VcPAS1 and VcPAS2. The Trp substitution with Leu destabilizes O_2 binding in both PaPAS and VcPAS2, but not VcPAS1. Based on the structural and functional similarities between PaPAS and VcPAS2, the tertiary structural arrangement of the VcPAS W276L should be more similar to that of the PaPAS in the ferric heme form, especially at the C-terminal DxT motif, as it is crucial for the PAS-to-HAMP signal relay. The structural alignment indicates a higher positional similarity of the DxT motif of VcPAS2 W276L to that of PaPAS in the CN^--bound form than the ferric form. Indeed, the overall organization of the secondary-structure elements of the ligand-free VcPAS2 W276L is very similar to

that of the CN-bound PaPAS (Figure 3-5). Therefore, the W276L mutation might mimic the ligand-bound state of VcPAS2. Structural comparison of VcPAS2 in both ferric and ligand-bound forms will be needed to unravel its ligand-induced conformational changes.

PAS-HAMP signaling mechanism of VcAer2

How multiple PAS domains in one signaling protein interact and integrate signals is still poorly understood. In VcAer2, one major difference between VcPAS1 and VcPAS2 is the requirement of the Iβ Trp for O_2-binding in the latter. The Iβ Trp in the distal heme-binding pocket is critical for ligating O_2 in both PaPAS and VcPAS2. In VcPAS2, the Trp276 residue stabilizes O_2 binding. On the contrary, most of the Trp151 substitutions in VcPAS1 did not affect the O_2-binding affinity. This evidence suggests that other residues in VcPAS1 play a role in O_2 stabilization. Potential O_2-stabilizing residues include Met52, Leu112, and Leu132, which all locate in the distal heme-binding pocket.

The roles of Met and Leu in O_2 binding has been extensively studied in other systems. RbcL2, a form III Rubisco in *Archaeoglobus fulgidus*, possess an unusually high affinity to O_2 [70]. Mutational studies have attributed this high affinity in part to interactions supplied by Met295, which composes a hydrophobic pocket along with other residues in the active site. Met295 is in close proximity to the highly conserved Arg275, which participates in substrate (RuBP) binding site. Substitution of Met295 lowers the affinity of the enzyme to O_2. In another example, mutational studies have shown that Leu16, which locates in the distal heme-binding pocket of *Alcaligenes*

xylosoxidans cytochrome c', is crucial for diatomic gas binding and ligand discrimination [70].

As the O_2-binding affinity of VcPAS1 is higher compared to VcPAS2 and PaPAS, the arrangement of residues in the heme-binding pocket of VcPAS1 may be different from those of VcPAS2 and PaPAS. In the VcPAS1 homology model, Met52 Leu112, and Leu132 are in close proximity to Trp151, and thus they may have a role in stabilizing O_2-binding. High-resolution structures and functional studies will be valuable in elucidating the O_2-binding stabilization mechanism of VcPAS1.

In several tandem PAS-containing signaling proteins, only one PAS domain serves as the sensor module [17-19, 33, 71]. Tlp3, the isoleucine receptor in *Campylobacter jejuni*, contains two periplasmic PAS domains [72]. The crystal structure of Tlp3 reveals two isoleucine-binding sites in the membrane-distal PAS but not in the membrane-proximal PAS [71]. The structural analysis suggests that the distal PAS adopts the closed form once bound to isoleucine, and induces the proximal PAS to be in the open form, which creates a piston displacement of the transmembrane helix, thus initiating the signal transduction cascade [71]. Similar to Tlp3, FixL and EcDOS are comprised of two tandem PAS domains with only one domain binding to heme, which thus exclusively functions as a sensor. In case of VcAer2, VcPAS1 has two-fold higher affinity to O_2 compared to VcPAS2. The deletion of VcPAS1 lowered the O_2 affinity of the VcAer2 receptor substantially (Table 3-2). However, VcAer2 can respond to O_2 when VcPAS1 does not bind to a heme molecule. This evidence suggests that VcPAS2 serves as a main O_2 sensor for VcAer2 while VcPAS1 functions as a regulator for VcPAS2. However, the higher O_2-binding affinity of

VcPAS1 implies that the domain might be necessary for sensing O_2 over a larger range of concentration.

One of the common themes in PAS signal transduction is the coexistence of PAS with other domains in a single modular signaling protein [2, 4]. To date, there are two models for PAS-HAMP signaling mechanisms. The EcAer adopts the lateral interaction between the PAS and HAMP domains, and follows a static-to-dynamic model to control aerotaxis [26, 41, 43]. When the PAS FAD is oxidized, the PAS β-scaffold directly interacts with the second helix of HAMP (AS2), enforcing the HAMP domain to be static and thus leading to a kinase-off output. The PAS-HAMP interaction is loosened when the PAS FAD is reduced, causing the HAMP domain to be dynamic, and resulting in a kinase-on output [26, 41]. On the other hand, PaAer2 does not utilize the direct PAS-HAMP interaction for interdomain communication. Rather, PaAer2 represents an in-line mechanism for PAS-HAMP interplay in which the signals induced by PAS structural changes are relayed to the downstream HAMP domain (HAMP4) [25].

It is still unclear how the signals generated by VcPAS domains are transduced to the HAMP and KCM domains. However, since VcAer2 and PaAer2 share the highly similar domain architectures, it is possible that VcAer2 also adopts the in-line signal transduction mechanism. In this case, O_2-induced structural changes in VcPAS2, will be subsequently transduced downstream to the HAMP domains without any physical interactions between the domains.

REFERENCES

[1] Schultz J, Milpetz F, Bork P, Ponting CP. SMART, a simple modular architecture research tool: identification of signaling domains. Proc Natl Acad Sci U S A. 1998;95:5857-64.

[2] Henry JT, Crosson S. Ligand-binding PAS domains in a genomic, cellular, and structural context. Annu Rev Microbiol. 2011;65:261-86.

[3] Taylor BL, Zhulin IB. PAS domains: internal sensors of oxygen, redox potential, and light. Microbiol Mol Biol Rev. 1999;63:479-506.

[4] Moglich A, Ayers RA, Moffat K. Structure and signaling mechanism of Per-ARNT-Sim domains. Structure. 2009;17:1282-94.

[5] Huang ZJ, Edery I, Rosbash M. PAS is a dimerization domain common to Drosophila period and several transcription factors. Nature. 1993;364:259-62.

[6] Nambu JR, Lewis JO, Wharton KA, Jr., Crews ST. The Drosophila single-minded gene encodes a helix-loop-helix protein that acts as a master regulator of CNS midline development. Cell. 1991;67:1157-67.

[7] Hoffman EC, Reyes H, Chu FF, Sander F, Conley LH, Brooks BA, et al. Cloning of a factor required for activity of the Ah (dioxin) receptor. Science. 1991;252:954-8.

[8] Finn RD, Mistry J, Schuster-Bockler B, Griffiths-Jones S, Hollich V, Lassmann T, et al. Pfam: clans, web tools and services. Nucleic Acids Res. 2006;34:D247-51.

[9] Finn RD, Mistry J, Tate J, Coggill P, Heger A, Pollington JE, et al. The Pfam protein families database. Nucleic Acids Res. 2010;38:D211-22.

[10] Galperin MY. Bacterial signal transduction network in a genomic perspective. Environ Microbiol. 2004;6:552-67.

[11] Krell T, Lacal J, Busch A, Silva-Jimenez H, Guazzaroni ME, Ramos JL. Bacterial sensor kinases: diversity in the recognition of environmental signals. Annu Rev Microbiol. 2010;64:539-59.

[12] Lacal J, Garcia-Fontana C, Munoz-Martinez F, Ramos JL, Krell T. Sensing of environmental signals: classification of chemoreceptors according to the size of their ligand binding regions. Environ Microbiol. 2010;12:2873-84.

[13] Rodgers KR. Heme-based sensors in biological systems. Curr Opin Chem Biol. 1999;3:158-67.

[14] Chan MK. Recent advances in heme-protein sensors. Curr Opin Chem Biol. 2001;5:216-22.

[15] Aono S. Biochemical and biophysical properties of the CO-sensing transcriptional activator CooA. Acc Chem Res. 2003;36:825-31.

[16] Sawai H, Sugimoto H, Shiro Y, Ishikawa H., Y. M, S. A. Structural basis for oxygen sensing and signal transduction of the heme-based sensor protein Aer1 from Psuedomonas aeruginosa. Chem Commun. 2012;48:6523-65.

[17] Hao B, Isaza C, Arndt J, Soltis M, Chan MK. Structure-based mechanism of O2 sensing and ligand discrimination by the FixL heme domain of Bradyrhizobium japonicum. Biochemistry. 2002;41:12952-8.

[18] Kurokawa H, Lee DS, Watanabe M, Sagami I, Mikami B, Raman CS, et al. A redox-controlled molecular switch revealed by the crystal structure of a bacterial heme PAS sensor. J Biol Chem. 2004;279:20186-93.

[19] Sasakura Y, Yoshimura-Suzuki T, Kurokawa H, Shimizu T. Structure-function relationships of EcDOS, a heme-regulated phosphodiesterase from Escherichia coli. Acc Chem Res. 2006;39:37-43.

[20] Boon EM, Marletta MA. Ligand discrimination in soluble guanylate cyclase and the H-NOX family of heme sensor proteins. Curr Opin Chem Biol. 2005;9:441-6.

[21] Gilles-Gonzalez MA, Gonzalez G. Signal transduction by heme-containing PAS-domain proteins. J Appl Physiol (1985). 2004;96:774-83.

[22] Gilles-Gonzalez MA, Gonzalez G. Heme-based sensors: defining characteristics, recent developments, and regulatory hypotheses. J Inorg Biochem. 2005;99:1-22.

[23] Mayfield JA, Dehner CA, DuBois JL. Recent advances in bacterial heme protein biochemistry. Curr Opin Chem Biol. 2011;15:260-6.

[24] Uchida T, Kitagawa T. Mechanism for transduction of the ligand-binding signal in heme-based gas sensory proteins revealed by resonance Raman spectroscopy. Acc Chem Res. 2005;38:662-70.

[25] Airola MV, Huh D, Sukomon N, Widom J, Sircar R, Borbat PP, et al. Architecture of the Soluble Receptor Aer2 Indicates an In-Line Mechanism for PAS and HAMP Domain Signaling. Journal of Molecular Biology. 2013;425:886-901.

[26] Campbell AJ, Watts KJ, Johnson MS, Taylor BL. Gain-of-function mutations cluster in distinct regions associated with the signalling pathway in the PAS domain of the aerotaxis receptor, Aer. Molecular Microbiology. 2010;77:575-86.

[27] Watts KJ, Johnson MS, Taylor BL. Different Conformations of the Kinase-On and Kinase-Off Signaling States in the Aer HAMP Domain. Journal of Bacteriology. 2011;193:4095-103.

[28] Taabazuing CY, Hangasky JA, Knapp MJ. Oxygen sensing strategies in mammals and bacteria. J Inorg Biochem. 2014;133:63-72.

[29] Aono S. The Dos family of globin-related sensors using PAS domains to accommodate haem acting as the active site for sensing external signals. Adv Microb Physiol. 2013;63:273-327.

[30] Gilles-Gonzalez MA, Ditta GS, Helinski DR. A haemoprotein with kinase activity encoded by the oxygen sensor of Rhizobium meliloti. Nature. 1991;350:170-2.

[31] Fischer HM. Genetic regulation of nitrogen fixation in rhizobia. Microbiol Rev. 1994;58:352-86.

[32] Fischer HM. Environmental regulation of rhizobial symbiotic nitrogen fixation genes. Trends Microbiol. 1996;4:317-20.

[33] Rodgers KR, Lukat-Rodgers GS. Insights into heme-based O2 sensing from structure-function relationships in the FixL proteins. J Inorg Biochem. 2005;99:963-77.

[34] Sasakura Y, Hirata S, Sugiyama S, Suzuki S, Taguchi S, Watanabe M, et al. Characterization of a direct oxygen sensor heme protein from Escherichia coli. Effects of the heme redox states and mutations at the heme-binding site on catalysis and structure. J Biol Chem. 2002;277:23821-7.

[35] Delgado-Nixon VM, Gonzalez G, Gilles-Gonzalez MA. Dos, a heme-binding PAS protein from Escherichia coli, is a direct oxygen sensor. Biochemistry. 2000;39:2685-91.

[36] Yoshimura-Suzuki T, Sagami I, Yokota N, Kurokawa H, Shimizu T. DOS(Ec), a heme-regulated phosphodiesterase, plays an important role in the regulation of the cyclic AMP level in Escherichia coli. J Bacteriol. 2005;187:6678-82.

[37] Taylor BL, Zhulin IB, Johnson MS. Aerotaxis and other energy-sensing behavior in bacteria. Annual Review Of Microbiology. 1999;53:103-28.

[38] Watts KJ, Sommer K, Fry SL, Johnson MS, Taylor BL. Function of the N-terminal cap of the PAS domain in signaling by the aerotaxis receptor Aer. Journal Of Bacteriology. 2006;188:2154-62.

[39] Watts KJ, Johnson MS, Taylor BL. Minimal requirements for oxygen sensing by the aerotaxis receptor Aer. Molecular Microbiology. 2006;59:1317-26.

[40] Bibikov SI, Biran, R., Rudd, K.E., and Parkinson, J.S. A signal tranducer for aerotaxis in Escherichia coli. J Bacteriol. 1997;179:4075-9.

[41] Garcia D, Watts KJ, Johnson MS, Taylor BL. Delineating PAS-HAMP interaction surfaces and signalling-associated changes in the aerotaxis receptor Aer. Mol Microbiol. 2016;100:156-72.

[42] Taylor BL, Rebbapragada A, Johnson MS. The FAD-PAS domain as a sensor for behavioral responses in Escherichia coli. Antioxidants & Redox Signaling. 2001;3:867-79.

[43] Taylor BL. Aer on the inside looking out: paradigm for a PAS-HAMP role in sensing oxygen, redox and energy. Molecular Microbiology. 2007;65:1415-24.

[44] Rebbapragada A, Johnson MS, Harding GP, Zuccarelli AJ, Fletcher HM, Zhulin IB, et al. The Aer protein and the serine chemoreceptor Tsr independently sense intracellular energy levels and transduce oxygen, redox, and energy signals for Escherichia coli behavior. Proc Natl Acad Sci U S A. 1997;94:10541-6.

[45] Samanta D, Widom J, Borbat PP, Freed JH, Crane BR. Bacterial Energy Sensor Aer Modulates the Activity of the Chemotaxis Kinase CheA Based on the Redox State of the Flavin Cofactor. J Biol Chem. 2016.

[46] Watts KJ, Taylor BL, Johnson MS. PAS/poly-HAMP signalling in Aer-2, a soluble haem-based sensor. Molecular Microbiology. 2011;79:686-99.

[47] Boin MA, Hase CC. Characterization of Vibrio cholerae aerotaxis. FEMS Microbiol Lett. 2007;276:193-201.

[48] Bryksin AV, Matsumura I. Overlap extension PCR cloning: a simple and reliable way to create recombinant plasmids. Biotechniques. 2010;48:463-5.

[49] Sudhamsu J, Kabir M, Airola MV, Patel BA, Yeh SR, Rousseau DL, et al. Co-expression of ferrochelatase allows for complete heme incorporation into recombinant proteins produced in E. coli. Protein Expr Purif. 2010;73:78-82.

[50] Otwinowski Z, Minor W. Processing of X-ray diffraction data collected in oscillation mode. Macromolecular Crystallography, Pt A. 1997;276:307-26.

[51] Emsley P, Lohkamp B, Scott WG, Cowtan K. Features and development of Coot. Acta Crystallogr D Biol Crystallogr. 2010;66:486-501.

[52] Adams PD, Afonine PV, Bunkoczi G, Chen VB, Echols N, Headd JJ, et al. The Phenix software for automated determination of macromolecular structures. Methods. 2011;55:94-106.

[53] Arnold K, Bordoli L, Kopp J, Schwede T. The SWISS-MODEL workspace: a web-based environment for protein structure homology modelling. Bioinformatics. 2006;22:195-201.

[54] Gong W, Hao B, Chan MK. New mechanistic insights from structural studies of the oxygen-sensing domain of Bradyrhizobium japonicum FixL. Biochemistry. 2000;39:3955-62.

[55] Key J, Moffat K. Crystal structures of deoxy and CO-bound bjFixLH reveal details of ligand recognition and signaling. Biochemistry. 2005;44:4627-35.

[56] Repik A, Rebbapragada A, Johnson MS, Haznedar JO, Zhulin IB, Taylor BL. PAS domain residues involved in signal transduction by the Aer redox sensor of Escherichia coli. Molecular Microbiology. 2000;36:806-16.

[57] Ma QH, Roy F, Herrmann S, Taylor BL, Johnson MS. The Aer protein of Escherichia coli forms a homodimer independent of the signaling domain and flavin adenine dinucleotide binding. Journal Of Bacteriology. 2004;186:7456-9.

[58] Herrmann S, Ma QH, Johnson MS, Repik AV, Taylor BL. PAS domain of the Aer redox sensor requires C-terminal residues for native-fold formation and flavin adenine dinucleotide binding. Journal Of Bacteriology. 2004;186:6782-91.

[59] Ayers RA, Moffat K. Changes in quaternary structure in the signaling mechanisms of PAS domains. Biochemistry. 2008;47:12078-86.

[60] Sevvana M, Vijayan V, Zweckstetter M, Reinelt S, Madden DR, Herbst-Irmer R, et al. A ligand-induced switch in the periplasmic domain of sensor histidine kinase CitA. J Mol Biol. 2008;377:512-23.

[61] Key J, Hefti M, Purcell EB, Moffat K. Structure of the redox sensor domain of Azotobacter vinelandii NifL at atomic resolution: Signaling, dimerization, and mechanism. Biochemistry. 2007;46:3614-23.

[62] Ma X, Sayed N, Baskaran P, Beuve A, van den Akker F. PAS-mediated dimerization of soluble guanylyl cyclase revealed by signal transduction histidine kinase domain crystal structure. J Biol Chem. 2008;283:1167-78.

[63] Nakasako M, Zikihara K, Matsuoka D, Katsura H, Tokutomi S. Structural basis of the LOV1 dimerization of Arabidopsis phototropins 1 and 2. J Mol Biol. 2008;381:718-33.

[64] Scheuermann TH, Stroud D, Sleet CE, Bayeh L, Shokri C, Wang H, et al. Isoform-Selective and Stereoselective Inhibition of Hypoxia Inducible Factor-2. J Med Chem. 2015;58:5930-41.

[65] Fedorov R, Schlichting I, Hartmann E, Domratcheva T, Fuhrmann M, Hegemann P. Crystal structures and molecular mechanism of a light-induced signaling switch: The Phot-LOV1 domain from Chlamydomonas reinhardtii. Biophys J. 2003;84:2474-82.

[66] Lee J, Tomchick DR, Brautigam CA, Machius M, Kort R, Hellingwerf KJ, et al. Changes at the KinA PAS-A dimerization interface influence histidine kinase function. Biochemistry. 2008;47:4051-64.

[67] Froehlich AC, Liu Y, Loros JJ, Dunlap JC. White Collar-1, a circadian blue light photoreceptor, binding to the frequency promoter. Science. 2002;297:815-9.

[68] Miyatake H, Mukai M, Park SY, Adachi S, Tamura K, Nakamura H, et al. Sensory mechanism of oxygen sensor FixL from Rhizobium meliloti: crystallographic, mutagenesis and resonance Raman spectroscopic studies. J Mol Biol. 2000;301:415-31.

[69] Park H, Suquet C, Satterlee JD, Kang C. Insights into signal transduction involving PAS domain oxygen-sensing heme proteins from the X-ray crystal structure of Escherichia coli Dos heme domain (Ec DosH). Biochemistry. 2004;43:2738-46.

[70] Kreel NE, Tabita FR. Substitutions at methionine 295 of Archaeoglobus fulgidus ribulose-1,5-bisphosphate carboxylase/oxygenase affect oxygen binding and CO2/O2 specificity. J Biol Chem. 2007;282:1341-51.

[71] Liu YC, Machuca MA, Beckham SA, Gunzburg MJ, Roujeinikova A. Structural basis for amino-acid recognition and transmembrane signalling by tandem Per-Arnt-Sim (tandem PAS) chemoreceptor sensory domains. Acta Crystallogr D Biol Crystallogr. 2015;71:2127-36.

[72] Rahman H, King RM, Shewell LK, Semchenko EA, Hartley-Tassell LE, Wilson JC, et al. Characterisation of a multi-ligand binding chemoreceptor CcmL (Tlp3) of Campylobacter jejuni. PLoS Pathog. 2014;10:e1003822.

CHAPTER 4

Conclusion

In the context of the recombinant HAMP domains, the stability and the dynamic properties of the Tsr HAMP conform to the biphasic stability model as purposed by Zhou *et al* [1]. The pulsed-ESR experiments enabled probing the transitions between the HAMP conformations that mediate the functional CCW [CCW(A)] and CW outputs. Overall, the conformational changes occur from, but not exclusively to, rotations of the HAMP helices as proposed by the gearbox model [2, 3], which were subsequently observed in several HAMP domains [4, 5]. Therefore, this research provides the intermediate view of the HAMP signaling mechanism as suggested by the structural and functional analyses of the PaAer2 poly HAMP domains [4, 6]. As the chimeric strategy provides greater stability to the Tsr HAMP and allows *in vivo* manipulations, the recombinant protein is possibly amenable to crystallization. In this case, further screening for mutations that confer high stability would be required for identifying candidates for crystallization.

The biochemical analyses of the VcPAS2 domain corroborate the role of the conserved Iβ Trp (Trp276) in O_2 ligation. The VcPAS2 W276L structure might represent the ligand-binding state of the VcPAS2 domain, and the side chain of the Iβ Trp aligns well with that of the CN^--bound PAS domain of PaAer2 [7, 8]. Interestingly, the Iβ Trp of VcPAS1 is not required for stabilizing O_2 as most substitutions of this Trp do not affect the O_2-binding affinity of the domain. Therefore, it is possible that

the VcPAS1 domain plays a role in regulating the activity of the VcPAS2 domain as observed in several signaling proteins with two continuous PAS domains, such as FixL and EcDos [9-11]. Further functional and structural studies will be valuable in elucidating the signaling interplays between the VcPAS1 and VcPAS2 domains.

In several chemoreceptors such as EcAer and PaAer2, PAS domains coexist with HAMP domains. Therefore, interactions between the two domains are critical for proper responses to environmental cues. As VcAer2 is homology to PaAer2, it is very likely that VcAer2 utilizes the in-line mechanism for its PAS-HAMP interplay. In this case, structural changes in VcPAS2 following ligand bindings induce conformational alterations in the downstream HAMP domains, which is subsequently transmitted the MCP domain. Biochemical and biophysical analyses, such as disulfide crosslinking and small-angle X-ray scattering (SAXS), are necessary to elucidate the PAS-HAMP interactions in the VcAer2 protein.

REFERENCES

[1] Zhou Q, Ames P, Parkinson JS. Biphasic control logic of HAMP domain signalling in the Escherichia coli serine chemoreceptor. Molecular Microbiology. 2011;80:596-611.

[2] Ferris HU, Zeth K, Hulko M, Dunin-Horkawicz S, Lupas AN. Axial helix rotation as a mechanism for signal regulation inferred from the crystallographic analysis of the E. coli serine chemoreceptor. J Struct Biol. 2014;186:349-56.

[3] Hulko M, Berndt F, Gruber M, Linder JU, Truffault V, Schultz A, et al. The HAMP domain structure implies helix rotation in transmembrane signaling. Cell. 2006;126:929-40.

[4] Airola MA, Watts KJ, Crane BR. Structure of concatenated HAMP domains provides a mechanism for signal transduction. Structure. 2010;18:436-48.

[5] Matamouros S, Hager KR, Miller SI. HAMP Domain Rotation and Tilting Movements Associated with Signal Transduction in the PhoQ Sensor Kinase. MBio. 2015;6:e00616-15.

[6] Airola MV, Sukomon N, Samanta D, Borbat PP, Freed JH, Watts KJ, et al. HAMP domain conformers that propagate opposite signals in bacterial chemoreceptors. PLoS Biol. 2013;11:e1001479.

[7] Airola MV, Huh D, Sukomon N, Widom J, Sircar R, Borbat PP, et al. Architecture of the Soluble Receptor Aer2 Indicates an In-Line Mechanism for PAS and HAMP Domain Signaling. Journal of Molecular Biology. 2013;425:886-901.

[8] Sawai H, Sugimoto H, Shiro Y, Ishikawa H., Y. M, S. A. Structural basis for oxygen sensing and signal transduction of the heme-based sensor protein Aer1 from Psuedomonas aeruginosa. Chem Commun. 2012;48:6523-65.

[9] Hao B, Isaza C, Arndt J, Soltis M, Chan MK. Structure-based mechanism of O2 sensing and ligand discrimination by the FixL heme domain of Bradyrhizobium japonicum. Biochemistry. 2002;41:12952-8.

[10] Kurokawa H, Lee DS, Watanabe M, Sagami I, Mikami B, Raman CS, et al. A redox-controlled molecular switch revealed by the crystal structure of a bacterial heme PAS sensor. J Biol Chem. 2004;279:20186-93.

[11] Sasakura Y, Yoshimura-Suzuki T, Kurokawa H, Shimizu T. Structure-function relationships of EcDOS, a heme-regulated phosphodiesterase from Escherichia coli. Acc Chem Res. 2006;39:37-43.

APPENDIX A

HAMP Domain Conformers That Propagate Opposite Signals in Bacterial Chemoreceptors[1]

Abstract

HAMP domains are signal relay modules in >26,000 receptors of bacteria, eukaryotes, and archaea that mediate processes involved in chemotaxis, pathogenesis, and biofilm formation. We identify two HAMP conformations distinguished by a four- to two-helix packing transition at the C-termini that send opposing signals in bacterial chemoreceptors. Crystal structures of signal-locked mutants establish the observed structure-to-function relationships. Pulsed dipolar electron spin resonance spectroscopy of spin-labeled soluble receptors active in cells verify that the crystallographically defined HAMP conformers are maintained in the receptors and influence the structure and activity of downstream domains accordingly. Mutation of HR2, a key residue for setting the HAMP conformation and generating an inhibitory signal, shifts HAMP structure and receptor output to an activating state. Another HR2 variant displays an inverted response with respect to ligand and demonstrates the fine energetic balance between "on" and "off" conformers. A DExG motif found in membrane proximal HAMP domains is shown to be critical for responses to extracellular ligand. Our findings directly correlate in vivo signaling with HAMP structure, stability, and dynamics to establish a comprehensive model for HAMP-mediated signal relay that consolidates existing views on how conformational signals

propagate in receptors. Moreover, we have developed a rational means to manipulate HAMP structure and function that may prove useful in the engineering of bacterial taxis responses.

---

[1]Reprinted from Airola MV, Sukomon N, Samanta D, Borbat PP, Freed JH, Watts KJ, et al. HAMP domain conformers that propagate opposite signals in bacterial chemoreceptors. PLoS Biol. 2013;11:e1001479.

Nattakan Sukomon cloned, expressed, purified, and crystallized Aer2 HAMP variants, performed PDS experiments, and analyzed X-ray crystallography and PDS data.

Introduction

The ability of single-celled organisms to sense, respond to, and adapt to their changing environment requires receptor proteins to convert extracellular signals into cellular responses [1]. Central to many of these signal transduction systems are HAMP domains, which act to couple sensory and output domains in over 26,000 different receptor proteins [2]. In transmembrane receptors, HAMP domains connect to transmembrane helices entering the cytoplasm and translate chemical, photo, and thermo stimuli to the output of cytoplasmic catalytic domains (mainly histidine kinases, adenylyl cyclases, methyl-accepting chemotaxis proteins [MCPs], and phosphatases) [3]. Deletion of HAMP domains disrupts the link between input and output units, generating receptors incapable of switching activity states upon stimulation [4].

HAMP domains are small modules, approximately 50 amino acids, that dimerize to form an entirely parallel four-helix bundle with two helices (AS1 and AS2) supplied from each subunit [3]. The AS1 and AS2 helices form a seven-residue pattern characteristic of coiled coils, termed a heptad repeat, with the repeat residues labeled *a* through *g*, and with the *a* and *d* positions hydrophobic in nature and pointing inward to form a buried core [5]. A semi-structured connector separates the AS1 and AS2 helices and contains two conserved hydrophobic residues, termed HR1 and HR2 (6). A spectrum of HAMP domain structures and conformations is now characterized for native and mutant HAMP domains, the most divergent of which differ by helix rotation, helix translation, and helix–helix crossing angle [5, 7-11]. Importantly, the transmembrane helices of characterized HAMP-containing receptors

are known to undergo small amplitude translations or rotations during signal transduction [12, 13].

The function and mechanism of HAMP domains have been most intensively studied in MCPs, which regulate bacterial chemotaxis and are archetypal models of bacterial transmembrane signaling [3]. Overall, MCPs have a modular construction comprising an extracellular ligand-sensing domain, a transmembrane helical region, a membrane proximal HAMP or tandem HAMP domain, and a kinase control module (KCM) containing the adaptation region and kinase coupling tip (Figure A-1) [14]. MCPs sense chemical gradients to direct bacterial cells towards or away from attractants and repellents through allosteric activation and inhibition of the histidine kinase CheA. CheA phosphorylates the response regulator CheY to generate CheY-P. Depending on the ratio of CheY to CheY-P, flagella rotate counterclockwise (CCW) or clockwise (CW). Cells bias their movement by alternating between bursts of straight swimming (CCW rotation) and tumbling (CW rotation) [3].

MCP activity is also modulated by an adaptation system composed of the methyltransferase CheR and the methylesterase CheB. CheR and CheB respectively methylate and demethylate specific Glu residues to compensate for ligand binding and to reverse signals to the kinase relayed by the HAMP domain [4]. The predominant *Escherichia coli* chemoreceptors Tar and Tsr have four (or five) Glu methylation sites on each subunit (EEEE); however, two sites are expressed as Gln residues (QEQE) and are subsequently deamidated by CheB [15]. By reestablishing an optimum response set point, the adaptation system allows MCPs to sense a wide concentration range of stimulants with remarkable sensitivity [14]. Importantly, the

adaptation system compensates for perturbations to receptor activity, i.e., demethylation/deamidation will thus attempt to "turn down" kinase-on states and methylation will "turn up" kinase-off states. Thus, only in the absence of the adaptation system (CheRB$^-$ cells) can the unbiased activity state of a given receptor be established [16].

The first HAMP domain structure, Af1503, was determined by nuclear magnetic resonance (NMR) from an orphan receptor from *Archaeoglobus fulgidus* [5]. We subsequently determined the structure of a poly-HAMP domain composed of three concatenated HAMP units from the *Pseudomonas aeruginosa* soluble receptor Aer2 [7]. The Aer2 HAMP domains are representative of a recently identified sequence cluster that comprises repeating units to form extended, linear poly-HAMP chains [7, 17]. These atypical HAMPs share similar residue conservation and overall structure with membrane-associated HAMP domains but differ in that they lack obvious signal input motifs [17, 18]. Aer2 is a soluble receptor that contains three N-terminal HAMP domains, a gas-sensing, heme-containing PAS domain, two additional HAMP domains, and an MCP KCM (Figure A-1) [19]. The three N-terminal HAMP domains of Aer2 (named HAMP1, HAMP2, and HAMP3 from N- to C-terminus) provide examples of two distinctly different conformations: HAMP1 and HAMP3 are similar to the Af1503 NMR structure, whereas HAMP2 has a comparatively distorted four-helix bundle structure in which the AS2 helices approximate a two-helix coiled coil and the AS1 helices splay outward at the C-terminal end. Importantly, a functionally critical hydrophobic residue in the helical connector [6], termed HR2, plays a clear role in stabilizing the HAMP2 structure by inserting between the

AS1/AS2 helices, but remains on the periphery and appears dispensable in the HAMP1-like conformers (Figure A-2). The alternating and divergent conformations of the Aer2 HAMP moieties led us to hypothesize that HAMP1 and HAMP2 may represent two sides of a conformational switch that could send opposing signals to an output domain [7].

Several additional mechanisms have been proposed for HAMP domain signal relay. Functional characterization of an extensive library of HAMP mutants in the *E. coli* serine receptor Tsr has led to a model of HAMP function in which activity states of HAMP variants lie on a biphasic curve of domain stability [16, 20]. Variants predicted to be very unstable or very stable do not activate CheA (CCW flagellar rotation), whereas variants of intermediate stability activate CheA (CW flagellar rotation). The "stable" CCW(A) state is proposed to be the functional off state, and the metastable CW state the physiological on state. The very unstable CCW(B) state arises from drastic mutations that perturb HAMP properties out of its natural range. The biphasic model explains several unusual variants in which methylation and demethylation have inverted effects on the ability to activate CheA. Correlation of the residue substitutions with domain stability is largely inferred based on the effects the mutations are likely to have on known HAMP structures, particularly that of Af1503 [16].

Our goal is to assign the conformational properties of the HAMP states in bacterial chemotaxis receptors that produce CW and CCW rotational behavior. Corresponding experiments have been carried out with the Af1503 HAMP grafted into chimeras of adenylate cyclase and sensor kinase output domains [8, 9, 21, 22]. There,

crystallographic and NMR spectroscopy data on isolated HAMP mutants were correlated with their ability to modulate cyclase or kinase activity. These data in part supported a model in which helical rotation within HAMP is responsible for downstream signaling; however, the conformational differences found among the crystallized HAMP mutants were more complex than simple helix rotations, and the correlation between the amount of rotation at the C-terminus of AS2 and the activity of the receptor was not striking across the entire set of variants tested.

A prime problem in structure–function studies of HAMP domains is the difficulty in mapping structural and biophysical properties of isolated HAMP domains to their functional states in transmembrane receptors. The problem is compounded by the sensitivity of HAMP domains to perturbations and the possibility that different conformational states produce similar outputs. The question then becomes: what are the essential conformational features HAMP domains enforce on output domains to set their activity states?

Here we investigate the downstream signaling and functional capabilities of structurally defined Aer2 HAMP domains in chimera MCP transmembrane receptors. We report that the two structural HAMP domain variants, HAMP1 and HAMP2, give rise to opposite CW and CCW downstream signals in vivo, and using spin-labeling distance measurements, we find that HAMP domains assume both conformations in solution. Crystal structures of HAMP domain mutants locked in activating signaling states confirm the structural relationship and provide insight into mechanisms of disrupting mutagenesis. Mutation of HR2, which is selectively important for the HAMP2 (CCW) conformation, shifts receptor bias towards a CW state. In addition, a

reconstituted, functional HAMP1 receptor confirms the role of the DExG signal input motif [17]. We also identify a novel inverse signaling HAMP1 mutant receptor with the same degree of ligand sensitivity as endogenous MCPs. Our collective results support a model in which HAMP domains switch primarily between the two conformations to propagate signals in bacterial chemoreceptors.

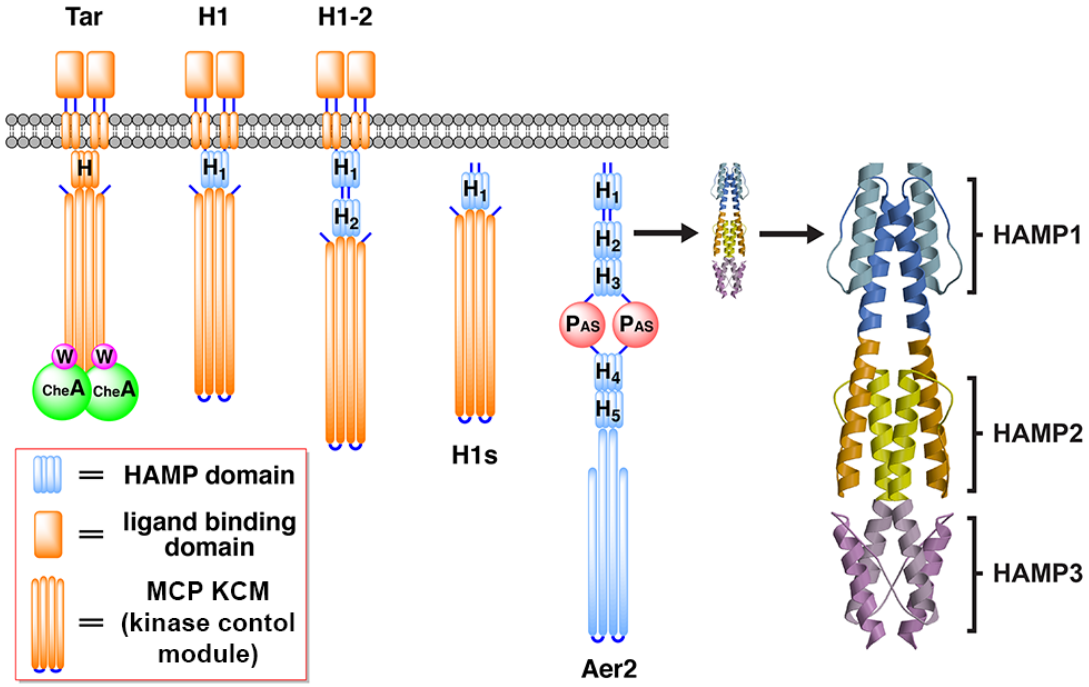

Figure A-1 Schematic of Aer2-Tar Chimeras.

The HAMP domain of Tar was replaced with single and poly-HAMP domains from Aer2 to generate chimeric receptors. Transmembrane ATCs (e.g., H1) contained the ligand binding domain and Tar KCM, both of which are necessary for modulating CheA kinase activity in response to aspartate. Soluble ATCs (e.g., H1s) comprised fusions of the Aer2 HAMP domains with only the Tar KCM. The structure of the three-unit Aer2 poly-HAMP domain (PDB: 3LNR) is shown on the right, with HAMP1 (blue), HAMP2 (yellow/orange), and HAMP3 (purple) colored accordingly.

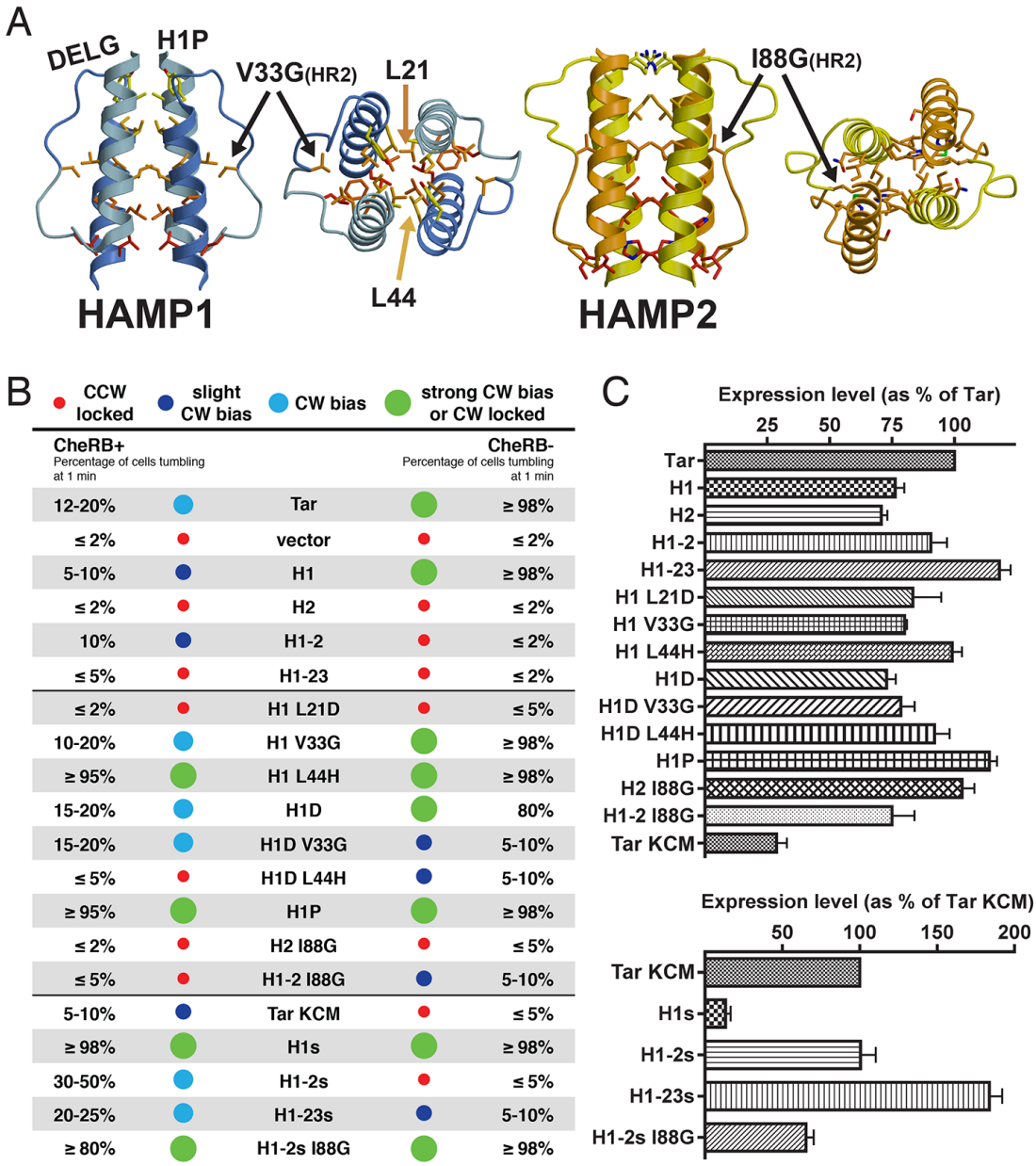

Figure A-2 Signaling biases and expression levels of ATC receptors.

(A) Structures of HAMP1 and HAMP2, highlighting positions of mutations reported in this study. HR2 (I88G) plays a prominent role in the HAMP2 hydrophobic core, inserting into the HAMP bundle between AS1 and AS2, while HR2 (V33G) in HAMP1 appears dispensable for bundle stability as it resides on the domain periphery.

L21 and L44 occupy core heptad positions inside the HAMP bundle. Membrane-associated HAMP domains contain a highly conserved DExG motif at the connector-AS2 junction and a less conserved Pro residue between TM2 and AS1. (B) Tumbling biases of transmembrane and soluble ATC receptors quantified by temporal assays in CheRB+ and CheRB− cells. Signaling biases are grouped into four categories: (1) CCW locked (<5% CW), (2) slight CW bias (5%–10% CW), (3) CW bias (10%–50% CW), and (4) strong CW bias (50%–95% CW) or CW locked (>95% CW). Temporal assays confirm H1 and H1-2 induce opposite outputs. The L44H mutation generates a CW locked receptor with or without the adaptation system. The soluble receptors H1s and H1-2s generate more distinct CW and CCW locked phenotypes in CheRB− cells than their transmembrane counterparts. Mutation of HR2 in H1-2s I88G switches receptor signaling from CCW to CW locked, which is consistent with HR2 stabilizing the CCW HAMP2 conformer. (C) Expression levels of ATC receptors in CheRB+ (BT3388) cells, normalized to that of Tar for transmembrane receptors and that of Tar KCM for soluble receptors.

Results

Two Structurally Characterized HAMP Domain Conformers Produce Opposite Downstream Signals

To understand HAMP signaling states, the preferred course would be to correlate the extensive genetic and functional data for the HAMP domains of the *E. coli* chemoreceptors Tar and Tsr with their structural and biophysical properties. Unfortunately, the *E. coli* HAMPs cannot be produced or studied in isolation or as soluble domain fusions. In contrast, the N-terminal Aer2 HAMP domains are highly amenable to structural characterization, but their contribution to Aer2 signaling is not well defined, and in fact, the function of Aer2 itself is not fully understood [19]. Thus, we have developed a chimeric system in which direct measurements of Aer2 HAMP conformation can be coupled to biological readouts.

Aer2–Tar chimeras (ATCs) were generated by replacing the HAMP domain of the *E. coli* aspartate receptor Tar with single or poly-HAMP domains from Aer2 (Figure A-1). These chimeric proteins were then expressed in *E. coli* cells lacking endogenous MCPs, and receptor function was assessed (Figure A-3; Table A-1). Direct measurements of cell tumbling frequencies (tumbling=CW, smooth swimming=CCW) were employed to confirm the flagellar output states of select receptors (Figure A-2). Receptors were scored in terms of percent CW bias, by counting the number of tumbling or smooth swimming cells after 1 min of observation, and were grouped into four categories: (1) CCW locked (<5% CW), (2) slight CW bias (5%–10% CW), (3) CW bias (10%–50% CW), and (4) strong CW bias (50%–95%) or CW locked (>95% CW). Prior to observation, cells were allowed to adapt for 5 min. Two strains that

either contained ($CheRB^+$, BT3388) or were devoid of ($CheRB^-$, UU2610) the methylation system were used to harbor ATC receptors. Changes in behavior between $CheRB^+$ and $CheRB^-$ indicate that the receptors assemble into functional clusters capable of activating CheA and responding to the adaptation system, at least to some degree. The $CheRB^-$ background provides an indication of intrinsic receptor activity in the absence of receptor modification. Select ATC receptors tested in strain UU2612, which is $CheRB^+$ but otherwise isogenic to UU2610, gave nearly identical responses to those expressed in BT3388. As expected, vector controls in both $CheRB^+$ and $CheRB^-$ cells were exclusively smooth swimming (≤2% CW) (Figure A-2). Tar produced a modest CW bias in $CheRB^+$ cells, and a CW locked phenotype in $CheRB^-$ cells. Thus, Tar alone is strongly CheA activating in its unmodified form (QEQE), whereas the adaptation system deactivates this receptor, largely by deamidating two of the methylation sites (QEQE to EEEE). This is similar to expression of Tsr, which produces a CW bias phenotype (25% CW) in $CheRB^+$ cells and a strong CW bias phenotype (75% CW) in $CheRB^-$ cells [16].

The H1 receptor, containing HAMP1 in place of the native Tar HAMP, behaved similar to Tar, being slightly CW biased in $CheRB^+$ cells and CW locked in $CheRB^-$ cells. On the other hand, the H1-2 receptor, containing HAMP1 and HAMP2 in tandem (the dash in H1-2 denotes the short helical linker) was similar to H1 in $CheRB^+$ cells but CCW locked in $CheRB^-$ cells. The contrasting behavior of H1 and H1-2 implies that the two different conformations of HAMP1 and HAMP2 send opposite signals to Tar KCM and elicit different responses from the adaptation system. The remaining unmutated ATCs were nearly exclusively CCW locked in both $CheRB^+$

and CheRB^{-} cells. Although all ATC receptors tested were expressed at normal levels (Figure A-2C), inactivity could indicate that these receptors do not assemble into functional clusters and/or are incapable of productive interactions with CheA and CheW. These additional factors may explain why the H1-23 receptor, which would be predicted to share the same HAMP conformer type and output as H1, displayed a CCW locked phenotype. Consequently, we limited our remaining studies to the functional receptors H1 and H1-2.

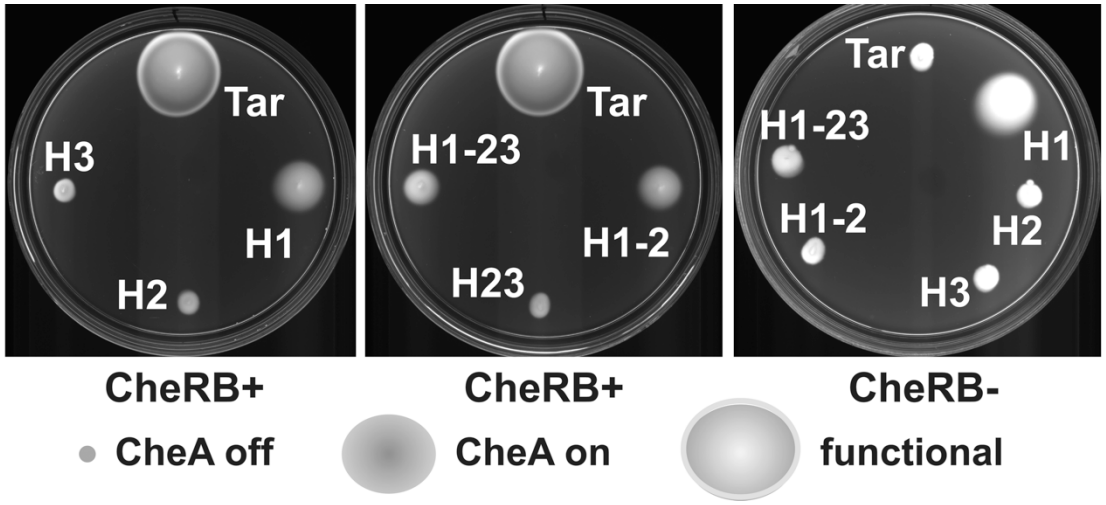

Figure A-3 Swim assays of ATCs.

Swim assays could distinguish between CheA inhibiting (CCW), CheA activating (CW), and functional receptors. H1 and H1-2, which have HAMP1 and HAMP2 attached to the KCM domain of Tar, exhibit similar downstream signals in adaptation-proficient cells (CheRB+) but opposite signals in CheRB− cells.

Table A-1 Tumbling biases of ATC receptors.
Tumbling biases were determined by temporal assays.

ATC	CheRB+ (BT3388)	CheRB- (UU2610)
Vector	CCW bias	CCW bias
Tar	CW bias	CW lock
H1	Slight CW bias	CW lock
H2	CCW bias	CCW bias
H3	Slight CW bias	Slight CW bias
H1-2	Slight CW bias	CCW bias
H23	CCW bias	Not tested
H1-23	CCW bias	CCW bias

Single Residue Substitutions Dramatically Affect ATC Phenotypes

Using our ATC system, we sought to better understand the principles underlying HAMP domain signal transduction by directly comparing in vivo signaling biases with the in vitro physical properties of point mutants that alter domain output. We thus generated single residue substitutions of ATC receptors with consideration of the extensive HAMP mutational data for the Tsr chemoreceptor as a guide. We focused mainly on H1 because of its functionality and the fact that HAMP1 is decoupled from HAMP2/3 in Aer2 1–172 by a short helical linker and hence is less likely to be dependent on HAMP2/3 for stability.

Cellular flagellar responses to single residue substitutions in H1 were varied, with roughly half of the substitutions having effects on signaling bias similar to those seen with equivalent substitutions in Tsr, and half having opposite effects (Table A-2). Notable was the L44H mutation, which generated a CW lock (i.e., exclusively tumbling) phenotype in both $CheRB^{+}$ and $CheRB^{-}$ cells (Figure A-2). Substitution of

HR2 in the connector (V33 and I88 in HAMP1 and HAMP2, respectively) tended to increase the CW bias of ATC receptors. Compared to H1, H1 V33G had increased CW bias in CheRB$^+$ cells and was also CW locked in CheRB$^-$ cells. H1-2 I88G displayed a slight CW bias in CheRB$^-$ cells, which differed from the CCW locked bias of H1-2. Overall, we established a set of HAMP domain mutants with defined phenotypes for structural and biochemical characterization. In general, HAMP1 substitutions that favored CCW output in Tsr could not be overexpressed as soluble proteins when produced in the Aer2 HAMP1 domain, whereas those that produced CW output were generally well tolerated. This suggests that CCW-biasing, but not CW, substitutions disrupt the native HAMP1-like conformation.

Table A-2 Tumbling biases of ATC mutant receptors.

HAMP Protein	Melting Temp (°C)	CheRB+ (BT3388)	CheRB- (UU2610)	Tsr Phenotype
Tar	-	CW bias	CW lock	-
H1	53	Slight CW bias	CW lock	-
L21D	39	CCW bias	CCW bias	CCW[28]
L29H	47	CCW bias	Slight CW bias	CCW lock[13]
V33G	39	CW bias	CW lock	CW lock[13]
L44H	43	Strong CW bias	CW lock	CCW[28]
H1D	39, 65	CW bias	Strong CW bias	-
L44N	Insoluble	Strong CW bias	Not tested	CCW[28]
L48E	Insoluble	CCW bias	Not tested	CCW[28]
L48G	Insoluble	CCW bias	Not tested	CCW[28]
L48Y	Insoluble	CW lock	CW lock	CCW[28]
H2	-	CCW bias	CCW bias	-
H2-I88G	Insoluble	CCW bias	CCW bias	-
H1-2	-	Slight CW bias	CCW bias	-
H1-2 I88G	Insoluble	CCW bias	Slight CW bias	-

Tumbling biases were determined by temporal assays. Melting temperatures of HAMP mutants, that could be successfully overexpressed in the context of Aer2 1-172, are shown. Some mutations resulted in insoluble protein upon overexpression. The extensive mutational library of Tsr mutants was used to select mutations and is shown for comparison.

1. Zhou Q, Ames P, & Parkinson JS (2011) Biphasic control logic of HAMP domain signalling in the Escherichia coli serine chemoreceptor. *Molecular Microbiology* 80(3):596-611.
2. Ames P, Zhou Q, & Parkinson JS (2008) Mutational analysis of the connector segment in the HAMP domain of Tsr, the Escherichia coli serine chemoreceptor. *Journal of Bacteriology* 190(20):6676-6685.

The DExG Motif Rescues Signal Input at the Membrane

To test whether ATCs were capable of receiving and transducing signal input, we carried out temporal assays to monitor flagellar responses to the attractant aspartate (Asp). H1 represented the most promising candidate, as it contained a single HAMP domain and was capable of CheA activation. However, H1 did not switch tumbling bias in response to Asp (Figure A-4).

We reasoned this could be due to the lack of two motifs often found in membrane-associated HAMP domains, but not present in the Aer2 HAMPs: (1) a DExG motif at the connector-AS2 junction and (2) a Pro residue at the beginning of AS1 conserved in many HAMP domains, including those of MCPs. Introducing DELG into H1, to produce H1D, generated a functional chemoreceptor with a clear CW-to-CCW switch in response to Asp (Figure A-4). In contrast, addition of the proline residue in AS1, to generate H1P, led to an unresponsive CW locked receptor. Combining the two motifs, into H1DP, crippled the previous gain of function. The H1D response was not as robust as that of Tar and required higher Asp concentrations to produce similar kinetics. The H1D mutant introduces an extra residue in AS2 because of a missing residue in this region of native HAMP1. As a control, and to test whether only the highly conserved Glu residue was required for function, we generated H1E, which adds a single Glu residue in the same position (Figure A-5). However, H1E failed to respond to Asp.

The DExG motif was introduced into all of the wild-type (WT) ATC receptors to test for functional reconstitution. Unlike H1, the DELG mutation did not affect the signaling bias or the ability of other ATC receptors to respond to Asp. A functional

Asp inhibitory response requires the ability to activate CheA. Thus, it was unsurprising that most ATCs remained nonresponsive. Somewhat surprisingly, H1D-2, which has the DExG motif added to HAMP1 in the context of H1-2 and can activate CheA, did not give an attractant response.

We assessed the effects of the DELG mutation on HAMP1 stability in the context of Aer2 1–172 (HAMP1-2/3). WT Aer2 1–172 unfolded in a single step, with a melting temperature (T_M) of 53°C. In contrast, the H1D protein had two consecutive unfolding steps (Figure A-6). At 39°C approximately two-thirds of helical structure was lost, whereas at 65°C the remaining one-third of helical content was lost. These results suggest that the DELG motif decouples HAMP1 from HAMP2/3, rendering HAMP1 with a T_M of 65°C and HAMP2/3 with a much lower T_M of 39°C. This interpretation derives from the consideration that cooperative unfolding of two-thirds of the helical content implies structural coupling of two adjacent HAMP domains, which are likely to be HAMP2 and HAMP3 as they share a much larger interface than HAMP1 and HAMP2, which are separated by a short linker. Decoupling between HAMP1 and HAMP2/3 is consistent with the lack of Asp response in the H1D-2 receptor, which may not be able to relay a conformational signal through the H1-2 junction. Our attempts to define the molecular basis of these effects were unsuccessful. The H1D protein failed to crystallize, and aggregation of the cysteine-engineered H1D-H1C protein complicated electron spin resonance (ESR) spin-labeling measurements (see below). However, given that H1D imparts signal input to HAMP1, we speculate that these effects may derive from an increased physical connection between the DExG motif and the upstream transmembrane helices.

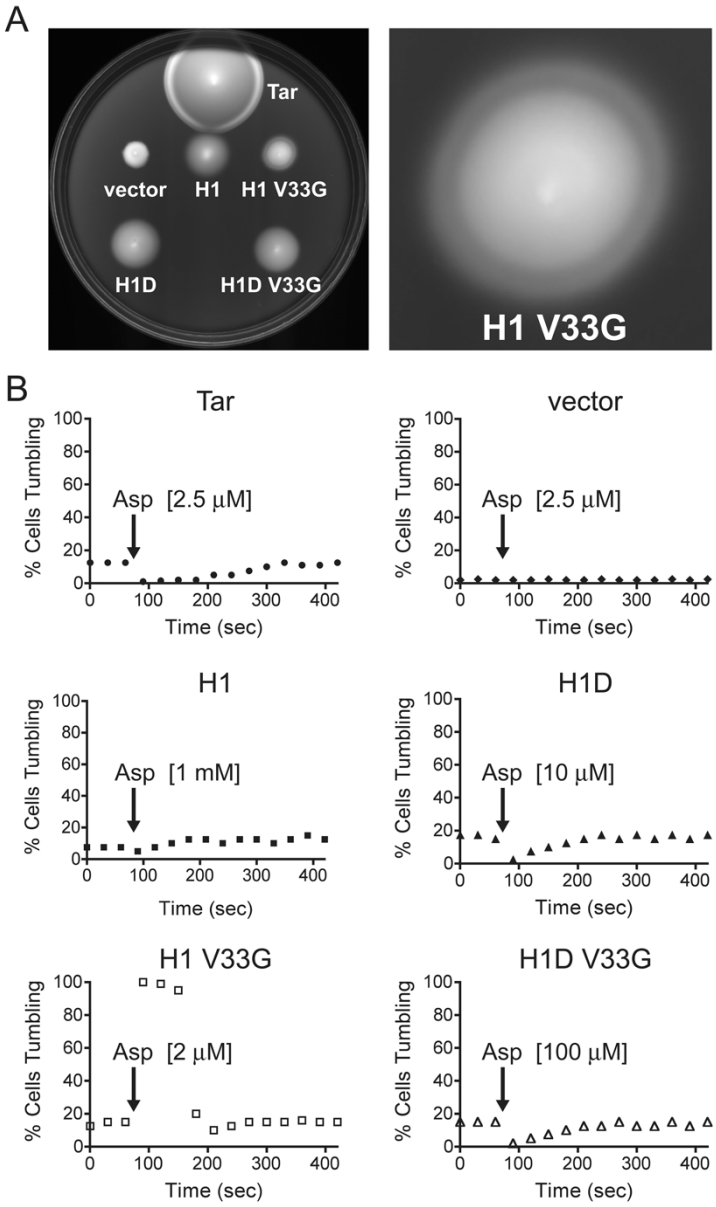

Figure A-4 H1D and H1 V33G receptors both respond to attractant, but with normal and inverse responses, respectively.

(A) Swim assays of ATC receptors on tryptone agar plates. Colonies with functional chemoreceptors generate a characteristic ring near the leading edge of an expanding colony as cells consume Asp and swim towards higher Asp concentrations. H1 V33G

generates an inverted ring, in comparison to Tar, which suggests an inverted CCW-to-CW response to Asp.

(B) Temporal assays of transmembrane receptors showing response and adaptation kinetics. CheRB+ cells expressing various receptors were allowed to reach adaptation equilibrium before Asp was added. Tumbling frequencies alter if receptors are capable of receiving and relaying signal input from TM2 to the output KCM. Tar responds in the normal direction, switching from 12.5% to 1% CW bias. After ~300 s, the adaptation system restores Tar CW bias to 12.5%. H1D has a normal Asp response, switching from 17.5% to 2.5% CW bias. H1 V33G displays an inverted response, switching from 16% to 100% CW bias upon Asp addition. A lower concentration of Asp is representative of increased receptor sensitivity.

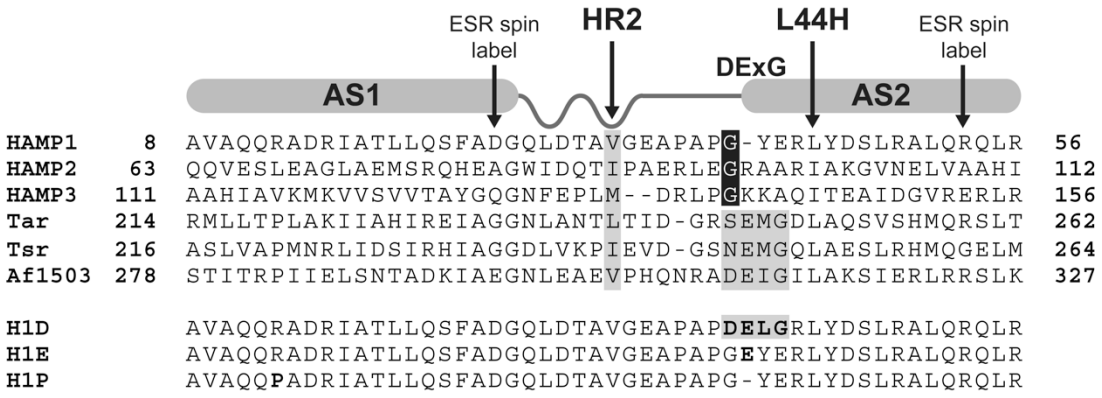

Figure A-5 HAMP domain alignment.

HAMP domain alignment highlighting the location of HR2, the CW locked L44H mutation, the DExG motif, the conserved glycine in divergent HAMPs, and ESR spin-labeling sites. The H1D mutant introduces an extra residue in AS2 of HAMP1; however, H1E, which also adds an extra residue, failed to switch in response to aspartate.

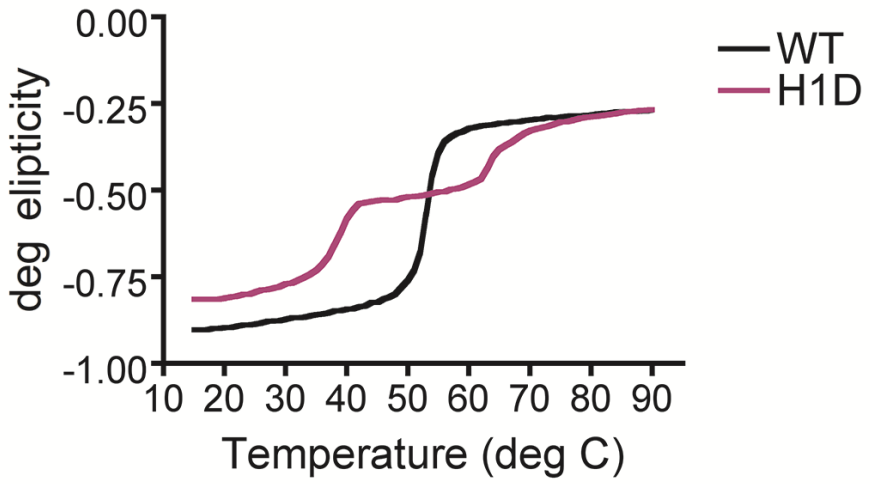

Figure A-6 The DELG mutation decouples HAMP1 from HAMP2/3.

Circular dichroism thermal melting curves of Aer2 1–172 WT and H1D proteins. WT protein unfolds in a single step and has a melting temperature of 53°C. H1D protein unfolds in two steps, one at 39°C and another at 65°C, which account for 2/3 and 1/3 of secondary structure, respectively. This suggests that the H1D mutation stabilizes HAMP1 and additionally decouples HAMP1 from HAMP2/3.

V33G Mutation produces a Hyper-Inverted Response to Aspartate

We investigated the ability of other mutations to induce Asp responses. Strikingly, swim assays of H1 V33G displayed a novel phenotype with an inverse ring (Figure A-4). Ring formation was validated by addition of Asp at the leading edge of expanding colonies, which caused ring flattening in both Tar and H1 V33G (Figure A-7). This odd ring pattern on plates suggested that H1 V33G exhibits an inverted response to Asp. Temporal assays confirmed an inverse Asp response by H1 V33G, in that Asp caused a drastic switch from 16% to 100% CW bias (Figure A-4). Notably, H1 V33G had high Asp sensitivity, displaying adaptation kinetics at concentrations similar to those of Tar. The H1D V33G variant, which combines the DELG and V33G substitutions, behaved similarly to H1D, although with significantly decreased sensitivity.

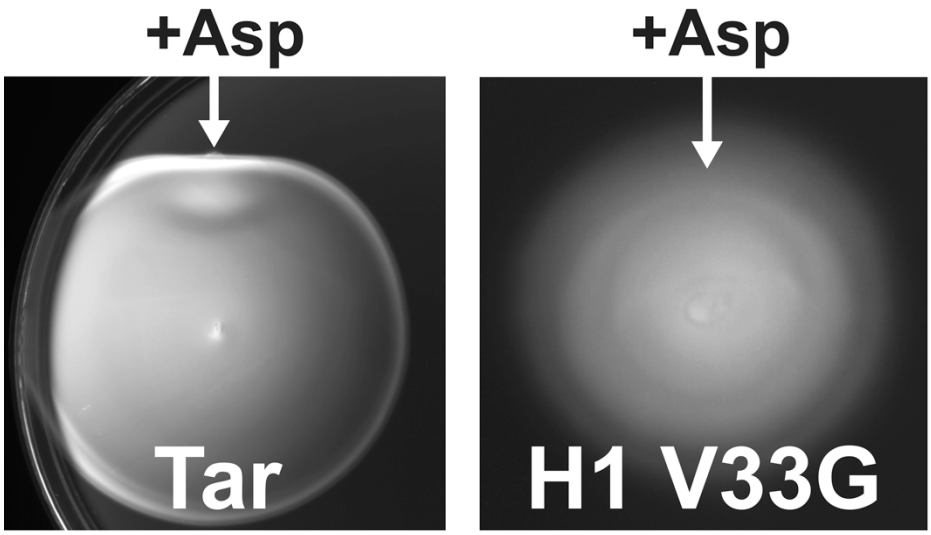

Figure A-7 Verification of aspartate rings by ring flattening.

Aspartate rings were verified by a flattening of the expanding ring after placing 2 µl of 0.5 M Asp on top of the semisoft agar, ~2 mm in front of the leading colony edge, and incubating plates for a further 5 h. Arrows highlight the flattened ring, which confirms the normal and inverse Asp responses of Tar and H1 V33G.

Crystal Structure of L44H and V33G Mutants Supports HAMP1 as the CW Signaling State

Based on our mutational analysis we aimed to determine the structure of CW locked variants to verify the CW signaling state as a HAMP1-like conformation. Crystals of L44H and V33G proteins were obtained in the context of Aer2 1–172 using conditions similar to those of the native protein [7]. V33G crystallized in the same space group as WT, but L44H produced a different crystal lattice. Complete datasets were collected to 1.9 Å resolution for L44H and to 2.9 Å resolution for V33G, and the structures were determined by molecular replacement.

The L44H mutation modified the HAMP1 domain structure while leaving the poly-HAMP2/3 domains largely unchanged (Figure A-8). The His44 side chain redirected from the bundle core towards AS1. This caused a tilt in the AS1 helix and a 5 Å shift at the top of AS1, resulting in a loss of secondary structure at the AS1 N-terminus. Despite these adjustments in AS1, the AS2 output helices superimposed with those of the native HAMP1 structure. In other words, the mutation did not alter the position of the HAMP1 AS2 helices, which must transmit the CW downstream signal.

The V33G mutation locally destabilized the connector around HR2 and increased mobility in this region of the protein, as evidenced by decreased electron density of the connector in the region of T31–V33 (Figure A-8). These changes had no effect on the helical positions of AS1 and AS2 compared to the WT structure, which is consistent with a HAMP1 conformer generating CW output. However, the increased flexibility of the connector and loss of the V33 side chain for packing into the bundle core should affect the ability of HR2 to stabilize the HAMP2 structure, and thus we expected this

substitution to disfavor conversion to a HAMP2-like conformer. In Aer2 1–172, HAMP1 and HAMP3 tolerated side chain removal at HR2 but HAMP2 did not (Table A-2).

Soluble ATC Receptors Are Active in Cells and Allow Direct Structure Function Correlations

In addition to full-length transmembrane chimeras, we constructed and assessed the activity of soluble chimeras that had the HAMP1 and HAMP2 domains fused to the Tar KCM (Figure A-1). These soluble chimeras, H1s and H1-2s, produced even more distinct phenotypes than their full-length analogs in *E. coli* (Figure A-2). Tar KCM produced slight CW bias in $CheRB^+$ cells, but nearly no CW behavior in $CheRB^-$ cells. Despite a substantially lower expression level than Tar KCM, H1s generated CW locked behavior in both $CheRB^+$ and $CheRB^-$ cells (Figure A-2). In contrast, H1-2s was CW biased in $CheRB^+$ cells, but CCW locked in $CheRB^-$ cells. These data reinforce the notion that HAMP1 induces a KCM conformation that gives a kinase-on state, and HAMP2 produces a kinase-off state. A striking result is found with H1-2s I88G. This mutation, which would be predicted to destabilize HAMP2, switched the H1-2s phenotype from CCW lock to CW lock in $CheRB^-$ cells (Figure A-2). The effect was similar, but somewhat muted, in the context of the compensating adaptation system. Importantly, the advantage of the soluble chimeras over their transmembrane counterparts is that their conformational properties can be directly probed in solution with spin-labeling techniques.

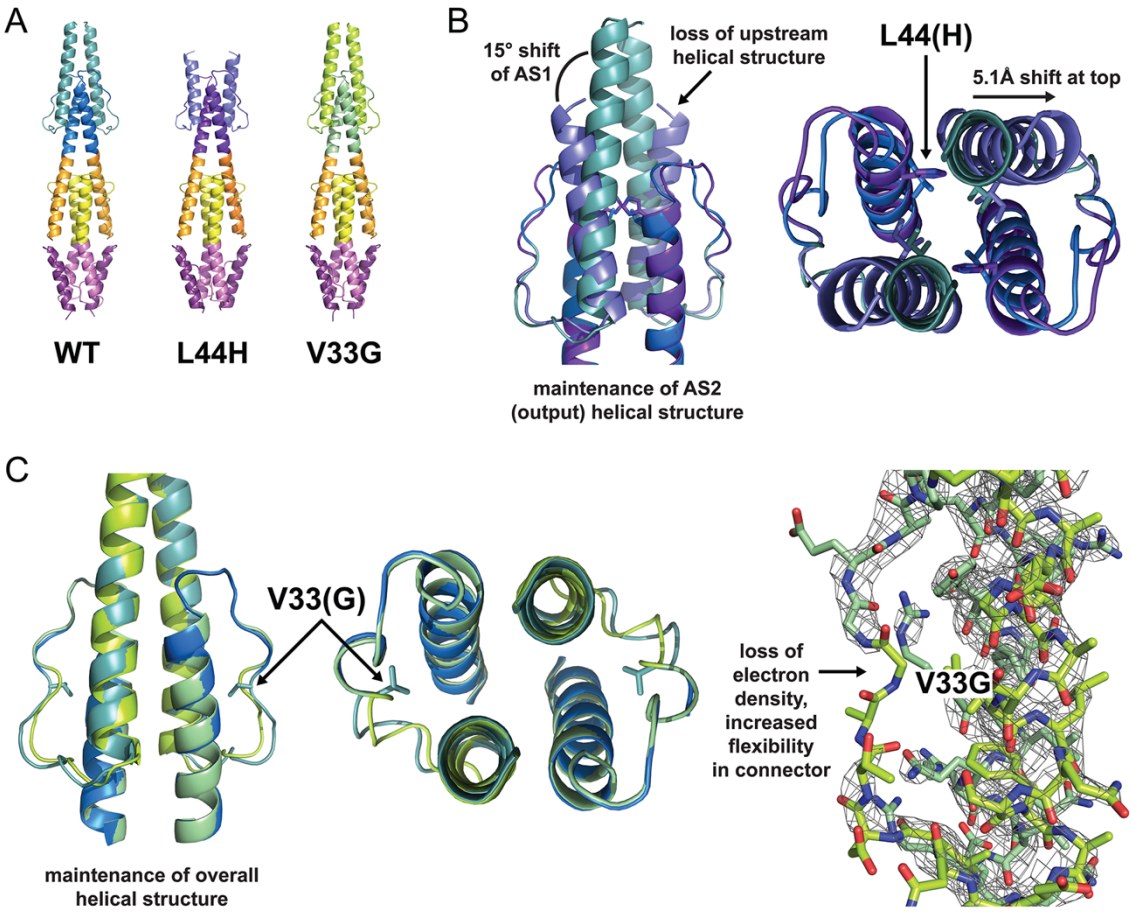

Figure A-8 Structure of L44H and V33G mutants.

(A) Crystal structure of Aer2 1–172 proteins, with HAMP1 colored blue (WT), purple (L44H), and green (V33G).

(B) Superposition of WT HAMP1 and CW locked L44H HAMP1 mutant. The L44H side chain redirects from the bundle core towards AS1, causing a 15° tilt of AS1 away from AS2 and a 5 Å shift at the top of AS1, which disrupts the upstream helical coiled coil. The positions of the AS2 output helices are identical to WT, which confirms that a HAMP1 structure generates CW output.

(C) Superposition of HAMP1 in WT and in the inverted signaling V33G mutant. Removal of HR2 in V33G does not affect the helical position of AS1 or AS2, suggesting that HR2 is dispensable to generate a HAMP1 conformer. 2Fo-Fc electron density maps of V33G (contoured at 2 σ) lack density in the surrounding HR2 connector region, suggesting increased flexibility of this region. Increased flexibility of HR2 due to Gly substitution would destabilize a HAMP2 conformer and thereby favor CW output.

Conformational Properties of Soluble HAMP Domains Fused to Tar

To directly correlate HAMP domain structure with in vivo signaling activity, we measured inter-subunit distance restraints on our soluble variants by site-specific spin labeling and pulsed dipolar ESR spectroscopy (PDS). Nitroxyl spin labels were attached to engineered Cys residues at three positions: (1) the C-terminal end of the AS1 helices, D26C and A81C; (2) the C-terminal end of the AS2 helices, R53C and A109C; and (3) in the KCM bundle directly across from the HAMP junction, E270C (Figure A-9). The reporter site in AS1 was chosen because of the large 6.5 Å difference in distance expected between the two conformations, and the reported functional tolerance of this site to mutation in Tsr [6]. The AS2 and KCM sites were chosen to report directly on the conformational changes immediately prior to and following the HAMP/KCM junction. The difference in inter-subunit separation at the AS1 site reflects the change in helix rotation and lateral translation that distinguish HAMP1 and HAMP2 [7]. This change in distance cannot be achieved by rotation of the helices alone. The AS2 site should produce a distinguishable 3.5 Å difference between the separations at the C-terminus for the two conformers and thus report on the signal being relayed to the coupled output domain.

As a control, we first conducted distance measurements of AS1 spin-labeled Aer2 1–172 (referred to as H1C AS1 and H2C AS1) to verify the separations expected by the crystal structure (Figure A-9; Table A-3). PDS distances of 32.4 Å for H1C AS1 and 39.7 Å for H2C AS1 matched well with the crystal structure separations, given that when combined, the two MTSSL spin labels can add up to 13 Å to the Cα–Cα separation of labeled residues. The 7 Å difference between H1C and H2C easily

distinguished the two conformers, and both pair-wise distance distributions had reasonably narrow shapes (Figure A-9). In the case of H1C AS1, the sharp peak is characteristic of a single conformation, but for H2C AS1 the broader line shape indicates some contribution from a more separated state of the labels. The closer proximity of the AS2 helices in HAMP2 than in HAMP1 was well reflected by PDS distances of 23.7 Å for H1C AS2 and 21.5 Å for H2C AS2, with both sites reporting narrow peak shapes (Figure A-9).

Next we monitored HAMP domain conformations within the soluble Tar KCM fusion receptors H1s and H1-2s (Figure A-9; Table A-3). The distance distribution of H1-2s AS1 remained centered around 39 Å, but appeared tighter and more symmetric than that of H2C AS1. In contrast, HAMP1 became more conformationally distributed when attached to the Tar KCM than in the context of Aer2 1–172. The H1s AS1 pair-wise distance distribution remained centered on 32 Å but became much broader, with a width at half the maximum peak height of 24.0 Å (Table A-3) and two peaks at 32 Å and 39 Å (Figure A-9). Thus, the conformation of H1-2s is consistent with a near exclusive HAMP2 conformation, whereas H1s has a broadly distributed conformation centered on a HAMP1-like state but likely also containing contributions from a HAMP2-like state. These structural states correlate well with the opposing CW and CCW locked phenotypes of H1s and H1-2s. Note that the ESR experiment did not measure dynamics directly, but a broad distribution can be reasonably interpreted as a molecule that dynamically exchanges among an ensemble of conformations.
The spin-label sites on AS2 and KCM in H1s and H1-2s produced an interesting similarity in distance and dynamics relative to AS1. H1s AS2 gave a broad

distribution centered at 27.1 Å for the inter-subunit distance, but a sharp bimodal distribution centered at 22.2 Å and 24.1 Å for H1-2s AS2 (Figure A-9; Table A-3). These differences in separation are consistent with the HAMP1 and HAMP2 structures in Aer2 1–172, where, in the case of the latter, the AS2 helices come tightly together to form an effective two-helix coiled coil. The relative separation and dynamics across the KCM junction were maintained, with H1-2s KCM sustaining a sharper distance distribution centered at 22.4 Å, and H1s KCM a longer, broader separation centered at 32.1 Å. Overall, the H1s and H1-2s distance distributions are consistent with near continuous four- and two-helix bundles across the H1/KCM junction, respectively, with the KCM helix retaining the dynamic and static features of the attached HAMP.

Table A-3 Inter-spin distance measurements by PDS.

Protein	AS1 (Å)	AS2 (Å)	KCM (Å)
H1 crystal	21.2	17.1	
H2 crystal	27.7	13.6	
H1C	32.4 (2.8)	23.7 (1.4)	
H2C	39.7 (5.2)	21.5 (2.2)	
H1s	32.6 (24.0)	27.1 (12.2)	32.1 (22.0)
H1-2s	42.7 (7.2)	22.2 (1.3), 24.1 (1.1)	22.4 (14.1)
H1-2s I88G	28.9 (29.0)	21.5 (7.0)	

The values shown in parentheses refer to the width (Å) at half of maximum peak height, and qualify peak broadening and conformational heterogeneity.

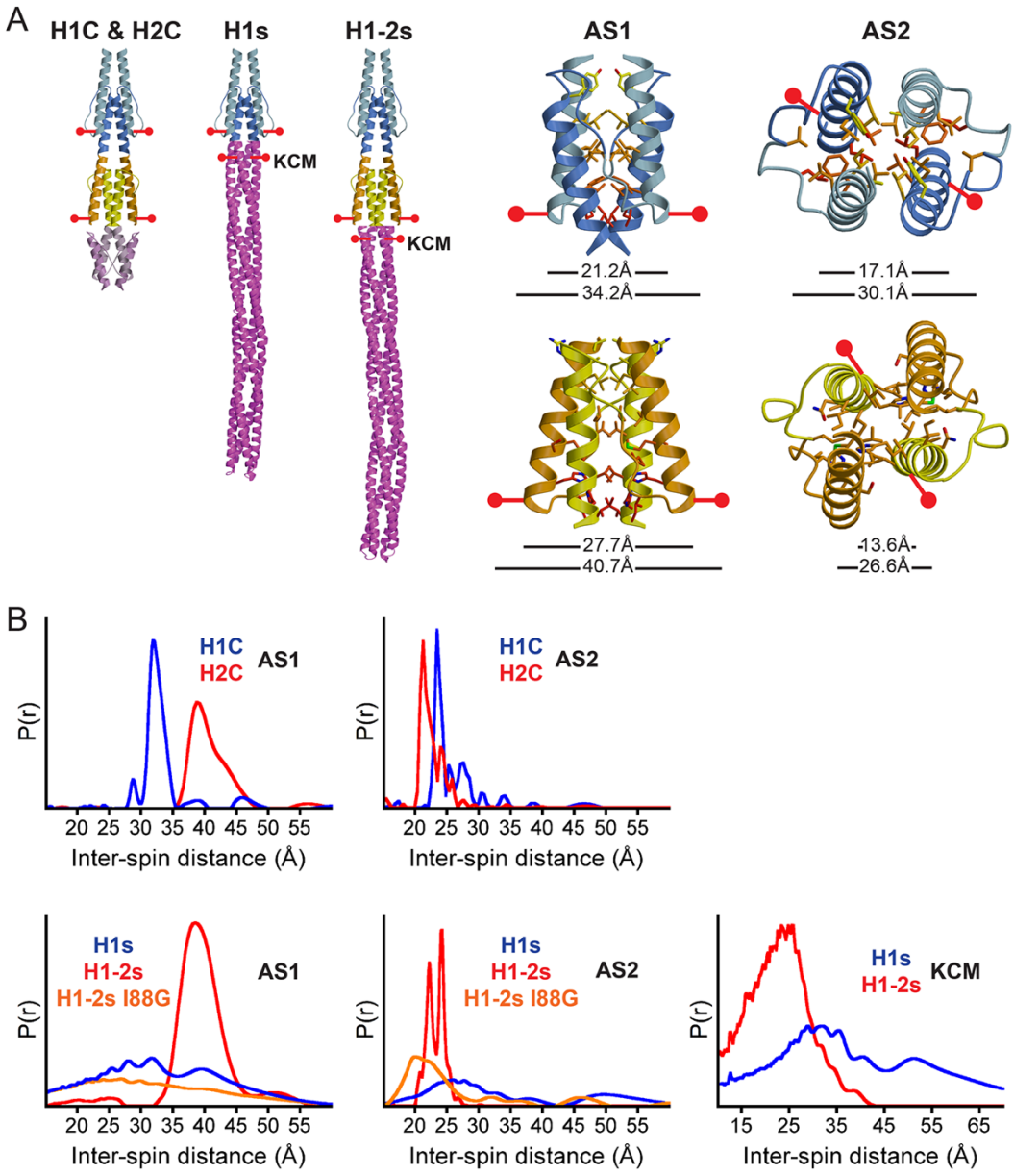

Figure A-9 Conformational properties of soluble receptors assessed by PDS.

(A) Schematic of spin-label sites in Aer2 1–172 (H1C and H2C) and soluble ATCs (H1s and H1-2s). Sites were chosen in AS1 and AS2 to maximize the distance separation expected to distinguish HAMP1 and HAMP2 in the crystal structure. Cα–

Cα distances from the crystal structure are shown (top distance). MTSSL spin labels can add up to 13 Å (bottom distance).

(B) Inter-spin distances measured by PDS of spin-labeled proteins. Pair-wise distance distributions (P[r]) of control samples (H1C and H2C) matched well with the differences in the crystal structure (Table A-3). Attachment to the Tar KCM (H1s) results in a more dynamic HAMP1 conformer, with broad distance distributions, which is indicative of conformation exchange between HAMP1 and HAMP2. HAMP2, in H1-2s, remains relatively static, with narrow distance peaks that are nearly identical to those of H2C. The H1-2s I88G HR2 mutant switches the conformational properties of HAMP2 towards a dynamic HAMP1 state, consistent with the CW locked phenotype in vivo. The two HAMP conformers have opposite effects downstream. HAMP2, which forms a two-helix coiled coil at the end of AS2, maintains similar distances across the junction in the KCM. HAMP1, which forms a four-helix coiled coil, maintains a longer, broader distance distribution. This suggests the structure of the AS2 helices is propagated downstream into the KCM helical bundle. Inter-spin distance distributions are tabulated in Table A-3

Substitution of HR2 Converts HAMP2 to a HAMP1-Like Conformation and Switches Output

Having established the CW signaling state as a HAMP1 conformer, we aimed to determine the conformational changes associated with the I88G mutation, which changes the behavior of H1-2s from CCW to CW locked in vivo. We reasoned the I88G mutation would alter the conformational equilibrium of HAMP2 to favor a HAMP1-like conformer. Using ESR distance measurements, we analyzed the H1-2s I88G structure in solution. As expected, the I88G mutation destabilized the rigid H1-2s conformation to generate a broad distance distribution (width at half the maximum peak height of 29.0 Å) centered at 28.9 Å for H1-2s I88G AS1 (Table A-3). This pair-wise distance distribution was nearly identical to that of H1s AS1 and indicative of conformational exchange (Figure A-9). The H1-2s I88G AS2 spin-spin distribution was also broad and overlapped with the distributed signal of H1s AS2, but also contained contribution from a short 21.5 Å distance that is most likely due to direct interactions between the spin labels and the bundle. Although the AS2 conformation in H1-2s I88G may not be identical to that in H1s, it is clearly different from that in H1-2s and shares the distributed properties of that in H1s. Thus, removing HR2 in HAMP2 shifted both receptor bias and HAMP structure toward a CW signaling HAMP1-like conformer. Given the conservation of HR2 and its importance structurally and functionally in CCW signaling, it is possible that other HAMP domains access a HAMP2-like conformation in their signaling mechanisms.

Discussion

Here we characterize the signaling properties of the Aer2 HAMP domains in chimeric transmembrane receptors and directly correlate structure and dynamics to cellular activities. As previously predicted [7], the HAMP1 and HAMP2 conformations generate CW and CCW signaling biases in bacterial chemoreceptors. Exchange between HAMP conformers is likely sufficient to induce CW biased signaling, whereas a more static HAMP2 conformer generates a CCW signal. Removal of HR2 destabilizes HAMP2, but not HAMP1, altering its structure and signaling bias to resemble those of HAMP1. Physical exchange between HAMP1 and HAMP2 conformers requires a downward motion of AS1 relative to AS2 and is consistent with the downward piston motion of TM2 produced by attractant binding in MCPs [12]. The most straightforward interpretation of our data produces a two-state model in which bacterial chemoreceptors switch primarily between HAMP1- and HAMP2-like states to propagate signals (Figure A-10).

The downstream effects of the two HAMP conformers provide important constraints on the output mechanism employed by MCPs. The transition between conformers involves multiple elements including helical translation, rotation, and tilts that are coupled to a rearrangement of the connector/HR2. Most relevant to the activity of downstream effector domains are the changes in position and dynamics of AS2. In HAMP1, the AS2 helices are part of a more standard four-helix bundle, whereas in the relatively distorted HAMP2, the AS2 helices resemble a two-helix coiled coil interaction. Two- and four-helix coiled coils differ with respect to the residues that contribute to the hydrophobic core. In a two-helix coiled coil,

the *a* and *d*residues form the core, while in a four-helix coiled coil the *a*, *d*, *e*, and *g* residues can all contribute to the core because of the greater packing contacts among the four helices. HAMP1-to-HAMP2 conversion rotates the AS2 helices in a CCW direction so that a "*g*" position (HAMP1) takes the place of what would otherwise be a "*c*" position (HAMP2) on the core periphery. (This corresponds to about a +55° rotation in Crick angle at the AS2 termini; however, the rotation in HAMP2 is also associated with substantial translation and tilting of the helices.) The HAMP2 AS2 conformation is then in line with the heptad pattern of hydrophobic residues entering the KCM. In the KCM, the *c* positions in-phase with HAMP2 tend to be hydrophilic and would thus disfavor placement as an out-of-phase *g* position. This is consistent with the proposed "stutter compensation" output mechanism based on helical discontinuities at AS2-output helix junctions [7, 20, 23]. The PDS data confirm that the helix separations across the junction follow those of AS2 in the two HAMP conformers, with position 270 appearing more two-helix-like and conformationally rigid when HAMP2 is attached, and more four-helix-like and broader when HAMP1 is attached. Given that the known structures of KCMs are consistently four-helix coiled coils, a switch to a distorted two-helix state would indeed destabilize the four-helix structure. Thus, these structural transitions appear consistent with the yin-yang and biphasic stability models for MCP signal transduction [16, 20, 24], where increased stability in HAMP decreases stability in the KCM that follows.

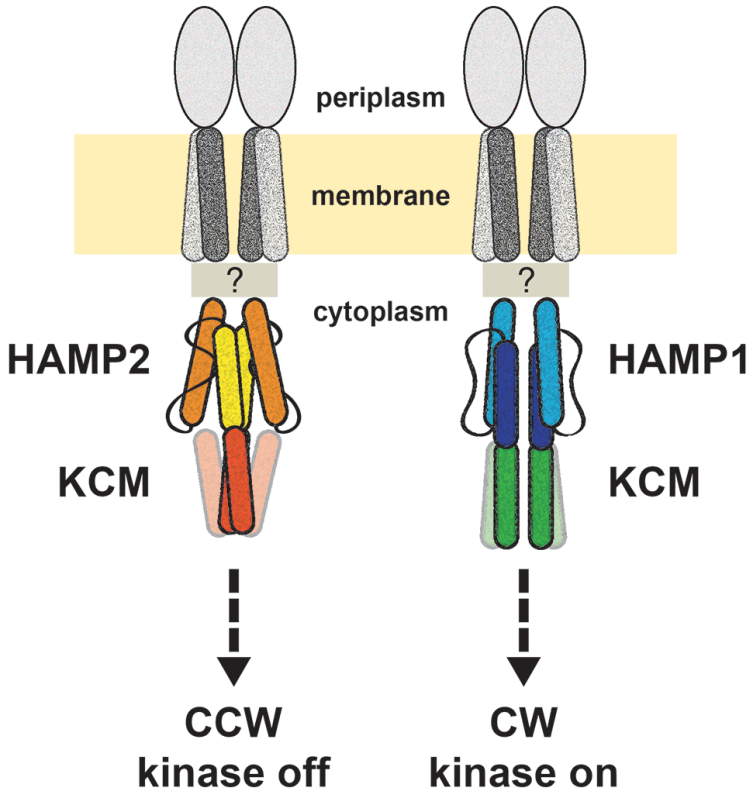

Figure A-10 Model for HAMP domain signal relay in bacterial chemoreceptors. The HAMP domains of MCPs exchange between HAMP1 and HAMP2 states to regulate bacterial chemotaxis. The conformation of HAMP2 imparts a two-helix coiled coil across the AS2/KCM junction, which results in CheA kinase inhibition and CCW flagella rotation. A dynamic HAMP1 forms a continuous four-helix coiled coil across the junction to generate kinase activation and CW flagella rotation.

Note that the KCM of Tar alone causes some CW output, but the kinase-on state is greatly enhanced when the HAMP1 domain is fused to Tar KCM. This stabilization cannot be explained by enhanced dimerization of the KCM because fusing the HAMP1 and HAMP2 domains, which stabilizes the dimer to an even greater extent (as judged by PDS), produces an opposite effect of exclusive CCW output. Furthermore, the expression level of H1s is substantially less than that of the Tar KCM domain itself, yet CW bias is higher; hence the CW lock does not derive from there being high levels of the KCM, which is known to activate CheA [25]. We conclude that HAMP1 exerts some conformational preference on the KCM that activates CheA, even in the absence of the transmembrane and ligand binding regions of Tar.

Consolidation of HAMP Signaling Models

Exchange between HAMP1 and HAMP2 conformers is also consistent with the biphasic HAMP signaling model [16]. In this case, a HAMP1 conformer would be assigned to the native kinase-on (CW) state. Notably, the PDS distributions of HAMP1 are broader than those of HAMP2, which supports a more dynamic on state predicted by the biphasic model. A HAMP2-like conformer would be assigned to the attractant-mimicking CCW(A) signaling state, given the importance of HR2 to the off state and its role in stabilizing the HAMP2 structure. PDS distributions of HAMP2 were narrower and more conformationally homogeneous than those of HAMP1, which indicates a more stable domain structure and thereby agrees with the increased stability indicated for the CCW(A) state in the biphasic model. The biphasic model

also predicts a second CCW(B) state where the HAMP domain is destabilized relative to the CW state. These states are largely found for mutations that are likely to disrupt the HAMP hydrophobic core but leave key hydrophobic residues at the C-terminal end of AS2 intact. Similar types of substitutions introduced into the Aer2 HAMP domains produced proteins that were not well expressed and hence difficult to study, which is consistent with highly destabilized domains. Nonetheless, CCW(B) lesions in Tsr do not completely unfold the HAMP domains because the mutant proteins are still able to exert a kinase-off conformation on the KCM. These results, taken with the structural data presented here, suggest that a key property of any CCW state may be the formation of a tight two-helix bundle at the C-terminal end of AS2. This may be achieved by a range of conformations in the upper HAMP that include those that resemble HAMP2, as well as those that disrupt the upper domain yet still allow close association of the AS2 helices.

Stability may be a difficult parameter to assign to specific HAMP variants, as its formal definition involves the free energy difference between defined states. As all HAMP domains are dynamic to some degree, an ensemble of conformational states is likely involved in their function. With regards to direct measurements of stability, as defined by cooperative helical unfolding, all Aer2 HAMP mutations were destabilizing irrespective of their shift in signaling bias (Figure A-11; Table A-2). Nonetheless, the HAMP domains of CW output receptors were indeed more dynamic, populating both HAMP1 and HAMP2 conformers. The conformational broadening of HAMP1 observed on fusion to the KCM suggests that an out-of-phase attachment of HAMP to the MCP KCM, which maintains the four-helix structure across the junction,

bestows the dynamic properties of the KCM coiled coil onto HAMP. The structure of HAMP2 remains relatively unaffected on fusion to the KCM, but in this case the KCM appears to adopt HAMP2-like properties. Thus, the HAMP domains of MCPs most likely oscillate between two states: a conformationally homogenous CCW state that closely resembles HAMP2 and a more conformationally heterogeneous CW state, whose mean atomic positions resemble HAMP1. In line with the reasoning of Parkinson and Falke and colleagues [16, 20, 24, 26], HAMP1 appears to stabilize the nascent on state inherent to the Tar KCM, whereas the more stable HAMP2 enforces a distorted four-helix bundle across the interface. Notably, the average conformations of the HAMP states and their dynamical properties change together; our data show that an activating HAMP conformation is more dynamic, which does not necessarily mean that any increase in HAMP dynamics is activating.

Studies of Af1503 HAMP fusions to dimerization histidine phosphorylation domains in the context of Taz, a chimera between the Tsr sensing domain and cytoplasmic regions of the sensor kinase EnvZ, found that mutations of key packing residues in the Af1503 HAMP alter the position of AS2 [9]. In particular, a substitution in the bundle core (A291F) that causes a CCW rotation of AS2 (+20° in Crick angle) is more readily able to undergo deactivation by attractant (Ser). Overall, the differences between the variant Af1503 HAMP structures characterized here are more modest than the differences between HAMP1 and HAMP2, and perhaps consistent with this, structural changes are not propagated far across the junction to the dimerization histidine phosphorylation domains. It is difficult to make direct comparison of the activity effects of Tar and Taz, as the signaling modules are quite

different; nonetheless, a rotational reorientation of AS2 is a common feature of structures that perturb output in both systems.

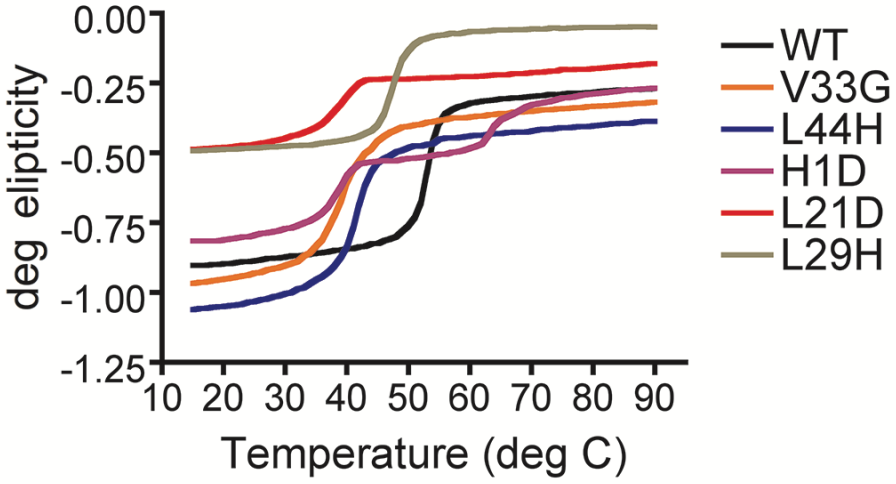

Figure A-11 Melting curves of HAMP1 mutants.

Circular dichroism thermal melting curves of Aer2 1–172 proteins. All mutations, with the exception of H1D, destabilized Aer2, resulting in a lower melting temperature. Overall, there was no correlation between stability and signaling bias.

Implications for Other HAMP Systems

Conversion between HAMP1 and HAMP2 states may also apply to other transmembrane receptors. For example, the transmembrane helices of NpHtrII are known to undergo a CW rotation upon light stimulation of the NpSRII-NpHtrII complex [13]. This motion is consistent with the helical rotation of AS1 required to convert between HAMP1 and HAMP2. In addition, the NpHtrII HAMP domain was reported to undergo dynamic oscillation at the C-terminal end of AS1 [27]. HAMP1 and HAMP2 conformational exchange could account for the dynamics of NpHtrII. Recently Wang et al. [28] reported ESR and labeling measurements using a more stable nanodisc-solubilized NpHtrII HAMP1-2 construct. Contrary to the previous report [27], they did not observe the unstable, dynamic HAMP state that had been seen in different salt concentrations. Upon light stimulation, they did observe alternating helical motions in the two NpHtrII HAMP domains, corresponding to conformational changes consistent with exchange between HAMP1 and HAMP2 conformers. This supports the idea that other HAMP domains may oscillate between HAMP1 and HAMP2 to change output states. Furthermore, the data indicated that signal transduction through tandem HAMP domains involves alternating switching in conformer states [28], as proposed from the Aer2 structures [7].

Although our model can be applied beyond the scope of MCPs, it is not clear if all ~26,000 identified HAMP domains utilize the same conformational signaling mechanism. Previous studies involving chimera transmembrane receptors suggest some HAMP domains share a conserved mechanism [29]. We report here that with minor modification the soluble HAMP domains of Aer2 can function within

transmembrane chemoreceptors and respond to ligand in both normal and inverse directions. However, as we have seen with HAMP1, attachment to up- and downstream domains may influence the conformation and/or dynamic properties of HAMP domains. Thus, although there is a significant body of evidence that HAMP domains are interchangeable modules sharing a conserved mechanism, it is possible these findings derive from a plastic property of HAMP domains that allows them to be molded in various ways by each input and output domain to which they are attached. For example, the large, flexible MCP KCMs may bestow dynamic properties upon MCP HAMP domains that are not found in sensor kinase HAMP domains.

The DExG Motif Distinguishes Membrane-Associated and Poly-HAMP Domains

The region that distinguishes canonical, membrane-associated, and divergent poly-HAMP domains is the connector-AS2 junction [17]. Canonical HAMPs contain the DExG motif, while divergent HAMPs conserve a single glycine [7]. Our finding that addition of the DExG motif reconstitutes transmembrane function into the divergent and soluble HAMP1 suggests that these two HAMP subtypes are distinguished mainly by their mode of signal input. Canonical HAMP domains require the DExG motif to couple to upstream transmembrane signals. In contrast, divergent HAMP domains require the conserved glycine to pack closely in a poly-HAMP chain. Currently, the role the DExG motif plays is unclear. In the Af1503 HAMP the conserved Glu of this motif hydrogen-bonds with the N-terminus of AS1 (Figure A-12) and thereby may couple conformational signals coming from the transmembrane helices into the connector. Alternatively, the motif may tune the conformational

equilibrium of the on and off states to make the off state more accessible to perturbations induced by ligand binding.

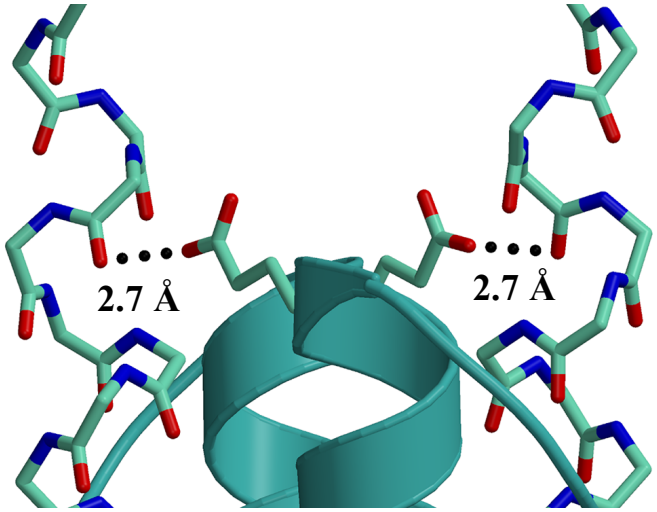

Figure A-12 The Glu in the DExG motif hydrogen-bonds to AS1 in the Af1503 structure. Structure of Af1503 (Protein Data Bank code 2ASW) highlighting hydrogen bond between E311 and carbonyl (T281) in AS1 [5].

HAMP Domain Mutational Effects

The L44H structure provides new insight into the structural consequences of HAMP domain residue substitutions that perturb function. In the L44H structure, the tilt of AS1 drives the helices apart, disrupting upstream helical packing and resulting in a loss of observed secondary structure at the N-terminus of AS1. In the context of a transmembrane MCP, if this helix disruption were maintained, it would decouple TM2 from AS1. Because the L44H variant is strongly CW biasing, and the H1 conformation generates CW output, we assume that the structure seen at the C-terminal domain in the crystal is maintained in the Tar fusions. However, within a transmembrane MCP, it is also possible that similar mutations maintain the TM2/AS1 junction and that the strain induced by the substitution disrupts, rather, the connectivity of the AS2/KCM junction. This idea offers the possibility that the phenotypes of some MCP mutants may derive from disruptions at the up- or downstream HAMP domain junctions and subsequent decoupling of signal input and output. Thus, it is perhaps not surprising that different types of residue substitutions at the same position can produce very different phenotypes, as seen in Tsr [16, 20]. Likewise, for similar reasons, the effects of several substitutions at different sites may not necessarily be additive. Such complex behavior results when the H1D substitution is present along with the L44H, V33G, or I88G substitutions (Figure A-2).

Inverted Signaling of H1 V33G: Potential Mechanisms and Application

The mechanism underlying H1 V33G inverted signaling is not completely understood; however, it is clear that a branched hydrophobic residue at HR2 is

important to achieve the HAMP2 conformation and CCW signaling state. Thus, it is perhaps reasonable that upon attractant binding, the V33G variant is unable to switch to a HAMP2 conformation. Unable to obtain the HAMP2 state, upstream perturbation causes the equilibrium to shift toward HAMP1. Stabilization of a HAMP1 state by V33G is evident by the effect of this mutation in the CheRB− background, where it produces an exclusively CW state. Nonetheless, introduction of the DExG motif overcomes the V33G lesion and restores a normal CCW response to attractant. Thus, the DExG motif must stabilize a CCW state despite the absence of HR2. Overall, the effects of these lesions underscore the fine balance between the CW and CCW conformational states that HAMP domains assume and the cooperative contributions of many residues to their relative stabilities and transitions.

Finally, the H1 V33G HAMP domain may provide a useful tool for engineering receptor-driven processes in bacteria. Substitution of H1D and H1 V33G into chimeric chemoreceptors should produce opposite chemotactic responses to the same ligand. This strategy could be applied to direct genetically modified bacteria towards or away from specific chemicals. This may be especially advantageous in remediation efforts for taxing bacteria towards chemicals that are normally repellants.

Materials and Methods

Bacterial Strains

ATC expression and behavioral assays mainly utilized two *E. coli* strains: BT3388 (*tar*, *tsr*, *trg*, *tap*, *aer*) [30] and a Δ*cheRB* strain UU2610 (*tar*, *tsr*, *trg*, *tap*, *aer*, *cheR*, *cheB*) (a gift from J. S. Parkinson), both of which lack all native chemoreceptors. For isogenic comparison, the *E. coli*strain UU2612 (*tar*, *tsr*, *trg*, *tap*, *aer*) was used (J. S. Parkinson).

Cloning and Mutation

E. coli Tar was cloned from genomic DNA into Litmus 28i with 5′ XbaI-NdeI and 3′ HindIII-XhoI restriction sites. Silent mutations were utilized to remove an internal NdeI site in Tar and to introduce BamHI and PmlI sites near the 5′ and 3′ boundaries of the Tar HAMP domain. To generate ATCs, Aer2 HAMP fragments were cloned into the engineered BamHI and PmlI sites of Tar/Litmus 28i. Final ATCs replaced the Tar HAMP domain (214–262) with Aer2 HAMP domains: H1 (8–56), H2 (63–112), H3 (109–156), H1-2 (8–56), H1-23 (8–156), and H23 (63–156). Full-length ATC receptors were transferred using NdeI and HindIII sites to the vector pKG116, which contained a salicylate inducible promoter. Soluble ATCs for in vivo studies were generated by ligating an Aer2 PCR fragment with a NdeI and PmlI digested Tar/pKG116 vector. For ESR studies, soluble ATCs were transferred to pET28 using NdeI and HindIII sites. All HAMP domain mutations were introduced using either the QuikChange strategy or overlap extension. The correct sequence for all clones was confirmed by direct nucleotide sequencing.

Quantification of Cell Tumbling Frequencies

Qualitative experiments were first carried out using standard swim assays in tryptone semisoft agar supplemented with 12.5 μg/ml chloramphenicol and 0.5 or 1 μM sodium salicylate. Plates were incubated at 30°C for 15–19 h. Aspartate rings were verified by placing 2 μl of 0.5 M aspartate on top of the semisoft agar, ~2 mm in front of the leading colony edge, and incubating plates for a further 5 h. Direct measurements of cell tumbling frequencies were carried out using temporal assays. *E. coli* cells harboring ATC plasmids were grown in tryptone broth, induced for 1 h with 2 μM sodium salicylate, washed and resuspended in KEP buffer (10 mM potassium phosphate, 0.1 mM EDTA [pH 7.0]), and then visualized by dark-field microscopy. Cells reached adaptation equilibrium after 5 min, after which cell tumbling frequencies were measured. The ability of ATC receptors to respond to aspartate was tested using temporal assays combined with monitoring of changes in tumbling frequency after the addition of various aspartate concentrations.

Expression Levels of ATC Receptors

Expression levels of proteins in BT3388 cells were analyzed by Western blotting after induction with 2 μM sodium salicylate, using antisera against the highly conserved region of Tsr (common to all chemoreceptors) (a gift from J. S. Parkinson). Bands were visualized on Western blots and quantified on a BioSpectrum digital imager (UVP).

Circular Dichroism Spectroscopy

Circular dichroism experiments on HAMP domain mutants were carried out using a AVIV Biomedical (model 202-01) spectropolarimeter. The protein sample (~0.5 mg/ml, in 10 mM sodium phosphate buffer [pH 7.5]) was heated 1°C per min and allowed to reach equilibrium for 2 min. After that, the degree of ellipticity was measured, averaged over 1 min, and plotted versus temperature.

Crystallization and Data Collection

Aer2 1–172 mutant proteins were purified as previously described for the WT protein [7] with the exception of induction temperature, which was reduced to 18°C. Crystals of Aer2 1–172 V33G protein were obtained in conditions and space group identical to those described previously for the WT protein [7]. Aer2 1–172 L44H protein (40 mg/ml) crystallized in a different space group ($P3_212$). L44H crystals were grown by vapor diffusion, mixing 1.5 µl of protein with 1.5 µl of well solution, against a reservoir containing 1.5–1.7 M $MgSO_4$ and 0.1 M Tris (pH 8.5) for 6–10 h at room temperature. Diffraction data were collected at the Cornell High Energy Synchrotron Source A1 beamline on an ADSC Quantum 210 CCD detector. Data were processed with HKL2000 [31].

Structure Determination and Refinement

V33G and L44H structures were determined by molecular replacement using Phenix AutoMR [32]. The structures of V33G and L44H were built using XFIT [33] and COOT [34], respectively, and structure refinement was carried out

using CNS [35] and Phenix [32], respectively, amidst cycles of manual model building, minimization, B-factor refinement, and solvent molecule placement to produce the final models (V33G, R-factor=23.5%, R_{free}=28.0%; L44H R-factor=20.8%, R_{free}=25.9%) (Table A-4).

Preparation of Spin-Labeled Proteins

All soluble ATC receptors were overexpressed in *E. coli* BL21 (DE3) cells at room temperature for 6–18 h using IPTG. Proteins were purified using a gravity Ni-column and size-exclusion chromatography on a Superdex 200 Hi-Load 26/60 column. Aer2 and Tar lack any native cysteine residues. Site-directed mutagenesis introduced cysteine residues for spin labeling in HAMP1 and HAMP2 at AS1 (D26 and A81) and AS2 (E53 and A107). A cysteine residue at E270 in Tar KCM was introduced two helix turns from the AS2/KCM junction, which starts at Tar D263. Spin labeling was accomplished as previously described [36] by incubating protein and MTSSL spin label with gentle mixing for 4 h at room temperature (H1C and H2C) or overnight at 4°C (H1s and H1-2s). Excess spin label was removed by buffer exchange using a desalting column. ESR measurements were conducted within 24 h of spin labeling, or protein was flash-frozen and thawed within 1 wk to ensure sample quality.

PDS Measurements

PDS measurements were conducted at the Advanced Electron Resonance Technology facility as previously described [36, 37]. Double electron electron resonance experiments were carried out at 17.35 GHz on a home-built 2D-FT ESR

spectrometer, with either 16-ns or 32-ns pump pulses [38]. Protein concentrations were in the range of 25–50 μM. Dipolar evolution times were typically about 2.5 microseconds. The baseline was approximated by a linear polynomial in most cases. Subsequently, distance distributions were calculated by Tikhonov regularization [39] and further refined by a maximum entropy regularization method [40].

Table A-4 Data collection and refinement statistics.

Data Collection		
	L44H	V33G
Wavelength (Å)	0.97918	0.97857
Space group	$P3_212$	$P4_32_12$
Cell parameters (Å)	a = b = 61.1, c = 81.4	a = b = 113.4, c = 65.0
Resolution (Å)	50-1.95 (1.98-1.95)	50-2.88 (2.93-2.88)
No. of reflections	138172	96286
No. of unique reflections	12812	10197
Completeness (%)	99.7 (100.0)	99.4 (100.0)
R_{sym} [a]	0.074 (0.366)	0.040 (0.349)
$I/\sigma(I)$	30.6 (6.8)	50.2 (8.4)
Refinement statistics		
Resolution range (Å)	50-1.95 Å (1.98-1.95)	50.0-2.88 Å (2.93-2.88)
R factor, %	20.8 (21.2)	23.5 (32.9)
R_{free}, %	25.9 (27.0)	28.0 (35.0)
Atoms (protein, solvent)	1149, 178	1229, 14
Mean B-values ($Å^2$)		
Protein	34.7	85.8
Solvent	51.3	65.0
R.m.s. deviations		
Bond lengths (Å)	0.004 Å	0.007 Å
Bond angles (deg)	0.98 deg	1.21 deg
Missing residues	1-6, 157-172	157-172

*Highest resolution shell is shown in parenthesis

REFERENCE

[1] Szurmant H, White RA, Hoch JA (2007) Sensor complexes regulating two-component signal transduction. Curr Opin Struct Biol 17: 706–715.

[2] Letunic I, Doerks T, Bork P (2012) SMART 7: recent updates to the protein domain annotation resource. Nucleic Acids Res 40: D302–D305.

[3) Parkinson JS (2010) Signaling mechanisms of HAMP domains in chemoreceptors and sensor kinases. Annu Rev Microbiol 64: 101–122.

[4] Hazelbauer GL, Falke JJ, Parkinson JS (2008) Bacterial chemoreceptors: high-performance signaling in networked arrays. Trends Biochem Sci 33: 9–19.

[5] Hulko M, Berndt F, Gruber M, Linder JU, Truffault V, et al. (2006) The HAMP domain structure implies helix rotation in transmembrane signaling. Cell 126: 929–940.

[6] Ames P, Zhou Q, Parkinson JS (2008) Mutational analysis of the connector segment in the HAMP domain of Tsr, the Escherichia coli serine chemoreceptor. J Bacteriol 190: 6676–6685.

[7] Airola MV, Watts KJ, Bilwes AM, Crane BR (2010) Structure of concatenated HAMP domains provides a mechanism for signal transduction. Structure 18: 436–448.

[8] Ferris HU, Dunin-Horkawicz S, Mondéjar LG, Hulko M, Hantke K, et al. (2011) The mechanisms of HAMP-mediated signaling in transmembrane receptors. Structure 19: 378–385.

[9] Ferris HU, Dunin-Horkawicz S, Hornig N, Hulko M, Martin J, et al. (2012) Mechanism of regulation of receptor histidine kinases. Structure 20: 56–66.

[10] Swain KE, Falke JJ (2007) Structure of the conserved HAMP domain in an intact, membrane-bound chemoreceptor: a disulfide mapping study. Biochemistry 46: 13684–13695.

[11] Watts KJ, Johnson MS, Taylor BL (2008) Structure-function relationships in the HAMP and proximal signaling domains of the aerotaxis receptor Aer. J Bacteriol 190: 2118–2127.

[12] Falke JJ, Hazelbauer GL (2001) Transmembrane signaling in bacterial chemoreceptors. Trends Biochem Sci 26: 257–265.

[13] Moukhametzianov R, Klare JP, Efremov R, Baeken C, Goppner A, et al. (2006) Development of the signal in sensory rhodopsin and its transfer to the cognate transducer. Nature 440: 115–119.

[14] Hazelbauer GL, Lai WC (2010) Bacterial chemoreceptors: providing enhanced features to two-component signaling. Curr Opin Microbiol 13: 124–132.

[15] Chao X, Muff TJ, Park SY, Zhang S, Pollard AM, et al. (2006) A receptor-modifying deamidase in complex with a signaling phosphatase reveals reciprocal regulation. Cell 124: 561–571.

[16] Zhou Q, Ames P, Parkinson JS (2011) Biphasic control logic of HAMP domain signalling in the Escherichia coli serine chemoreceptor. Mol Microbiol 80: 596–611.

[17] Dunin-Horkawicz S, Lupas AN (2010) Comprehensive analysis of HAMP domains: implications for transmembrane signal transduction. J Mol Biol 397: 1156–1174.

[18] Airola MV, Watts KJ, Crane BR (2010) Identifying divergent HAMP domains and poly-HAMP chains. J Biol Chem 285: le7.

[19] Watts KJ, Taylor BL, Johnson MS (2011) PAS/poly-HAMP signalling in Aer-2, a soluble haem-based sensor. Mol Microbiol 79: 686–699.

[20] Zhou Q, Ames P, Parkinson JS (2009) Mutational analyses of HAMP helices suggest a dynamic bundle model of input-output signalling in chemoreceptors. Mol Microbiol 73: 801–814.

[21] Linder JU, Schultz JE (2010) Transmembrane receptor chimeras to probe HAMP domain function. Methods Enzymol 471: 115–123.

[22]] Mondéjar LG, Lupas A, Schultz A, Schultz JE (2012) HAMP domain-mediated signal transduction probed with a mycobacterial adenylyl cyclase as a reporter. J Biol Chem 287: 1022–1031.

[23] Stewart V, Chen LL (2010) The S helix mediates signal transmission as a HAMP domain coiled-coil extension in the NarX nitrate sensor from Escherichia coli K-12. J Bacteriol 192: 734–745.

[24] Swain KE, Gonzalez MA, Falke JJ (2009) Engineered socket study of signaling through a four-helix bundle: evidence for a yin-yang mechanism in the kinase control module of the aspartate receptor. Biochemistry 48: 9266–9277.

[25] Ames P, Yu YA, Parkinson JS (1996) Methylation segments are not required for chemotactic signalling by cytoplasmic fragments of Tsr, the methyl-accepting serine chemoreceptor of Escherichia coli. Mol Microbiol 19: 737–746.

[26] Starrett DJ, Falke JJ (2005) Adaptation mechanism of the aspartate receptor: electrostatics of the adaptation subdomain play a key role in modulating kinase activity. Biochemistry 44: 1550–1560.

[27] Doebber M, Bordignon E, Klare JP, Holterhues J, Martell S, et al. (2008) Salt-driven equilibrium between two conformations in the HAMP domain from Natronomonas pharaonis—the language of signal transfer? J Biol Chem 283: 28691–28701.

[28] Wang J, Sasaki J, Tsai A, Spudich JL (2012) HAMP domain signal relay mechanism in a sensory rhodopsin-transducer complex. J Biol Chem 287: 21316–21325.

[29] Appleman JA, Chen LL, Stewart V (2003) Probing conservation of HAMP linker structure and signal transduction mechanism through analysis of hybrid sensor kinases. J Bacteriol 185: 4872–4882.

[30] Yu HS, Saw JH, Hou S, Larsen RW, Watts KJ, et al. (2002) Aerotactic responses in bacteria to photoreleased oxygen. FEMS Microbiol Lett 217: 237–242.

[31] Otwinowski Z, Minor W (1997) Processing of X-ray diffraction data collected in oscillation mode. In: Carter CW Jr, Sweet RM, editors. Methods in enzymology, Volume 276: macromolecular crystallography, part A. pp. 307–326.

[32] Adams PD, Afonine PV, Bunkoczi G, Chen VB, Davis IW, et al. (2010) PHENIX: a comprehensive Python-based system for macromolecular structure solution. Acta Crystallogr D Biol Crystallogr 66: 213–221.

(33) McRee DE (1999) XtalView Xfit—a versatile program for manipulating atomic coordinates and electron density. J Struct Biol 125: 156–165.

[34] Emsley P, Cowtan K (2004) Coot: model-building tools for molecular graphics. Acta Crystallogr D Biol Crystallogr 60: 2126–2132.

[35] Brunger AT, Adams PD, Clore GM, DeLano WL, Gros P, et al. (1998) Crystallography & NMR system: a new software suite for macromolecular structure determination. Acta Crystallogr D Biol Crystallogr 54: 905–921.

[36] Bhatnagar J, Borbat PP, Pollard AM, Bilwes AM, Freed JH, et al. (2010) Structure of the ternary complex formed by a chemotaxis receptor signaling domain,

the CheA histidine kinase, and the coupling protein CheW as determined by pulsed dipolar ESR spectroscopy. Biochemistry 49: 3824–3841.

[37] Borbat PP, Freed JH (2007) Measuring distances by pulsed dipolar ESR spectroscopy: spin-labeled histidine kinases. Methods Enzymol 423: 52–116.

[38] Park SY, Borbat PP, Gonzalez-Bonet G, Bhatnagar J, Pollard AM, et al. (2006) Reconstruction of the chemotaxis receptor–kinase assembly. Nat Struct Mol Biol 13: 400–407.

[39] Chiang YW, Borbat PP, Freed JH (2005) The determination of pair distance distributions by pulsed ESR using Tikhonov regularization. J Magn Reson 172: 279–295.

[40] Chiang YW, Borbat PP, Freed JH (2005) Maximum entropy: a complement to Tikhonov regularization for determination of pair distance distributions by pulsed ESR. J Magn Reson 177: 184–196.

APPENDIX B

Architecture of the Soluble Receptor Aer2 Indicates an In-Line Mechanism for PAS and HAMP Domain Signaling[1]

Abstract

Bacterial receptors typically contain modular architectures with distinct functional domains that combine to send signals in response to stimuli. Although the properties of individual components have been investigated in many contexts, there is little information about how diverse sets of modules work together in full-length receptors. Here, we investigate the architecture of Aer2, a soluble gas-sensing receptor that has emerged as a model for PAS (Per–Arnt–Sim) and poly-HAMP (histidine kinase–adenylyl cyclase–methyl-accepting chemotaxis protein–phosphatase) domain signaling. The crystal structure of the heme-binding PAS domain in the ferric, ligand-free form, in comparison to the previously determined cyanide-bound state, identifies conformational changes induced by ligand binding that are likely essential for the signaling mechanism. Heme-pocket alternations share some similarities with the heme-based PAS sensors FixL and EcDOS but propagate to the Iβ strand in a manner predicted to alter PAS–PAS associations and the downstream HAMP junction within full-length Aer2. Small-angle X-ray scattering of PAS and poly-HAMP domain fragments of increasing complexity allow unambiguous domain assignments and reveal a linear quaternary structure. The Aer2 PAS dimeric crystal structure fits well within ab initio small-angle X-ray scattering molecular envelopes, and pulsed dipolar

ESR measurements of inter-PAS distances confirm the crystallographic PAS arrangement within Aer2. Spectroscopic and pull-down assays fail to detect direct interactions between the PAS and HAMP domains. Overall, the Aer2 signaling mechanism differs from the Escherichia coli Aer paradigm, where sideon PAS–HAMP contacts are key. We propose an in-line model for Aer2 signaling, where ligand binding induces alterations in PAS domain structure and subunit association that is relayed through the poly-HAMP junction to downstream domains.

---

[1]Reprinted from Airola MV, Huh D, Sukomon N, Widom J, Sircar R, Borbat PP, et al. Architecture of the Soluble Receptor Aer2 Indicates an In-Line Mechanism for PAS and HAMP Domain Signaling. J Mol Biol. 2013;425:886-901.

Nattakan Sukomon expressed, purified, crystallized, and collected diffraction data of the surface entropy reduction variants of the Aer2 PAS domain, performed pull-down experiments, and measured UV-visible absorption spectra of the ligand-free and CN-bound Aer2 PAS proteins.

Introduction

Two-component systems allow bacteria to respond to environmental changes and are therefore necessary for their survival. Signaling cascades are initiated by modular receptors that combine different functional domains to sense signals and relay changes to the activity of an enzymatic or non-enzymatic effector module. PAS (Per–Arnt–Sim) and HAMP (histidine kinase–adenylyl cyclase–methyl-accepting chemotaxis protein–phosphatase) domains are two of the most common components [1–3]. Found in over 29,000 and 26,000 proteins [4], respectively, they regulate the same large class of effectors including histidine kinases, adenylyl cyclases, methyl-accepting chemotaxis proteins, phosphatases, GGDEF, and EAL domains [1,5]. PAS domains often utilize a noncovalently bound cofactor (e.g., FAD or heme) that enables sensing of light, oxygen, voltage, and chemical stimuli [2,5]. HAMP domains are signal relay modules that couple input and output domains [1,3]. The *Escherichia coli* aerotaxis receptor (EcAer) is the best-studied PAS–HAMP system, where signals are relayed through direct side-on PAS and HAMP domain interactions in this integral membrane protein [1,6,7]. How signal transduction occurs in other multi-domain receptors is a major open question.

The *Pseudomonas aeruginosa* soluble receptor Aer2 has emerged as a promising system to investigate signal transduction by coupled PAS and HAMP domains [8]. The domain architecture of Aer2 comprises three N-terminal HAMP domains (collectively known as a poly-HAMP domain) [Protein Data Bank (PDB) code: 3LNR] [9], a heme-binding PAS domain (PDB codes: 3V0L and 4HI4) [10], two C-terminal HAMP domains, and a kinase-control module (KCM) typical of

methyl-accepting chemotaxis proteins (Figure B-1 and B-2) [8]. Unlike EcAer, PaAer2 contains no integral membrane helices and, thus, allows the study of interdomain signaling without the complication of the membrane component, which EcAer requires for function. The biological function of Aer2 is not yet clear. One report suggested that Aer2 is involved in mediating aerotaxis in P. aeruginosa [11], but this finding has not been confirmed [8,12,13]. Nevertheless, Aer2 can interact with the chemotaxis system of *E. coli* to mediate repellent responses to O2, nitric oxide (NO), and CO [8]. Interestingly, deletion of CheB2, which is expressed from the same operon as Aer2 and likely mediates Aer2 adaptation, was necessary for *P. aeruginosa* pathogenesis in a *Caenorhabditis elegans* infection model [14]. Thus, although how Aer2 relates to chemotaxis in *P. aeruginosa* is currently unclear, Aer2 is relevant to infection by *P. aeruginosa*.

The crystal structure of the Aer2 PAS domain was recently determined with bound cyanide (CN^-) [10]. The structure revealed a unique heme-binding PAS fold that is similar in overall architecture to the characterized heme-binding PAS domains of FixL [15–17] and EcDOS [18,19], but different in important ways, which include primarily the regions surrounding the heme pocket and the mode of heme ligation. In addition, Aer2 PAS differs from the extracellular, heme c-binding PAS domains from Geobacter sulfurreducens. 20 This has raised the interesting question of precisely how the Aer2 PAS domain signals in response to ligand binding. Furthermore, how do the Aer2 PAS domains communicate with their downstream HAMP domains and why are the N-terminal HAMP domains, which occur prior to the sensing domain, necessary for function? To answer these questions, we coupled structural data of the unligated

ferric PAS domain using X-ray crystallography and low-resolution small-angle X-ray scattering (SAXS) of PAS and poly-HAMP domains to establish the domain architecture of Aer2 and reveal conformational properties of the protein relevant to its signaling mechanism.

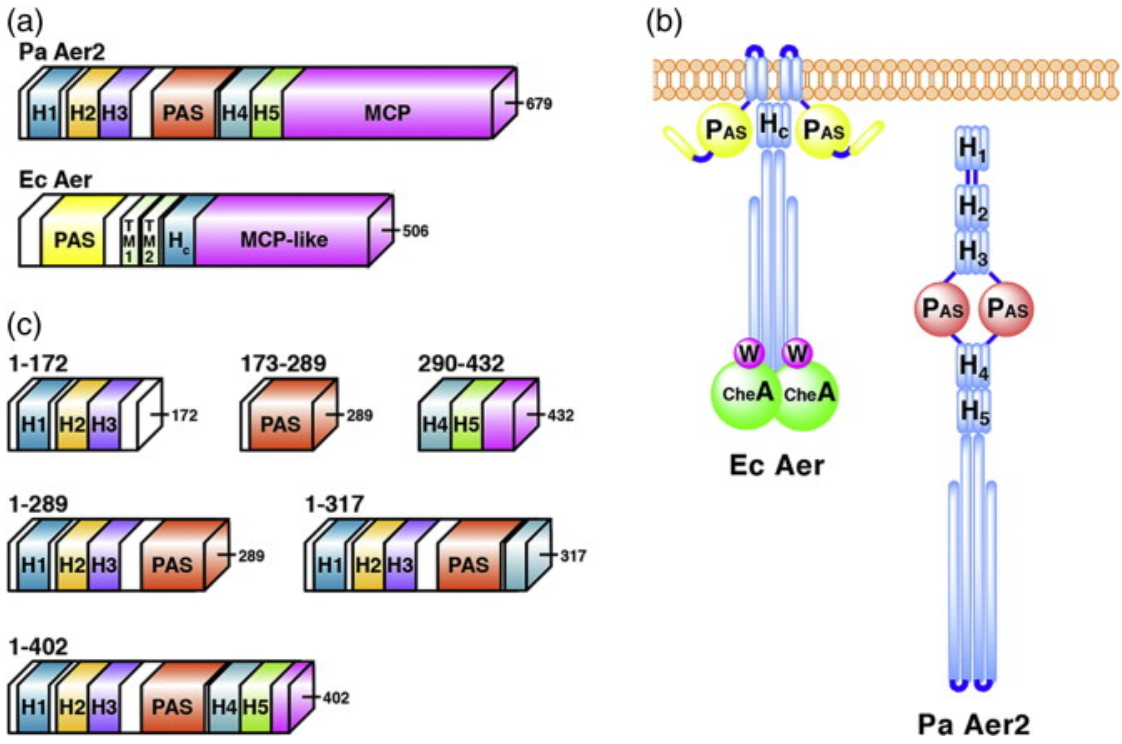

Figure B-1 Domain architecture of PAS and HAMP domains in *Pa*Aer2 and *Ec*Aer.

(a) Schematic representation of full-length *Pa*Aer2 and *Ec*Aer proteins.

(b) Cartoon representation of full-length proteins displaying known PAS and HAMP domain interactions in *Ec*Aer and *Pa*Aer2.

(c) Schematic representation of truncated *Pa*Aer2 proteins used in this study.

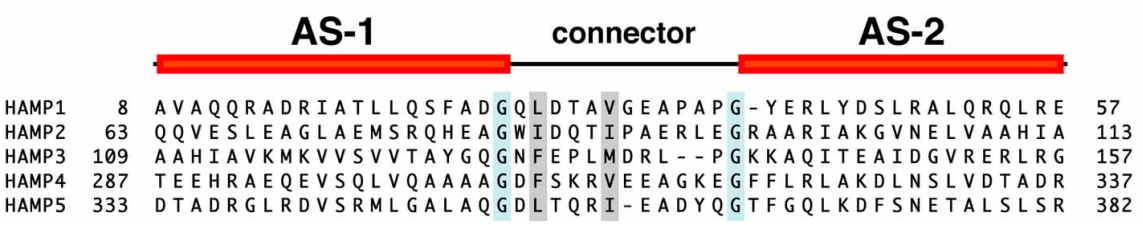

Figure B-2 The Aer2 receptor contains five HAMP domains. Sequence alignment of the HAMP domains in Aer2. HAMP domains consist of two helices (AS-1 and AS-2) and a semi-structured connector which folds into a dimeric, parallel four-helix bundle. Conserved glycine residues and hydrophobic residues (HR1 and HR2) in the connector are shown in blue and grey respectively. HAMP2-3 and HAMP4-5 are concatenated to form di-HAMP domains.

Materials and methods

Protein expression and purification

Various fragments (1–172, 173–289, 290–432, 1–289, 1– 317, and 1–402) of the gene encoding *P. aeruginosa* PAO1 Aer2 were cloned into the pET28a vector between NdeI and HindIII restriction sites, which added a cleavable N-terminal His tag. The surface entropy reduction substitutions (K176A and E275A) were generated in Aer2 173–289 and full-length Aer2 1–679 using PCR (K176A-PAS) and site-directed mutagenesis. For overexpression, plasmids were transformed into BL21 (DE3) cells, grown at 37 ° C in Luria Broth to an OD600 (optical density at 600 nm) of 0.6 and incubated with 100 mM IPTG at either 18 °C (1–402), 23 °C (1–172, 1–289, 1–317, and 173–289), or 37 °C (290–432) for 20 h (18 °C and 23 °C) or 6 h (37 °C)

before harvesting cells. Co-expression with E. coli ferrochelatase was necessary to promote full heme incorporation in Aer2 1–402 as previously described.26 Proteins were purified using a Ni-NTA column following the manufacturer's recommended protocol (Qiagen). After thrombin digestion, His tag free protein was applied to either a Superdex 75 26-60 Hi-Prep Column (1– 172, 173–289, 290–432) or a Superdex 200 26-60 Hi-Prep Column (1–289, 1–317, and 1–402). Size-exclusion columns were equilibrated with either 25 mM Tris, pH 7.5, 150 mM NaCl (1–172 and 290–432), 20 mM imidazole, pH 8.0, and 50 mM NaCl (1–289, 173–289, and 173–307) or 20 mM imidazole, pH 8.0, 100 mM NaCl, and 5% glycerol (1–402). Aer2 PAS fragments required imidazole for long-term stability. Concentrated protein was aliquoted, flash frozen, and stored at −80 °C.

Behavioral assays

To determine any effects of the entropy reduction substitutions K176A and E275A on full-length Aer2 function, we independently introduced both lesions into pLH1 [8], expressed them in E. coli BT3388 [45], and tested them for their response to oxygen in a gas perfusion chamber [8]. Mutants were induced with 200 μM IPTG and their swimming behavior was observed after the addition or removal of oxygen.

Crystallization and data collection

Crystals of Aer2 173–289 K176A E275A protein (20 - 40 mg/mL) were grown by vapor diffusion, mixing 1.5 μL of protein with 1.5 μL of well solution, against a reservoir containing 5–20% polyethylene glycol 4K, 0.2 M NaOAc, and 0.1 M Tris,

pH 8.5–9.0 for 1–2 weeks at 17 °C. Diffraction data were collected at the Cornell High Energy Synchrotron Source A1 beamline on an ADSC Quantum 210 CCD. Data were processed with HKL2000 [46].

Structure determination and refinement

The ferric Aer2 PAS structure was determined by molecular replacement with PHENIX AutoMR47 using the CN-bound Aer2 PAS structure (PDB code: 3VOL) [10] truncated from 183–287 with the heme removed. The structure was built using Coot [48] and structure refinement was carried out using PHENIX [47], amid cycles of manual model building, minimization, B-factor refinement, and non-crystallographic symmetry to produce the final model (R-factor = 22.8, Rfree= 24.8) (Table B-1).

UV-visible absorption spectroscopy

Absorption spectra for Aer2 proteins were recorded at 25 °C in stoppered quartz cuvettes with an Agilent 8453 UV-Visible Absorption Spectrophotometer. Ferrous samples were prepared in an anaerobic glovebox by diluting concentrated protein in previously degassed sample buffer and treating with the reducing agent dithionite. Subsequent addition of the NO-releasing compound NOC-7 produced the ferrous–NO complex. Ferrous–NO complexes could also be generated by addition of 1 μM ascorbate and NOC-7. Oxy complexes were generated by either adding cold, non-degassed buffer to dithionite-treated ferrous Aer2 or by addition of 1 μM ascorbate in an aerobic environment. Ferric species were generated by addition of the oxidizing agent $Fe(CN)_6$. Subsequent treatment with KCN produced the ferric–CN− complex.

Multiple rounds of buffer exchange were conducted to remove any trace of imidazole prior to spectroscopic measurements.

Pull-down assays

Pull-down assays were carried out in binding buffer composed of 50 mM Tris, pH 7.5, 150 mM NaCl, and 50 mM imidazole in an aerobic environment. Proteins were incubated with 30 mL washed Ni-NTA resin for 30 min and washed with binding buffer. SDS-loading buffer was added to Ni-NTA resin and used for SDS-PAGE analysis.

SAXS data collection

SAXS data were collected at the SIBYLS beamline (Advanced Light Source, Lawrence Berkeley National Laboratories) using a MarCCD 165 detector capable of fast frame transfer mode. Protein samples at various concentrations and matching buffer samples were loaded into a 96-well plate and transferred to a helium-purged sample chamber using a Hamilton robot. Data were collected for short (0.5 s), long (5 s), and short (0.5 s) exposure times. Samples were checked for radiation damage by comparing data from both short exposure times. Guinier plots were used to evaluate potential sample aggregation and protein concentration effects. Initial data of Aer2 1–402 indicated inter-particle repulsion (decreased scattering at I0 with increasing protein concentration) [28]. Buffer modification to 20 mM imidazole, pH 7.0, 200 mM NaCl, and 5% glycerol alleviated this effect, generating monodisperse samples suitable for SAXS analysis.

SAXS data evaluation and ab initio reconstruction

Prior to analysis, scattering from matching buffer samples was subtracted to generate scattering curves due to protein alone. Guinier plots of buffer-subtracted scattering curves were analyzed using PRIMUS [49] and used to calculate the radius of gyration (Rg) and intensity at zero scattering angle (I0). All Guinier plot values reported include a range extending to Rg×1.3. To optimize signal-to-noise ratios, we created merged data sets from short exposures for small values of q and long exposures for large values of q. Pair-distribution functions [P(r)] were generated using GNOM [50] and used for ab initio shape reconstruction using DAMMIN [29]. Ten independent ab initio runs were compared and averaged using SUPCOMB [51] and DAMAVER [52] to generate the final molecular envelopes. Crystal structures of Aer2 fragments 1–172 and 173–289 were manually fit into the envelopes. HAMP2/3 (residues 66–156) were used to model HAMP4/5.

Pulsed dipolar ESR distance measurements

Purified Aer2 1–402 S183C was spin-labeled by gentle mixing with excess MTSSL overnight at 4 °C. Excess spin label was removed by buffer exchange and protein was used immediately for ESR analysis. PDS measurements were conducted at the AdvanCed Electron Resonance Technology facility as previously described.53,54 Double electron–electron resonance experiments were carried out at 17.35 GHz on a home-built 2D-FT ESR spectrometer, with either 16-ns or 32-ns pump pulses [55]. Protein concentrations were in the range of 25–50 μM. The baseline was approximated by a linear polynomial in most cases. Subsequently, distance distributions were

calculated by Tikhonov regularization56 and further refined by a maximum entropy regularization method [57]. Construction of structural model of full-length Aer2 The full-length model for Aer2 was manually constructed using PyMOL by arranging crystal structures of Aer2 PAS fragments in accordance with Dmax values from scattering data.

Accession numbers

The coordinates and structure factors for the ferric Aer2 PAS domain have been deposited in the PDB with PDB code 4HI4.

Results

Crystal structure of Aer2 PAS

The structure of Aer2 PAS in the ferric heme state was determined at 2.3 Å (Table B-1) using the surface entropy reduction method [21,22] to reduce mobility of exposed loops. A variant protein containing the residue substitutions K176A and E275A (neither of which substantially affected the ability of full-length Aer2 to respond to oxygen) was readily crystallized, and the structure was determined by molecular replacement with the CN^- bound form as a probe. In comparison with FixL and EcDOS, Aer2 represents a novel heme b-binding PAS domain. Aer2 maintains the central Aβ, Bβ, Hβ, and Iβ PAS core2,5 but adopts a different structure between its Cα and Gβ elements to create a different cavity for heme binding (Figure B-3). Cα/Dα form an extended, nearly continuous helix kinked at Ala209, which breaks with the i to i+ 4 main-chain hydrogen-bonding pattern. This extension of Cα and Dα borders the heme edge and is compensated for by an abbreviated and repositioned turn between Gβ and Hβ. The Eα found in EcDOS and FixL distorts into a 310 helix (Eη in Aer2) with two i to i+ 3 main-chain hydrogen bonds. Surprisingly, the Fα helix does not supply the heme-ligating His residue as in FixL and EcDOS, despite two His residues being located on this helix in Aer2 PAS, including His239, which would be predicted by sequence alignments to be the proximal heme ligand8 (Figure B-4). Instead, His234 on Eη serves as the proximal heme ligand. As a result, Fα, Gβ, and the heme moiety all adopt unique atomic positions in Aer2 PAS compared to EcDOS and FixL. The two Aer2 PAS His residues, including His239, project from the solvent-exposed face of the Fα helix. In EcDOS and FixL, the ligand stabilizing Met and Arg

residues are located in the distal heme pocket constructed from the divergent region around Gβ. Rather in Aer2 PAS, a conserved Trp residue near the C-terminal end of Iβ interacts with the distal CN^- ligand in the CN-bound structure [10]. Overall, the structure of Aer2 highlights the degree of structural variability of the Cα-Gβ cofactor-binding pockets of PAS domains, which can supply a variety of ligands and adopt quite different conformations to accommodate the same cofactor.

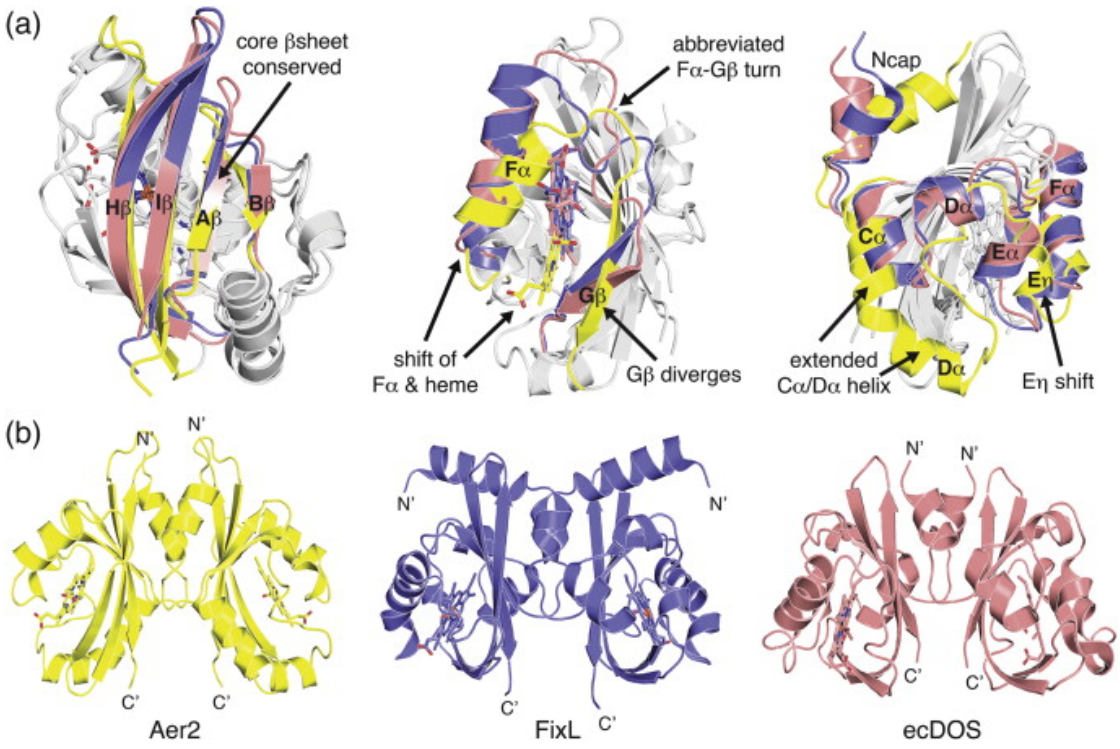

Figure B-3 Aer2 is a novel heme-binding PAS domain that forms a parallel PAS dimer. (a) Structural alignment of the heme-binding PAS domains of Aer2 (yellow, PDB code: 4HI4), FixL (purple, PDB code: 1D06), and *Ec*DOS (pink, PDB code: 1V9Z). Aer2 conserves the core β-sheet (left) but adopts a novel conformation between the Cα helix and Gβ strand elements (middle and right) to bind heme in a unique way.

(b) The ferric Aer2 PAS domain forms a parallel dimer with the Ncap and β-sheet at the interface. FixL and *Ec*DOS form similar parallel dimers but with different orientations of the PAS domains.

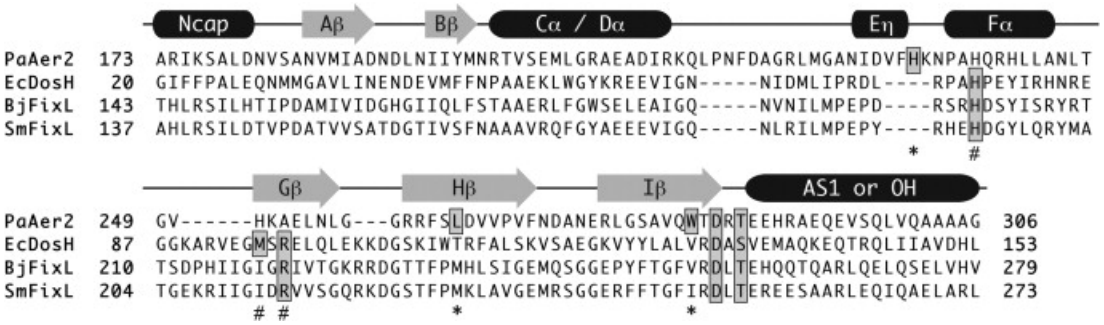

Figure B-4 Sequence alignment of Aer2 with other heme-binding PAS domains. Sequence alignment of *Pa*Aer2, *Ec*Dos, *Bradyrhizobium japonicum* FixL (*Bj*FixL), and *Sinorhizobium meliloti* FixL (*Sm*FixL) with secondary-structure elements above. The proximal heme-coordinating histidine and distal ligand stabilizing residues are highlighted in gray. Residues important for *Pa*Aer2 are denoted by the symbol *, while those for *Ec*DOS/FixL are denoted by the symbol #. The C-terminal DxT motif is highlighted in gray.

Table B-1 Data collection and refinement statistics

Wavelength (Å)	0.97720
Resolution range (Å)	50–2.3 (2.34–2.3)
Space group	$P2_12_12_1$
Unit cell dimensions	
a, *b*, *c* (Å)	67.37, 67.44, 117.87
α, β, γ (°)	90, 90, 90
Total reflections	159,302
Unique reflections	24,338
Multiplicity	6.5 (6.6)
Completeness (%)	99.7 (97.3)
Mean $I/\sigma(I)$	18.1 (7.0)
Wilson *B*-factor	28.3
R_{sym}	0.074 (0.32)
R-factor	0.228 (0.227)
R_{free}	0.248 (0.276)
Number of atoms	4101
Macromolecules	3685
Ligands	197
Water	67
Protein residues	476
RMS bonds (Å)	0.009
RMS angles (°)	1.23
Ramachandran favored (%)	99
Ramachandran outliers (%)	0
Clashscore	20.03
Average *B*-factor	22.2
Macromolecules	21.6
Solvent	21.8

Parallel PAS dimer

Aer2 PAS forms a parallel dimer in the crystallographic asymmetric unit with extensive contacts between the Ncap helices and β-sheets (Figure B-3). This interface is consistent with typical modes of PAS dimerization [2]. The Ncap helices point upward and reside slightly below the Gβ–Hβ loop. The C-termini of the Iβ strands align and face the opposite direction with the Cα carbons separated by 16.3 Å. This is approximately the same distance of separation predicted for the AS1–AS1′ helices of the downstream HAMP domain. A large pocket between the Ncap helices is lined with hydrophobic residues and is occupied by solvent molecules. FixL and EcDOS have also been crystallized as parallel dimers but with different PAS domain orientations (Figure B-3). Aer2 PAS displays a tendency to dimerize in the crystal but is primarily a monomer in solution, as assessed by size-exclusion chromatography.8 However, the crystallographically observed dimer may well be relevant to the full-length receptor where the dimeric HAMP domains above and below would bring the PAS domains in close proximity.

Conformational changes associated with ligand binding

Important structural differences in the ferric heme state of Aer2 PAS compared to the CN-bound structure emanate from the ligand-binding region. These differences are consistent whether any of the four crystallographically unique molecules in the ligand-free structure are superimposed on the CN^-- bound structure. Strikingly, the Trp283 indole group that hydrogen bonds with bound CN^- rotates approximately 90° in the absence of ligand and Leu264 contracts toward the iron center to occupy the

position where CN− binds (Figure B-5). This shift in the position of Leu264 due to CN^- coordination displaces Gβ, Hβ, and the C-terminus of Iβ toward the dimer interface, with the Cα atoms of these β- strands moving by ~ 2.0 Å. The heme itself also shifts up toward Leu264 1.5–2.0 Å upon ligand binding and the surrounding regions of the proximal heme pocket adjust accordingly. The positions of residues in the Hβ–Iβ loop also differ by 3–4.5 Å in the two structures and couple to a similar magnitude shift in the Ncap helix, which packs against this loop at the dimer interface. The movement of the C-terminal Iβ strand, which appears to respond directly to the rotation of Trp283, causes a nearly 3.0-Å displacement toward the dimer for the C-terminal

DxT motif (Figure B-5). This motif is a conserved feature of PAS domains, couples directly to the C-terminal HAMP domain in Aer2, and is known to undergo changes in different signaling states [2]. Overall, the differences between the free and CN^--bound monomers are substantial and likely reflect the conformational changes utilized by Aer2 to respond to diatomic ligands. Importantly, if the CN^--bound structure is superimposed on the ligand-free parallel PAS dimer found in the Aer2 PAS crystals, the shifts of the Ncap helix and the Gβ– Hβ–Iβ strands cause collisions across the dimer interface that make the CN^--bound form incompatible with the ligand-free structure (Figure B-5). In particular, the C-terminal end of Hβ and the Ncap helix collide in the modeled dimer. Thus, ligand binding to Aer2 would in the least rearrange PAS–PAS interactions based on the parallel crystallographic dimer and may cause substantial changes to the junction between Iβ and the downstream HAMP domain.

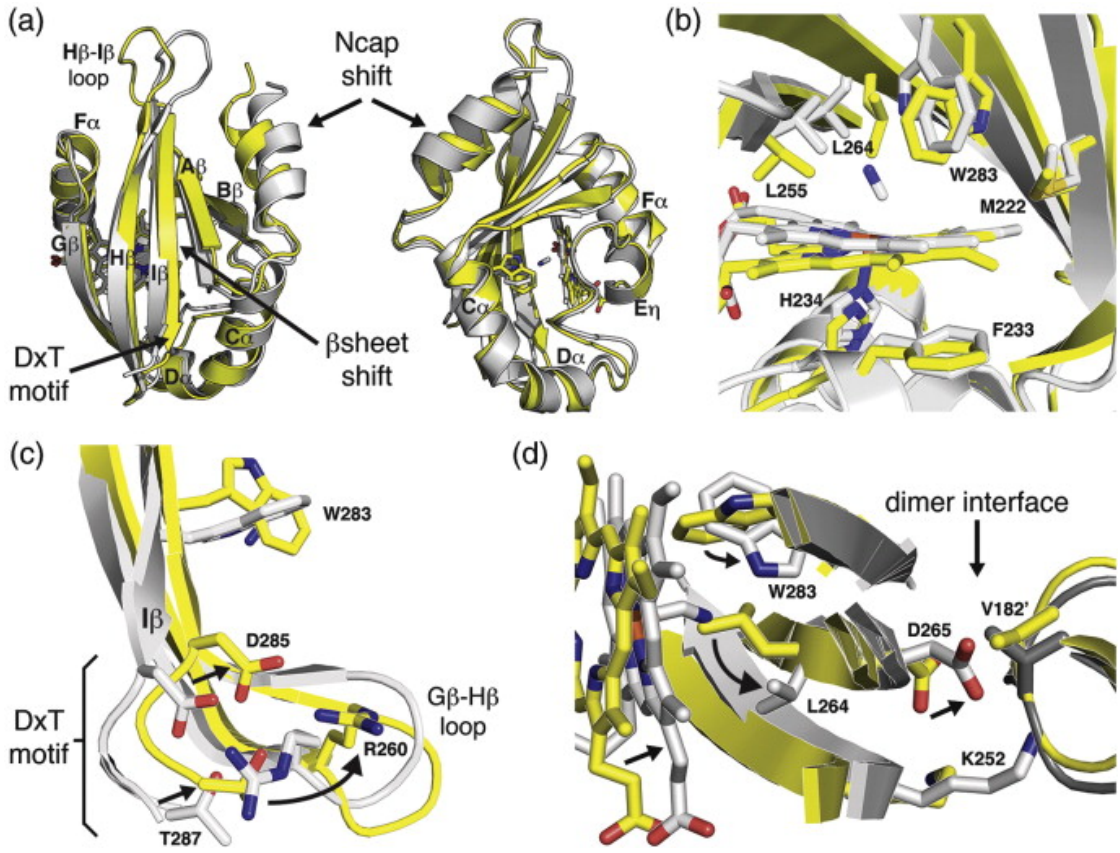

Figure B-5 Conformational changes associated with ligand binding.

Structural alignment of ferric (yellow) and CN-bound (gray) Aer2 PAS domains.

(a) The absence of ligand alters the PAS domain structure, shifting the β-sheet and Ncap helix.

(b) The active site rearranges in the absence of ligand with the Trp283 side chain, which interacts with bound CN, rotating 90° and the Leu264 side chain moving over the iron center.

(c) Ligand-induced conformational changes propagate to the DxT motif, at the C-terminal end of the Iβ strand, and associated Gβ–Hβ loop.

(d) A superposition of the CN-bound structure on the ferric dimer structure reveals that the CN-bound monomer is incompatible with the ferric dimer. Asp265, which is adjacent to Leu264 in Hβ, collides with Val182, located at the C-terminal end of the Ncap, across the dimer interface. Superimposed CN-bound PAS molecules are shown as light gray (left) and dark gray (right).

The HAMP domains of Aer2 do not alter the local heme environment

Next, we aimed to determine how ligand binding might propagate from the Aer2 PAS domain to the downstream HAMP domains. We first asked whether Aer2 utilizes a similar mechanism as EcAer where side-on PAS/HAMP interactions mediate interdomain communication. Since EcAer requires the HAMP domain for stable FAD binding [23–25], we reasoned that the HAMP domains might affect the spectroscopic properties of the Aer2 PAS domain. Initial characterization of PAS and PAS/HAMP fragments found substantial differences in UV-visible spectra. However, we determined that rather than this being due to the presence of the HAMP domains, it was caused by improper iron incorporation, as detected by fluorescence spectroscopy, which resulted in a mixture of heme and protoporphyrin IX (heme lacking iron). Improper iron incorporation only occurred in the purified PAS/HAMP fragment [26,27]. Co-expression of Aer2 with ferrochelatase, which catalyzes the insertion of iron into protoporphyrin IX, resulted in full heme incorporation [26]. The resulting UV-visible spectra of PAS and PAS/HAMP fragments were now identical for all redox and ligation states assayed (Figure B-6; Table B-2). Thus, the HAMP domains

do not alter the local environment surrounding the Aer2 PAS domain as monitored by UV-visible spectroscopy.

Table B-2 UV-visible absorption maxima for Aer2 PAS domains with and without HAMP domains

	PAS (173–289)			PAS/HAMP (1–402)		
	Soret	β	α	Soret	β	α
Fe(III)	393	511	646	396	511	645
Fe(II)	433	560		432	561	
Fe(II)-O_2	418	543	577	418	543	577
Fe(II)-NO	419	534	568	419	533	567
Fe(III)-CN	422	545		421	545	

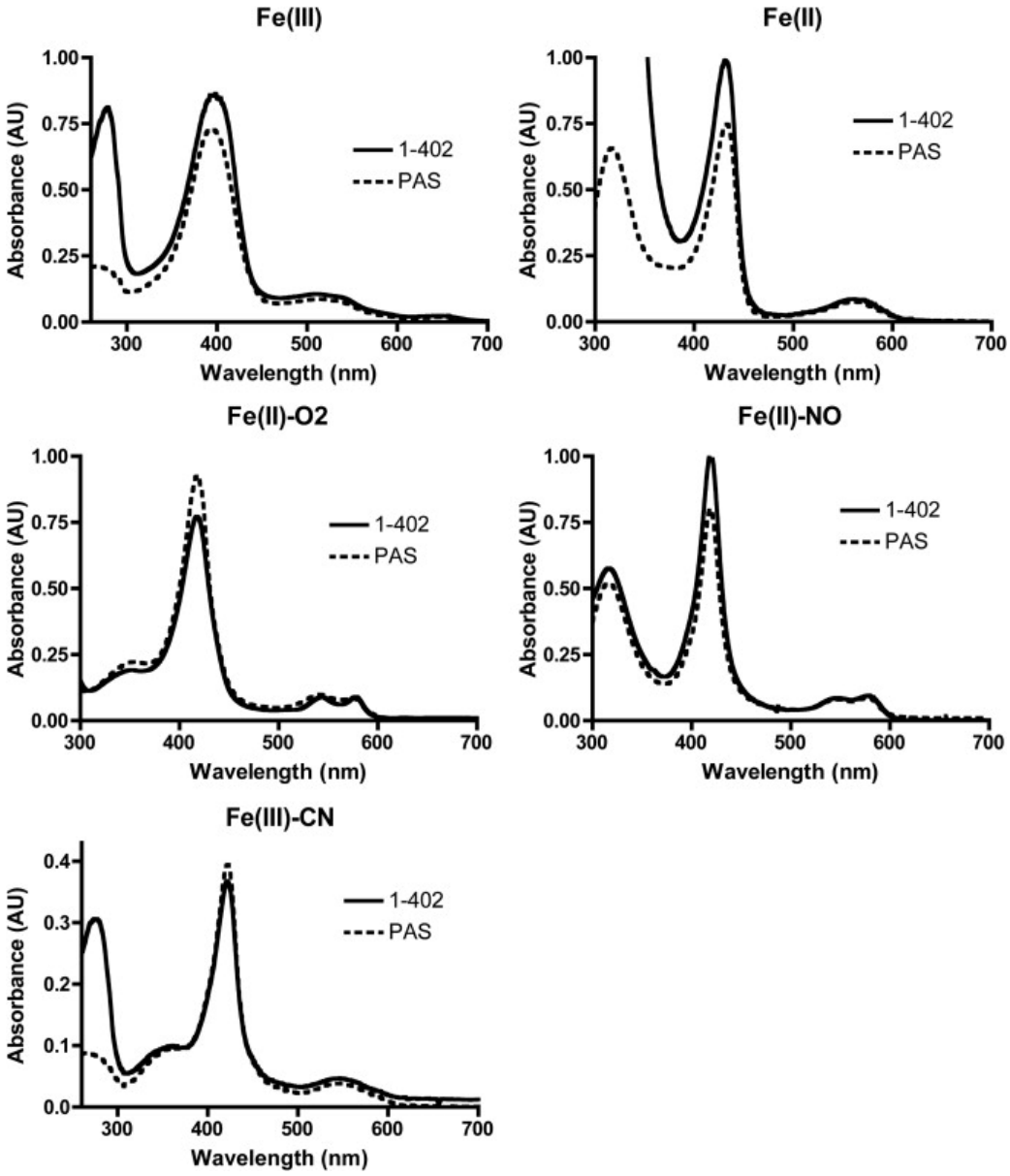

Figure B-6 The HAMP domains do not affect the UV-visible absorption spectra of the heme-binding PAS domain. UV-visible absorption spectra of purified Aer2 PAS (173–289) and PAS/HAMP (1–402) proteins in ferric, ferrous, Fe(II)-O_2, Fe(II)-NO, and Fe(III)-CN redox and ligation states. Absorption maxima (Table B-2) and peak shape are identical in both Aer2 protein fragments.

The PAS and HAMP domains do not form stable complexes

The lack of spectroscopic changes does not necessarily rule out PAS and HAMP domain interactions in Aer2 since the heme environment is spatially removed from the likely contact interface involving the β-sheet. To directly assess interdomain interactions, we used pull-down assays of individually purified domains. The PAS domain failed to pull down with both HAMP1–2/3 and HAMP4/5 (Figure B-7). In addition, HAMP1–2/3–PAS failed to pull-down HAMP4/5. This suggests that the PAS and HAMP domains do not form stable complexes but these data do not exclude the possibility of transient interactions, especially during signal transduction.

Determination of quaternary structure using SAXS

Defining the domain juxtapositions within the quaternary structure of Aer2 should provide important clues to the mechanism of signal transduction. SAXS gives detailed information on mass distribution in molecules and can provide low-resolution molecular envelopes that are particularly useful to reconstruct quaternary structure when atomic structures of individual domains are known.28 To unambiguously identify the domain arrangement in Aer2, we collected SAXS data on progressively larger protein fragments: 1–172, 1–317, and 1–402. Conditions were optimized to ensure that experimental data were suitable for analysis (see Experimental Procedures). In summary, Guinier analysis and a plot of the intensity at zero scattering angle (I0) versus concentration (Table B-3; Figure B-8) indicated that all samples were monodisperse and suitable for ab initio reconstruction. In addition, a maximum distance (Dmax) for each receptor fragment was determined by calculating the pairwise electron density distribution function [P(r)]. Ten *ab initio* reconstructions

were carried out for each Aer2 fragment using DAMMIN [29] and the resulting models were compared and averaged to generate final envelopes (Figure B-9). The *ab initio* reconstructions clearly distinguished the N-terminal poly-HAMP domains in each fragment (Figure A-9). A wider envelope is found below HAMP3 and is consistent with a PAS dimer residing in this position. C-terminal extensions to PAS project downward and suggest that HAMP4/5 lies below the PAS dimer. In addition, the Dmax values increased with the addition of each domain (Table B-3), which is consistent with a linear domain arrangement. Interestingly, a kink was observed at the PAS–HAMP4 junction. This feature was consistent among the various reconstructions. It may result from an inherent flexibility between the domains or simply be an artifact given the highly elongated nature of Aer2. Elongated structures require increased search volumes compared to globular proteins, making ab initio reconstructions less accurate [28].

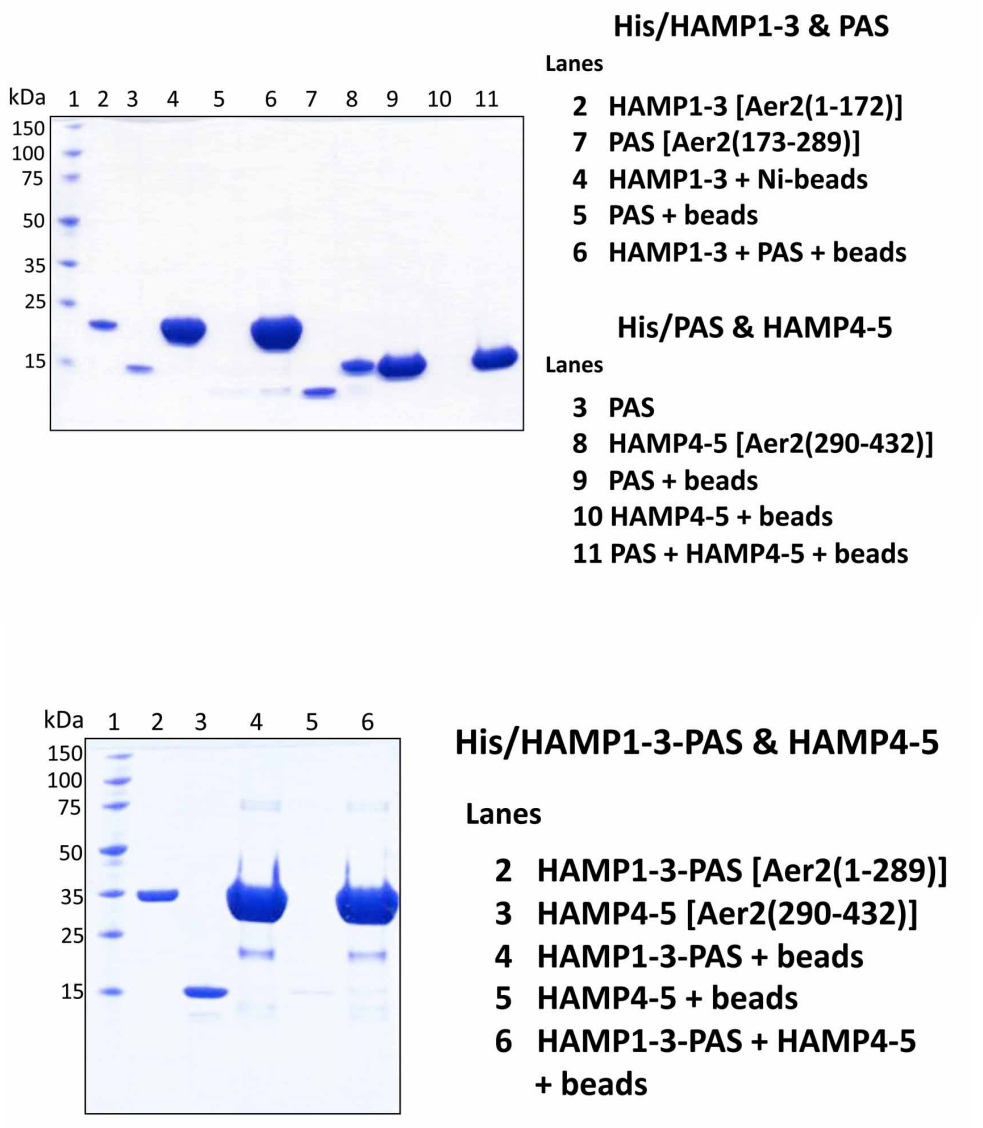

Figure B-7 Pull-down assays of Aer2 PAS and HAMP domain protein fragments. Pull-down assays with His-tagged proteins were unable to detect binding of the PAS domain to either HAMP1-3 or HAMP4-5 fragments.

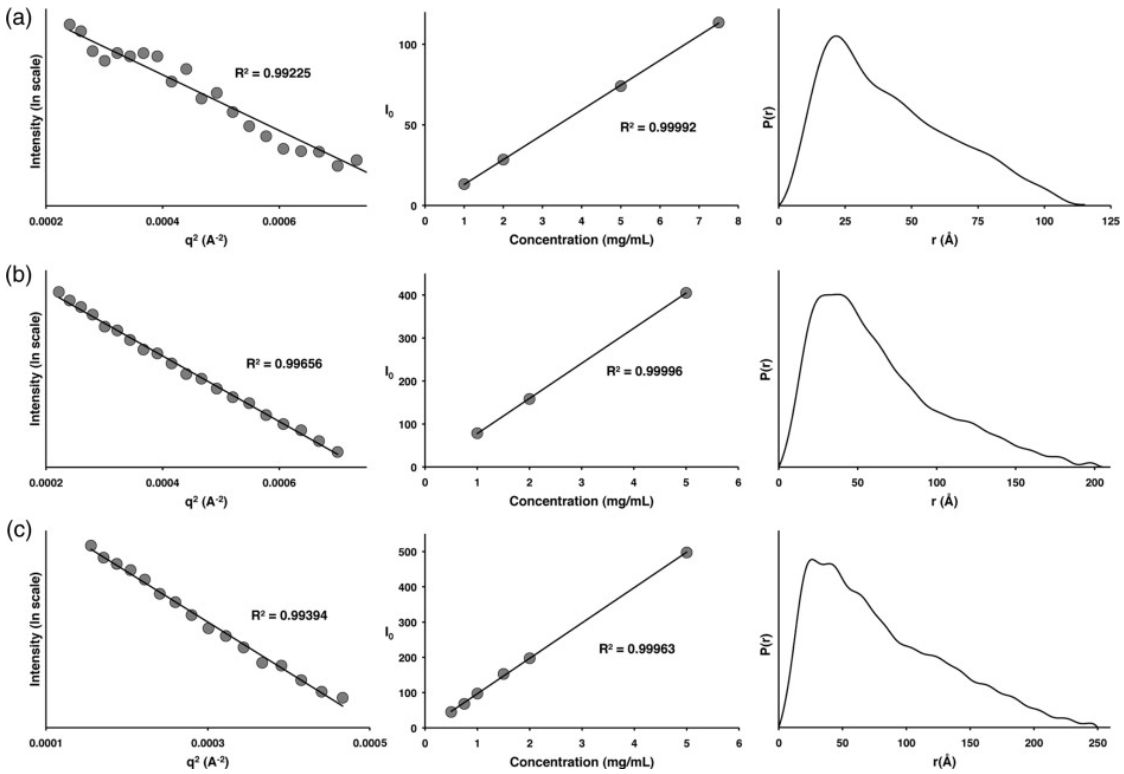

Figure B-8 SAXS parameters for data validation and interpretation. Guinier plot (left), I_0 *versus* protein concentration (middle), and $P(r)$ *versus* r (Å) (right) for (a) Aer2 1–172, (b) Aer2 1–317, and (c) Aer2 1–402 proteins. I_0, intensity at zero scattering angle; $P(r)$, pairwise electron density distribution. Linear plots indicate that the Aer2 protein samples are monodisperse and suitable for further analysis. D_{max} values were determined from $P(r)$ distributions.

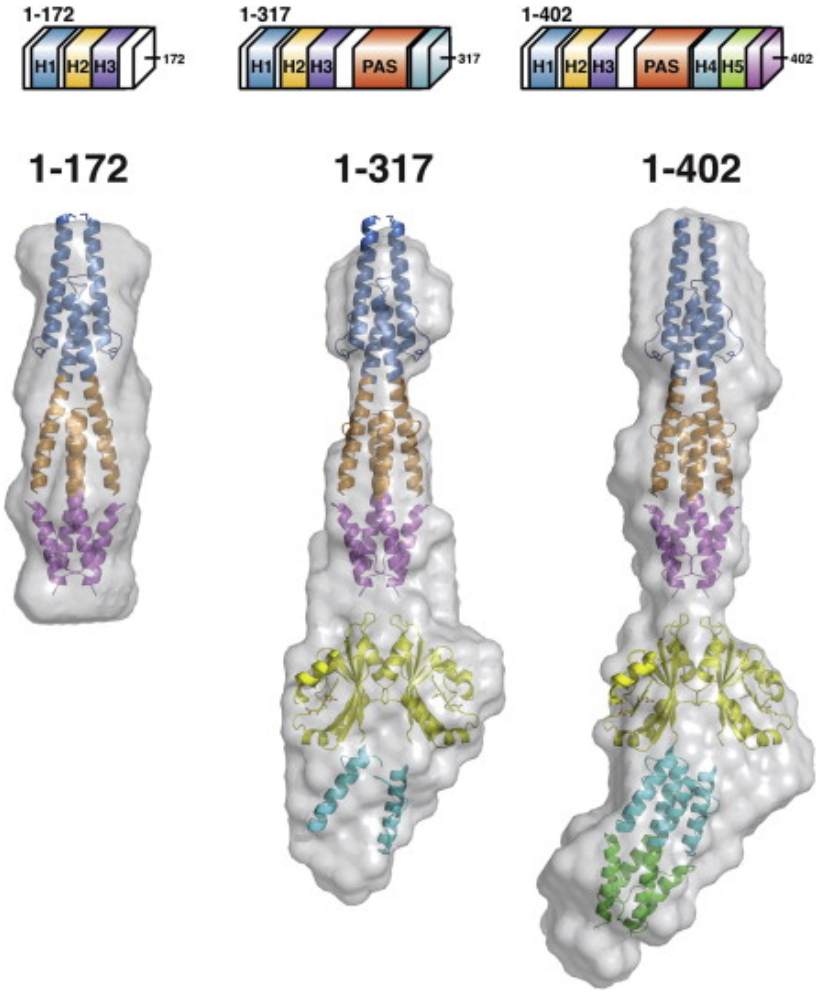

Figure B-9 *Ab initio* SAXS reconstructions of Aer2 protein fragments. Molecular envelopes (gray) generated from scattering data of Aer2 protein fragments 1–172 (HAMP1–2/3), 1–317 (HAMP1–2/3, PAS, and HAMP4 AS-1/connector), and 1–402 (HAMP1–2/3, PAS, HAMP4/5, and 20 residues of the KCM). Due to the elongated nature of Aer2, protein fragments of increasing molecular weight were used to allow clear identification of quaternary structure. Crystal structures of Aer2 HAMP1–2/3 (PDB code: 3LNR) and the PAS dimer (PDB code: 4HI4) were manually placed and fit well inside the envelopes. HAMP2/3 of Aer2 was used as a model for HAMP4/5.

Table B-3 SAXS parameters for data validation and interpretation

	1–172	1–317	1–402
Experimental			
q range ($Å^{-1}$)	0.0155–0.319	0.0149–0.319	0.01247–0.319
Resolution (Å)	402–19.7	422–19.7	504–19.7
R_g (Guinier plot) (Å)	32.4	45.8	62.7
R_g [$P(r)$] (Å)	34.1	52.8	67.8
D_{max} (Å)	115	205	250
Ab initio SAXS model			
Goodness of fit (χ^2)	1.02	1.16	1.31
Normal spatial discrepancy	1.00	0.64	0.69
R_g model (Å)	32.0	51.8	66.4
D_{max} model (Å)	112.2	193	237.8
Structural model			
D_{max} model (Å)	112	207	241

D_{max} values determined from experimental data, *ab initio* model, and structural model correlate well for each Aer2 protein fragment.

Interdomain distances defined by pulsed ESR are only consistent with a PAS dimer

We aimed to confirm the linear domain arrangement and lack of side-on PAS/HAMP interactions with pulsed dipolar ESR spectroscopy (PDS) distance measurements of spin-labeled Aer2. We spinlabeled Aer2 1–402 and assessed the interdomain PAS–PAS distance by monitoring the magnetic dipolar interactions between spins. We chose to spin label at position S183, which is solvent exposed near the PAS dimer interface and should provide an intersubunit Cα –Cα distance of 11.7 Å if the crystallographic parallel dimer of Aer2PAS is maintained in the larger protein (Figure A-10). (Corresponding residues in the FixL and EcDOS dimeric structures are

also near each other, with distances of 12.5 and 17.1 Å.) However, the 183 side chain is constrained by the dimer interface to project into solvent away from the symmetry axis of the dimer. Modeling S183Cnitroxide spin labels at the two corresponding 183 positions gives an intersubunit distance of ~ 26 Å between nitroxides (Figure A-10). PDS distance measurements of MTSSL spin-labeled Aer2 1–402 S183C gave a strong dipolar signal and sharp P(r) distribution centered at 26.7 Å, in good agreement with the expected distance based on the crystal structure (Figure A-10). There is no question that the presence of a HAMP domain between the PAS domains would greatly increase this distance by ~ 26 Å; thus, the experimental ESR distance measurements are only consistent with a dimeric PAS architecture within Aer2.

Model for Aer2 architecture

A final model of the Aer2 receptor architecture was produced using information derived from crystallography, SAXS, and ESR data (Figure A-11). The ab initio molecular envelopes and Dmax values support a linear domain organization, with a PAS dimer sandwiched between the N- and C-terminal HAMP domains. This arrangement is consistent with the short, three-amino-acid linker between the PAS and HAMP4 termini, whereas in EcAer, the PAS and HAMP domains are separated by an F1 helical region and two transmembrane helices. Overall, the architecture of soluble Aer2 differs drastically from the membrane-integrated EcAer and thereby implies an "in-line" mechanism for signal transduction between PAS and HAMP domains, much like those proposed for chemotaxis receptors, sensor kinases, and sensory rhodopsin transducers.

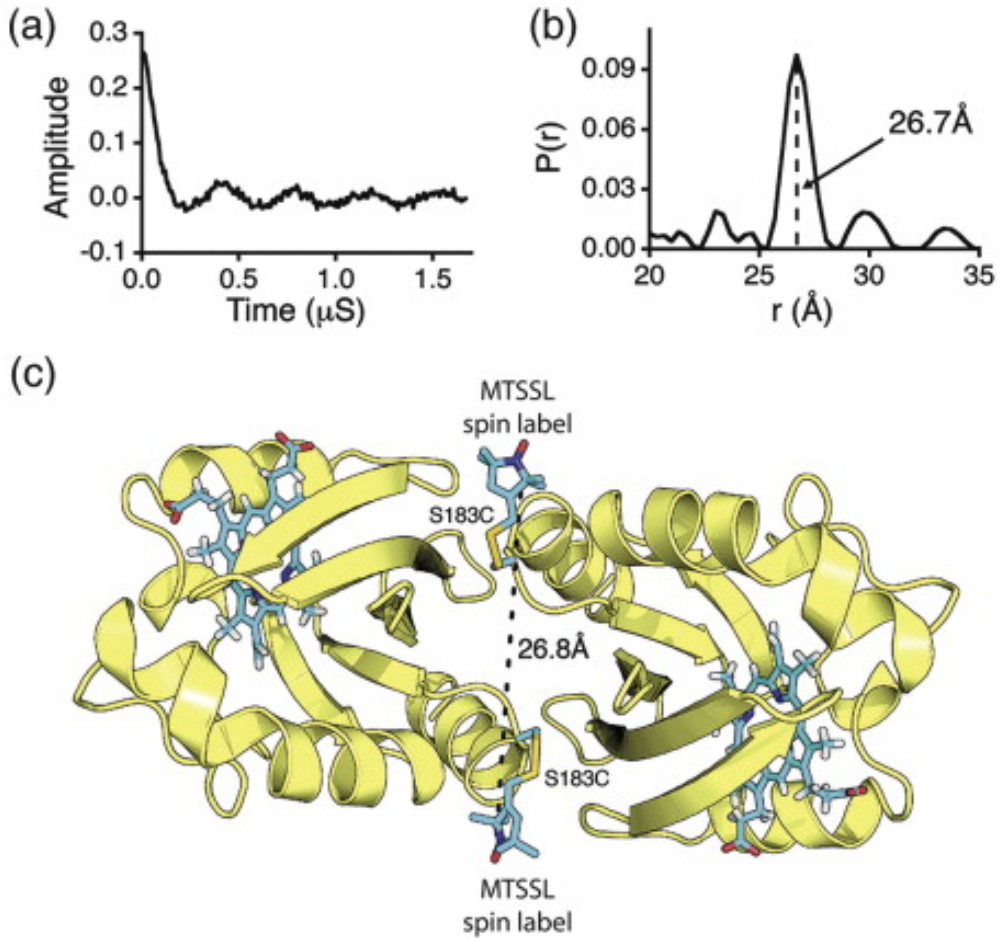

Figure B-10 Interdomain distance is only consistent with a PAS dimer.

(a) Time domain signal and (b) corresponding probability distance distribution [$P(r)$] for spin-labeled Aer2 1–402 S183C. A sharp $P(r)$ centered at 26.8 Å is smaller than the diameter of a HAMP domain and fully consistent with the ferric Aer2 PAS dimer. (c) Model of MTSSL spin-labeled Aer2 S183C PAS dimer. The dimer interface directs the two spin labels (blue) away from each other to add approximately 15 Å to the S183 C^{α}–C^{α} atom distance.

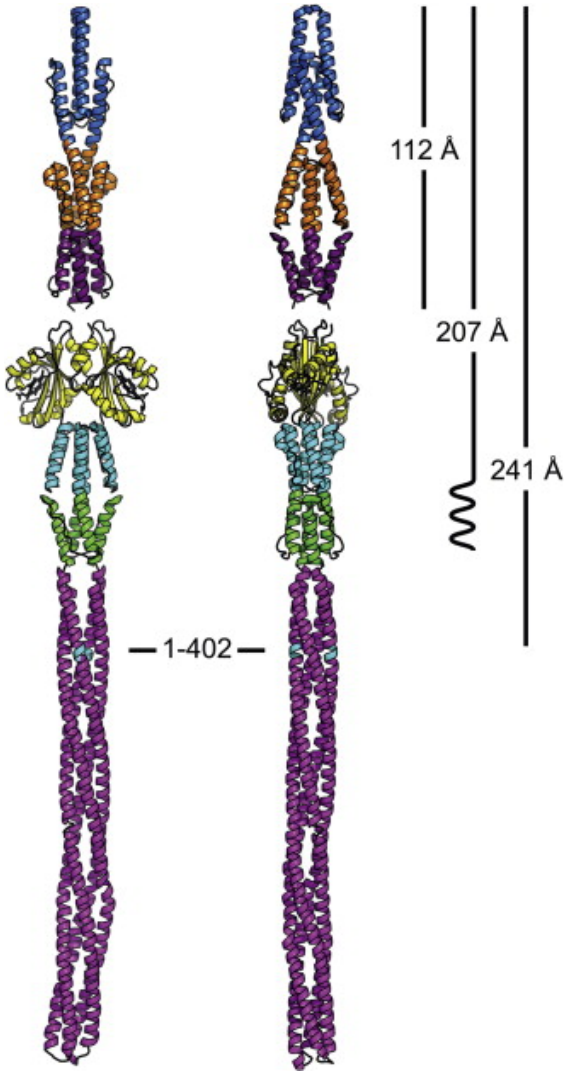

Figure B-11 Structural model of Aer2 receptor with a linear domain arrangement. Full-length model of the soluble receptor Aer2 using structural information reported in this study. D_{max} values derived from the SAXS data are displayed on the right and are consistent with the linear domain arrangement as shown. A small region, comprising residues 158–172, predicted to be of helical structure would connect HAMP3 and the PAS domains. The methyl-accepting chemotaxis protein module (purple) is modeled from *Thermotoga maritima*1143 (PDB code: 2CH7).

Discussion

An in-line PAS and HAMP domain signaling mechanism in Aer2

The aerotaxis receptor EcAer has served as a paradigm for PAS and HAMP domain signaling for more than a decade [6]. EcAer is a transmembrane protein that has proved difficult to characterize structurally; however, through biochemical and genetic methods, the signaling mechanism has been well characterized [7,24,25,30–37]. In EcAer, an F1 linker and two transmembrane helices separate the cytoplasmic PAS and HAMP domains.35,38 Signal relay occurs through direct side-on interdomain interactions between the PAS β-sheet and the cognate HAMP AS2 helix [7] (K.J.W., M.S. Johnson, and B.L. Taylor, unpublished data). It is noteworthy that this is an atypical type of interdomain signaling for both PAS and HAMP domains. In general, PAS domains interact with other PAS domains through pseudo symmetric interfaces formed by the β-sheets or Ncaps2,5 and HAMP domains receive signal input from connected transmembrane helices.

To shed light on the signaling mechanisms in other PAS and HAMP domain systems, we have investigated the architecture of the soluble receptor Aer2. This also represents the first structural characterization of poly-HAMP domains connected to a sensing domain. We have visualized the ligand-induced PAS domain conformational changes between ferric and ferric CN^--bound states and, combined with atomic resolution structures, defined the quaternary structure of the soluble receptor Aer2 using SAXS. Ab initio molecular envelopes and Dmax values clearly establish that the PAS and poly-HAMP domains of Aer2 are arranged in a linear fashion. Thus, the mechanism by which PAS and HAMP communicate in Aer2 must be different than

that of EcAer. If Aer2 does not utilize side-on interactions, then how does ligand binding propagate to the downstream HAMP domains? Based on the work presented herein and on previous work, we hypothesize that signal relay occurs through changes at the junction between the PAS and HAMP domains caused by changes in PAS–PAS subunit orientations brought about by ligand binding. Namely, that changes at the C-terminal end of the PAS domain affect the conformation and signaling state of HAMP4, in a manner more similar to transmembrane signal input. Based on the dimeric crystal structure and matching ESR distance, we propose that Aer2 contains a PAS domain dimer and that alterations in subunit interactions, which result from ligand binding in the heme center, affect the conformation of HAMP4 AS1. Although the Aer2 PAS domains only have a weak affinity for dimerization in isolation,8 they are held in close proximity by the constitutively dimeric N- and C-terminal HAMP domains. This may explain why the N-terminal HAMP domains are required for function,8 even though they are not physically located between the input and output domains. In this scenario, a weak PAS dimerization affinity is preferential to allow perturbations at the PAS–PAS interface to be induced by ligand binding. In contrast, a very stable PAS dimer would be less able to respond to stimuli by altering the subunit interface.

Overall, these considerations lead to a model where the N-terminal poly-HAMPs are required as a dimerization motif. In support of this, Aer2 peptides lacking HAMP2 and HAMP3 cannot respond to changes in gas concentrations [8]. Changes in ligation state cause conformational changes in PAS that propagate from the ligand binding site (e.g., rotation of Trp283 and contraction of Leu264) to shift the β-sheet,

reposition the Ncap helix, and alter the position of the C-terminal DxT motif, which connects directly to the downstream HAMP. This shifts the PAS monomer–dimer equilibrium or alternatively causes a rearrangement of the PAS dimer. The changes in PAS dimerization are interpreted by HAMP4/5 and relayed to the KCM of the methyl-accepting chemotaxis protein module to regulate kinase activity. The orientation of the PAS domains relative to HAMP1–3 may also change in response to the ~ 3-Å change in Ncap helix position. However, due to its peripheral association with the PAS core, the position of the N-terminal helix could be affected by its lack of attachment to HAMP3 in the isolated PAS domain structures.

Comparison with conformational changes in other heme-binding PAS domains

FixL, EcDOS, and Aer2, the three PAS domains structurally defined in different ligation states, appear to utilize different signaling mechanisms but nevertheless share some common themes for ligand-induced conformational changes. In EcDOS, Met95 serves as the distal ligand in the six-coordinate ferrous state.18,19 Oxygen binding purges Met95 far from the active site and the side chain of Arg97 flips downward to hydrogen bond with and stabilize bound O_2 (Figure A-12). The active-site changes are propagated and coupled to a total rearrangement of the Fα–Gβ loop between residues Gly88 and Leu99. Other regions of the protein, including the core β- sheet, are nearly unchanged with the exception of the Leu99 and Tyr80 side chains. The ligand-induced conformational changes in FixL also occur in the Fα–Gβ loop but are relatively minor in comparison to EcDOS. FixL is five-coordinate in the ferrous state. Bound O2 is stabilized by the side chain of Arg200, which moves inward

from the periphery of the active site (Figure A-12) [39]. Ile215 moves in the opposite direction, from the active site toward the periphery, and His214 alters its position to continue hydrogen bonding with the propionate group of heme. Overall, both EcDOS and FixL share a similar mechanism in that ligand binding is stabilized by an Arg residue and conformational changes are mainly localized to the Fα–Gβ loop, which contain the distal heme-coordinating and/or ligand-stabilizing residues. Analogous to the movement of Met95/Arg97 in EcDOS and Ile215/Arg220 in FixL, $CN^{-}-$ binding in Aer2 PAS displaces Leu264 from above the hemeiron center, and rotation of the indole group of Trp283, which is already in the active site, facilitates a hydrogen bond to CN^{-}. However, in contrast to FixL and EcDOS, the ferric and CN^{-}-bound structures of Aer2 differ not only in the active site but also throughout the entire domain, including the core β- sheet and Ncap. These global changes stem from the central location of the distal active-site residues in Aer2, which reside in the Iβ (Trp283) and Hβ (Leu264) strands and not in Fα–Gβ loop/Gβ strand. The magnitude of these changes is not as large as the drastic shifts observed in the Fα–Gβ loop in EcDOS, but importantly they affect the position of the C-terminal portion of the Iβ strand, Ncap, and dimer interface that more clearly illustrates the functional outcome of ligand binding in comparison to the localized movements observed for EcDOS and FixL. Overall, there is a similarity in the general mechanism of ligand-induced conformational changes in that one active-site residue moves outward to allow ligand binding and another moves inward to hydrogen bond and stabilize bound ligand.

Although the heme-binding PAS domains characterized thus far utilize different means to generate their respective signaling states, coordination of a diatomic

ligand to the heme cofactor of these PAS sensors appears to be the key determinant in propagating conformational signals, as opposed to a change in heme redox state. In Aer2, any diatomic ligand capable of hydrogen bonding with its distal atom would be predicted to induce the same structural changes we observe with CN^-. This may explain why Aer2 gives nearly equivalent chemotaxis repellent responses in *E. coli* with saturating levels of O_2, NO, or CO [8], the latter being isoelectronic with CN^-. When ligation state control dominates, CN^- can effectively mimic other diatomic ligands. The kinase activity of BjFixL is regulated nearly equivalently by O2 binding the ferrous heme or CN^- binding the ferric form.40 Also, EcDOS is activated by both O_2 and CO [41] and CN^- binding to EcDOS induces similar allosteric changes in subunit interactions as CO or O_2 [42]. In contrast, CN^- will not activate the heme-based CO transcription factor CooA, but this is because CN^- is not a strong enough ligand to displace a protein-based proline ligand to the heme [43]. Variant forms of CooA that have been engineered to be five-coordinate bind CN^- and respond with an activated transcriptional response [44].

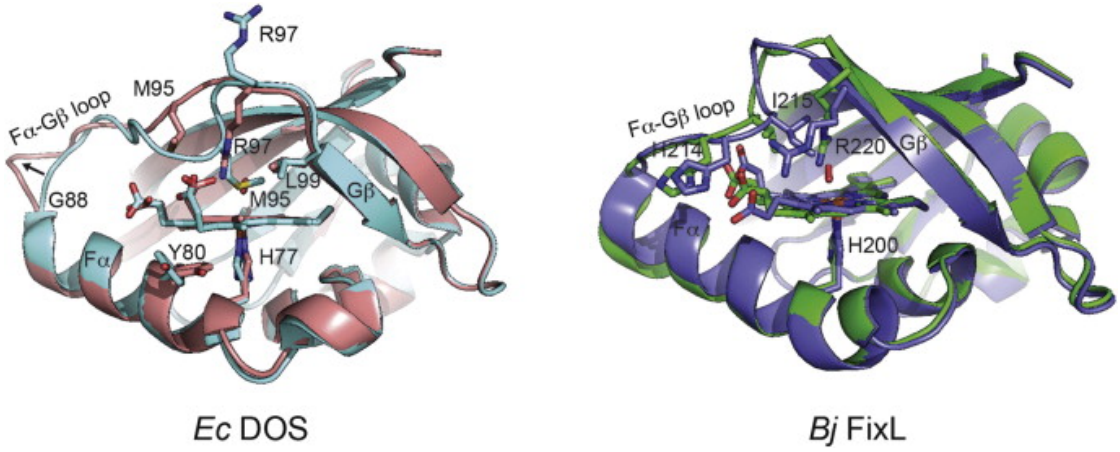

Figure B-12 Conformational changes in *Ec*DOS and FixL PAS domains. Superposition of *Ec*DOS (PDB code: 1S66) and *Bj*FixL (PDB codes: 1LSW and 1DP6) PAS domains in ferrous (blue, green) and O_2 bound (pink, purple) states. The Fe(II) state of *Ec*DOS is six-coordinate with Met95 serving as the distal ligand. O_2binding displaces Met95 and is stabilized by Arg97. O_2 binding is coupled to a rearrangement of the Fα–Gβ loop. In FixL, O_2 binding also causes a rearrangement of the Fα–Gβ loop. Ile215 moves away from the heme center, whereas Arg220 moves toward the heme center to hydrogen bond with molecular oxygen.

Endogenous ligands

The endogenous ligands sensed by Aer2 are currently not known; however, the considerable differences between ferric and ferric- CN^- structures that can propagate to the downstream HAMP domains suggest that Aer2 switches between these two conformers during signaling. The response of Aer2 to CN− is not established, but all diatomic ligands tested (O_2, NO, and CO) generate the same chemotactic response in *E. coli* cells expressing Aer2 [8]. Reaction toward these ligands indicates that Aer2

obtains the ferrous form within cells. Nonetheless, the CN^--bound form, which favors ferric coordination, is likely a reasonable mimic for the ferrous ligation states of O_2, NO, and CO. The broad UV-visible spectral features of the Aer2 heme cofactor in either the ferric or ferrous form indicate that the heme is five-coordinate in the absence of ligand, regardless of redox state. Moreover, the conformational differences we observe between the ligand-bound and free forms stem from a coordinated diatomic ligand that is capable of accepting a hydrogen bond from Trp283 and excludes Leu264 from the active center. We suspect that this is the critical factor in rearranging the PAS conformation, not the redox state of the heme per se. CN^- simply allows a ligated state to be trapped by the ferric form. Nonetheless, determining structures of Aer2 in different redox/ligation states is an area of active investigation and will aid in determining the endogenous ligand and function of Aer2.

Summary

We determined the structure of Aer2 PAS with a five-coordinate ferric heme, which, in comparison with the six-coordinate ferric–CN− structure, provides a view of conformation changes associated with ligand binding. In addition, we have reconstructed the structure of the soluble receptor Aer2 by combining atomic-resolution structures of the individual PAS and HAMP domains with solution SAXS data. The resulting model indicates that the Aer2 PAS and HAMP domains do not directly interact but are arranged in a linear fashion, consistent with the results of both UV-visible spectra, pull-down assays, and ESR distance measurements. Based on the

structural architecture, a mechanism of signal transduction likely involves changes in PAS–PAS subunit association in response to changes in the ligation state of the heme iron. Overall, the quaternary structure of Aer2 establishes an in-line model for PAS–HAMP signaling that differs considerably from previously characterized systems, yet may be widely applicable to other signaling proteins that fuse sensory domains directly to HAMP modules.

REFERENCES

[1] Parkinson, J. S. (2010). Signaling mechanisms of HAMP domains in chemoreceptors and sensor kinases. Annu. Rev. Microbiol. 64, 101–122.

[2] Möglich, A., Ayers, R. A. & Moffat, K. (2009). Structure and signaling mechanism of Per–ARNT–Sim domains. Structure, 17, 1282–1294.
[
3] Dunin-Horkawicz, S. & Lupas, A. N. (2010). Comprehensive analysis of HAMP domains: implications for transmembrane signal transduction. J. Mol. Biol. 397, 1156–1174.

[4] Schultz, J., Milpetz, F., Bork, P. & Ponting, C. P. (1998). SMART, a simple modular architecture research tool: identification of signaling domains. Proc. Natl Acad. Sci. USA, 95, 5857–5864.

[5] Henry, J. T. & Crosson, S. (2011). Ligand binding PAS domains in a genomic, cellular, and structural context. Annu. Rev. Microbiol. 65, 261–286.

[6] Taylor, B. L. (2007). Aer on the inside looking out: paradigm for a PAS–HAMP role in sensing oxygen, redox and energy. Mol. Microbiol. 65, 1415–1424.

[7] Campbell, A. J., Watts, K. J., Johnson, M. S. & Taylor, B. L. (2010). Gain-of-function mutations cluster in distinct regions associated with the signalling pathway in the PAS domain of the aerotaxis receptor, Aer. Mol. Microbiol. 77, 575–586.

[8] Watts, K. J., Taylor, B. L. & Johnson, M. S. (2011). PAS/poly-HAMP signalling in Aer-2, a soluble haembased sensor. Mol. Microbiol. 79, 686–699.

[9] Airola, M. V., Watts, K. J., Bilwes, A. M. & Crane, B. R. (2010). Structure of concatenated HAMP domains provides a mechanism for signal transduction. Structure, 18, 436–448.

[10] Sawai, H. et al. (2012). Structural basis for oxygen sensing and signal transduction of the heme-based sensor protein Aer2 from Pseudomonas aeruginosa. Chem. Commun. 48, 6523–6525.

[11] Hong, C. S. et al. (2004). Chemotaxis proteins and transducers for aerotaxis in Pseudomonas aeruginosa. FEMS Microbiol. Lett. 231, 247–252.

[12] Ferrández, A., Hawkins, A. C., Summerfield, D. T. & Harwood, C. S. (2002). Cluster II che genes from Pseudomonas aeruginosa are required for an optimal chemotactic response. J. Bacteriol. 184, 4374–4383.

[13] Güvener, Z. T., Tifrea, D. F. & Harwood, C. S. (2006). Two different Pseudomonas aeruginosa chemosensory signal transduction complexes localize to cell poles and form and remould in stationary phase. Mol. Microbiol. 61, 106–118.

[14] Garvis, S., Munder, A., Ball, G., de Bentzmann, S., Wiehlmann, L., Ewbank, J. J. et al. (2009). Caenorhabditis elegans semi-automated liquid screen reveals a specialized role for the chemotaxis gene cheB2 in Pseudomonas aeruginosa virulence. PLoS Pathog. 5, e1000540.

[15] Gong, W., Hao, B., Mansy, S. S., Gonzalez, G., GillesGonzalez, M. A. & Chan, M. K. (1998). Structure of a biological oxygen sensor: a new mechanism for heme-driven signal transduction. Proc. Natl Acad. Sci. USA, 95, 15177–15182.

[16] Key, J. & Moffat, K. (2005). Crystal structures of deoxy and CO-bound bj FixLH reveal details of ligand recognition and signaling. Biochemistry, 44, 4627–4635.

[17] Miyatake, H., Mukai, M., Park, S. Y., Adachi, S., Tamura, K., Nakamura, H. et al. (2000). Sensory mechanism of oxygen sensor FixL from Rhizobium meliloti: crystallographic, mutagenesis and resonance Raman spectroscopic studies. J. Mol. Biol. 301, 415.

[18] Kurokawa, H., Lee, D. S., Watanabe, M., Sagami, I., Mikami, B., Raman, C. S. & Shimizu, T. (2004). A redox-controlled molecular switch revealed by the crystal structure of a bacterial heme PAS sensor. J. Biol. Chem. 279, 20186–20193.

[19] Park, H. J., Suquet, C., Satterlee, J. D. & Kang, C. H. (2004). Insights into signal transduction involving PAS domain oxygen-sensing heme proteins from the X-ray crystal structure of Escherichia coli Dos heme domain (Ec DosH). Biochemistry, 43, 2738–2746.

[20] Pokkuluri, P., Pessanha, M., Londer, Y. Y., Wood, S. J., Duke, N. E., Wilton, R. et al. (2008). Structures and solution properties of two novel periplasmic sensor domains with c-type heme from chemotaxis proteins of Geobacter sulfurreducens: implications for signal transduction. J. Mol. Biol. 377, 1498–1517.

[21] Derewenda, Z. S. & Vekilov, P. G. (2005). Entropy and surface engineering in protein crystallization. Acta Crystallogr., Sect. D: Biol. Crystallogr. 62, 116–124.

[22] Cooper, D. R., Boczek, T., Grelewska, K., Pinkowska, M., Sikorska, M., Zawadzki, M. & Derewenda, Z. (2007). Protein crystallization by surface entropy reduction: optimization of the SER strategy. Acta Crystallogr., Sect. D: Biol. Crystallogr. 63, 636–645.

[23] Herrmann, S., Ma, Q., Johnson, M. S., Repik, A. V. & Taylor, B. L. (2004). PAS domain of the Aer redox sensor requires C-terminal residues for native-fold formation and flavin adenine dinucleotide binding. J. Bacteriol. 186, 6782–6791.

[24] Bibikov, S. I., Barnes, L. A., Gitin, Y. & Parkinson, J. S. (2000). Domain organization and flavin adenine dinucleotide-binding determinants in the aerotaxis signal transducer Aer of Escherichia coli. Proc. Natl Acad. Sci. USA, 97, 5830–5835.
[25] Ma, Q., Johnson, M. S. & Taylor, B. L. (2005). Genetic analysis of the HAMP domain of the Aer aerotaxis sensor localizes flavin adenine dinucleotide-binding determinants to the AS-2 helix. J. Bacteriol. 187, 193–201.

[26] Sudhamsu, J., Kabir, M., Airola, M. V., Patel, B. A., Yeh, S. R., Rousseasu, D. L. & Crane, B. R. (2010). Co-expression of ferrochelatase allows for complete heme incorporation into recombinant proteins produced in E. coli. Protein Expr. Purif. 73, 78–82.

[27] Airola, M. V., Du, J., Dawson, J. H. & Crane, B. R. (2010). Heme binding to the mammalian circadian clock protein period 2 is nonspecific. Biochemistry, 49, 4327–4338.

[28] Putnam, C. D., Hammel, M., Hura, G. L. & Tainer, J. A. (2007). X-ray solution scattering (SAXS) combined with crystallography and computation: defining accurate macromolecular structures, conformations and assemblies in solution. Q. Rev. Biophys. 40, 191–285.

[29] Svergun, D. (1999). Restoring low resolution structure of biological macromolecules from solution scattering using simulated annealing. Biophys. J. 76, 2879.

[30] Watts, K. J., Sommer, K., Fry, S. L., Johnson, M. S. & Taylor, B. L. (2006). Function of the N-terminal cap of the PAS domain in signaling by the aerotaxis receptor Aer. J. Bacteriol. 188, 2154–2162.

[31] Watts, K. J., Johnson, M. S. & Taylor, B. L. (2006). Minimal requirements for oxygen sensing by the aerotaxis receptor Aer. Mol. Microbiol. 59, 1317–1326.

[32] Watts, K. J., Johnson, M. S. & Taylor, B. L. (2008). Structure–function relationships in the HAMP and proximal signaling domains of the aerotaxis receptor Aer. J. Bacteriol. 190, 2118–2127.

[33] Watts, K. J., Johnson, M. S. & Taylor, B. L. (2011). Different conformations of the kinase-on and kinaseoff signaling states in the Aer HAMP domain. J. Bacteriol. 193, 4095–4103.

[34] Watts, K. J., Ma, Q., Johnson, M. S. & Taylor, B. L. (2004). Interactions between the PAS and HAMP domains of the Escherichia coli aerotaxis receptor Aer. J. Bacteriol. 186, 7440–7449.

[35] Campbell, A. J., Watts, K. J., Johnson, M. S. & Taylor, B. L. (2011). Role of the F1 region in the Escherichia coli aerotaxis receptor Aer. J. Bacteriol. 193, 358–366.

[36] Burón-Barral, M. C., Gosink, K. K. & Parkinson, J. S. (2006). Loss- and gain-of-function mutations in the F1- HAMP region of the Escherichia coli aerotaxis transducer Aer. J. Bacteriol. 188, 3477–3486.

[37] Repik, A., Rebbapragada, A., Johnson, M. S., Haznedar, J. O., Zhulin, I. B. & Taylor, B. L. (2002). PAS domain residues involved in signal transduction by the Aer redox sensor of Escherichia coli. Mol. Microbiol. 36, 806–816.

[38] Amin, D. N., Taylor, B. L. & Johnson, M. S. (2007). Organization of the aerotaxis receptor Aer in the membrane of Escherichia coli. J. Bacteriol. 189, 7206–7212.

[39] Hao, B., Isaza, C., Arndt, J., Soltis, M. & Chan, M. K. (2002). Structure-based mechanism of O2 sensing and ligand discrimination by the FixL heme domain of Bradyrhizobium japonicum. Biochemistry, 41, 12952–12958.

[40] Tuckerman, J. R., Gonzalez, G., Dioum, E. M. & Gilles-Gonzalez, M. A. (2002). Ligand and oxidationstate specific regulation of the heme-based oxygen sensor FixL from Sinorhizobium meliloti. Biochemistry, 41, 6170–6177.

[41] Hiroto, T. & Toru, S. (2006). Phosphodiesterase activity of Ec DOS, a heme-regulated enzyme from Escherichia coli, toward 3′,5′-cyclic diguanylic acid is obviously enhanced by O2 and CO Binding. Chem. Lett. 35, 970–971.

[42] Lechauve, C., Bouzhir-Sima, L., Yamashita, T., Marden, M. C., Vos, M. H., Liebl, U. & Kiger, L. (2009). Heme ligand binding properties and intradimer interactions in the full-length sensor protein DOS from Escherichia coli and its isolated heme domain. J. Biol. Chem. 284, 36146–36159.

[43] Youn, H., Kerby, R. L. & Roberts, G. P. (2003). The role of the hydrophobic distal heme pocket of CooA in ligand sensing and response. J. Biol. Chem. 278, 2333–2340.

[44] Thorsteinsson, M. V., Kerby, R. L. & Roberts, G. P. (2000). Altering the specificity of CooA, the carbon monoxide-sensing transcriptional activator: characterization of CooA variants that bind cyanide in the FeII form with high affinity. Biochemistry, 39, 8284–8290.

[45] Yu, H. S., Saw, J. H., Hou, S., Larsen, R. W., Watts, K. J., Johnson, M. S. et al. (2006). Aerotactic responses in bacteria to photoreleased oxygen. FEMS Microbiol. Lett. 217, 237–242.

[46] Otwinowski, Z. & Minor, W. (1997). Processing of Xray diffraction data collected in oscillation mode. Macromol. Crystallogr. A, 276, 307–326.

[47] Adams, P. D., Afonine, P. V., Bunkoczi, G., Chen, V. B., Davis, I. W., Echols, N. et al. (2010). PHENIX: a comprehensive Python-based system for macromolecular structure solution. Acta Crystallogr., Sect. D: Biol. Crystallogr. 66, 213–221.

[48] Emsley, P. & Cowtan, K. (2004). Coot: model-building tools for molecular graphics. Acta Crystallogr., Sect. D: Biol. Crystallogr. 60, 2126–2132.

[49] Konarev, P. V., Volkov, V. V., Sokolova, A. V., Koch, M. H. J. & Svergun, D. I. (2003). PRIMUS: a Windows PC-based system for small-angle scattering data analysis. J. Appl. Crystallogr. 36, 1277–1282.

[50] Svergun, D. (1992). Determination of the regularization parameter in indirect-transform methods using perceptual criteria. J. Appl. Crystallogr. 25, 495–503.

[51] Kozin, M. B. & Svergun, D. I. (2001). Automated matching of high-and low-resolution structural models. J. Appl. Crystallogr. 34, 33–41.

[52] Volkov, V. V. & Svergun, D. I. (2003). Uniqueness of ab initio shape determination in small-angle scattering. J. Appl. Crystallogr. 36, 860–864.

[53] Bhatnagar, J., Borbat, P. P., Pollard, A. M., Bilwes, A. M., Freed, J. H. & Crane, B. R. (2010). Structure of the ternary complex formed by a chemotaxis receptor signaling domain, the CheA histidine kinase, and the coupling protein CheW as determined by pulsed dipolar ESR spectroscopy. Biochemistry, 49, 3824–3841.

[54] Borbat, P. P. & Freed, J. H. (2007). Measuring distances by pulsed dipolar ESR spectroscopy: spinlabeled histidine kinases. Methods Enzymol. 423, 52–116.

[55] Park, S. Y., Borbat, P. P., Gonzalez-Bonet, G., Bhatnagar, J., Pollard, A. M., Freed, J. H. et al. (2006). Reconstruction of the chemotaxis receptor– kinase assembly. Nat. Struct. Mol. Biol. 13, 400–407.

[56] Chiang, Y. W., Borbat, P. P. & Freed, J. H. (2005). The determination of pair distance distributions by pulsed ESR using Tikhonov regularization. J. Magn. Reson. 172, 279–295.

[57] Chiang, Y. W., Borbat, P. P. & Freed, J. H. (2005). Maximum entropy: a complement to Tikhonov regularization for determination of pair distance distributions by pulsed ESR. J. Magn. Reson. 177, 184–196.